Antibodies, conjugates, and uses thereof

Field of the invention

The present invention relates to antibodies, antigen-binding fragments thereof and fragment-drug conjugates (FDCs) which bind to the human MET-receptor (cMET), methods for discovering and making anti-cMET FDCs and their use in the treatment of cancer and other diseases.

Background of the invention

Cancer is a leading cause of global deaths, and according to the World Health Organisation (https://gco.iarc.fr) accounted for 10 million deaths in 2020. The most common cancers include lung (~1.8 million cases/year), colon and rectum (~935 000), liver (~830 000), stomach (~760 000) and breast (~685 000). Poor permeation [1] and multi-drug resistance [2] in solid tumours are two important challenges which lead to the failure of current treatment methods. The tumour microenvironment (TME) in solid tumours poses physical challenges for the effective and homogenous delivery of cancer treatments. Intra-tumoral drug penetration is hindered by the physical barriers brought on by the tumour stroma, disruption and disorganisation of the extracellular matrix increasing tissue stiffness/solid stress, impaired lymphatic drainage which consequently increases hydrostatic pressure and increased vascular permeability 'leaky vasculature' causing irregular intra-tumour blood flow [3]. Poor drug penetration and distribution leads to marginal doses reaching the tumour resulting in acquired resistance and treatment failure [1].

One approach to increase cancer therapy effectiveness is to use combination of drugs with different or complementary mechanisms of action and non-overlapping clinical toxicities [4]. Antibody-Drug Conjugates (ADCs) are a well-established form of targeted therapy, making an impact in cancer primarily, but also in infectious diseases, inflammatory diseases and other indications [5,6]. Here, a specific monoclonal antibody (MAb) enables the selective accumulation of an effector payload in the required target tissue (e.g., tumour) whilst normal, non-targeted organs eliminate and clear the ADC or its components. ADCs, designed around the standard whole Immunoglobulin (Ig) structure, primarily IgG, have a long circulatory half-life due to the presence of the Fc-domain (which interacts with the neonatal Fc-receptor, FcRn). However, the large size also presents many limitations such as slow and ineffective tumour and organ penetration and long-term exposure of payloads to non-targeted tissues [6,7].

cMET overexpression relative to that of normal tissues has been observed in many types of solid human malignancies including gastric, colorectal, pancreatic, lung, head and neck, ovarian, breast, renal, prostate, bladder, nasopharyngeal, gliomas, osteosarcomas and melanomas (Table 1). Due to the poor clinical prognosis of solid tumours overexpressing cMET, and the toxicities caused by broad-spectrum chemotherapeutic treatments used today as well as insufficient drug dosage reaching all parts of the tumour, an opportunity is presented for the development of targeted therapeutics against this receptor.

Furthermore, MAb or ADC distribution following extravasation from the vasculature is further impeded by cellular internalization and subsequent endocytic clearance at the tumour periphery (an effect known as the "binding-site barrier"), leading to poor penetration and regions of marginal antibody concentrations [8-10]. It follows that higher binding-affinity, multi-valent avidity and higher antigen expression, especially at the tumour edge, can retard MAb tumour percolation and impair homogeneous distribution. Although this barrier can be overcome by increasing the dose of therapeutic agent administered to patients, this can lead to significant side effects, particularly with cytotoxic agents such as ADCs.

An alternative approach is to improve penetration and diffusion using smaller formats such as antibody fragments (e.g., Fab fragments (~50 kDa), single-chain variable fragments (scFv ~30 kDa) and single-domain antibodies (sdAb 12–15 kDa)) and peptides [11]. Although these formats possess higher extravasation and intra-tumoural diffusion rates, the overall percentage tumour uptake is low because the elimination rates for smaller formats is higher compared to full-size antibody molecules. Immunoglobulins possess a half-life of at least 20 days for most therapeutic MAbs [9,12]. Antibody fragments lacking an Fc region have half-lives of minutes-hours for formats whose size falls below the glomerular filtration cut-off (approx. 30–50 kDa) [7,11]. The rapid elimination rate after systemic delivery prevents most antibody fragments from saturating the tumour and achieving a uniform distribution.

Due to its targeting/localization effect, ADCs increase the tumour concentration of the targeted payload, therefore lower doses are required to reach the tumour to effectively destroy the targeted cells. More recent thinking suggests that ADCs have a similar maximum tolerated dose as the equivalent payload but improve efficacy though targeted delivery [13]. Moreover, depending on the chemical nature of the drug and its release in the tumour (either intracellular or extracellular), some payloads can subsequently diffuse and kill surrounding non-targeted tumour cells ("bystander killing") [14]. Consequently, these features, in some way, help ameliorate the drawbacks of the heterogeneous tumour

distribution, but does not solve the problem, especially for intractable or poorly vascularised tumours.

Despite >90% of cancers being solid tumours, only 6/12 of the approved ADCs are for solid tumours (trastuzumab-emtansine, famtrastuzumab-deruxtecan, directed against HER2, enfortumab-vedotin against Nectin-4, Sacituzumab govitecan against TROP-2, tisotumab vedotin against tissue factor and mirvetuximab sorvtansine against folate receptor alpha) which highlights the difficulty in applying ADCs to these diseases [5]. An estimated 100 or more other ADCs are currently under clinical development (www.clinicaltrials.gov) but the failure rate for solid tumours is disproportionately higher compared to haematological cancers (https://beacon-intelligence.com). The availability of target antigens expressed on the surface of tumour cells and the approval of the use of ADCs have seen success in the area of haematological malignancies. Solid tumours however display antigens which are tumour associated and have varying levels of over-expression. These antigens are not exclusively found on the surface of these solid tumours but are also expressed on normal tissues at lower levels bringing about challenges with on-target off-tumour toxicity [6]. High doses, poor biophysical properties (e.g., aggregating) and the presence of an Fc-region can lead to off-target toxicities [15]. Biochemical improvements to ADCs have driven the success in this area such as improved linker chemistry preventing premature release, increased payload loading achieving higher drug:antibody ratios (DAR) for more tolerable payloads, and the discovery of new warheads with different mechanisms of action and membrane-permeable payloads [5,6,16,17].

The addition of a cytotoxic payload to pre-existing targeted therapy illustrates the value of tumour-specific cytotoxin delivery. Trastuzumab-emtansine was able to broadly improve patient outcomes compared to the non-conjugated trastuzumab MAb and this was further improved by trastuzumab-deruxtecan [5,6,18] which is now widely acknowledged to have a transformative clinical impact in HER2-positive breast cancer [18].

cMET overexpression relative to that of normal tissues has been observed in many types of solid human malignancies including gastric, colorectal, pancreatic, lung, head and neck, ovarian, breast, renal, prostate, bladder, nasopharyngeal, gliomas, osteosarcomas and melanomas (Table 1). Due to the poor clinical prognosis of solid tumours overexpressing cMET, and the toxicities caused by broad-spectrum chemotherapeutic treatments used today as well as insufficient drug dosage reaching all parts of the tumour, the inventors identified an opportunity which is presented for the development of targeted therapeutics against this receptor.

The inventors have developed novel anti-cMET antibodies and antigen-binding fragments thereof, along with antibody-drug and fragment-drug conjugates. These antibodies have surprising beneficial properties in terms of cMET binding, and tumour penetration and clearance.

Summary of the invention

In a first aspect the invention provides an antibody or antigen-binding fragment thereof that specifically binds to the MET receptor (cMET), wherein the antibody or antigen-binding fragment thereof comprises a heavy chain variable region (VH) comprising the Complementarity Determining Region (CDRs) CDR-H1, CDR-H2, and CDR-H3 of SEQ ID NO. 1, or a variant thereof having at least 80% sequence identity to SEQ ID NO. 1, and comprises a light chain variable region (VL) comprising the CDRs CDR-L1, CDR-L2, and CDR-L3 of SEQ ID NOs. 196 or 2, or a variant thereof having at least 80% sequence identity with SEQ ID NOs. 196 or 2.

In a particular embodiment of the first aspect of the invention there is provided an antibody or antigen-binding fragment thereof that specifically binds to the MET receptor (cMET), wherein: (i) the antibody or antigen-binding fragment thereof comprises a heavy chain variable region (VH) comprising the Complementarity Determining Regions (CDRs) CDR-H1, CDR-H2, and CDR-H3 of SEQ ID NO. 1, or a variant thereof having at least 90% sequence identity to SEQ ID NO. 1, and comprises a light chain variable region (VL) comprising the CDRs CDR-L1, CDR-L2, and CDR-L3 of SEQ ID NOs.196 or 2, or a variant thereof having at least 90% sequence identity with SEQ ID NOs.196 or 2; or (ii) the antibody or antigen-binding fragment thereof comprises a heavy chain variable region (VH) comprising the Complementarity Determining Regions (CDRs) CDR-H1, CDR-H2, and CDR-H3 of SEQ ID NO. 21, or a variant thereof having at least 90% sequence identity to SEQ ID NO. 21, and comprises a light chain variable region (VL) comprising the CDRs CDR-L1, CDR-L2, and CDR-L3 of SEQ ID NO. 22, or a variant thereof having at least 90% sequence identity with SEQ ID NO. 22.

In some embodiments of the first aspect of the invention, the antibody or antigen-binding fragment thereof comprises a VL comprising the CDRs of SEQ ID NO. 196.

In some embodiments, the antibodies and antigen-binding fragments disclosed herein have advantageous properties in terms of cMET binding and blocking of cMET signalling. The application also discloses the antibodies and antigen-binding fragments thereof conjugated to payloads which demonstrate advantageous properties in tumour

penetration, tumour payload delivery, serum half-life and bioavailability, normal tissue exposure and tumour clearance.

By "cMET" we mean the MET receptor, which is also referred to as hepatocyte growth factor receptor, HGF receptor, HGFR, and MET. The mesenchymal-epithelial transition factor gene referred to as MET is a proto-oncogene which encodes a cell surface tyrosine kinase receptor (cMET) for hepatocyte growth factor (HGF)/scattering factor (SF) ligand. Upon ligand binding cMET forms a homo-dimer leading to trans-phosphorylation which activates several pathways including phosphoinositide 3-kinase (P13K)/AKT (protein kinase B), mitogen-activated protein kinase Ras/(MAPK), Janus kinase/signal transducers and activators of transcription (JAK/STAT), SRC and WNT/β catenin [19,20].

The HGF/cMET pathway in normal physiology is involved in embryogenesis, normal cellular growth, cell motility, cell survival, wound healing, angiogenesis and tissue regeneration. The HGF/cMET pathway regulates disease progression by reducing oxidative stress, inflammation, apoptosis and fibrosis. cMET is expressed in vascular, lymphatic endothelial cells and hematopoietic cells, skin, GI tract and lungs at low normal levels and can increase upon tissue repair, regeneration or during inflammation. cMET is also expressed at low levels in normal liver, kidney, pancreas, prostate, muscle and bone marrow, during embryogenesis and adulthood [19].

MET overexpression, genomic amplification, translocations, sub-gene deletions, point mutations and alternative splicing can lead to the aberrant expression of the MET proto-oncogene. This is a major cause of the dysregulation of the cMET autocrine and paracrine signalling pathway [21]. Over-expression of the HGF ligand can also lead to aberrant cMET signalling. These alterations, leading to cMET activation have been observed in many human malignancies associated with invasive growth, tumour cell motility, angiogenesis, and poor clinical prognosis [20-23]. cMET expression strongly and significantly correlates with poor prognosis and patient outcomes in multiple clinical examples of cancer and is highly implicated in other cancers (Table 1). In some cases, genetic defects in MET lead to activation which renders tumour cells 'addicted' (i.e. highly dependent on this pathway for growth and survival) to MET-oncogene signalling [22]. More often than not cMET protein over-expression is not the outcome of MET gene mutations which occur in ~6% of cMET-over-expressing cancers [21]. MET gene amplification frequency in solid tumours (<2%) is described in the AACR GENIE registry (https://www.aacr.org/professionals/research/aacr-project-genie) [23].

The MET gene is translated as a single chain precursor of 1390 residues and transported to the golgi for glycosylation. Furin cleaves the protein to form a disulphide-linked alpha

and beta chain heterodimer. The extracellular portion of cMET comprises 3 domains, SEMA (semaphorin, a 7-bladed beta propeller structure which includes the HGF-binding site) domain, PSI (plexin-semaphorin-integrin-domain) and 4 IPT (immunoglobulin-plexin-transcription) repeats. The intracellular domains comprise a juxtamembrane sequence, the tyrosine kinase catalytic domain and carboxyl-terminal sequences [19].

cMET overexpression relative to that of normal tissues has been observed in many types of solid human malignancies including gastric, colorectal, pancreatic, lung, head and neck, ovarian, breast, renal, prostate, bladder, nasopharyngeal, gliomas, osteosarcomas and melanomas (Table 1). Due to the poor clinical prognosis of solid tumours overexpressing cMET, and the toxicities caused by broad-spectrum chemotherapeutic treatments used today as well as insufficient drug dosage reaching all parts of the tumour, an opportunity is presented for the development of targeted therapeutics against this receptor.

Table 1: cMET expression in tumours

Cancer type	Notes
Gastric [23-25]	Overexpressed (43-55%), MET-amplified (5-21%), significantly poor impact on survival
Lung [26,27]	Overexpressed (35-72%), MET-amplified (2-5%), mutation (3-4%), associated with significantly worse overall survival
Oesophageal [28,29]	Overexpressed (44-69%) in adenocarcinoma, MET-amplified (4%), mutations (1%) rare in oesophageal squamous cell carcinoma, associated with a significantly shorter 5-year disease specific and OS with an increased likelihood to develop local and distant metastases
Ovarian [30,31]	Overexpressed in early stage (65%) and late-stage disease (80.8%), MET-amplification in clear-cell adenocarcinomas (22%) and mutations in 6% clear-cell adenocarcinomas, high expression of c-Met increases the risk of metastasis and is negatively correlated with prognosis, cMET overexpression correlates with adverse outcomes for patients
Renal [32,33]	16-80% overexpression, 47% >2-4 MET copies per nucleus, 7% 4 copies per nucleus and 46% 2 copies per nucleus (study with 572 tumours), mutations observed in patients with hereditary papillary RCC and in 13% of sporadic papillary RCC, c-Met overexpression associated with significantly worse prognosis (RCC). Elevated cMET/HGFR expression correlates with worse cancer specific survival and MET upregulation is associated with unfavourable prognosis.
Thyroid [34]	70-80% overexpressed Met protein present in papillary carcinomas (116 thyroid tumours)
Head and Neck [35,36]	20% highly overexpressed, cMET overexpression associated with significantly worse overall survival
Liver [37]	30% overexpressed in hepatocellular carcinoma, MET amplification is rate (<5%)
Bladder [38]	Overexpressed (59%), 0.8% rare amplification of the MET gene, 1.9% of cases from a study of 569 cases have MET mutations (rare), Phosphorylated cMET leads to highly malignant disease and poor overall survival.
Breast [39,40]	Overexpressed (54.5%), MET-amplified (4.7%), MET mutations (~9%), increased over expression of c-Met correlates with reduced overall survival in patients
Melanoma [41]	Upregulated in uveal melanoma in response to kinase inhibitors

Osteosarcoma [42]	cMET inhibitors active in osteosarcoma
Glioma [43]	cMET involved in glioma tumour initiating cells
Nasopharyngeal [44]	Positive expression on 70% of patient samples
Colorectal [45-47]	Highly expressed in up to 67% primary carcinomas, gene amplification in up to 18%, activating mutations in ~5%, poor prognostic factor for survival
Prostate [48]	Observed expression and associated poorer outcomes
Haematological	Expression in diffuse large B-cell lymphoma with poorer prognosis

cMET overexpression can be defined by an immunohistochemistry (IHC) H-score (range 0-300) of 200-300 (High, 3+), 100-200 (Medium, 2+), 50-100 (Low, 1+) or 0-50 (Negative, 0) [49]. Briefly, IHC staining protocol for cMET overexpression has been developed using the Ventana cMet CONFIRM (SP44) kit. Tissue samples are stained with the Ventana antibody and then scored by determining the percentages of target tissue cells staining at various intensity levels of low to high [50].

Other methods to determine cMET over-expression levels can also include RNA *In Situ* Hybridization Assays, silver In Situ Hybridization Assays (SISH) or Quantitative real-time polymerase chain reaction (qPCR).

cMET expression determination by protein-based methods such as IHC is cost-effective and well established in clinical settings but does not discriminate between MET-oncogene addicted and non-addicted tumour cells [21,22].

The MET properties described above position this oncogene target as an important prognostic factor and a valuable drug target for numerous applications in clinical oncology [51-55].

There has been a major effort to develop small molecule cMET pathway inhibitors (e.g., crizotinib, cabozantinib, capmatinib, tepotinib, and glesatinib). Cabozantinib (Cabometyx®/Cometriq®) and crizotinib (Xalkori®) are FDA/EMA-approved and marketed drugs but many others have failed clinical development primarily due to poor tolerability or low efficacy (often related to poor patient selection resulting in patients whose tumours are not oncogene addicted and less sensitive to cMET inhibition) [22,51]. Small molecule inhibitors (SMIs) block ATP-phosphorylation of the cMET tyrosine kinase preventing downstream signalling and broad specificity for ATP-binding sites makes them specific for related kinases such as VEGFR, RET, AXL and others.

Cabozantinib is approved for thyroid, liver and kidney cancer but has shown disappointing results in other major solid tumours with side effects such as severe bleeding, blood clots,

hypertension, gastro-intestinal toxicities. Crizotinib is approved for ALK/ROS-mutated non small-cell lung cancer with serious adverse effects including liver toxicity (fatal in 0.1% patients), interstitial lung disease (severe/fatal in 0.5%), pneumonitis, cardiac effects and neutropenia. This indicates a need for better tolerated drugs.

cMET expression in tumours is also associated with resistance to targeted therapies against other receptors or signalling pathways. For example, in NSCLC, patients become resistant to epidermal growth factor receptor (EGFR) inhibitors [27] with MET-gene amplification occurring as a by-pass mechanism in 5-20% of resistant patients and HGF over-expression occurring in a higher number of patients. Vascular endothelial growth factor (VEGF) pathway resistance is also seen [20]. This has resulted in therapeutic strategies utilizing cMET cross-reactive SMI's and bispecific MAbs (e.g. amivantamab) and ADCs.

Single agent anti-cMET MAbs (e.g., onartuzumab, emibetuzumab, SAIT-301, and ABT700), or single agent anti-HGF MAbs (e.g. ficlatuzumab, rilotumumab) which aim to inhibit cMET signalling have met with limited clinical success [20,22] for many of the reasons mentioned above. Total cMET protein levels (determined by IHC) does not correlate well with pathway activation leading to lack of efficacy in the selected patient population [54]

For example, onartuzumab (MetMAb) is a humanized antagonistic anti-cMET MAb [22]. Clinical trials in Phase III for lung cancer in combination with Erlotinib was terminated due to lack of efficacy [55]. Rilotumumab, which binds to HGF and inhibits HGF/cMET signalling, was terminated in Phase III due to increased deaths compared to chemotherapy alone [55].

Delivering a cytotoxic payload directly to tumour cells via a MAb against the cMET receptor ensures cell death via irreversible cellular damage independent of cMET-mediated proliferative cell signalling and thus overcomes many of the limitations of inhibitory MAbs or SMIs. A number of ADCs (and MAbs) are in development where the MAb component, due to its bivalent structure must be designed not to cause cMET cross-linking and induced signalling agonism [51]. This can be achieved by engineering the hinge region or using biparatopic MAbs which enable cMET clustering but not signalling. However, high affinity or high avidity MAbs can inhibit tumour penetration due to the binding site barrier effect [9]. Cross-linking receptors can induce or speed up their internalization but too rapid internalization can also inhibit tumour mass penetration [56].

WO2018/098035 describes an anti-cMET ADC comprising MMAE payload which demonstrated tumour killing efficacy in a range of human tumour xenograft models at 1-3mg/kg given intraperitoneally one to four doses. However, the development of this ADC was discontinued. Abbvie are currently developing a cMET ADC, called telisotuzumab

vedotin, ABBV399, comprising the MMAE payload, (EP3636273B1) which demonstrated tumour cure efficacy in human tumour xenograft models at six doses of 3mg/kg (cumulative dose of 18mg/kg) in tumours which express high to moderate levels of cMET target. No efficacy was seen at six doses of 1mg/kg (cumulative dose of 6mg/kg). ABBV399 was ineffective in cancer models with low-cMET expression, with a threshold of >100,000 receptors/cell being described. Greater than 50% maximal cell killing was not observed in call lines with less than 50,000 receptors/cell [51,57]. Telisotuzumab vedotin is in advanced stage (Phase II) clinical trials for NSCLC and has demonstrated good tolerability at 2.7mg/kg [58] and RECIST-qualified tumour regression responses in patients expressing high (3+) to moderate (2+) cMET levels with high-cMET expressing patients responding more favourably (LUMINOSITY Phase II Trial, EGFR-Wild type, cMET-high, ORR-52.2%, EGFR-Wild type, cMET-intermediate, ORR-24.1% [59]. This suggests stratification of patients based on cMET protein expression may lead to better patient outcomes when using an ADC and a high-DAR FDC approach with the potential to deliver more cytotoxic payload per receptor could be additionally beneficial for patients expressing lower levels of cMET. The most common any-grade adverse events were peripheral sensory neuropathy, nausea, and hypoalbuminemia (20-25%).

Other cMET ADCs are in development at earlier stages such as TR1801 (PBD payload) which is in Phase I [35], SHRA1403 (auristatin payload, [60]), cIRCR201-dPBD (PBD payload, [61]) and BYON3521 (duocarmycin payload, [62]). Bispecific cMET ADCs include AZD9592 [63] specifically to address EGFR co-expression and resistance to EGFR inhibitors in lung cancer. cMET ADCs with ultra-potent (IC_{50} in the pM range) DNA damaging payloads pose a toxicity concern as Abbvie discontinued development (EP3636273B1) as did Immunogen (HucMET27-DGN549). Generally, ultra-potent alkylating, DNA damaging payloads and ADCs against other targets using highly potent payloads such as PBDs have been discontinued due to poor tolerability and an almost 50% failure rate [15].

ADCs are complex molecules to discover and develop. There are many parameters that need to be optimized, sometimes empirically, but increasingly, it is well established that there are some key design features [5,6]. The physical and chemical stability (e.g. aggregation, pI, hydrophobicity) of an ADC can potentially impact its efficacy, toxicity and immunogenicity and many other potentially dose-limiting toxicities involved Fc-receptor binding and prolonged exposure to normal tissues [15,64] and general methods for designing and making ADCs are described [5,6,65].

Idiopathic pulmonary fibrosis (IPF) is a progressive lung fibrosing disease which is poorly understood. It is characterized by progressive lung scarring leading to respiratory failure

and death, with a median survival from diagnosis of ~3 years [66]. Many therapies have been tested for this harmful condition, yet none have demonstrated effectiveness in modifying respiratory-specific or all-cause mortality in IPF [67]. The aberrant proliferative events in IPF resemble that of malignant transformation in cancer [66] which could encourage the use of cancer drugs for IPF. The key histological feature of IPF is shown in the "fibroblast foci", aggregates of actively proliferating fibroblasts and myofibroblasts-cells which can also harbour MET in its activated form. Therefore, RTK inhibitors such as those against cMET could be efficacious in IPF [66].

There are currently two FDA–approved drugs for the treatment of IPF: pirfenidone (Esbriet®) and nintedanib (Ofev®). Pirfenidone is a pyridone derivative which exhibits anti-inflammatory and anti-fibrotic effects (via downregulation of transforming growth factor-β (TGF-β), a central signalling pathway in fibrosis). Nintedanib is a broad-spectrum-tyrosine kinase inhibitor, originally used as anti-vascular cancer chemotherapy. Nintedanib's anti-fibrotic activity via inhibition of key growth factor signalling pathways involved in pulmonary fibrosis (e.g., platelet-derived growth factor (PDGF), vascular endothelial growth factor (VEGF), and fibroblast growth factor (FGF). Nintedanib also competitively inhibits both non-receptor tyrosine kinases (nRTKs) including Lck, Lyn, and Src. Therefore, nintedanib action resembles the broad spectrum tyrosine kinase inhibitors used in anti-cMET cancer therapy. Pirfenidone and nintedanib have demonstrated efficacy in clinical trials, slowing the decline in forced vital capacity typical of IPF progression. Despite these two agents, therapeutic options for patients living with this condition remain very limited. More recently, TAS-115, a highly specific, SMI of VEGF receptor 2 (VEGFR2) and cMET originally discovered as an antitumor therapeutic [68] has shown therapeutic promise with good tolerability. HGF signals through cMET to upregulate expression of proangiogenic VEGF. Blocking both pathways by inhibiting RTK phosphorylation with TAS-115 was shown to effectively decrease tumour vascularization and size with minimal toxicity and off-target effects. Applied in the IPF setting, TAS-115 could modulate inflammation associated with fibrosis as demonstrated in preclinical models, better than nintedanib [69].

Therefore, as in cancer, cMET-induced invasive growth is emerging as a target for IPF, due to the proliferative nature of this disease in the lung. Signalling inhibitors aim to reduce the proliferation of damaging fibroblasts. This suggests that cMET receptor could be a candidate for the targeted delivery of chemical modulator-drugs to dampen down inflammation or proliferation. This would increase the local concentration of such therapeutic drugs and reduce the off-target systemic adverse effects of broadly-acting SMI drugs.

In some embodiments, the antibody or antigen-binding fragment thereof is capable of blocking cMET signalling.

In some embodiments, the antibody or antigen-binding fragment thereof binds cMET with high affinity, or with higher affinity than an alternative anti-cMET antibody. Affinity can be expressed by measuring the KD (dissociation constant, or equilibrium dissociation constant, expressed in M) or KA (association constant, or equilibrium association constant, expressed in M^{-1}) of a particular antibody or antigen-binding fragment when binding cMET. The KD and KA may be calculated by measuring the association rate constant (ka, expressed in $M^{-1}s^{-1}$) and dissociation rate constant (kd, expressed in s^{-1}). KA is calculated by ka/kd. KD is calculated by kd/ka.

Therefore, by "higher affinity" we mean that the antibody or antigen binding fragment thereof has a higher KA and/or a lower KD than an alternative anti-cMET antibody or antigen binding fragment. In some preferred embodiments, the antibody or antigen binding fragment has a lower KD (i.e. a higher binding affinity) than an alternative anti-cMET antibody or antigen binding fragment. In some embodiments, the antibody or antigen binding fragment thereof has a higher ka and/or a lower kd than an alternative anti-cMET antibody or antigen binding fragment.

In some embodiments, the antibody or antigen-binding fragment thereof binds cMET with an affinity KD of less than 10nM. In some embodiments, the antibody or antigen-binding fragment thereof binds cMET with an affinity KD of less than 5nM. In some embodiments, the antibody or antigen-binding fragment thereof binds cMET with an affinity KD of less than 4nM. In some embodiments, the antibody or antigen-binding fragment thereof binds cMET with an affinity KD of less than 3nM. In some embodiments, the antibody or antigen-binding fragment thereof binds cMET with an affinity KD of less than 2nM.

In some embodiments, the antibody or antigen-binding fragment thereof binds cMET with an affinity KD of less than 1nM.

In some embodiments, the antibody or antigen-binding fragment thereof of the first aspect comprises a heavy chain variable region (VH) comprising the Complementarity Determining Region (CDRs) CDR-H1, CDR-H2, and CDR-H3 of SEQ ID NO. 1, or a variant thereof having at least 80% sequence identity to SEQ ID NO. 1, for example a variant having at least 85%, 90%, 91%, 92%, 93%, 94%, 95%, 96%, 97%, 98%, or 99% identity. In some embodiments, the VH has at least 90% identity with SEQ ID NO. 1 (i.e. up to 10% variance). In some preferred embodiments, the VH has at least 93% identity with SEQ ID NO. 1 (i.e. up to 7% variance).

The CDR sequences described herein are defined according to the Kabat system.

In some embodiments, the antibody or antigen-binding fragment thereof of the first aspect comprises a light chain variable region (VL) comprising the CDRs CDR-L1, CDR-L2, and CDR-L3 of SEQ ID NOs. 196 or 2, or a variant thereof having at least 80% sequence identity with SEQ ID NOs. 196 or 2, for example a variant having at least 85%, 90%, 91%, 92%, 93%, 94%, 95%, 96%, 97%, 98%, or 99% identity. In some embodiments, the VL has at least 90% identity with SEQ ID NOs. 196 or 2 (i.e. up to 10% variance). In some preferred embodiments, the VL has at least 91% identity with SEQ ID NOs. 196 or 2 (i.e. up to 9% variance).

In some embodiments, the antibody or antigen-binding fragment thereof of the first aspect comprises a heavy chain variable region (VH) comprising the Complementarity Determining Region (CDRs) CDR-H1, CDR-H2, and CDR-H3 of SEQ ID NO. 21, or a variant thereof having at least 90% sequence identity to SEQ ID NO. 21, for example a variant having at least 91%, 92%, 93%, 94%, 95%, 96%, 97%, 98%, or 99% identity. In some embodiments, the VH has at least 90% identity with SEQ ID NO. 21 (i.e. up to 10% variance). In some preferred embodiments, the VH has at least 91% identity with SEQ ID NO. 21 (i.e. up to 9% variance).

In some embodiments, the antibody or antigen-binding fragment thereof of the first aspect comprises a light chain variable region (VL) comprising the CDRs CDR-L1, CDR-L2, and CDR-L3 of SEQ ID NO. 22, or a variant thereof having at least 90% sequence identity with SEQ ID NO. 22, for example a variant having at least 91%, 92%, 93%, 94%, 95%, 96%, 97%, 98%, or 99% identity. In some embodiments, the VH has at least 90% identity with SEQ ID NO. 22 (i.e. up to 10% variance). In some preferred embodiments, the VH has at least 91% identity with SEQ ID NO. 22 (i.e. up to 9% variance).

In some embodiments, the antibody or antigen-binding fragment thereof of the first aspect comprises any combination of 6 CDR sequences set out in Table A and/or Table B. For example, the antibody or antigen-binding fragment thereof of the first aspect comprises the 6 CDR sequences of any clone listed in Table A and/or Table B.

In some embodiments, the antibody or antigen-binding fragment thereof of the first aspect comprises any pair of VH and VL sequences set out in Table A and/or Table B. For example, the antibody or antigen-binding fragment thereof of the first aspect comprises the VH and VL sequences of any clone listed in Table A and/or Table B.

Table A

Clone	VH SEQ ID	VH CDR1 SEQ ID	VH CDR2 SEQ ID	VH CDR3 SEQ ID	VL SEQ ID	VL CDR1 SEQ ID	VL CDR2 SEQ ID	VL CDR3 SEQ ID
3A2	3	23	115	30	4	36	40	45
20F6	3	23	115	30	6	37	41	45
49G5	5	23	115	31	6	37	41	45
53D11	3	23	115	30	8	37	41	46
59D5	3	23	115	30	78	37	41	125
49A6	71	23	115	119	6	37	41	45
55G9	72	23	115	120	6	37	41	45
55A3	73	23	115	121	6	37	41	45
54E11	3	23	115	30	79	37	41	126
59D4	3	23	115	30	80	37	41	127
59A10	3	23	115	30	81	37	41	128
65C2	3	23	115	30	82	37	41	129
53G1	3	23	115	30	83	37	41	130
65A3	3	23	115	30	84	37	41	131
65G6	3	23	115	30	85	37	41	132
53G9	3	23	115	30	86	37	41	133
58H11	3	23	115	30	87	37	41	134
59E5	3	23	115	30	88	37	41	135
59H2	3	23	115	30	89	37	41	136
59A6	3	23	115	30	90	37	41	137
59A2	3	23	115	30	91	37	41	138
59D10	3	23	115	30	92	37	41	139
58A9	3	23	115	30	93	37	41	140
74C3	74	23	115	30	94	37	41	141
59H6	3	23	115	30	95	37	41	142
64B2	75	23	115	30	96	37	41	143
52G1	3	23	115	30	97	37	41	144
58A2	3	23	115	30	98	37	41	145
52D5	3	23	115	30	99	37	41	146
71D4	76	27	115	30	100	37	41	147
75G7	3	23	115	30	101	37	41	148
71C2	3	23	115	30	102	37	41	149
71F11	3	23	115	30	103	37	41	150
77F3	7	23	115	31	8	37	41	46
126A8B	77	23	116	32	8	37	41	46
129D5BTY	1	23	28	32	196	37	197	198
129D5B	1	23	28	32	2	37	41	46
139B2	9	23	115	31	10	37	41	46

139D2	11	23	115	31	12	37	41	46
139D7	13	23	115	31	12	37	41	46

Table B

Clone	VH SEQ ID	VH CDR1 SEQ ID	VH CDR2 SEQ ID	VH CDR3 SEQ ID	VL SEQ ID	VL CDR1 SEQ ID	VL CDR2 SEQ ID	VL CDR3 SEQ ID
26B5	14	23	29	33	15	38	42	47
83B11D	16	23	29	33	17	38	43	48
94C2	18	23	29	34	17	38	43	48
94C3	104	23	29	122	17	38	43	48
94E6	105	23	29	123	17	38	43	48
112F2	106	113	29	34	17	38	43	48
112G4	107	113	117	122	17	38	43	48
113A3	106	113	29	34	110	38	43	151
113G8	107	113	117	122	111	38	43	152
115C7	108	114	29	34	112	38	43	153
116A5	104	23	29	122	20	39	43	47
121H3B	109	23	118	124	20	39	43	47
115D1D	19	23	29	35	20	39	43	47
131D5S	21	27	29	35	22	39	44	47

In some embodiments of the first aspect of the invention, the VH comprises the CDRs of SEQ ID NO. 1 and the VL comprises the CDRs of SEQ ID NO. 2.

In some embodiments of the first aspect of the invention, the VH comprises the CDRs of SEQ ID NO. 1 and the VL comprises the CDRs of SEQ ID NO. 196.

In some embodiments of the first aspect of the invention, the VH comprises the CDRs of SEQ ID NO. 3 and the VL comprises the CDRs of SEQ ID NO. 4.

In some embodiments of the first aspect of the invention, the VH comprises the CDRs of SEQ ID NO. 3 and the VL comprises the CDRs of SEQ ID NO. 6.

In some embodiments of the first aspect of the invention, the VH comprises the CDRs of SEQ ID NO. 3 and the VL comprises the CDRs of SEQ ID NO. 8.

In some embodiments of the first aspect of the invention, the VH comprises the CDRs of SEQ ID NO. 5 and the VL comprises the CDRs of SEQ ID NO. 6.

In some embodiments of the first aspect of the invention, the VH comprises the CDRs of SEQ ID NO. 7 and the VL comprises the CDRs of SEQ ID NO. 8.

In some embodiments of the first aspect of the invention, the VH comprises the CDRs of SEQ ID NO. 9 and the VL comprises the CDRs of SEQ ID NO. 10.

In some embodiments of the first aspect of the invention, the VH comprises the CDRs of SEQ ID NO. 11 and the VL comprises the CDRs of SEQ ID NO. 12.

In some embodiments of the first aspect of the invention, the VH comprises the CDRs of SEQ ID NO. 13 and the VL comprises the CDRs of SEQ ID NO. 12.

In some embodiments of the first aspect of the invention, the VH comprises the CDRs of SEQ ID NO. 14 and the VL comprises the CDRs of SEQ ID NO. 15.

In some embodiments of the first aspect of the invention, the VH comprises the CDRs of SEQ ID NO. 16 and the VL comprises the CDRs of SEQ ID NO. 17.

In some embodiments of the first aspect of the invention, the VH comprises the CDRs of SEQ ID NO. 18 and the VL comprises the CDRs of SEQ ID NO. 17.

In some embodiments of the first aspect of the invention, the VH comprises the CDRs of SEQ ID NO. 19 and the VL comprises the CDRs of SEQ ID NO. 20.

In some embodiments of the first aspect of the invention, the VH comprises the CDRs of SEQ ID NO. 21 and the VL comprises the CDRs of SEQ ID NO. 22.

In some embodiments of the first aspect of the invention, the VH comprises SEQ ID NO. 3 and the VL comprises SEQ ID NO. 8.

In some embodiments of the first aspect of the invention, the VH comprises SEQ ID NO. 5 and the VL comprises SEQ ID NO. 6.

In some embodiments of the first aspect of the invention, the VH comprises SEQ ID NO. 7 and the VL comprises SEQ ID NO. 8.

In some embodiments of the first aspect of the invention, the VH comprises SEQ ID NO. 9 and the VL comprises SEQ ID NO. 10.

In some embodiments of the first aspect of the invention, the VH comprises SEQ ID NO. 11 and the VL comprises SEQ ID NO. 12.

In some embodiments of the first aspect of the invention, the VH comprises SEQ ID NO. 13 and the VL comprises SEQ ID NO. 12.

In some embodiments of the first aspect of the invention, the VH comprises SEQ ID NO. 14 and the VL comprises SEQ ID NO. 15.

In some embodiments of the first aspect of the invention, the VH comprises SEQ ID NO. 16 and the VL comprises SEQ ID NO. 17.

In some embodiments of the first aspect of the invention, the VH comprises SEQ ID NO. 18 and the VL comprises SEQ ID NO. 17.

In some embodiments of the first aspect of the invention, the VH comprises SEQ ID NO. 19 and the VL comprises SEQ ID NO. 20.

In some embodiments of the first aspect of the invention, the VH comprises SEQ ID NO. 21 and the VL comprises SEQ ID NO. 22.

In some embodiments, the antibody or antigen-binding fragment of any of the preceding claims, wherein the VH comprises the following CDRs:

a) CDR-H1: **[SEQ ID NO. 23]** or an amino acid sequence having at least 80% identity therewith, for example at least 85%, 90%, 91%, 92%, 93%, 94%, 95%, 96%, 97%, 98%, or 99% identity, preferably with at least 80% identity; and/or
b) CDR-H2: **[SEQ ID NO. 28]** or an amino acid sequence having at least 80% identity therewith, for example at least 85%, 90%, 91%, 92%, 93%, 94%, 95%, 96%, 97%, 98%, or 99% identity, preferably with at least 88% identity; and/or
c) CDR-H3: **[SEQ ID NO. 32]** or an amino acid sequence having at least 65% identity therewith, for example at least 70%, 75%, 80%, 85%, 90%, 91%, 92%, 93%, 94%, 95%, 96%, 97%, 98%, or 99% identity, preferably with at least 67% identity.

In some embodiments, the antibody or antigen-binding fragment of any of the preceding claims, wherein the VH comprises the following CDRs:

a) CDR-H1: **[SEQ ID NO. 27]** or an amino acid sequence having at least 60% identity therewith, for example at least 60%, 65%, 70%, 75%, 80%, 85%, 90%, 91%, 92%, 93%, 94%, 95%, 96%, 97%, 98%, or 99% identity, preferably with at least 60% identity; and/or
b) CDR-H2: **[SEQ ID NO. 29]** or an amino acid sequence having at least 80% identity therewith, for example at least 85%, 90%, 91%, 92%, 93%, 94%, 95%, 96%, 97%, 98%, or 99% identity, preferably with at least 82% identity; and/or
c) CDR-H3: **[SEQ ID NO. 35]** or an amino acid sequence having at least 60% identity therewith, for example at least 65%, 70%, 75%, 80%, 85%, 90%, 91%, 92%, 93%, 94%, 95%, 96%, 97%, 98%, or 99% identity, preferably with at least 69% identity.

In some preferred embodiments, the VH comprises the CDRs of SEQ ID NOs 23, 28, and 32. In some preferred embodiments, the VH comprises the CDRs of SEQ ID NOs 27, 29, and 35.

In some other embodiments, the VH comprises the CDRs of any of the following combinations:

(i) SEQ ID NOs 23, 115, and 30 (clones 3A2, 20F6, and 53D11);
(ii) SEQ ID NOs 23, 115, and 31 (clones 49G5, 139B2, 139D2, 139D7 and 77F3);
(iii) SEQ ID NOs 23, 29, and 33 (clone 26B5);
(iv) SEQ ID NOs 23, 29, and 33 (clone 83B11D);
(v) SEQ ID NOs 23, 29, and 34 (clone 94C2);
(vi) SEQ ID NOs 23, 29, and 35 (clone 115D1D);
(vii) SEQ ID NOs 27, 29, and 35 (clone 131D5s);
(viii) SEQ ID NOs 23, 28, and 32 (clone 129D5B/129D5BTY).

In some embodiments, the antibody or antigen-binding fragment comprises a VH having the amino acid sequence of SEQ ID NO. 1, or a variant having at least 80% sequence identity therewith, for example at least 85%, 90%, 91%, 92%, 93%, 94%, 95%, 96%, 97%, 98%, or 99% identity. In some preferred embodiments, the variant has around 93% identity with SEQ ID NO. 1. In some preferred embodiments, the antibody or antigen-binding fragment comprises a VH having the amino acid sequence of SEQ ID NO. 1.

In some embodiments, the antibody or antigen-binding fragment comprises a VH having the amino acid sequence of SEQ ID NO. 21, or a variant having at least 90% sequence identity therewith, for example at least 91%, 92%, 93%, 94%, 95%, 96%, 97%, 98%, or 99% identity. In some preferred embodiments, the variant has around 91% identity with SEQ ID NO. 21. In some preferred embodiments, the antibody or antigen-binding fragment comprises a VH having the amino acid sequence of SEQ ID NO. 21.

In some preferred embodiments, the antibody or antigen-binding fragment comprises a VH having the amino acid sequence of SEQ ID NOs 3, 5, 7, 9, 11, 13, 14, 16, 18, 19, or 21.

In some embodiments, the VL comprises the following CDRs:

a) CDR-L1: **[SEQ ID NO. 37]** or an amino acid sequence having at least 80% identity therewith, for example at least 85%, 90%, 91%, 92%, 93%, 94%, 95%, 96%, 97%, 98%, or 99% identity, preferably having at least 85% identity; and/or
b) CDR-L2: **[SEQ ID NOs. 197 or 41]** or an amino acid sequence having at least 70% identity therewith, for example at least 70%, 75%, 80%, 85%, 90%, 91%, 92%, 93%, 94%, 95%, 96%, 97%, 98%, or 99% identity, preferably having at least 71% identity; and/or
c) CDR-L3: **[SEQ ID NOs. 198 or 46]** or an amino acid sequence having at least 55% identity therewith, for example at least 60%, 65%, 70%, 75%, 80%, 85%, 90%, 91%, 92%, 93%, 94%, 95%, 96%, 97%, 98%, or 99% identity, preferably having at least 55% identity.

In some embodiments, the VL comprises the following CDRs:

a) CDR-L1: **[SEQ ID NO. 37]** or an amino acid sequence having at least 80% identity therewith, for example at least 85%, 90%, 91%, 92%, 93%, 94%, 95%, 96%, 97%, 98%, or 99% identity, preferably having at least 85% identity; and/or
b) CDR-L2: **[SEQ ID NO. 197]** or an amino acid sequence having at least 70% identity therewith, for example at least 70%, 75%, 80%, 85%, 90%, 91%, 92%, 93%, 94%, 95%, 96%, 97%, 98%, or 99% identity, preferably having at least 71% identity; and/or
c) CDR-L3: **[SEQ ID NO. 198]** or an amino acid sequence having at least 55% identity therewith, for example at least 60%, 65%, 70%, 75%, 80%, 85%, 90%, 91%, 92%, 93%, 94%, 95%, 96%, 97%, 98%, or 99% identity, preferably having at least 55% identity.

In some embodiments, the VL comprises the following CDRs:

a) CDR-L1: **[SEQ ID NO. 39]** or an amino acid sequence having at least 80% identity therewith, for example at least 85%, 90%, 91%, 92%, 93%, 94%, 95%, 96%, 97%, 98%, or 99% identity, preferably having at least 92% identity; and/or
b) CDR-L2: **[SEQ ID NO. 44]** or an amino acid sequence having at least 55% identity therewith, for example at least 60%, 65%, 70%, 75%, 80%, 85%, 90%, 91%, 92%, 93%, 94%, 95%, 96%, 97%, 98%, or 99% identity, preferably having at least 57% identity; and/or
c) CDR-L3: **[SEQ ID NO. 47]** or an amino acid sequence having at least 55% identity therewith, for example at least 60%, 65%, 70%, 75%, 80%, 85%, 90%, 91%, 92%, 93%, 94%, 95%, 96%, 97%, 98%, or 99% identity, preferably having at least 55% identity.

In some embodiments, the VL comprises the CDRs of SEQ ID NOs 37, 41, and 46. In some embodiments, the VL comprises the CDRs of SEQ ID NOs 39, 44, and 47.

In some other embodiments, the VL comprises the CDRs of any of the following combinations:

(i) SEQ ID NOs 36, 40, and 45 (clone 3A2);
(ii) SEQ ID NOs 37, 41, and 45 (clones 20F6 and 49G5);
(iii) SEQ ID NOs 37, 41, and 46 (clones 129D5B, 53D11, 139B2, 139D2, 139D7 and 77F3);
(iv) SEQ ID NOs 37, 197, and 198 (clone 129D5BTY);
(v) SEQ ID NOs 38, 42, and 47 (clone 26B5);
(vi) SEQ ID NOs 38, 43, and 48 (clones 83B11D and 94C2);
(vii) SEQ ID NOs 39, 43, and 47 (clone 115D1D); and
(viii) SEQ ID NOs 39, 44, and 47 (clone 131D5s).

In some embodiments, the antibody or antigen-binding fragment comprises a VL having the amino acid sequence of SEQ ID NO. 2, or a variant having at least 90% sequence identity therewith, for example at least 91%, 92%, 93%, 94%, 95%, 96%, 97%, 98%, or 99% identity. In some preferred embodiments, the variant has around 91% identity with SEQ ID NO. 2. In some preferred embodiments, the antibody or antigen-binding fragment comprises a VL having the amino acid sequence of SEQ ID NO. 2.

In some embodiments, the antibody or antigen-binding fragment comprises a VL having the amino acid sequence of SEQ ID NO. 196, or a variant having at least 90% sequence identity therewith, for example at least 91%, 92%, 93%, 94%, 95%, 96%, 97%, 98%, or 99% identity. In some preferred embodiments, the variant has around 91% identity with SEQ ID NO. 196. In some preferred embodiments, the antibody or antigen-binding fragment comprises a VL having the amino acid sequence of SEQ ID NO. 196.

In some embodiments, the antibody or antigen-binding fragment comprises a VL having the amino acid sequence of SEQ ID NO. 22, or a variant having at least 90% sequence identity therewith, for example at least 91%, 92%, 93%, 94%, 95%, 96%, 97%, 98%, or 99% identity. In some preferred embodiments, the variant has around 91% identity with SEQ ID NO. 22. In some preferred embodiments, the antibody or antigen-binding fragment comprises a VL having the amino acid sequence of SEQ ID NO. 22.

In some preferred embodiments, the antibody or antigen-binding fragment comprises a VL having the amino acid sequence of SEQ ID NOs 196, 2, 4, 6, 8, 10, 12, 15, 17, 20, or 22.

In some embodiments, the antibody or antigen-binding fragment comprising the following CDRs:

a) CDR-H1: **[SEQ ID NO. 23]** or an amino acid sequence having at least 80% identity therewith, for example at least 85%, 90%, 91%, 92%, 93%, 94%, 95%, 96%, 97%, 98%, or 99% identity, preferably with at least 80% identity; and/or
b) CDR-H2: **[SEQ ID NO. 28]** or an amino acid sequence having at least 80% identity therewith, for example at least 85%, 90%, 91%, 92%, 93%, 94%, 95%, 96%, 97%, 98%, or 99% identity, preferably with at least 88% identity; and/or
c) CDR-H3: **[SEQ ID NO. 32]** or an amino acid sequence having at least 60% identity therewith, for example at least 65%, 70%, 75%, 80%, 85%, 90%, 91%, 92%, 93%, 94%, 95%, 96%, 97%, 98%, or 99% identity, preferably with at least 67% identity; and/or
d) CDR-L1: **[SEQ ID NO. 37]** or an amino acid sequence having at least 80% identity therewith, for example at least 85%, 90%, 91%, 92%, 93%, 94%, 95%, 96%, 97%, 98%, or 99% identity, preferably having at least 85% identity; and/or
e) CDR-L2: **[SEQ ID NO. 41]** or an amino acid sequence having at least 70% identity therewith, for example at least 75%, 80%, 85%, 90%, 91%, 92%, 93%, 94%, 95%, 96%, 97%, 98%, or 99% identity, preferably having at least 71% identity; and/or

f) CDR-L3: **[SEQ ID NO. 46]** or an amino acid sequence having at least 55% identity therewith, for example at least 60%, 65%, 70%, 75%, 80%, 85%, 90%, 91%, 92%, 93%, 94%, 95%, 96%, 97%, 98%, or 99% identity, preferably having at least 55% identity.

In some embodiments, the antibody or antigen-binding fragment comprising the following CDRs:

a) CDR-H1: **[SEQ ID NO. 23]** or an amino acid sequence having at least 80% identity therewith, for example at least 85%, 90%, 91%, 92%, 93%, 94%, 95%, 96%, 97%, 98%, or 99% identity, preferably with at least 80% identity; and/or
b) CDR-H2: **[SEQ ID NO. 28]** or an amino acid sequence having at least 80% identity therewith, for example at least 85%, 90%, 91%, 92%, 93%, 94%, 95%, 96%, 97%, 98%, or 99% identity, preferably with at least 88% identity; and/or
c) CDR-H3: **[SEQ ID NO. 32]** or an amino acid sequence having at least 60% identity therewith, for example at least 65%, 70%, 75%, 80%, 85%, 90%, 91%, 92%, 93%, 94%, 95%, 96%, 97%, 98%, or 99% identity, preferably with at least 67% identity; and/or
d) CDR-L1: **[SEQ ID NO. 37]** or an amino acid sequence having at least 80% identity therewith, for example at least 85%, 90%, 91%, 92%, 93%, 94%, 95%, 96%, 97%, 98%, or 99% identity, preferably having at least 85% identity; and/or
e) CDR-L2: **[SEQ ID NO. 197]** or an amino acid sequence having at least 70% identity therewith, for example at least 75%, 80%, 85%, 90%, 91%, 92%, 93%, 94%, 95%, 96%, 97%, 98%, or 99% identity, preferably having at least 71% identity; and/or
f) CDR-L3: **[SEQ ID NO. 198]** or an amino acid sequence having at least 55% identity therewith, for example at least 60%, 65%, 70%, 75%, 80%, 85%, 90%, 91%, 92%, 93%, 94%, 95%, 96%, 97%, 98%, or 99% identity, preferably having at least 55% identity.

In some embodiments, the antibody or antigen-binding fragment comprising the following CDRs:

a) CDR-H1: **[SEQ ID NO. 27]** or an amino acid sequence having at least 60% identity therewith, for example at least 60%, 65%, 70%, 75%, 80%, 85%, 90%, 91%, 92%, 93%, 94%, 95%, 96%, 97%, 98%, or 99% identity, preferably with at least 60% identity; and/or
b) CDR-H2: **[SEQ ID NO. 29]** or an amino acid sequence having at least 80% identity therewith, for example at least 85%, 90%, 91%, 92%, 93%, 94%, 95%, 96%, 97%, 98%, or 99% identity, preferably with at least 82% identity; and/or

c) CDR-H3: **[SEQ ID NO. 35]** or an amino acid sequence having at least 60% identity therewith, for example at least 65%, 70%, 75%, 80%, 85%, 90%, 91%, 92%, 93%, 94%, 95%, 96%, 97%, 98%, or 99% identity, preferably with at least 69% identity; and/or

d) CDR-L1: **[SEQ ID NO. 39]** or an amino acid sequence having at least 80% identity therewith, for example at least 85%, 90%, 91%, 92%, 93%, 94%, 95%, 96%, 97%, 98%, or 99% identity, preferably having at least 92% identity; and/or

e) CDR-L2: **[SEQ ID NO. 44]** or an amino acid sequence having at least 55% identity therewith, for example at least 60%, 65%, 70%, 75%, 80%, 85%, 90%, 91%, 92%, 93%, 94%, 95%, 96%, 97%, 98%, or 99% identity, preferably having at least 57% identity; and/or

f) CDR-L3: **[SEQ ID NO. 47]** or an amino acid sequence having at least 55% identity therewith, for example at least 60%, 65%, 70%, 75%, 80%, 85%, 90%, 91%, 92%, 93%, 94%, 95%, 96%, 97%, 98%, or 99% identity, preferably having at least 55% identity.

In some embodiments, the antibody or antigen-binding fragment thereof preferably comprises the following combination of CDRs: SEQ ID NOs. 23, 28, 32, 37, 41, and 46.

In some embodiments, the antibody or antigen-binding fragment thereof preferably comprises the following combination of CDRs: SEQ ID NOs. 23, 28, 32, 37, 197, and 198.

In some embodiments, the antibody or antigen-binding fragment thereof preferably comprises the following combination of CDRs: SEQ ID NOs. 27, 29, 35, 39, 44, and 47.

In some other embodiments, the antibody or antigen-binding fragment thereof comprises one of the following combinations of CDRs:

(i) SEQ ID NOs. 23, 115, 30, 36, 40, and 45 (clone 3A2);
(ii) SEQ ID NOs. 23, 115, 30, 37, 41, and 45 (clone 20F6);
(iii) SEQ ID NOs. 23, 115, 31, 37, 41, and 45 (clone 49G5);
(iv) SEQ ID NOs. 23, 115, 30, 37, 41, and 46 (clone 53D11);
(v) SEQ ID NOs. 23, 115, 31, 37, 41, and 46 (clone 77F3);
(vi) SEQ ID NOs. 23, 29, 33, 38, 42, and 47 (clone 26B5);
(vii) SEQ ID NOs. 23, 29, 33, 38, 43, and 48 (clone 83B11D);
(viii) SEQ ID NOs. 23, 29, 34, 38, 43, and 48 (clone 94C2);
(ix) SEQ ID NOs. 23, 29, 35, 39, 43, and 47 (clone 115D1D);
(x) SEQ ID NOs. 27, 29, 35, 39, 44, and 47 (clone 131D5s);

(xi) SEQ ID NOs. 23, 28, 32, 37, 41, and 46 (clone 129D5B); and

(xii) SEQ ID NOs. 23, 28, 32, 37, 197, and 198 (clone 129D5BTY).

In any listed embodiment or any listed clone, CDR-L2 may have SEQ ID NO. 41 replaced by SEQ ID NO. 197 and/or CDR-L3 may have SEQ ID NO. 46 replaced by CDR SEQ ID NO. 198.

In some embodiments, the antibody or antigen-binding fragment thereof comprises a heavy chain variable region having the amino acid sequence of SEQ ID NO: 1 and a light chain variable region having the amino acid sequence of SEQ ID NO: 2, or an amino acid sequence having at least 80% sequence identity therewith, for example at least 85%, 90%, or 95% sequence identity. In some preferred embodiments, the antibody or antigen-binding fragment thereof comprises a heavy chain variable region having the amino acid sequence of SEQ ID NO: 1 and a light chain variable region having the amino acid sequence of SEQ ID NO: 2, or an amino acid sequence having at least 90% sequence identity therewith, preferably at least 91%, 92%, 93%, 94%, 95%, 96%, 97%, 98%, or 99% sequence identity therewith.

In some embodiments, the antibody or antigen-binding fragment thereof comprises a heavy chain variable region having the amino acid sequence of SEQ ID NO: 1 and a light chain variable region having the amino acid sequence of SEQ ID NO: 196, or an amino acid sequence having at least 80% sequence identity therewith, for example at least 85%, 90%, or 95% sequence identity. In some preferred embodiments, the antibody or antigen-binding fragment thereof comprises a heavy chain variable region having the amino acid sequence of SEQ ID NO: 1 and a light chain variable region having the amino acid sequence of SEQ ID NO: 196, or an amino acid sequence having at least 90% sequence identity therewith, preferably at least 91%, 92%, 93%, 94%, 95%, 96%, 97%, 98%, or 99% sequence identity therewith.

In some embodiments, the antibody or antigen-binding fragment thereof comprises a heavy chain variable region having the amino acid sequence of SEQ ID NO: 21 and a light chain variable region having the amino acid sequence of SEQ ID NO: 22, or an amino acid sequence having at least 80% sequence identity therewith, for example at least 85%, 90%, or 95% sequence identity. In some preferred embodiments, the antibody or antigen-binding fragment thereof comprises a heavy chain variable region having the amino acid sequence of SEQ ID NO: 21 and a light chain variable region having the amino acid sequence of SEQ ID NO: 22, or an amino acid sequence having at least 90% sequence

identity therewith, preferably at least 91%, 92%, 93%, 94%, 95%, 96%, 97%, 98%, or 99% sequence identity therewith.

In some embodiments, the antibody or antigen-binding fragment thereof is an antigen-binding fragment.

In some embodiments, the antigen-binding fragment is selected from: scFv, Fv, Fab, F(ab)2, Fab-SH, dsFv, sdAb, di-scFvs bi-scFv, Fcabs, diabodies, scFv-Fc/minibody, triabody, tetrabody, tandAb, half antibody (Unibody) and domain antibodies.

In some particularly preferred embodiments, the antigen-binding fragment is an scFv.

By "antibody" we include substantially intact antibody molecules, as well as chimeric antibodies, humanised antibodies, human antibodies (wherein at least one amino acid is mutated relative to the naturally occurring human antibodies), single chain antibodies, biparatopic antibodies, antibody heavy chains, antibody light chains, homodimers and heterodimers of antibody heavy and/or light chains, and antigen binding fragments and derivatives of the same.

By "antigen-binding fragment" we mean a functional fragment of an antibody that is capable of binding to cMET.

It is preferred if the antibody fragment excludes the Fc region of a whole antibody. In particular, it is preferred if the antibody fragment does not include the CH2 and CH3 regions of a whole antibody.

The advantages of using antibody fragments, rather than whole antibodies, are several-fold. The smaller size of the fragments may lead to improved pharmacological properties, such as better penetration of solid tissue. Moreover, antigen-binding fragments such as Fab, Fv, ScFv and dAb antibody fragments can be expressed in and secreted from *E. coli,* thus allowing the economic production of large amounts of the said fragments.

Antibody fragments are functional portions of whole immunoglobulins that possess advantageous properties over complete antibodies such as faster penetration into dense or solid tumours, reduced cross-reactivity with normal tissues and more rapid clearance from the circulation, thus reducing normal tissue exposure overall. It is well known in the art that antibody fragments demonstrate faster pharmacokinetics, dispersing into tissues and eliminating more rapidly (ADME-adsorption, distribution, metabolism and excretion

properties). They are also easier to produce in more cost-effective systems such as microbial expression systems [70].

Antibody fragments can be produced by chemical or enzymatic cleavage, but, more preferably, are produced using recombinant DNA technology. The latter allows for indefinite protein expression in prokaryotic or eukaryotic cell lines and genetic modification leading to fragments with enhanced or additional properties. Antibody fragments normally possess at least one variable (V-) domain because V-domains contain the complementarity-determining regions (CDRs) or loops for antigen binding [71]. More recently, CDR-like loops have been inserted into non-variable domains (e.g. constant-heavy-3, CH3 domains) enabling these domains to bind to useful or predetermined targets [72].

For antibody fragments to be used effectively as carrier vehicles for cytotoxic drugs, they must possess biophysical properties that allow high drug loading via chemical conjugation (or strong and specific non-covalent interactions) without detrimentally affecting protein stability, antibody-antigen binding, and drug-favourable properties such as solubility, aggregation and immunogenicity. Very rarely are these features inherent to antibody fragments [73] so these additional benefits must be engineered into antibody fragments, or preferably be selected from naturally-occurring antibodies to make them practically useful [74,75]. One example of such a feature is the incorporation of additional or more optimally distributed surface lysine residues onto antibody fragments, thus increasing its capacity for drug conjugation using amine-directed chemistry. Other amino acids could be used, such as optimally distributed cysteines, tyrosines, glutamates, aspartates, arginines, asparagines, histidines and serines, but lysines are more preferable due to the well-established and successful chemical approaches for conjugation and relative inertness to conjugation without specific activating groups (chapter 10 in [76]). Non-natural amino acids such as p-Acetylphenylalanine and formyl-glycine can also be used [77]. The identification of positions for antibody fragment modification can be by direct analysis of the 3-dimensional structure of the antibody fragment (or parental whole antibody), if available, or by homology modelling using a number of software resources such as Phyre [78]. The criteria for selecting positions include: (1) the use of amino acids already favoured or conserved at that position (identified from databases such as IMGT or Kabat [79]) or through practical demonstration by making and testing antibody fragment mutants; (2) Distribution of residues away from positions that would interfere with antigen binding; and, (3) Separation of conjugating residues so that they do not sterically hinder (or predicted to hinder) each other during chemical reactions or drug release reactions or form highly hydrophobic patches leading to aggregation.

All of the antigen-binding fragments described herein are built from the same building blocks, i.e. the variable domains of the heavy and light chains, and therefore would be expected to function in a similar manner. Variable domains of antibodies (i.e. the V_H and V_L domains that form an scFv), are compact, discrete domains that are highly conserved.

Therefore, fragments other than scFvs that also comprise a V_H and V_L region would be expected to conjugate and behave in a similar way to an scFv as has been particularly exemplified in the specification. Furthermore, the fragments discussed herein are all structurally very similar to the exemplified scFv fragments, with only subtle differences in their formats, as discussed below:

Fvs, including ds-Fvs, are structurally very similar to scFvs, and have almost identical surfaces where the conjugation occurs, differing only in the linker which is not involved in the conjugation reaction.

Fab fragments comprise the V_H and V_L regions together with the first constant region, and they therefore are very structurally similar to scFvs.

Therefore, Fab (and Fab-SH) fragments are structurally similar to scFvs, such that the claimed conjugates produced using Fab or Fab-SH fragments would reasonably be expected to function in a similar manner to the exemplified scFvs.

Bi-specific scFvs (bs-scFv) and di/bi-scFvs have the scFv format discussed above, but consist of two scFvs tethered by a linker. It is widely acknowledged in the art that the structure of one of the scFv units in a bivalent or trivalent scFv multimer would be the same as the parental scFv.

As these fragments have double the identical surface area to scFvs, the lysine content and distribution would be expected to be identical to the scFv, and it would therefore be expected that a bs-scFv or di/bi-scFv to work in the same way.

Diabodies are bi-valent scFvs where the V_H-V_L domains are arranged in a head-to-tail format.

As discussed herein, it will be appreciated that the antibodies and antigen binding fragments of the invention may alternatively comprise variants of the above-defined sequences. The antibodies and antigen binding fragments thereof may have at least 60%

sequence identity with any of the sequences disclosed herein. For example, they may have at least 60%, at least 65%, at least 70%, at least 75%, at least 80%, at least 85%, at least 90%, at least 95%, or at least 99% sequence identity.

The antibodies and antigen binding fragments thereof may alternatively be a variant of a specific sequence disclosed herein, wherein said variant comprises mutations at one or more positions relative to the parent sequence. By "mutation" we include insertions, deletions and substitutions. Accordingly a variant may be a substitution, deletion or addition variant. A variant polypeptide may comprise 1, 2, 3, 4, 5, 6, 7, 8, 9, up to 10, up to 20, up to 30, up to 40, up to 50, up to 75 or more amino acid mutations, in a preferred embodiment. The mutations may be either conservative or non-conservative. For example, conservative substitution refers to the substitution of an amino acid within the same general class (e.g. an acidic amino acid, a basic amino acid, a non-polar amino acid, a polar amino acid or an aromatic amino acid) by another amino acid within the same class. Thus, the meaning of a conservative amino acid substitution and non-conservative amino acid substitution is well known in the art.

"Deletion" variants may comprise the deletion of individual amino acids, deletion of small groups of amino acids such as 2, 3, 4 or 5 amino acids, or deletion of larger amino acid regions, such as the deletion of specific amino acid domains or other features. "Substitution" variants preferably involve the replacement of one or more amino acids with the same number of amino acids and making conservative amino acid substitutions. For example, an amino acid may be substituted with an alternative amino acid having similar properties, for example, another basic amino acid, another acidic amino acid, another neutral amino acid, another charged amino acid, another hydrophilic amino acid, another hydrophobic amino acid, another polar amino acid, another aromatic amino acid or another aliphatic amino acid. Some properties of the 20 main amino acids which can be used to select suitable substituents are as follows:

Ala, A	aliphatic, hydrophobic, neutral	Met, M	hydrophobic, neutral
Cys, C	polar, hydrophobic, neutral	Asn, N	polar, hydrophilic, neutral
Asp, D	polar, hydrophilic, charged (-)	Pro, P	hydrophobic, neutral
Glu, E	polar, hydrophilic, charged (-)	Gln, Q	polar, hydrophilic, neutral
Phe, F	aromatic, hydrophobic, neutral	Arg, R	polar, hydrophilic, charged (+)
Gly, G	aliphatic, neutral	Ser, S	polar, hydrophilic, neutral
His, H	aromatic, polar, hydrophilic, charged (+)	Thr, T	polar, hydrophilic, neutral
Ile, I	aliphatic, hydrophobic, neutral	Val, V	aliphatic, hydrophobic, neutral

Lys, K	polar, hydrophilic, charged (+)	Trp, W	aromatic, hydrophobic, neutral
Leu, L	aliphatic, hydrophobic, neutral	Tyr, Y	aromatic, polar, hydrophobic

Amino acids herein may be referred to by full name, three letter code or single letter code. Preferred "variants" include those in which instead of the naturally occurring amino acid the amino acid which appears in the sequence is a structural analog thereof. Amino acids used in the sequences may also be derivatised or modified, *e.g.* labelled, providing the function of the antibody is not significantly adversely affected.

Derivatives and variants as described above may be prepared during synthesis of the antibody or by post-production modification or by peptide synthesis or by native chemical ligation of peptides, or when the antibody is in recombinant form using the known techniques of site-directed mutagenesis, random mutagenesis, or enzymatic cleavage and/or ligation of nucleic acids.

Suitable variants may be at least 70% homologous to a sequence disclosed herein, preferably at least 80% or 90% and more preferably at least 95%, 97% or 99% homologous thereto.

Preferably variants have an amino acid sequence which has more than 60%, or more than 70%, *e.g*. 75 or 80%, preferably more than 85%, e.g. more than 90 or 95% amino acid identity to a sequence as shown in the sequences disclosed herein (*e.g*. the VH or VL region sequences, or CDR sequences therein). This level of amino acid identity may be seen across the full length of the relevant SEQ ID NO sequence or over a part of the sequence, such as across 20, 30, 50, 75, 100, 150, 200 or more amino acids, depending on the size of the full-length polypeptide.

For example, variants of the above CDR sequences may comprise one, two three, four, five, six, seven, eight or more amino acid mutations relative to the reference sequence (such as a deletion, substitution and/or insertion of an amino acid).

The percent sequence identity between two polypeptides may be determined using suitable computer programs, for example the GAP program of the University of Wisconsin Genetic Computing Group and it will be appreciated that percent identity is calculated in relation to polypeptides whose sequences have been aligned optimally. Methods for determining sequence identity are known to those skilled in the art.

The alignment may alternatively be carried out using the Clustal W program (as described in [80], which is incorporated herein by reference). The parameters used may be as follows:

Fast pairwise alignment parameters: K-tuple(word) size; 1, window size; 5, gap penalty; 3, number of top diagonals; 5. Scoring method: x percent.

Multiple alignment parameters: gap open penalty; 10, gap extension penalty; 0.05. Scoring matrix: BLOSUM.

Alternatively, the BESTFIT program may be used to determine local sequence alignments. Also included within the scope of the invention are modified versions of antibodies and antigen-binding fragments thereof, e.g. modified by the covalent attachment of polyethylene glycol or other suitable polymers (see below).

Methods of generating antibodies and antibody fragments are well known in the art. For example, antibodies may be generated via any one of several methods which employ induction of *in vivo* production of antibody molecules, screening of immunoglobulin libraries [75,81] or generation of monoclonal antibody molecules by cell lines in culture. These include, but are not limited to, the hybridoma technique, the human B-cell hybridoma technique, and the Epstein-Barr virus (EBV)-hybridoma technique [82-85].

Suitable monoclonal antibodies to selected antigens may be prepared by known techniques, for example those disclosed in [86].

Likewise, antibody fragments can be obtained using methods well known in the art (see, for example [87]. For example, antibody fragments according to the present invention can be prepared by proteolytic hydrolysis of the antibody or by expression in *E. coli* or mammalian cells (e.g. Chinese hamster ovary cell culture or other protein expression systems) of DNA encoding the fragment. Alternatively, antibody fragments can be obtained by pepsin or papain digestion of whole antibodies by conventional methods.

It will be appreciated by persons skilled in the art that for human therapy or diagnostics, human or humanised antibodies are preferably used. Humanised forms of non-human (e.g. murine) antibodies are genetically engineered chimeric antibodies or antibody fragments having preferably minimal-portions derived from non-human antibodies. Humanised antibodies include antibodies in which complementary determining regions of a human antibody (recipient antibody) are replaced by residues from a complementary determining region of a non-human species (donor antibody) such as mouse, rat of rabbit having the desired functionality. In some instances, Fv framework residues of the human

antibody are replaced by corresponding non-human residues. Humanised antibodies may also comprise residues which are found neither in the recipient antibody nor in the imported complementarity determining region or framework sequences. In general, the humanised antibody will comprise substantially all of at least one, and typically two, variable domains, in which all or substantially all of the complementarity determining regions correspond to those of a non-human antibody and all, or substantially all, of the framework regions correspond to those of a relevant human consensus sequence. Humanised antibodies optimally also include at least a portion of an antibody constant region, such as an Fc region, typically derived from a human antibody (see, for example, [88-90].

Methods for humanising non-human antibodies are well known in the art. Generally, the humanised antibody has one or more amino acid residues introduced into it from a source which is non-human. These non-human amino acid residues, often referred to as imported residues, are typically taken from an imported variable domain. Humanisation can be essentially performed as described (see, for example, [88,89,91]; US 4,816,567) by substituting human complementarity determining regions with corresponding rodent complementarity determining regions. Accordingly, such humanised antibodies are chimaeric antibodies, wherein substantially less than an intact human variable domain has been substituted by the corresponding sequence from a non-human species. In practice, humanised antibodies may be typically human antibodies in which some complementarity determining region residues and possibly some framework residues are substituted by residues from analogous sites in rodent antibodies.

Human antibodies can also be identified using various techniques known in the art, including phage display libraries (see, for example, [92-95]).

Once suitable antibodies are obtained, they may be tested for binding activity, for example by ELISA.

In some embodiments, the antibody or antigen-binding fragment thereof disclosed herein comprises a heavy chain constant region, or part thereof.

In some embodiments, the heavy chain constant region is of an immunoglobulin subtype selected from the group consisting of IgG1, IgG2, IgG3 and IgG4.

In some embodiments, the heavy chain constant region is of an immunoglobulin subtype IgG1.

In some embodiments, the antibody or antigen-binding fragment thereof disclosed herein comprises a light chain constant region, or part thereof.

In some embodiments, the light chain constant region is of a kappa or lambda light chain. In some embodiments, the constant region is a human or humanised constant region.

In some embodiments, the antibodies, antigen-binding fragments and conjugates disclosed herein have an IC50 of 100nM or lower.

The half maximal inhibitory concentration (IC50) is a measure of the effectiveness of a substance in inhibiting a specific biological or biochemical function. This measure indicates how much of a particular drug or other substance (inhibitor) is needed to inhibit a given biological process (or component thereof) by half. Determination of the IC50 for a given compound is a routine matter, and typically is determined by constructing a dose-response curve and examining the effect of different concentrations of antagonist on reversing agonist activity. The IC50 value is calculated by determining the concentration needed to inhibit half of the maximum biological response of the agonist.

In some embodiments, the antibodies, antigen-binding fragments and conjugates disclosed herein have a serum half-life of at least 2 hours, optionally the serum half-life of at least 2 hours is measured in rodents or in humans. In some embodiments, the serum half-life is preferably 4 hours, alternatively 8, 16, 32, 64 or 128 hours. In some preferred embodiments, the serum half-life is measured in humans.

In some embodiments, the conjugates disclosed herein have a longer serum-half life than the unconjugated antibodies or antigen-binding fragments. In some embodiments, serum half-life is also referred to as bioavailability.

Serum half-life is the calculated duration of time for a serum level of a compound to be reduced to half its initial value. Bioavailability can be defined as the area-under-curve (AUC) in a plasma concentration vs time pharmacokinetic plot and is related to serum half-life. Determination of the serum half-life or bioavailability for a given compound is a routine matter, and typically is determined by measuring the amounts of drug in the serum over time following compound administration to an organism. Serum half-life or bioavailability is important clinically, as it will determine the dosage regime required in order to consistently achieve a serum level of drug within a clinically effective range.

In some embodiments, the payloads, when coupled to the antibody or antigen-binding fragment, are separated by a distance of at least two amino acids (3.5 to 7.5 angstroms). In some embodiments, the payloads, when coupled to the antibody or antigen-binding fragment, are separated by a distance of two amino acids (3.5 to 7.5 angstroms), three amino acids (9 to 12 angstroms), four amino acids (10 to 15 angstroms), five amino acids (15 to 20 angstroms) or six amino acids (20 to 25 angstroms).

In some embodiments, the antibody or antigen-binding fragment thereof disclosed herein further comprises a payload. By "payload" we mean a drug molecule that is conjugated to the antibody or antigen-binding fragment thereof. The drug molecule may be a cytotoxic or cytostatic agent. The drug molecule is in some preferred embodiments a small molecule payload. In some embodiments, the payload is conjugated to the antibody or antigen-binding fragment via a linker. In some embodiments, the antibody/antigen-binding fragment conjugated to the payload is referred to as an antibody-drug conjugate (ADC).

Despite the many advances made in the ADC field over recent years, it is clear that significant problems associated with the biophysical or biological properties of ADCs that result in ineffective or poorly tolerated compounds are often encountered. For example, an anti-CD33 ADC (gemtuzumab ozogamicin) was approved to treat acute myeloid leukaemia in 2000 but was withdrawn in 2010 due to liver toxicity, patients' deaths and poor efficacy compared to existing therapies [5]. In another example, trastuzumab emtansine, already approved for HER2-expressing breast cancer in 2013, was not approved for HER2-expressing gastric cancer in 2015 due to lack of efficacy [18]. In another example, traztuzumab deruxtecan demonstrated high efficacy in HER2-expressing breast cancer but progression-free survival and other key outcomes are much poorer for HER2-expressing gastric cancer [96] which is known to be more heterogenous and difficult to treat [97,98]. A review carried out by the FDA concluded that the major dose-limiting toxicities of ADCs were due to payload exposure to normal tissues [99] and many examples of so-called ultra-potent (low pM IC_{50}) ADCs have failed due to a narrow therapeutic window compared to ADCs built with less potent payloads [15].

To date, all of the approved and advanced clinical stage ADCs are based upon full-length immunoglobulins coupled to a payload. The immunoglobulin format has size and avidity properties which limits its penetration into solid tumours [9,56] and ineffective penetration is a noted as a significant factor in cancer therapy [100]. Highly penetrating peptides and small molecule ligands have been developed as alternative delivery vehicles for drug-conjugates but quite often these have to be administered more frequently and due to kidney clearance, can induce toxicities related to renal excretion [9]. Recombinant

antibody fragments such as single-chain Fvs (scFvs) and Fabs have also been considered as smaller delivery vehicles for drug-conjugates [7,11] but their design and low drug:antibody ratio (DAR) has not made them viable drug candidates. Antikor Biopharma Ltd has previously described an approach using antibody fragments such as scFvs with a DAR of at least 5 coupled in such a way that leads to antibody fragment drug conjugates (FDCs) with high affinity, high potency, manageable tolerability, good pharmacokinetics and good biophysical properties that lead to FDC products that viable commercial products [WO2016/046574].

Accordingly, another aspect of the present invention provides ADCs based on antibody fragments, herein known as antibody Fragment Drug Conjugates (FDCs), against cMET using the anti-cMET antibody sequences described herein which avoids the complication of hinge manipulation or bi-valency or multi-valency leading to possible cMET agonism.

cMET FDCs enable delivery of payloads to cMET-expressing cell surface receptor, and subsequent internalization of the FDC to deliver the payload intracellularly, whilst exhibiting no agonist activity. Surprisingly, cMET FDCs internalise as well as bivalent ADCs resulting in effective payload delivery to tumours. cMET FDCs have a faster plasma half-life and lower bioavailability than comparable ADCs but surprisingly demonstrate a higher quantity of payload delivered to tumours in the early time points and furthermore demonstrate lower liver payload uptake as would be expected for a format carrying a high quantity of payload. Notably and surprisingly, cMET FDCs are able to elicit complete tumour regression after four doses of 1mg/kg (cumulative dose of 4mg/kg) whereas an ADC against the same target with the same payload was ineffective at a cumulative dose of 6mg/kg [57].

Described herein, cMET FDCs demonstrate high biophysical and thermal stability which is unexpectedly higher than other phage-display selected human scFvs conjugated to similar linker-payloads. cMET FDCs can be made with a variety of linker payloads which suggests that cMET FDCs can have utility in many types of tumours irrespective of their sensitivity to particular payload classes and diseases beyond cancer such as other proliferative conditions like Idiopathic Pulmonary Fibrosis where a payload also needs to be delivered to cMET-overexpressing tissues. As a further advantage, cMET FDCs do not possess an Fc-domain which removes any cross-reaction with Fc-receptors. Fc-gamma receptor binding is an important factor in many dose limiting ADC toxicities such as thrombocytopenia [64], and can also be a factor in damaging Fc-gamma receptor bearing immune cells (e.g. macrophages) which are needed for mounting an effective immune response to cancer or infections.

In some embodiments, the cMET FDC binds cMET with an affinity KD of less than 50nM, 40nM, 30nM, 20nM, 10nM, 5nM or less than 1nM.

In certain embodiments, the cMET FDC binds cMET with an affinity KD of less than 10nM.

In some embodiments, the payload is coupled to the antibody or antigen-binding fragment thereof with a coupling ratio (payload:antibody or antigen-binding fragment) of at least 2:1, at least 3:1, at least 4:1, at least 5:1, at least 6:1, at least 7:1, at least 8:1, at least 9:1 or at least 10:1.

In some preferred embodiments, the coupling ratio (payload:antibody or antigen-binding fragment) is at least 6:1.

In some embodiments, the payload comprises, but is not limited to, at least one of:

- A toxin (cytotoxic and/or cytostatic agent);
- An immunoregulatory/immunostimulatory agent;
- An anti-inflammatory agent;
- A protein-degradation agent (PROTAC);
- A radionucleotide/PET agent;
- A fluorescent dye.

The cytotoxic and/or cytostatic agents may be any agents known to inhibit the growth and/or replication of and/or kill cells and in particular cancer/tumour cells. Numerous agents having cytotoxic and/or cytostatic properties are known in the literature. Non-limiting examples of classes of cytotoxic and/or cytostatic agents include antimitotic agents, topoisomerase I inhibitors, topoisomerase II inhibitors, DNA alkylating agents, DNA cross-linking agents, DNA intercalating agents, DNA groove binding agents, DNA strand-cleavage agents including enediynes, kinase inhibitors, RNA/DNA anti-metabolites, RNA polymerase (transcription) inhibitors, protein synthesis inhibitors, cell-cycle modulators, apoptosis regulators, mitochondria inhibitors, nuclear export inhibitors and N-myristoyl transferase inhibitors.

The toxin may be selected from the group consisting of:

- An auristatin such as MMAE (monomethyl auristatin E) and MMAF (monomethyl auristatin F);
- Hemiasterlins;
- A maytansinoid such as maytansine, DM1, DM4 and DM21;
- A camptothecin (exatecan, DXd, Belotecan, SN-38, 7-aminomethyl-(10,11-methylenedioxy)-camptothecin, 7-aminoethyl-(10,11-methylenedioxy)-

camptothecin, 7-Aminomethyl-(10-Methyl, 11-Fluoro)-camptothecin, 7-Aminoethyl-(10-Methyl, 11-Fluoro)-camptothecin;

- A kinase inhibitor such as nintedanib;
- A transcription inhibitor (triptolide, α-amanatin);
- Immunoregulatory agent such as glucocorticoids (Dexamethasone, Budesonide);
- Immunostimulatory agents such as toll-like receptors TLR7/8 (imidazoquinoline, T785) and STING agonists such as XMT-1621, IMSA172;
- A DNA alkylating agent such as Duocarmycin, Duocarmycin-SA, seco-DUBA;
- A tubulysin;
- An anthracycline derivative such as PNU-159682, doxorubicin;
- A cryptophycin;
- An enediyne (calicheamicin, uncialamycin);
- A nicotinamide phosphoribosylytransferase (NAMPT) inhibitor such as FK-866 (daporinad) and analogues;
- A pyrrole-based kinesin spindle protein (KSP) inhibitor such as Filasenib;
- A PROTAC such as BET/BRD4 degraders (MZ1 (BRD4/VHL)), GNE-987 (BRD4/VHL);
- A protein synthesis inhibitor (HSP90 inhibitor) like geldanamycin, (a splicing inhibitor) such as Thailanstatin A;
- A Bcl-xL inhibitor such as clezutoclax.
- An inhibitor of N-myristoyl transferase

In some preferred embodiments, the payload is exatecan.

Antimitotic Agents

Microtubules are long filamentous protein polymers consisting of heterodimers of α- and β-tubulin which are involved in a number of cellular processes critical to cellular function, including organelle and vesicle transport, cell migration and mitosis. These polymers are assembled and disassembled in a highly controlled process within cells. The main role of microtubules is to separate and segregate chromosomes during cell division. Thus, tubulin inhibitors interfere with cell division by preventing the two pairs of chromosomes from separating into two daughter cells [101].

In certain embodiments the toxin may be an auristatin which refers to a family of antimitotic agents derived from the natural product dolastatin-10 which is a highly potent linear pentapeptide isolated from Dolabella Auricularia, a sea hare [102]. Dolastatin-10 and its analogues are extremely potent cytotoxic antineoplastic agents, exhibiting picomolar GI_{50} values in most cancer cell proliferation assays [103]. The potent antiproliferative activity is caused by the ability to strongly bind to tubulin and inhibit

microtubule assembly and tubulin-dependent GTP hydrolysis, resulting in accumulation of cells in the G2/M phase of the cell proliferation cycle resulting in cell cycle arrest and apoptosis. Detailed binding studies have shown that dolastatin-10 and the auristatins bind to a region which overlaps with that of the vinca site but extends significantly further and near the exchangeable GTP binding site termed the peptide site. Dolastatin-10 and the auristatins bind at the α,β-tubulin interphase, inducing a curved conformation that is incompatible with the straight structure of microtubules. In addition to effects on tubulin dynamics, it was soon recognised that dolastatin-10 and related synthetic auristatin analogues also have strong anti-vascular effects. However, dolastatin-10 and other derivatives failed to demonstrate meaningful clinical activities as single-agents due to severe dose-limiting adverse effects. However, targeted delivery to the tumour can reduce systemic toxicity and result in clinical benefit.

Examples of auristatins include monomethyl auristatin E (MMAE), monomethyl auristatin F (MMAF), auristatin F, auristatin F hydroxylpropylamide (AF-HPA), monomethyl auristatin D (MMAD), monomethyl auristatin F methylester (MMAF-OMe), PF-06380101. Suitable auristatins are described in WO2002088172, WO2005081711, US6323315, US5663149, US5530097 and US5504191.

Dolastatin-15 is a related seven-subunit depsipeptide also obtained from Dolabella Auricularia see [US4879278]. Many synthetic analogues of this natural product have been prepared, among which cemadotin (LU-103793) and tasidotin (ILX651) have entered clinical trials [104]. For exemplary drugs and analogues from dolastatin-10 see, US5410024, US5599902, US5635483 and US6323315.

In certain embodiments, the toxin may be from the hemiasterlin family. Hemiasterlins are a family of cytotoxic tripeptides that were initially isolated from the South African marine sponge Hemiasterella minor [105]. Hemiasterlin and its synthetic analogues like Taltobulin (HTI-286) show nanomolar cytotoxic potency and probably bind to the 'peptide binding site' shared with dolastatins and cryptophycins and inhibit tubulin assembly triggering mitotic arrest and subsequent apoptosis. In comparison with other marine peptides, hemiasterlins have the advantage of a simpler structure allowing the preparation of many synthetic analogues like taltobutin which is less sensitive to P-glycoprotein drug transporters. For exemplary hemiasterlin derivatives as ADC payloads see WO2016123582 which describes 3-aminophenylhemiasterlin and its derivatives.

In certain embodiments, the toxin may be a maytansinoid. The term maytansinoid refers to benzoansamacrolide, a class of highly potent antimitotics originally isolated from the

African shrub Maytenus ovatus. Maytansinol, which has the same macrocyclic system as in maytansine but with a C3-hydroxyl instead of the C3-acetyl-N-methyl-alanine side chain. Maytansinoids are derivatives of maytansinol with modified C3-side chains that are typically C3-esters [106,107]. Maytansine binds tubulin at the vinca-binding site, similar to vinca alkaloids, thereby depolymerizing tubulin and inducing mitotic arrest in the G2/M phase [108]. Similar to the auristatins, maytansine in its original form yielded a narrow therapeutic window due to associated neurological and gastrointestinal toxicities. Consequently, synthetic maytansine derivatives were synthesized that possessed 100–1000-fold increases in potency while also including modifications to enable targeted delivery [109].

Exemplary maytansinoids or maytansinoid analogues including maytansinol are described [110] and US5416064. C3-esters of simple carboxylic acids are described in US4317821. C3-esters with derivatives of N-methyl-L-alanine are described in US4260608. Exemplary maytansinoids such as DM1, DM3, DM4 and DM21 or maytansinoid analogues including maytansinol are described in US6716821, US7276497 and US20180296694.

In certain embodiments the toxin may be a cryptophycin. Cryptopycins are a family of 16-membered cyclic depsipeptides, first isolated from terrestrial blue-green algae. They are potent tubulin-binding antimitotic agents, inhibiting mitotic spindle function of cells in the G2M phase of the cell cycle resulting in apoptotic cell death [111]. Cryptophycins have demonstrated excellent activity against a broad spectrum of solid tumours with potency in the picomolar range [112] and unlike other antitubulin agents they have a major advantage in that they are insensitive to the ABC transporters P-gP and MRP, which are implicated in multidrug resistance [113].

Although cryptophycins have failed as stand-alone drugs due to toxicity, their very high potency (picomolar potency on a panel of tumor cells) and lack of PgP susceptibility make them potential candidates as payloads in targeted delivery [114]. Exemplary cryptophycin compounds are described in US6680311 and US20180078656.

In certain embodiments the toxin may be a tubulysin. Tubulysins are a family of naturally occurring cytotoxic tetrapeptides isolated from mycobacterium cultures [115]. Tubulysins are potent inhibitors microtubule polymerisation, causing rapid disintegration of the cytoskeleton of dividing cells in the G2/M phase leading to apoptosis. Binding is to the peptide binding site like the dolostatins making tubulysins extremely potent cytotoxic agents at sub-nanomolar concentrations against a variety of cancer types especially multidrug resistant lines [116]. This activity has led to significant interest in the tubulysins

as targeted anticancer agents. Exemplary tubulysin compounds are described in, US20210188906, WO2021262910, US20170326247, WO2017134547, US20160340386, and WO2015157594.

In certain embodiments the toxin may be a taxane. Paclitaxel (Taxol), Docetaxel and Cabazitaxel, Larotaxel, TPI 287 and MAC-321 represent the taxane family of drugs which have demonstrated remarkable efficacy against solid tumours such as ovarian and breast cancer. Paclitaxel was first isolated from the Pacific Yew tree Taxus brevifolia and its antitumour activity was first reported in 1971. Paclitaxel works by promoting tubulin polymerisation by stabilising microtubules from depolymerisation, thus causing cell cycle arrest in the G2M stage of the cell cycle, leading to apoptotic cell death. Exemplary paclitaxel and analogues are described in [117].

In certain embodiments the toxin may be a vinca alkaloid and their synthetic analogues. Vincristine and vinblastine are complex molecule produced by the leaves of the rosy periwinkle plant. They block the polymerisation of tubulin into microtubules and inhibit mitotic progression resulting in apoptotic cell death. The lead compounds vinblastine and vincristine have been employed in clinical practice for more than thirty years and remain widely used to this day. Several hundred derivatives have been synthesised and evaluated for their pharmacological activities [118]. Vinorelbine (Navelbine) is a semi-synthetic vinca-alkaloid with broad spectrum of activity in breast and non-small cell lung cancer with fewer side effects than other vinca alkaloids. Other examples include 4-deacetyl-vinblastine-3-carboxyhydrazide which was evaluated as a conjugate [119] and N-(3-hydroxypropyl)vindesine alanine which was conjugated to a polyacetal polymer. Exemplary vinca alkaloids include vincristine, vinblastine, vindesine and navelbine and those disclosed in US20020103136 and US20100305149.

In certain embodiments the toxin may be eribulin. Eribulin is a synthetic analogue of the macrocycle halichondrin B, a complex polyether macrolide first isolated from the Asian marine sponge Halichondria okadai [120]. Eribulin binds specifically to the β-tubulin subunit on the (+)-end of a microtubule, inhibiting elongation but having no effect on microtubule depolymerisation. Eribulin (as the mesylate salt) was approved by the FDA for the treatment of metastatic breast cancer and is being investigated for use in other tumour types including bladder, lung and. In addition to antimitotic effects, eribulin appears to act through some non-mitotic pathways which may contribute to its overall antitumour activity. An eribulin derivative modified with a cathepsin-cleavable dipeptide valine-citrulline is described in [121]. Exemplary eribulin compounds are described in WO2017151979 and WO2023061466.

In certain embodiments, the toxin may be an epothilone and their synthetic analogues. The epothilones are a group of closely related antitubulin cytotoxic macrocylic lactones with a mechanism of action similar to the taxanes in which they bind to the same αβ-tubulin heterodimer, promoting tubulin polymerisation by stabilising microtubules from depolymerisation, thus causing cell cycle arrest in the G2M stage of the cell cycle, leading to apoptotic cell death [122]. The epothilones were originally identified as metabolites produced by the soil-dwelling myxobacterium Sorangium celulosum and by 2008 epothilones A-F were identified and characterised. Epothilones A and B have strong antiproliferative activity against different types of cancer cells and have been found to also exert their effects on taxol resistant cancers. Exemplary epothilone compounds include epithilone A, B, C, D, E, and F and derivatives thereof. Suitable epithilone compounds and derivatives are Ixabepilone (Ixempra, BMS-247550), Utidelone (depoxythilone), Sagopilone (ZK-EPO) and Patupilone (EPO906). Additional exemplary derivatives are described in US6989450, WO9719086, WO9907692, WO9927890 and WO2017066606.

DNA targeting agents

Topoisomerase I inhibitors: Topoisomerases are nuclear enzymes that regulate the three-dimensional geometry (topology) of DNA and enable supercoiled DNA to relax. Regulation of DNA supercoiling is essential to DNA transcription and replication, when the DNA helix must unwind to permit proper function of the enzymatic machinery involved these processes. In order to relieve the topological stress caused by supercoiling, the enzymes topoisomerase I and topoisomerase II (Topo I and II) produce single or double-strand breaks respectively, followed by re-sealing, thus reducing the tension in the DNA strand without leaving damaging nicks. Topoisomerase I works by breaking only one strand of DNA, followed by attachment of the free phosphate residue of the broken strand to a tyrosine residue of the enzyme. The complex then rotates, relieving the supercoiled tension of the DNA, and the two ends are then re-sealed. Topoisomerase II works in a related manner but cleaves both strands of DNA simultaneously, passing a complete duplex strand through the cut, followed by re-sealing of both ends. Topoisomerase inhibitors affect the activity of Topo I and II, with most acting to block the re-sealing process, leading to cell death by apoptosis [123]. Topoisomerases are considered essential proteins for all human cell division to take place properly. They are overexpressed in cancer cells, where the higher activity of topoisomerase enzymes accelerates the rate of cell division making the inhibition of these enzymes important anticancer drug targets. In certain embodiments, the toxin may be a topoisomerase I or II inhibitor.

In certain embodiments the toxin may be a camptothecin. The term 'camptothecin' as used herein is intended to mean a camptothecin or camptothecin derivative that functions as a topoisomerase I inhibitor. Camptothecin (CPT) was the first specific topo I inhibitor to be discovered. It is a quinoline plant alkaloid isolated from the Chinese plant Camptotheca acuminata and has a novel pentacyclic structure. The cytotoxic effect of camptothecin and its analogues is due the inhibition of the religation step that normally reseals the parent strand of DNA causing an irreversible double-strand DNA break, arresting the process of cell division, resulting in cell death [124].

Exemplary camptothecins that may be used in accordance with the present invention include topotecan, exatecan, DX-8951f, DXd, irinotecan, SN28, belotecan, 9-aminocamptothecin, rubitecan, silatecan, lurtotecan, diflometotecan, namitecan, gimatecan, cositecan, rubitecan, FL118 (7-methyl-10,11-methylenedioxy-20(RS)-camptothecin and its 7-alkylamino derivatives (7-methyl, ethyl, propyl, butyl), 7-n-butyl-10-aminocamptothecin, 7-n-butyl-9-amino-10,11-methylenedioxy camptothecin, 4-Amino-9-ethyl-5-fluoro-9-hydroxy-1,2,3,9,12,15-hexahydro-camptothecin, 7-methylamino-(10-methyl,11-fluoro)-camptothecin, 7-trihydroxmethylaminomethyl-(10,11-methylenedioxy)-camptothecin. Exemplary camptothecin compounds also include those described in [125]. Exemplary camptothecin compounds are further described in WO2022232834, WO2022093800, WO2022015656, WO2022155347, WO2022253035, WO2022246576, WO2022058395, WO2020219287 and WO2019236954.

Camptothecin has a novel pentacyclic ring structure of and to distinguish modifications and derivatives each ring given a label A-E. Exemplary ring modified camptothecins are described in [126]. In camptothecin the presence of a 6-membered α-hydrocy lactone E-ring is regarded as an important feature as it interacts with human Topo I through Arg364 and Asp533 residues and confers antiproliferative activity. However, this lactone E ring is unstable in plasma at physiological pH resulting short half-life and low therapeutic efficacy. E-ring modified camptothecin derivatives such as an expanded 7-membered β-hydroxy lactone like diflomotecan have been developed and also derivatives where the size of the E-ring has been reduced from 6-membered to 5-membered. One such active derivative is S39625 [127]. Derivatives where the E ring has been opened are also being explored.

Non-camptothecin topoisomerase I inhibitors: Several non-camptothecin derivatives have recently been developed as topo I inhibitors including indenoisoquinolines including exemplary compounds NSC 725776 and NSC 724998 [128], dibenzonaphthyridione (benzophenanthridine) [129]. Exemplary compounds include GENZ-644282 [130], ARC-111 (topovale) and other derivatives. Evodiamine is a quinazoline-carbolin alkaloid

isolated from the Chinese herb Evodia rutaecarpa and is a potent topo I inhibitor. Many synthetic derivatives of evodiamine have been found to manifest potent antitumour activity [131].

Nemorubicin, a doxorubicin analogue bearing a 2(S)-methoxy-4-morpholinyl chain is a potent antitumour agent that induces DNA strand breaks primarily through topoisomerase-I cleavage and is active in cells resistant to topoisomerase II inhibitors. But nemorubicin also exerts its antitumour action through a novel mechanism different to that of other anthracyclines, involving the inhibition of DNA nucleotide excision repair (NER) [132]. Exemplary nemorubicin analogues are described in US20140227299 and WO2008092796.

Topoisomerase II inhibitors: Exemplary approved topoisomerase II inhibitors that can be used in accordance with the present invention are etoposide, teniposide, doxorubicin, idarubicin, epirubicin, and mitoxantrone. Topoisomerase II is a multi-subunit enzyme which uses ATP to pass an intact helix through a transient double-stranded break in DNA to modulate DNA topology [133]. After strand passage, the DNA backbone is religated and DNA structure restored. It has been suggested that cancer cells rely on the topo II enzyme more than healthy cells since they divide more rapidly. Therefore, normally reversible DNA strand breaks are converted into lethal breaks by processes such as transcription and replication causing errors in DNA synthesis and promoting apoptosis [134]. Etoposide is a semi-synthetic glucoside analogue of epi-podophyllotoxin, a toxin lignan (from the rhizome of the wild mandrake, Podophyllum peltatum). Etoposide and derivatives act as non-intercalating topo II poisons, preventing topoisomerase II from religating cleaved DNA [135].

The largest group of topo II inhibitors are the anthracyclines. Anthracyclines also intercalate into DNA and form reactive metabolites that interact with many intracellular molecules and biologic effects of the anthracyclines are not based solely on topoisomerase II activity [136]. In certain embodiments, the toxin may be a topoisomerase II inhibitor.

In certain embodiments the toxin may be doxorubicin. Doxorubicin refers to members of the family of anthracyclines derived from a naturally occurring group of antitumour antibiotics and include daunorubicin, epirubicin and idarubicin. The mechanism of action of doxorubicin is common to all anthracyclines and involves DNA intercalation. The planar anthraquinone aromatic ring nucleus inserts between the base pairs of the DNA double helix, perpendicular to the double-strand axis. The complex is then stabilised by various hydrogen bonds, hydrophobic interactions and Van der Waals forces. By forming intercalated adducts, doxorubicin inhibits both DNA and RNA polymerases, leading to

arrest of DNA replication and RNA transcription. Doxorubucin also binds to the DNA-topoisomerase complex in proximity to the scission site of DNA, thus preventing its repair and triggering apoptosis by inhibiting cellular division at the G1 and G2 phases [137]. Doxorubicin and the other anthracyclines can undergo one- and two-electron reduction, since they are members of the quinone family, producing reactive compounds that damage macromolecules and lipid membranes. Exemplary anthracyclines are described in [138].

Mitoxantrone is a simplified anthracenedione that binds to topoisomerase II resulting in cleavable complexes that induce DNA strand breaks. Mitoxantrone lacks the ability to form the quinone-type free radicals thought to account for anthracycline cardiotoxicity and is the only agent of its class approved for clinical use. In some embodiments, the toxin is mitoxantrone.

PNU-159682 is liver metabolite of nemorubicin and is about three orders of magnitude more potent than its parent molecule on cultured human tumour cells. It is a potent topo II inhibitor amongst other poorly understood modes of action and is effective regardless of the cell cycle unlike doxorubicin. PNU-159682 is not an efflux pump substrate and is able to bypass resistance mechanisms observed with known tubulin inhibitors like MMAE and DM1 [139]. In some embodiments, the toxin is PNU-159682.

Several analogues of these anthracyclines are in various stages of clinical development. PNU-159548, an alkycycline daunorubicin derivative, has demonstrated antineoplastic activity in animal models with reduced cardiotoxicity compared to doxorubicin [140]. Ethonafide is an anthracene-containing derivative of amonafide which inhibits topoisomerase II and may have less toxicity than other anthracene-containing agents. Exemplary PNU-159682 derivatives are described in [141]. In some embodiments, the toxin is PNU-159548 or ethonafide.

In certain embodiments, the toxin may be a duocarmycin. Duocarmycins are a family of DNA minor groove-binding compounds with exquisite cytotoxicity originally identified in Streptomyces [142]. Their unique mechanism of action involves DNA minor-groove binding and alkylation of adenine forming DNA-adducts which disrupt the DNA helix ultimately leading to cell death. A key advantage of duocarmycins and its analogues is the ability to exert their effects on any phase of the cell cycle acting on both dividing and non-dividing cells. Structurally, duocarmycins contain a DNA-binding moiety that selectively interacts with DNA strands and a DNA-alkylating unit that possess a spirocyclic cyclopropapyrroloindole (CPI) moiety and many synthetic duocarmycin analogues maintain these structural features. The alkylating CPI unit can also be derivatised in its

ring-opened chloromethyl aromatic (seco) form, forming prodrugs that contain a phenolic hydroxyl group producing a cyclopropane-containing cytotoxin, via a process known as spirocyclisation, to prevent spontaneous cyclisation, the phenolic hydroxyl group must be modified usually via a pro-drug strategy.

Exemplary duocarmycins and analogues include CC-1065, duocarmycin SA, duocarmycin TM, duocarmycin A, adozelesin, bizelesin, carzelesin, seco-adezelesin, DC0-NH2, DC1, DC1SMe, DC41SMe, (+)-CBI-CDPI1, (+)-CBI-CDPI2, DC41, DC4SMe, DC10SMe, DU-257, DU-86, KW-2189, seco-duocarmycin-SA, duocarmycin MB, duocarmycin GA, duocarmycin B2 [143,144]. Duocarmycins are DNA mono-alkylators, by connecting two duocarmycin-type units per molecule, DNA-cross-linking via double alkylation is achieved and these derivatives display significantly greater potency than duocarmycins. The CXI dimers [dimers containing, for example cyclopropapyrroloindole (CPI), cyclopropabenzindole (CBI) or cyclopropathienoindole (CTI) moieties] are the main class of potent bis-alkylating payloads. Exemplary CXI dimers are described [145].

In certain embodiments, the toxin may be a Pyrrolobenzodiazepine (PBDs). PBDs were discovered in the 1960s and are an important class of sequence-selective DNA-interactive agents that bind covalently to guanine bases within the minor groove of DNA. There are now two recognized subfamilies of pyrrolobenzodiazepines, the first is the PBD monomer subfamily that represents the agents originally discovered in cultures of Streptomyces species (e.g., anthramycin and tomaymycin). The PBD monomers are remarkable in possessing a 3-dimensional shape that allows them to fit perfectly within the minor groove of DNA, once located in a position of low energy in the groove (i.e., a preferred DNA sequence), largely dictated by substituents, the electrophilic imine then alkylates the amine group of an adjacent guanine base, thus producing a robust covalent adduct capable of blocking biological processes such as transcription factor binding and RNA polymerase progression. The PBD monomers have both antibacterial properties and selective cytotoxicity toward tumour cells. The second subfamily, the PBD dimers, are not naturally occurring but are synthetic derivatives, the first examples were designed to span greater lengths of DNA than the PBD monomers, to have enhanced sequence-selectivity, and to form DNA cross-links that might be more difficult for tumour cells to repair. It is now known that PBD dimers can form both inter-strand and intra-strand cross-links, as well as monoadducts under certain conditions, although the interstrand cross-linked adduct is still thought to be the most toxic in cells. The perfect fit of a PBD dimer in the DNA minor groove results in negligible distortion of the DNA helix, thus potentially avoiding DNA-repair mechanisms and drug resistance.

Exemplary pyrrolobenzodiazepine (PBDs), which expressly include dimers and analogues, include but are not limited to those described in [146,147]. Duocarmycin-PBD dimers are heterodimeric compounds fomed by linking together two different alkylating subunits derived from duocarmycin and pyrrolobenzodiazepine (PBD) classes of DNA-minor groove-alkylating agents. Exemplary duocarmycin-PBD dimers are described in [148].

In certain embodiments, the toxin may be a mitomycin. Mitomycins are a family of aziridine-containing natural products isolated from Streptomyces caespitosus, the best-known members being mitomycin A, B and C. Mitomycin C has significant antitumour properties and is active against a variety of tumours including breast, stomach, oesophagus, bladder and NSCLC. The main mechanism of action of mitomycin is through *in situ* bioreduction resulting in a bis-electrophile that can alkylate a range of cellular nucleophiles with DNA alkylation as the main mechanism of action. The reductive activation mechanism confers selectivity towards particular tumour types, especially hypoxic solid tumours. Exemplary mitomycins are described in [149,150].

In some embodiments, the toxin may be a nitrogen mustard. Nitrogen mustards are some of the earliest examples of DNA alkylating agents, these act either as mono-alkylators or as intra- and interstrand cross-linkers. Exemplary nitrogen mustards are chlorambucil (Leukeran™) and bendamustine (Levact™). Site-directed nitrogen mustards include melphalan (Alkeran™) which is an L-phenylalanine derivative designed for selective uptake by tumour cells in which protein synthesis may be occurring. The oligopyrrole antibiotics netropsin and distamycin A (and related synthetic heteropyrrole/imidazole 'lexitropsin' analogues) are well-documented minor groove binders. Attaching nitrogen mustards to their analogues results in increased cytotoxicity, highly specific alkylation at adenines and broad spectrum solid tumour activity. This work culminated in the development of tallimustine. Bis-benzimidazoles are also well-characterised reversible minor groove binding ligands, with extensive studies on the lead compound Hoechst 33258 whose analogues with aniline mustards attached by a variable-length polymethylene chain showed chain length-dependent patterns of DNA alkylation and are potent. Exemplary derivatives are described in [151].

Further approaches utilise selective bioactivation of prodrug forms where there are biochemical differences between tumour and normal tissues. Cyclophosphamide (Endoxana™) is one example of a metabolic prodrug that requires enzymic activation by phosphoramide hydrolysis by phosophoramidases, releasing the active agent which alkylates guanine bases resulting in mono-adducts and both intra-and inter-strand cross-links. Other mechanisms of alkylation of DNA are through aziridines and epoxides. The

active species involved in DNA alkylation by nitrogen mustards is an aziridinium cation and several aziridine derivatives have been tested as antitumour agents like Carboquone, Diaziquone (AZQ) and BZQ. The high reactivity of epoxides towards nucleophilic groups in biomolecules has led to the development of numerous DNA alkylating drugs like Treosulfan which alkylates DNA at guanine bases and has been used in the treatment of ovarian cancer.

The nitrosoureas are a class of alkylating agents that decompose to produce alkylating compounds under physiologic conditions, the predominant mechanism being base catalysed decomposition to a chloroethyl diazonium moiety which reacts with DNA to form a unique inter-strand DNA cross-link. Currently the most clinically relevant nitrosoureas are Carmustine (BCNU), Lomustine, Nimustine (ACNU) and Streptozotocin.

The platinum antitumor agents are complexes of platinum with ligands that can be displaced by nucleophilic (electron-rich) nitrogens in nucleic acids. All platinum agents act as pro-drugs, in that they require the removal of their labile chloride or carboxylate ligands, through their displacement by water, before they can bind DNA. When binding to DNA, platinum complexes predominantly do so through the formation of a coordination bond at the N7 site of guanosine residues. Simultaneous binding at a second, adjacent nucleotide, typically another guanosine base, results in inter-strand cross-linking, significant bending and unwinding of the DNA which prevents transcription and replication. The cascade effect of this binding is the induction of apoptotic cell death. Exemplary platinum drugs are cisplatin, carboplatin (Paraplatin), oxaliplatin (Eloxatin), nedaplatin, loboplatin, picoplatin, heptaplatin, teraplatin, iproplatin, satraplatin and ormaplatin

In certain embodiments, the toxin may be an enediyne. Enediynes are highly cytotoxic DNA damaging natural products produced through microbial secondary metabolism. The enediyne natural products share a common structural motif containing two acetylenic groups conjugated to a double bond or incipient double bond within a 9- or 10-membered carbocycle [152]. Exemplary 9-membered enediynes include neocarzinostatin, kedarcidin, maduropeptin, C-1027 and N1999A2. These molecules, except for N1999A2, generally are found in complex with a cognate apoprotein that binds the enediyne chromophore to generate a stable chromoprotein. Exemplary 10-membered enediynes can be divided into two subfamilies: the calicheamicin-like enediynes including the calicheamicins, the esperamicins, namenamicin and shishijimicins, and the anthraquinone-fused enediynes including dynemicin, uncialamycin, the tiancimycins and the yangpumicins [153].
The conjugated carbocycle drives the shared mode of action for the enediynes. Electronic rearrangement of the enediyne carbocycle (cycloaromatization) generates a benzenoid

diradical that drives enediyne-induced cytotoxicity. Enediyne natural products with a 9-membered carbocycle can proceed through either the Myers-Saito or Bergman rearrangement pathways depending on their architecture, whereas all known 10-membered enediynes proceed through the Bergman rearrangement. These DNA lesions are responsible for the cytotoxicity of enediyne natural products [154]. Exemplary enediyne antibiotics are described in [155,156].

Although there are many anticancer drugs that interact with DNA by initially intercalating, there are also classes of drugs whose main mode of action is intercalation. Intercalation involves the insertion between the base pairs of DNA, perpendicular to the axis of the helix of a flat, fused aromatic molecule. This unwinding results in local structural changes in the helix such as lengthening or twisting of the base pairs and lead to the interference of recognition and function of DNA-associated proteins such as polymerases, transcription factors and DNA repair systems. Exemplary monofunctional intercalating agent is ellipticine and its analogues. Ellipticine is an alkaloid isolated from the leaves of Ochrosia elliptica and has potent anticancer properties. Ellipticines are multimodal anticancer agents because they exert their biological activity via several modes of action with intercalation and topoisomerase II inhibition the best established. Exemplary ellipticine derivatives are celiptium, datelleptium, the olivacine derivative S-16020 and intoplicine.

In order to increase the binding constant of intercalating compounds, bifunctional of polyfunctional compounds have been designed. Bifunctional intercalators (bis-intercalators) contain two intercalating units, normally cationic, separated by a spacer chain that must be long enough to allow double intercalation to take place. Exemplary bis-intercalators are ditercalinium and elinafide. Further examples of both mono-and bis-intercalators are described in [157].

Tyrosine Kinase Inhibitors

Protein kinases are enzymes that catalyse phosphorylation and are divided into three categories: serine, threonine or tyrosine kinases. Tyrosine kinases function by catalysing the transfer of a phosphoryl group from a nucleoside triphosphate donor to the hydroxyl group of tyrosine residues on protein substrates and then triggering the activation of downstream signalling cascades. In cancer a variety of kinase families are involved in cell cycle progression, cell proliferation, motility and angiogenesis. Abnormal activation of tyrosine kinases due to mutations, translocations, or amplifications is implicated in tumorigenesis, progression, invasion, and metastasis of malignancies [158]. As such, tyrosine kinases have emerged as major targets for drug discovery [159].

Fibrosis denotes an excessive deposition of collagen and other extracellular matrix (ECM) components in tissue. Deposition of collagen is part of physiological wound healing but when this process becomes abnormal, connective tissue replaces normal parenchyma, leading to tissue destruction and impairment of organ function. This pathologic process can affect several organs, causing diverse chronic diseases such as idiopathic pulmonary fibrosis (IPF) [160]. An exemplary compound for the treatment of IPF is nintedanib. Nintedanib is a small molecule, competitive, triple angiokinase inhibitor that targets multiple receptor tyrosine kinases (RTKs) and non-receptor tyrosine kinases (nRTKs). Many of these RTKs are implicated in lung fibrosis and tumour angiogenesis, so nintedanib is therefore used in the treatment of proliferative diseases such as idiopathic pulmonary fibrosis, non-small cell lung cancer, and systemic sclerosis-associated interstitial lung disease. The specific RTKs that nintedanib inhibits are platelet-derived growth factor (PDGFR) α and β, fibroblast growth factor receptor (FGFR) 1-3, vascular endothelial growth factor receptor (VEGFR) 1-3, and Fns-Like tyrosine kinase-3 (FLT3). Nintedanib binds to the ATP-binding pocket of these receptors and inhibits their activity, thereby blocking signalling cascades that result in the proliferation and migration of lung fibroblasts. Nintedanib also inhibits kinase signalling pathways in various cells within tumour tissues, including endothelial cells, pericytes, smooth muscle cells, and cells contributing to angiogenesis, culminating in an inhibition of cell proliferation and apoptosis of affected tumour cells [161]. Exemplary derivatives of nintedanib include the αvβ6 targeting-nintedanib conjugates [162].

In some embodiments, the payload is a tyrosine kinase inhibitor selected from the group consisting of nintedanib, afatinib, axitinib, bosutinib, crizotinib, dasatinib [163] erlotinib, fostamatinib, gefitinib, ibrutinib, imanitib, lapatinib, mubritinib, nilotinib, pazopanib, pegaptanib, sorafenib, sunitinib, Lenvatinib, linifanib, tivozanibvandetanib, vemurafenib, CEP-701 (lesaurtinib), INCB018424 (ruxolitinib), ARRY-142886 (selemetinib), ARRY-438162 (binimetinib).

Transcription inhibitors

Transcription has a fundamental role in cell development, activity and proliferation. Transcription is regulated by RNA polymerase II (RNApol II) that directly binds to DNA and involves transcription factors that form complexes with RNApol II to initiate transcription and co-regulators that mediate chromatin structure and accessibility.

In certain embodiments, the toxin maybe an amatoxin. Amatoxins (including alpha-amanitin, beta-amanitin and amanitin) are natural and highly potent RNApol II inhibitors derived from the Amanita phalloides mushroom. They are cyclic peptides composed of 8

amino acids and inhibit specifically the DNA-dependent RNA polymerase II of mammalian cells, affecting transcription and protein biosynthesis, stopping growth and proliferation [164]. Exemplary amatoxins include alpha-amanitins, beta-amanitins, gamma amanitins, eta amanitins, amanulin, amanullic acid, amanisamide, amanon and proamanulin. Amatoxins are described in [165].

Another strategy to stop DNA transcription is to inhibit transcription factors. Transition factors are essential to RNApol II attachment to the DNA at the initiation step. Triptolide, a natural compound derived from the Chinese medicinal herb called "thunder god vine", is highly cytotoxic against a variety of solid tumour cell-lines and one of its main modes of action is as an inhibitor of both RNA Pol I- and RNA Pol II dependent transcriptions. Minnelide is a water-soluble pro-drug of triptolide currently being evaluated as an anticancer drug. Exemplary triptolide derivatives are described in [166].

Histone deacetylases (HDACs) are epigenetic regulators that regulate the histone tail, chromatin conformation, protein-DNA interaction and are therefore involved in various cellular processes including transcription and protein regulation. They have been found to be overexpressed or overactivated in cancer cells and are thought to be involved in increased proliferation, migration and invasion. Exemplary HDAC inhibitors that may be used in accordance with the present invention include Vorinostat, Romidepsin, Panobinostat, and Belinostat.

In certain embodiments, the toxin maybe a thailanstatin, or an analogue or derivative thereof. Thailanstatin A and its analogues are RNA splicing inhibitors. RNA splicing controls metabolism, angiogenesis, cancer cell proliferation and metastasis mainly by excision of introns and exons that are responsible for the complex cellular mechanism of transforming RNA to mRNA. They can also directly control the initiation, elongation, and termination of transcription and are potent antiproliferative drugs capable of targeting cells that are actively dividing and quiescent. Thailanstatin is a natural product originally isolated from Brucella Thailandensis msmb43 and activated by binding to the SF3b subunit of the spliceosome U2 snRNA subcomplex. The thailanstatin family has a strong binding and inhibitory effect on spliceosomes by inhibiting the eukaryotic mRNA splicing pathway, resulting in low nanomolar IC50 values for a variety of cancer cell lines. Exemplary Thailanstatin A derivatives are described in [167].

In certain embodiments, the toxin maybe a kinesin spindle protein inhibitor. Kinesin spindle protein (KSP, synonyms: Eg5, KIF11) is an ATP-dependent motor protein involved in the separation of centrosomes in the G2/M phase of the cell cycle. High expression in

certain solid tumours (breast, pancreatic and bladder cancers) is associated with poor prognosis. The blockade of this essential event in mitosis with small molecule KSP inhibitors (KSPis), results in high antitumor potency. Also, Eg5 expression is specific to proliferating cells and is not expressed in the cells of the nervous system so avoiding the neurological side effects of classic microtubule targeting agents. Exemplary small molecule KSP inhibitors are Ispinesib and Filanesib. Further examples are described in [168].

In certain embodiments, the toxin maybe a NAMPT inhibitor. Niacinamide phosphate ribose transferase (NAMPT), which converts nicotinamide into nicotinamide mononucleotide, is a rate-limiting enzyme that controls the concentration of NAD^+ within cells. When NAMPT is suppressed, NAD^+ levels drop below the level required for metabolism, leading to an energy crisis and eventually, cell death. In contrast to many other cytotoxic molecules, the cell death following depletion of NAD proceeds via a nonapoptotic and proinflammatory mechanism termed oncosis. Exemplary NAMPT inhibitors that may be used in accordance with the present invention include FK-866, CHS-828, GMX-1777, GMX-17778, GPP 78 hydrochloride, ST 118804, STF31. Further examples are described in [169].

In certain embodiments, the toxin maybe a Bcl-xL inhibitor. Bcl-xL is an anti-apoptotic protein that plays an important role in tumour formation, metastasis, and drug resistance. Apoptosis is a highly regulated cellular process. Aberration in apoptosis is a common characteristic of various disorders. Therefore, proteins involved in apoptosis are prime targets in multiple therapies. Compared to other antiapoptotic proteins, the expression of Bcl-xL is common in solid tumours and apoptosis of cancer cells can theoretically be triggered by drugs blocking the BH3 binding domain on Bcl-xL. However, Bcl-xL is critical for platelet survival, and pan-inhibitors of Bcl-xL may produce platelet toxicity [170].
Exemplary BcL-xL and Bcl-2 inhibitors are navitoclax, venetoclax, GX-070 (obatoclax), gossypol acetic acid (AT-101, sabutoclax), WEHI-539), ABT-737 and those described in [171]; exemplary compounds are described in WO2017/214301 and WO2017/214282.

Further exemplary compounds that may be used in accordance with the present invention are G3139 (Oblimersen), Bcl-2-targeting antisense oligonucleotide IPI-194 and IPI-565, HGS1029, GDC-0145, GDC-0152, LCL-161, LBW-242, Bcl-2 family members, death domain proteins, TNF family members, Toll family members and/or NF-kappa-B proteins.

In certain embodiments, the toxin maybe an immune stimulating agent such as toll-like receptor agonists (e.g. TLR 7/8 agonists) or STING agonists. Tumour immunity involves T cells, macrophages, dendritic cells, etc., which transform cold tumours (immunologically inactive) into hot tumours (immunologically active) through immunomodulation, and

ultimately enhance the effect of immunotherapy. Novel cancer immunotherapies, such as checkpoint inhibitors, have proven to be a vital approach for the treatment of an increasing number of cancers [172]. While these therapies successfully modulate the immune system to eradicate metastases, their success does not translate well to "cold" or "non-T cell-inflamed" tumours that lack sufficient T cell infiltrates or exhibit immune suppression prior to treatment. One approach to overcome this resistance is to activate the patients innate immune system/response via known signalling pathways, including toll-like receptor (TLR) 7/8, nucleotide-binding oligomerization domain, and cGAS-STING and promote tumour-specific T cell recruitment [173].

STING and TLR agonists constitute the two main categories of immune stimulants, however, the systemic administration of potent STING and TLR agonists is associated with severe toxicity caused by cytokine release syndrome. Their conjugation to proteins or antibodies could be one approach in exploiting their strong antitumour potential together with better tolerability. Several chemical scaffolds have been identified as starting points to generate potent TLR7/8 agonists, including purines (loxoribine), imidazoquinolines (imiquimod and resiquimod), deazapurines (compounds described in WO 2015/16827 benzazepines (motolimod) and various others [174]. These compounds all bind in the 2′3-cGMP site of the TLR7/8 proteins (which share a high degree of sequence homology and function). Exemplary compounds are CL264, UC-1V150, D18, and T785. Further exemplary compounds are described in WO 2018/191746 and WO 2020/056192.

The stimulator of interferon genes (STING) is a key regulator in the natural immune signalling pathway and has the function of initiating the body's natural immune defence response and promoting the formation of adaptive immunity by T cells. The STING-mediated type I interferon signalling pathway is a major discovery in the field of natural immunity, providing a new target for tumour immunotherapy. Activating the STING pathway can induce the expression and secretion of type I interferons and a variety of other cytokines, activate the natural immune response, promote the anti-tumour immune response. Natural agonist, cGAMP and other synthetic cyclic dinucleotide (CDN) derivatives have been the main starting point for the development of STING agonists, non-CDN small molecule STING agonists have also been identified, such as dimeric amidobenzimidazole (diABZI) like XMT-1621, these function by mimicking the native ligand of STING, 2′3′-cGAMP. Exemplary compounds are described in [175,176].

In certain embodiments, the toxin maybe a PROTAC. Proteolysis Targeting Chimeric Molecules (PROTACs) are bifunctional molecules that bring together the E3 ligase with the target protein thus allowing its ubiquitination and degradation by the proteasome. Instead

of directly inhibiting its target protein, PROTACs trigger its degradation with several potential clinical advantages such as prolonged effect, catalytic activity and therefore very potent cytotoxicity. PROTACs can benefit from being targeted inside the cell to overcome their limited cell permeability. Exemplary compounds are MZ1 (BRD4/VHL), GNE-9787 (BRD4/VHL), BRD4/VHL, BRD4/CRBN, Era/VHL, Era/XIP, BRM/VHL, TGFbR2/CRBN, other examples are described in [177].

In certain embodiments, the toxin maybe an anti-inflammatory agent. In the treatment of immunological disease (inflammation associated with various diseases), glucocorticoid receptor modulators (GRMs) are often the first line of treatment. However, GRM can cause musculoskeletal (osteoporosis and decreased bone density), endocrine, and gastrointestinal side effects and other toxicities, limiting their beneficial therapeutic effects (especially in long-term use). Multiple medicinal chemistry programs have targeted small molecule selective glucocorticoid receptor modulators which would minimize GR transactivation (believed to be responsible for the unwanted side effects) while maintaining GR transrepression (believed to be responsible for the desired anti-inflammatory effects). Exemplary glucocorticoid receptor modulators are dexamethasone, prednisolone, and budesonide. Further examples are described in [178,179], WO 2017/062271, WO2017/210471, WO2019/136487, WO2022/150637.

In certain embodiments the toxin may be an antimetabolite. Antimetabolites are anticancer agents that are analogues of naturally occurring essential metabolites. They work by either blocking biochemical pathways essential for cell growth and division i.e., as enzyme inhibitors) or by incorporating themselves into nucleic acids (i.e., DNA or RNA) and act as 'false substrates' for relevant polymerases, thus blocking relevant down-stream processes such as replication and transcription. Although the enzymes inhibited by antimetabolites are also present in normal cells, some selectivity towards cancer cells is possible due to their faster cell division rates.

Most antimetabolites interfere with nucleic acid synthesis and the production of DNA or RNA by two main mechanisms: By competing for sites of enzymes that participate in essential biosynthetic processes or by incorporating into nucleic acids, inhibiting their normal function and triggering apoptosis. One class of antimetabolites are the antifolates, these bind tightly to dihydrofolate reductase (DHFR) thereby inhibiting folate metabolism. Through this inhibition, thymidylate synthesis is blocked, and thus, purine biosynthesis which can then no longer be incorporated into DNA; examples of antifolates include methotrexate, pemetrexed, pralatrexate, raltitrexed, nolatrexed, lometrexol, ZD9331, PT523. Purine antimetabolites inhibit several enzymes at various points in the purine

synthesis pathway and examples include 6-mercaptopurine, azathioprine, fludarabine phosphate, cladribine, clofarabine, nelarabine. Similar to the purine antimetabolites are the pyrimidine antimetabolites, these inhibit the synthesis of DNA in the S-phase and block the movement of cells through the G1/S part of the cell cycle. Exemplary drugs include 5-fluoroucil, tegafur, capecitabine, doxifluridine, cytarabine, gemcitabine, and decitabine, azacytidine [180-182].

In certain embodiments the toxin maybe a N-myristolytransferase (NMT) inhibitor. Myristoylation, is a lipid modification to a specific group of proteins and involves the N-terminal modification of proteins with myristic acid, a 14-carbon fatty acid, that allows them to interact with other proteins or membranes. Myristoylation plays vital roles in protein–protein interactions, signal transduction, immune regulation and tumour development. It is catalysed by the enzyme *N*-myristoyltransferase (NMT) which introduces irreversible changes to human proteins. NMT inhibitors have been shown to inhibit the viability and growth of various cancers and represent a novel class of ADC payloads that exploit cancer cell dependency on myristloylated proteins [183]. Exemplary small-molecule NMT inhibitors are described in WO 2022/058745.

In some embodiments, the payload is a microtubule inhibitor (MTI), a DNA-damaging agent, a topoisomerase inhibitor, a steroid, a tyrosine kinase inhibitor, or an immuno-modulatory drug. In some embodiments, the payload is an MTI, a DNA-damaging agent, or a topoisomerase inhibitor.

In some embodiments, the MTI is an auristatin or a derivative thereof. In some embodiments, the auristatin is mono-methyl auristatin E (MMAE) or mono-methyl auristatin F (MMAF). In some embodiments, the DNA-damaging agent is a nicking agent, an alkylator, or an intercalating agent. In some embodiments, the topoisomerase inhibitor is a camptothecin or a derivative thereof. In some embodiments, the steroid is desxamethasone. In some embodiments, the tyrosine kinase inhibitor is nintedanib. In some embodiments, the immuno-modulatory drug is a Toll-Like Receptor 7/8 agonist drug.

In some embodiments, the antigen-binding fragment is a single chain Fv and the payload is MMAE, and wherein the payload is coupled to the scFv with a coupling ratio (payload:scFv) of 6:1.

In some embodiments, the antigen-binding fragment is a single chain Fv and the payload is a mono-methyl auristatin E (MMAE) comprising a glucuronide and branched PEG linker, wherein the MMAE is conjugated onto surface lysine residues of the scFv.

Specific examples of compounds according to the invention include, but are not limited to, where:

(i) the antigen-binding fragment is an scFv and the payload is MMAE;
(ii) the antigen-binding fragment is an scFv and the payload is MMAF;
(iii) the antigen-binding fragment is an scFv and the payload is SN38;
(iv) the antigen-binding fragment is an scFv and the payload is exatecan;
(v) the antigen-binding fragment is an scFv and the payload is Dxd;
(vi) the antigen-binding fragment is an scFv and the payload is belotecan;
(vii) the antigen-binding fragment is an scFv and the payload is triplotide;
(viii) the antigen-binding fragment is an scFv and the payload is nintedanib;
(ix) the antigen-binding fragment is an scFv and the payload is dexamethasone;
(x) the antigen-binding fragment is an scFv and the payload is of N^1-benzylamino imidazoquinoline;
(xi) the antigen-binding fragment is an scFv and the payload is GENZ-644282.

In some embodiments, the payload is conjugated to the antibody or antigen-binding fragment thereof via a linker.

In the present invention, the term 'linker' refers to any chemical moiety capable of linking a payload as described to an antibody or antigen binding fragment thereof. The linkers may be monovalent such that they covalently link a single payload to a single site on the antibody fragment, or the linker maybe polyvalent such that they link more than one payload to a single site on the antibody fragment. The linkers connect the payload to the antibody fragment by forming a covalent linkage to the payload at one location and a covalent linkage to the antibody fragment at another. The covalent linkages are formed by reaction between functional groups on the linker and functional groups on the payload and antibody fragments.

The term 'linker' includes (i) unconjugated forms of the linker that include a functional group capable of covalently linking the linker to the payload and a functional group capable of covalently linking the linker to the antibody fragment (ii) partially conjugated forms of the linker that includes a functional group capable of covalently linking the linker to the antibody fragment that is covalently linked to a payload, or *vice versa,* and (iii) fully conjugated forms of the linker that is covalently linked to both payload and antibody fragment.

The linker may be chemically or biologically stable or resistant to cleavage (a 'non-cleavable linker') or the linker may be susceptible to cleavage or include linkages that are designed to release the payload upon internalisation within the cell (a 'cleavable linker'). These cleavable linkers are designed to cleave and/or self-immolate or otherwise breakdown specifically or non-specifically inside cells. The term 'self-immolate' refers to an at least bifunctional molecule that can be included in a linker that degrades spontaneously after an initial reaction has taken place and thereby releasing the payload. Polyvalent linkers that may be used to link many payloads to a single antibody molecule include Mersanas Fleximer™ technology which incorporated payloads into a solubilising polyacetal backbone via a sequence of ester bonds, other approaches use dendritic type linkers.

Cleavable linkers

In certain embodiments, the linker is cleavable *in vivo*. Cleavable linkers may include chemically or enzymatically unstable or degradable linkages. Cleavable linkers generally rely on processes inside cells to liberate the payload, such as reduction in the cytoplasm, acid induced cleavage in the lysosomes or endosomes, or cleavage by specific proteases or other proteolytic enzymes within the cell [184]. In certain embodiments, a linker comprises a chemically labile group such as hydrazone and/or disulphide groups. These types of linkers exploit differential properties between the plasma and some cytoplasmic compartments. The intracellular conditions to facilitate drug release for hydrazone containing linkers are the acidic environment of endosomes and lysosomes, while disulphide containing linkers are reduced in the cytosol, which contain high concentrations of reductive agents like glutathione.

Acid cleavable linkers aim to exploit the acidity of the endosomes (pH 5.5-6.2) and lysosomes (pH 4.5-5.0) whilst maintaining stability in circulation at pH 7.4. Acid-labile groups such as hydrazone remain intact during systemic circulation in the blood's neutral pH and undergo hydrolysis, releasing the payload once internalised into the endosome and lysosome compartments of the cell. Other acid sensitive functional groups used in linkers include a carbonates and esters.

Disulphide containing linkers are designed to release the payload upon internalisation inside cells, they thermodynamically stable at physiological pH but are susceptible to nucleophilic attack from thiols. In blood plasma, the dominant thiol species is the reduced form of human serum albumin (HSA), however its reactivity towards large molecules is hampered because the free thiol-containing residue (Cys34) is in a crevice and has limited solvent exposure. In contrast, the cytosol contains high levels of glutathione, a thiol-

containing small molecule tripeptide. This difference between the reductive potential of the blood plasma and the cytosol enables selective intracellular release of the payload. Also, tumours can have hypoxic regions, resulting in enhanced or elevated levels of reductive enzymes and higher glutathione concentrations. The *in vivo* stability of disulphide linkers may be further enhanced by chemical modification of the linker, e.g., increasing steric protection around the disulphide which makes the linker less susceptible to reduction.

Enzyme cleavable linkers utilise the high or elevated levels of unique hydrolytic enzymes like cathepsins that reside in the lysosomes of cells and offer an opportunity for the selective cleavage of linkers and the intracellular release of the payload [185]. Such linkers are typically peptide-based or include peptidic regions that act as substrates for these enzymes. Cathepsin B is a ubiquitous cysteine protease whose properties do not differ very much from species to species. It is never found extracellularly, except in pathological conditions such as metastatic tumours. Therefore, conjugates produced with cathepsin B-cleavable linkers are likely to be stable in circulation. Release of a drug from an antibody occurs specifically due to the action of lysosomal proteases, e.g, cathepsin and plasmin.

Exemplary cleavable peptides that can be used in accordance with the present invention include, but are not limited to dipeptides, tripeptides, tetrapeptides and pentapeptides. Dipeptides are often preferred over longer peptides due to the hydrophobicity of longer peptides. Exemplary dipeptides that may be used in some embodiments of the invention include but are not limited to alanine-alanine (ala-ala), valine-alanine (val-ala), valine-citrulline (val-cit), alanine-phenylalanine (ala-phe), phenylalanine-lysine (phe-lys), phenlyalanine-homolysine (phe-homolys) and N-metyl-valine-citrulline(Me-val-cit). Exemplary tripeptides include but are not limited to glycine-valine-citrulline (gly-val-cit), glycine-glycine-glycine (gly-gly-gly), valine-lysine-glycine (val-lys-gly) and alanine-alanine-alanine (ala-ala-ala). Exemplary tetrapeptides include but are not limited to glycine-glycine-phenylalanine-glycine (gly-gly-phe-gly) and glycine-phenylalanine-leucine-glycine (gly-phe-leu-gly).

A peptide may comprise naturally occurring and/or non-natural amino acid residues. The term "naturally occurring amino acid" refer to Ala, Asp, Cys, Glu, Phe, Gly, His, Ile, Lys, Leu, Met, Asn, Pro, Gln, Arg, Ser, Thr, Val, Trp, and Tyr. "Non-natural amino acids" (i.e., amino acids that do not occur naturally) include, by way of non-limiting examples, homoserine, homoarginine, citrulline, phenylglycine, taurine, iodotyrosine, seleno-cysteine, norleucine (Nle), norvaline (Nva), beta-alanine, L- or D-naphthalanine, ornithine (Orn), and the like. Peptides can be designed and optimized for enzymatic cleavage by a

particular enzyme, for example, a tumour-associated protease, cathepsin B, C and D, or a plasmin protease.

Amino acids also include the D-forms of natural and non-natural amino acids. "D-" designates an amino acid having the "D" (dextrorotary) configuration, as opposed to the configuration in the naturally occurring ("L-") amino acids. A variety of di-, tri-and tetrapeptides cleavable linkers have been described that link various payloads to antibodies [185,186], WO2019/195665.

The linker described herein may be an enzymatically cleavable linker. Enzymatically cleavable linkers may include a self-immolative spacer to spatially separate the drug from the site of enzymatic cleavage and is a di- or tri-functional chemical moiety that is capable of covalently linking together two or three chemical moieties. The direct attachment of a payload to a peptide linker can impair enzymatic release or result in proteolytic release of an amino acid adduct of the payload, thereby impairing its activity. The use of a self-immolative spacer allows for the elimination of the fully active, chemically unmodified drug upon amide bond hydrolysis. A typical self-immolative spacer is the bifunctional para-aminobenzyl alcohol group, which is linked to the peptide through the amino group, forming an amide bond, while amine containing payloads may be attached through carbamate functionalities to the benzylic hydroxyl group of the linker (PABC). The resulting prodrugs are activated upon protease-mediated cleavage (for example with cathepsin B), payload release is thermodynamically driven and takes place after amide bond hydrolysis via either an electron cascade for PABC type linkers (1,4-, 1,6-, or 1,8-elimination) or an intramolecular nucleophilic cyclisation. 1,6-elimination from a typical PABC spacer result in the release of the unmodified payload, carbon dioxide, an aza-quinone methide and remnants of the linker group [187]. The self-immolative spacer maintains enzymic activity, independent from the payload and variants of the self-immolative spacer where the PABC has been replaced by a heterocyclic spacer like amino-thiazole have also been described in US7754681.

Glycosidase-cleavable linkers

In some embodiments, the linker in accordance with the present invention is a glycosidase-cleavable linker. Another class of proteolytic enzymes that are only found in lysosomes are the β-glucuronidases. β-glucuronidases are hydrolytic enzymes in the glycosidase class that catalyse the breakdown of β-glucuronic acid residues in polysaccharides. Their exclusivity and abundance in the lysosomal compartment of cells, overexpression in some tumour types and little enzyme activity outside of cells make them ideal candidates for use in enzyme cleavable linkers [188]. The incorporation of a β-glucuronic acid moiety

into a linker, results in facile release of the drug through cleavage of the β-glucuronide-glycosidic bond by the lysosomal enzyme β-glucuronidase. Also, β-Glucuronic acid-based linkers can also be linked to a self-immolative spacer (similar to the PABC used with peptidic linkers) but using a para-hydroxybenzyl alcohol group. However, in this case attachment to the antibody is achieved through substituents on the space molecule (an amine or carboxylic acid group) *ortho-* to the enzyme-cleavable moiety.

A variety of cleavable β-glucuronic acid-based linkers useful for linking drugs such as auristatins, camptothecins, doxorubicin analogues, CBI minor-groove binders and cryptophycins to antibodies have been described [189-191]. Due to the hydrophilic nature of β-glucuronides, β-glucuronic acid-based linkers may be used to minimise or overcome payload induced aggregation of antibody conjugates, especially when trying to achieve high drug loadings with very hydrophobic drugs. The hydrophilicity of β-glucuronic acid-based linkers and the overall antibody-drug conjugate can be further increase by the incorporation of linear or branched polyethylene glycols, crown or aza-crown ethers, cyclodextrins, polysarcosines or chito-oligosaccharides like Chetosensar™ through branching points on the linker. This can greatly reduce plasma clearance, thereby increasing exposure and *in vivo* efficacy [192-195].

By modifying the β-glucuronide linker to contain a dimethylethylene diamine (DMED) self-immolative spacer phenolic or alcohol containing drugs could be enzymatically released. Drug release involves enzymatic deglucuronidation, 1,6-elimination, decarboxylation, and cyclization of the DMED carbamate to the cyclic urea to liberate the free phenol or alcohol functionalised drug [196]. Similar to β-glucuronidase cleavable linkers, β-galactosidase cleavable linkers have also been described. This lysosomal enzyme is also over expressed in certain tumour types and is analogous to β-glucuronidase in its hydrolytic activity but instead hydrolyses β-galactoside [197].

Other lysosomal enzymes that have been exploited as enzymatic triggers to release payloads in cancer cells include lysosomal acid pyrophosphatase and acid phosphatase, these enzymes hydrolyse pyrophosphates and terminal mono-phosphates respectively to their parent alcohols. A pyrophosphate containing linker has been described for use with alcohol-linked glucocorticoid payloads [198].

Sulfatases are another group of lysosomal enzymes which have high activity in the lysosome and low activity in human and rodent plasma. A number of different sulfatases reside in the lysosome, catalysing the hydrolysis of alkylsulfate esters to alcohols but they also display arylsulfatase activity. Arylsulfate linker motifs have been designed that after

hydrolysis, a alkoxybenzyl carbamate is revealed which is primed for spontaneous 1,6-elimination of an amine containing payload [199].

Non-cleavable Linkers

In some embodiments, the linker for use in the present invention is a non-cleavable linker. Unlike cleavable linkers, non-cleavable linkers do not have a triggerable moiety which ultimately separates the active drug from the antibody through a specific cleavage mechanism but instead release an active metabolite upon complete digestion of the antibody component after internalisation and lysosomal processing

With a non-cleavable linker, the linker, along with the amino acid residue of the antibody to which the linker is attached, remains connected to the payload, and this whole construct becomes the active metabolite. Since the linker stays attached to the drug after cellular processing, it must be linked at a position which does not interfere significantly with binding of the drug to its target (activity) [200].

Bioconjugation

In some embodiments, the payload is directly conjugated to the antibody or antigen-binding fragment thereof at an amino acid. In some embodiments, the direct coupling is via a lysine or cysteine residue on the surface of the antibody or antigen-binding fragment thereof. In some preferred embodiments, the direct coupling is via a lysine residue on the surface of the antibody or antigen-binding fragment thereof.

In some embodiments, the payload is indirectly conjugated to the antibody or antigen-binding fragment thereof at an amino acid, which may be a lysine or cysteine reside. In some embodiments, the indirect coupling is via a thiol or maleimide.

There are many ways to conjugate cytotoxic drugs to antibodies and antibody fragments [76,201]. This is summarised in Table 2. Lysine residues are favourable for conjugation because they can be present multiply on the surface of antibodies without causing detrimental effects such as unwanted cross-linking and due to the nucleophilicity of the ε-amino side chain (see also WO2016/046574 for example). For example, conjugation onto lysines can be direct (Table 2), using drugs or drug-linkers that possess and N- hydroxy-succinimide esters (and their more soluble 3-sulfonated analogues), a tetrafluorophenyl ester (and its sulphonated analogue) pentafluorophenyl ester, an isothiocyanate, a β-lactam reactive group or a mixed anhydride. Other lesser known/used direct lysine conjugations involve sulfonyl halides, acylfluorides, iminoboronates, diazonium salts, aldehydes and sulphonylacrylates [202]. Indirect methods for lysine conjugation include

derivatising the amino group with a bifunctional linker (such as those available from Pierce Chemicals (Thermo) and Quanta Bioscience) to generate a secondary reactive group, such as 2-iminothiolane to generate a reactive thiol for conjugating to drugs or drug-linkers with thiol or maleimide reactive groups. Some lysine residues may be particularly prone to conjugation owing to enhanced nucleophilicity due to the microenvironment around that residue [203]. This allows for more site-selective modifications of lysine residues via a two-step methodology such as via a phospha-Mannich reaction whereby the lysine amine first undergoes imine formation with an aldehyde reagent, followed by attack of the imine with a nucleophilic triethylphosphite reagent to generate a stable link. Further functionalisation can then be carried out using a hydroxylamine terminated payload [204]. Reactive lysines can also be modified with methylsulfone phenyloxadiazole (MS-PODA) modified payloads. Further conjugation methods are known such as native chemical ligation [205], site specific conjugation including using enzymes [206]. Enzymes can provide exquisite specificity for bioconjugation, and one example of a lysine-targeting enzyme is sortase A from *Staphylococcus aureus,* which catalyses the covalent ligation between two amino acids via an isopeptide bond. Sortase A recognises the primary acid sequence LPXTG – it first cleaves the amide bond between threonine and glycine, undergoing a thioesterification with its active site cysteine and the carbonyl group of threonine. This thioester can be substituted by an amino group to form a stable amide bond. It is possible to use this activity to achieve site-specific modification of lysine residues in a wide range of proteins. Another enzyme that can be used for bioconjugation is microbial transglutaminase (MTG), which catalyses the formation of amide bonds between the γ-carboxyamide group of glutamine and the ε-amine group of lysine. This occurs by initial thioesterification, by attack of the active site cysteine on the γ-carboxyamide and loss of ammonia; and finally amide formation by reaction with the primary amine of the lysine. MTG is a cheap, readily available enzyme that functions under a diverse range of different temperatures, salt concentrations, and pH. Using this approach that one can utilise MTG into targeting lysine residues as acyl acceptors on a antibodies and proteins. Another reported chemoenzymatic method for lysine acylation is called 'lysine acylation using conjugation enzymes' (LACE). This approach uses a small ubiquitin-like modifier (SUMO)-conjugating Ubc9 enzyme, which can identify an IKXE sequence on proteins, alongside a functionalised thioester as an acyl donor. This strategy enables the site-selective modification of the lysine residue within the IKXE tag. Another approach one can use, involves transforming the ε-amino sidechain of lysine into a biorthogonal moiety either directly by transforming the ε-amino group into an azide or by a two-step approach involving a bis-functional cross-linker carrying a lysine reactive group and a biorthogonal reactive moiety. These bifunctional linkers will be well known to the skilled person.

Cysteine residues also offer a particularly attractive target for protein bioconjugation due to the exceptionally high nucleophilicity of the deprotonated thiolate side chain at physiological pH and the ability via mutagenesis to insert cysteine residues. The go-to method for cysteine modification usually remains the use of maleimides. Cysteine modification occurs most commonly by 1,4-conjugate addition to N-substituted maleimides. Maleimides are particularly attractive reagents due to their synthetic accessibility and rapid reaction rates with cysteine under mild conditions Maleimide reagents allow extraordinary fast labelling with acceptable cysteine selectivity. Furthermore, a variety of maleimide derivatives, including dyes, affinity probes and crosslinkers, are commercially available, allowing easy access without the need of synthetic expertise. However, maleimides suffer from stability issues, thus rendering conjugation products unstable under certain conditions. Although maleimides are the most common cysteine-selective reagents, a variety of novel linkers have been used to functionalise cysteines, avoiding the instability issues of traditional maleimides, for example, iodoacetamides bromomaleimides, carbonylacrylic reagents and N-alkyl vinylpyridine salts [206,207].

Recent conjugation methods include the use of methylsulphonylphenyloxadiazole reactive linkers to form thioethers [208] and disulphide bridging technologies.

In recent years, genetic code expansion (GCE) techniques have enabled the incorporation of non-canonical amino acids (ncAAs) into antibody sequences, resulting in an efficient approach to the site-specific modification of antibodies through bioorthogonal bioconjugation. The most common bioorthogonal approach for bioconjugation involves 'click' chemistry. For various purposes, there are several types of reactions under 'click' chemistry including strain-promoted azido-alkyne cycloaddition (SPAAC) Cu-catalyzed azido-alkyne cycloaddition (CuAAC), Staudinger ligation, cycloaddition reactions between a tetrazine and a trans-alkene or a strained alkyne (IeDDA), reactions between an isocyanopropyl group and tetrazine and Diels–Alder reactions between a cyclopentadienone and a strained alkyne [209]. Other biorthogonal chemistries involve oxime-ligation onto para-acetyl-phenylalanine (ncAA).

Other bioconjugation strategies involve tyrosine selective labelling via the use of a tyrosine-click reaction [210]. Site-selective histidine modification which poses a challenge due to competition from other more nucleophilic residues such as lysine or cysteine has been developed involving a "chemical linchpin". This linchpin is a bifunctional reagent containing both aldehyde and epoxide reactive groups. First, all available lysine residues were transiently protected via reaction with the aldehyde moiety. Next, proximal histidine

residues react with the pendant epoxide to afford irreversible modification. Finally, reformation of the aldehyde enables modification of this installed bioorthogonal handle via oxime formation. Selective modification of arginine residues via condensation of its guanidine side chain with a 4-azidophenyl glyoxal (APG) reagent enables the direct introduction of a bioorthogonal azido group onto the antibody, which can subsequently be modified via SPAAC reaction to conjugate various payloads [211].

In some embodiments, the payload is conjugated to the antibody or antigen-binding fragment thereof by direct conjugation of payloads bearing an N- hydroxy-succinimide ester to multiple lysine residues. In some other embodiments, the payload is conjugated to the antibody or antigen-binding fragment thereof by indirect conjugation to lysine residues wherein the cross-linker SMCC is used to modify surface lysine residues, generating a reducible thiol for conjugating to drugs or drug-linkers bearing a thiol or maleimide group. Mixtures of drugs with the same reactive group can be used in the chemical conjugation reaction to generate conjugates with more than one cytotoxic therapeutic drug type or a combination of therapeutic drug and diagnostic agent such as a fluorescent dye [212]. Such conjugates could potentially be useful for overcoming drug resistance or allowing combined imaging and treatment (theranostic).

Therefore, in some embodiments, the antibody or antigen-binding fragment thereof is conjugated to multiple types of payloads. For example, the same antibody or antigen-binding fragment may be conjugated to two types of payloads, three types of payloads, four types of payloads, five types of payloads, or six types of payloads.

Table 2: Bonds for linking groups-Direct Conjugation

Reactive group on protein	**Complementary group on drug**	**Resulting linking group**
Amines/Anilines	Activated esters	Amides
	Cyanates	Ureas
	Isothiocyanates	Thioureas
	Imidoester	Amidines
	Activated carboxylic acids	Amides
	Acyl azides	Amides
	Acyl halides	Amides
	Acyl nitriles	Amides
	Aryl halides	Aryl amines
	Alkyl halides	Alkyl amines

	Anhydrides	Amides/Imides
	Aldehydes	Imines
	Sulphonyl halides	Sulphonamides
	Sulphonate esters	Alkyl amines
	Halotriazines	Aminotriazines
	Sulphonylacrylates	Amines
	α,β-unsaturated sulphonamide	Amines
	β-lactams	Amides
Amines	Epoxides	Alkyl amines
Thiols	Maleimides	Thioethers
	Haloacetamides	Thioethers
	Alkyl halides	Thioethers
	Aryl halides	Aryl thioether
	Acrylamides	Thioethers
	Aziridines	Thioethers
	Epoxides	Thioethers
	Disulphides	Disulphides
	Vinylsulphones	Thioethers
	Ethynylphosphonamidates	Thioethers
Alcohols/Phenols	Acyl halides	Esters
	Acyl nitriles	Esters
	Alkyl halides	Ethers
	Anhydrides	Esters
	Halotriazines	Triazinyl ethers
	Isocyanates	Urethanes/Carbamates
Alcohols	Activated carboxylic acids	Esters
	Phosphoramidites	Phosphite esters
	Silyl halides	Silyl ethers
	Epoxides	Ethers
Carboxylic acids	Alkyl halides	Esters
	Epoxides	Esters
	Diazoalkanes	Esters
Activated carboxylic acids	Amines/Anilines	Amides
	Alcohols	Esters
	Hydrazines	Hydrazides

Aldehydes/Ketones	Hydrazines	Hydrazones
	Hydroxyamines	Oximes
	Amines	Imines
Ketone (unnatural amino acids))	Hydroxylamines	Oximes
Azides (unnatural amino acids)	Alkynes	1,2,3-triazoles
	Strained alkynes	1,2,3-triazoles
Alkyne	Tetrazine	Pyridazine
Aldehyde (formyl glycine)	Hydrazines	Azacarboline

Combination therapies

Combination therapy is important for maximizing patient outcomes by combining different mechanisms of drug action to obtain a larger therapeutic effect without significantly increasing adverse effects and thus widening the therapeutic window. Combining the action of trastuzumab antibody with chemotherapy lapatinib is well known in the art and accepted clinical practice for breast cancer (https://www.esmo.org/guidelines/guidelines-by-topic/breast-cancer). Immuno-oncology drugs, notably checkpoint inhibitors (CPI) such as anti-CTLA4 (ipilimumab), anti-PD1 (nivolumab, pembrolizumab) and anti-PDL1 (atezolizumab) have transformed the landscape of oncology therapy for diseases such as melanoma, lung and renal cancer by reversing tumour-mediated immune suppression [172]. However, not all patients benefit from durable responses and immune-oncology drugs are being increasingly used in combination. CPI drugs combined with standard-of-care cytotoxic chemotherapy can lead to increased toxicity, therefore CPI drugs combined with targeted chemotherapy (i.e., antibody drug conjugates) have gained much interest [213]. ADCs are known to kill tumours by a variety of mechanisms in addition to the concept of delivering a damaging payload to a targeted cell. One key mechanism the 'immunogenic cell death' where the payload-mediated cytotoxicity causes tumour cells to release immunogenic signals that elicit a separate adaptive and innate immune response.

Damage-associate molecular patterns (DAMPs) released by tumour cells dying due to ADC killing include signals such as heat-shock proteins, calreticulin, ATP and high mobility group-1 (HMGB1) proteins which stimulated immune-mediated clearance. Less than 10% of chemotherapy drugs are ICD-inducing, but payloads such as auristatins and anthracyclins stimulate immune cells *in vitro* and *in vivo* and can enhance the effect of CPIs. Tubulin destabilizing payloads such as maytanines can directly activate and stimulate the maturation of dendritic cells, thus enhancing the immune system. Taken together, there is a rationale for killing tumours with an ADC which enhances immunity which is

further enhanced by IO drugs. This has been demonstrated in preclinical animal models [214]. Immunoglobulin-based ADCs often retain inherent immune-activating functions due to the presence of an IgG1 Fc-domain. This can elicit toxicities and damage the specific cells that are required for immune function. For example, Fc-interaction with megakaryocytes Fc-receptors is one reason why ADCs cause dose-limiting thrombocytopenia [15,64,213]. Therefore, many developers have chosen to use immunologically-silent Fc domain (e.g. IgG4) to reduce inadvertent immune cell damage. Antibody fragments such as single-chain Fvs lack an Fc-domain and are not expected to cause Fc/Fc-gamma-receptor mediated toxicities. There is therefore a rationale for combining cMET FDCs in this invention with IO/CPI drugs which may elicit a superior combination effect compared to ADCs due to the lack of an Fc-domain.

Clinical trials in breast, urothelial, lung and ovarian cancer are ongoing with promising results in terms of early responses and safety profile. Cancers which do not respond well to IO drugs, the so-called immunologically cold cancers (low tumour mutational burden such as ovarian or prostate cancer [215]), could benefit more significantly from an ADC-mediated stimulation of the immune system.

Therefore, in some embodiments, the antibodies, antigen-binding fragments and ADCs disclosed herein may be combined in a formulation with one or more of the following: a chemotherapeutic agent, an immune-oncology drug, a monoclonal antibody, or a checkpoint inhibitor.

Combination with other therapeutic modalities such as CART-cells, gene therapy, other forms of chemotherapy, other forms of monoclonal antibody therapy are also possible with the antibodies, antigen-binding fragments and ADCs disclosed herein.

Another aspect of the invention provides a pharmaceutical composition comprising the antibody or antigen-binding fragment or ADC disclosed herein and a pharmaceutically-acceptable carrier, excipient or diluent.

Another aspect of the invention provides an antibody or antigen-binding fragment or ADC or pharmaceutical composition as defined herein for use in medicine.

Another aspect of the invention provides an antibody or antigen-binding fragment or pharmaceutical composition or ADC as defined herein for use in the diagnosis, treatment and/or prevention of a disease. In some embodiments, the disease is selected from cancer, benign tumours, infectious diseases including bacterial, viral, fungal,

trypanosome, nematode and prion infections, cardiovascular disease, autoimmune disease.

Another aspect of the invention provides an antibody or antigen-binding fragment or ADC or pharmaceutical composition as defined herein for use in the manufacture of a medicament for the treatment and/or prevention of a disease selected from cancer, benign tumours, infectious diseases including bacterial, viral, fungal, trypanosome, nematode and prion infections, cardiovascular disease, and autoimmune disease.

In some preferred embodiments, the disease is cancer. In some preferred embodiments, the disease is idiopathic pulmonary fibrosis (IPF).

In some embodiments, the disease is cancer of the colon, lung, breast, head/neck, prostate, skin, stomach/gastrointestinal, oesophageal, bladder, glioma, renal, ovarian, thyroid and bone. In some preferred embodiments, the disease is a gastric cancer or gastric tumour.

Another aspect of the invention provides a process of making a compound (i.e. an ADC or FDC) as defined herein comprising the steps of:

(i) providing a payload as defined herein;
(ii) providing the antibody or antigen-binding fragment as defined herein;
(iii) conjugating the payload and the antibody or antigen binding fragment thereof.

In some embodiments, the conjugation takes place in the presence of at least one polar aprotic solvent and an aqueous buffer. In some embodiments, the conjugation is via a linker between the payload and the antibody or antigen-binding fragment. The linker can be any linker as described herein.

In some embodiments, the process comprises the step of:

(iv) combining the compound with a pharmaceutically-acceptable carrier to form a pharmaceutical composition.

References

1. Minchinton AI, Tannock IF. Nat Rev Cancer. 2006 6:583-92.
2. Lei ZN, Tian Q, Teng QX, Wurpel JND, Zeng L, Pan Y, Chen ZS. MedComm 2023;4:e265.
3. Brown JM and Giaccia AJ. Cancer Research. 1998; 58:1408-1416.
4. Cruz E and Kayser V. Biologics: Target and Therapy. 2019; 13: 33-51

5. Fu Z, Li S, Han S, Shi C, Zhang Y. Signal Transduct Target Ther. 2022;7:93.
6. Teicher BA, Morris J. Curr Cancer Drug Targets. 2022;22(6):463-529..
7. Deonarain MP. Drug Discov. Today Technol. 2018, 30:47-53.
8. Baker JHE, Kyle AH, Reinsberg SA, et al. Clin Exp Metastasis. 2018;35:691–705
9. Thurber GM, Schmidt MM, Wittrup KD. Adv Drug Deliv Rev. 2008;60:1421–1434.
10. Fujimori K, Covell DG, Fletcher JE, Weinstein. J Nucl Med. 1990;31:1191–1198
11. Deonarain MP, Yahioglu G. Expert Opin Drug Discov. 2021,16:613-624.
12. Chiu ML, Goulet DR, Teplyakov A, Gilliland GL. Antibody Structure and Function: The Basis for Engineering Therapeutics. Antibodies (Basel). 2019,8:55
13. Colombo R and Rich JR Cancer Cell 2022;40:1255-1263.
14. Li F, Emmerton KK, Jonas M, et al. Cancer Res. 2016;76(9):2710–2719.
15. Nguyen TD, Bordeau BM, Balthasar JP. Cancers (Basel). 2023;15:713.
16. Tumey L.N. in, Innovations for Next-Generation Antibody-Drug Conjugates, Cancer Drug Discovery and Development, Springer International Publishing, 2018. pp187 (M. Damelin, Ed)
17. Conilh L, Sadilkova L et al. J. Haemaol Oncol 2023;16:3
18. Von Arx C, De Placido P et al Cancer Treat Rev. 2023;113:102500.
19. Petrini I. Annals Trans Med 2015, 3;82.
20. Rivas S et al. Int J Mol Sci. 2022, 23;13898
21. Raghav K et al. Cancer Treat Rev, 2018, 66;95-103.
22. Comoglio PM et al. Nat Rev cancer. 2018, 18; 341
23. Peng Z, Zhu Y, Wang Q, et al., PLoS One. 2014; 9(1).
24. Lu J and Teng L. Int. J. of Molecular Medicine. 2013; 32:1247-1254.
25. Wu ZW, Sha Y, Chen Q et al., World Journal of Clinical Cases. 2021; 9: 3350-3355.
26. Salgia R. Mol. Can. Ther. 2017; 16(4).
27. Wu YL, Soo RA et al. Cancer Treat Rev. 2017 Dec;61:70-81.
28. Mesteri I, Schoppmann SF, et al., European Journal of Cancer. 2014; 50(7): 1354-1360.
29. Chan E, Alkhasawneh A, et al., Journal of Gastrointestinal Oncology. 2016; 7(6): 838-847.
30. Wang H, Tan M, et al., Int. J. Molecular Sciences. 2015; 16(2): 3391-3404.
31. Yamamoto S, Tsuda Hitoshi, Miyai K. *Modern Pathology.* 2011; 24: 1146-1155.
32. Kim JH, Kim JB and Kim HS. Oncotarget. 2017; 8(43): 75478-75487.
33. Macher-Goeppinger S, Keith M, Endris V et al., Oncotarget. 2017; 8: 1046-1057.
34. Zanetti A, Stoppacciaro A, et al., Journal of Pathology. 1998; 186: 287-291.
35. Gymnopoulos M, Betancourt O et al. J. Mol Oncol. 2020;14:54-68.
36. Vsiansky V, Gumulec J et al. Sci Rep. 2018;8:10370.
37. Szparecki G, Ilczuk T, et al., Folia Biologica (Praha). 2017; 63: 146-154.

38. Mukae Y, Miyata Y, Nakamura Y et al., Oncology Letters. 2020; 20(1): 135-144.
39. Jia L, Yang X, Tian W et al., Medical Science Monitor. 2018; 24: 8239-8249.
40. Melo Gagliato D, Fontes Jardim D, et al., *Clinical Breast Cancer.* 2014; 14(6): 468-474.
41. Ohara M, Saito K et al. Cancers (Basel). 2021;13:1104
42. Chen W, Wu S et al. Onco Targets Ther. 2021;14:4791-4804
43. Rath P, Lal B et al. Transl Oncol. 2013;6:104-11
44. Luan T and Yu Y. Int J Clin Exp Med. 2014;7:5583-7.
45. Lee SJ, Lee J et al. Clin Colorectal Cancer. 2018;17:165-169
46. Gayyed MF, Abd El-Maqsoud NM et al. J Gastrointest Oncol. 2015;6:618-27.
47. Yao HP, Tong XM, Hudson R, Wang MH. J Exp Clin Cancer Res. 2020;39:198
48. Knudsen BS and Edlund M. Adv Cancer Res. 2004;91:31-67
49. Immunohistochemistry in tumor diagnostics Tuffaha M, Guski H & Kristiansen G Eds), Springer Publishing 2018
50. Wang M et al. Annals Diag. Pathol 2018, 35;69-78.
51. Yao H-P et al. Drug Discovery Today, 2021, 26, 106-121.
52. Puccini A et al. Drug Safety, 2019; 42;211-233.
53. De Silva DM, Roy A, et al. Biochem Soc Trans. 2017;45:855-870.
54. Hughes VS & Siemann DW. Trends in Cancer, 2018, 4, 94-97
55. Bradley CA, Salto-Tellez M et al. Nat Rev Clin Oncol. 2017;14:562-576.
56. Vasalou C, Helmlinger G, Gomes B. PLoS One. 2015;10:e0118977
57. Wang J, Anderson MG et al. Clin Cancer Res. 2017;23:992-1000
58. Strickler JH, Weekes CD et al. J Clin Oncol. 2018;36:3298-3306.
59. Camidge DR, Barlesi F et al. J Clin Oncol. 2023 Feb 10;41(5):1105-1115.
60. Yang C, Zhao X et al. Xenobiotica. 2019;49:1097-1105.
61. Min B, Jin J et al. ACS Omega. 2020;5:25798-25809.
62. Groothuis PG, Jacobs DCH et al. Mol. Cancer Ther. 2023;22:765-777.
63. Comer F et al (2023). AZD9592: An EGFR-cMET bispecific antibody-drug conjugate (ADC) targeting key oncogenic drivers in non-small-cell lung cancer (NSCLC) and beyond. Cancer Research 83 (suppl) abtract 5736
64. Mahalingaiah PK, Ciurlionis R et al. Pharmacol Ther. 2019;200:110-125.
65. Dumontet C, Reichert JM et al. Nat Rev Drug Discov. 2023;22:641-661.
66. Stella GM, Gentile A et al. J Transl Med. 2016;14:256.
67. Canestaro WJ, Forrester SH et al. Mol Cancer Ther. 2013;12:2685-96
68. Fujita H, Miyadera K et al., Mol. Cancer Ther. 2013:12:2685-96
69. Koyama K, Goto H et al. Am J Respir Cell Mol Biol. 2019 Apr;60(4):478-487.
70. De Marco A. Microb Cell Fact. 2009, 8:26
71. Carter PJ. Nat Rev Immunol. 2006, 6: 343-57

72. Wozniak-Knopp, G et al. Protein Eng. Des. Sel. 2010, 23, 289-297
73. Wörn A & Plückthun A. J Mol Biol. 2001, 305:989-1010
74. Schaefer JV & Plückthun A. Protein Eng Des Sel. 2012, 25:485-506
75. Winter G et al., 1991, Nature 349:293-299
76. Ducry, L (Ed) (2013), Antibody-Drug Conjugates, Methods in Molecular Biology volume 1045, Humana Press
77. Behrens CR and Liu B. MAbs. 2014, 6:46-53.
78. Kelley LA & Sternberg MJ. Nat Protoc. 2009; 4: 363-71
79. Chames, P (Ed.), Antibody Engineering: Methods and Protocols, Second Edition, Methods in Molecular Biology, vol. 907, Chapter 1
80. Thompson JD et al., Nuc. Acid Res. 1994, 22:4673-4680
81. Orlandi R et al., Proc. Natl. Acad. Sci. U.S.A. 1989, 86:3833-3837;
82. Kohler D et al., 1975. Nature 256:4950497;
83. Kozbor D et al., 1985. J. Immunol. Methods 81:31-42;
84. Cote RJ et al., Proc. Natl. Acad. Sci. USA 1983, 80:2026-2030;
85. Cole SPC et al., Mol. Cell. Biol. 1984, 62:109-120.
86. Hurrell, J.G.R in Monoclonal Hybridoma Antibodies: Techniques and Applications", (CRC Press, 1982).
87. Harlow & Lane, 1988, Antibodies: A Laboratory Manual (Cold Spring Harbor Laboratory, New York).
88. Jones PT et al., 1986. Nature 321:522-525;
89. Riechmann L et al., 1988, Nature 332:323-329
90. Presta LG Curr. Op. Struct. Biol. 1992, 2:593-596).
91. Verhoeyen M et al., Science 1998, 239:1534-1536
92. Hoogenboom & Winter, 1991, J. Mol. Biol. 227:381
93. Marks JD et al., J. Mol. Biol. 1991, 222:581
94. Cole et al., 1985, In: Monoclonal antibodies and Cancer Therapy, Alan R. Liss, pp. 77
95. Boerner P et al., J. Immunol. 1991, 147:86-95.
96. Thuss-Patience PC, Shah MA et al., Lancet Oncol. 2017;18:640-653.
97. Lordick F, Allum W et al., Cancer Treat Rev. 2014;40:692-700.
98. Yver A, Agatsuma T, Soria JC. Ann Oncol. 2020;31:430-434.
99. Saber H, Leighton JK. Regul Toxicol Pharmacol. 2015;71:444-52.
100. Bartelink IH, Jones EF et al., Clin Pharmacol Ther. 2019 ;106:148-163.
101. Alberts, B et. al. in Molecular Biology of the Cell, Garland Science, Ney York, 4th edition, 2002, E. B. Garon
102. Pettit GR, Kamano Y et al., J. Am. Chem. Soc. 1987, 109(22), 6883-6885
103. E. Flahive, J. Srirangam, Anticancer Agents from Natural Products 2nd ed. CRC Press, 2011, 263-290

104. Kerbrat P, Dieras V et al., Eur. J. Cancer 2003, 39, 317-320
105. Chen H, Arnst KE, Miller DD, Li W Molecules, 2017, 22, 1281
106. Yu, T-W, H. G. Floss, G. M. Gragg and D. J. Newman. Anticancer Agents from Natural Products 2nd ed. CRC Press, 2011, 407-427
107. Zafar S, Armaghan M et al. Biomed. Pharmacother. 2023;165,115039
108. Remillard, S, Rebhun LI et al. Science (New York, NY. 1975;189(4207):1002–5
109. Oroudjev E, Lopus M et al. Mol. Can. Ther. 2010, 9(10), 2700-2713
110. Kupchan SM, Sneden AT et al. J. Med. Chem. 1978, 21(1), 31-37]
111. Moobery SL, Busquets L, Tien G Int. J. Cancer 1997, 73, 440-448
112. Trimurtulu G, Ohtani I, Patterson GML, Moore RE, Corbett TH, Valeriote FA, Demchik L J. Am. Chem. Soc., 1994, 116, 4729-4737
113. Smith CD, Zhang X et al., Cancer Res. 1994, 54, 3779-3784
114. Verma VA, Pillow TH et al., Bioorg. Med. Chem. Lett. 2015, 25(4), 864-868
115. Sasie F, Steinmetz H et al., J. Antibiot. 2000, 53, 879-885
116. Murray BC, Peterson MT, Fecik RA Nat. Prod. Reps. 2015, 32, 654-662
117. Ojima I, Geng X et al., J. Med. Chem. 2002, 45, 5620-5623
118. Fahy J Curr. Pharm. Design 2001, 7(13), 1181-1197
119. Laguzza BC, Nichols CL et al., J. Med. Chem. 1989, 32, 548-555
120. Hirata, S, Y, Uemura D Pure Appl. Chem. 1986, 58, 701-710
121. Cheng X, Li J et al., Mol. Cancer Ther. 2018, 17(12) 2665-2675
122. Goodin S, Kane MP, Rubin EH J. Clin. Oncol. 2004, 15(22), 15-25
123. Pommier Y ACS Chem. Biol. 2013, 8, 82-95
124. Iyer L and Ratain MJ Cancer Chemother. Pharmacol., 1998, 42, S31-S43
125. Wani MC, Nicholas AW et al., J. Med. Chem. 1987, 30, 1774-1779
126. Talukdar A, Kundu B et al., Eur. J. Med. Chem. 2022, 236, 114304
127. Tagakagi K, Dexheimer TS et al., Mol. Can. Ther. 2007, 6, 3229-3238
128. Kummar S, Chen A et al. Cancer Chemother. Pharmacol., 2016, 78, 73-81
129. Kurtzberg LS, Roth S et al. Clin. Can. Res. 2011, 17, 2777-2787
130. Nishida M, terayabashi T et al. Nat. Comm. Biology, 2022, 5, 982-995
131. Liang Z, Lei F et al. J. Med. Cem. 2022, 228, 113960
132. M. Broggini Top. Curr. Chem. 208, 283, 191
133. Watt PM and Hickson ID. Biochem. J. 1994, 303, 681-695
134. Broggini M, Anthracycline Chemistry II, Topics in Current Chemistry 2007, vol. 283, 191-206
135. Fortune JM and Osheroff N Proc. Nucleic Acid Res. Mol. Biol. 2000, 64, 221-253
136. Swift LP, Rephali A et al., Cancer Res. 2006, 66, 4863-4871
137. Tacar, O et. al. J. Pharm. Pharmacol. 2013, 61(8), 933-938
138. Swedan HK, Kassab AE et al., Bioorganic Chemistry 2023, 136, 106548

139. Yu SF, Zheng B et al., Clin. Cancer Res. 2015, 21, 3298–306
140. Geroni C, Ripamonti M et al. Cancer Res. 2001, 61, 1983-1990
141. Yu SF, Zheng B et al., Clin. Cancer Res. 2015, 21(14), 3298-306
142. Hanka LJ, Dietz A et al., J. Antibiot. 1978, 31, 1211–1217
143. Yao HP, Zhao H, Hudson R et al., Drug Disc. Today 2021, 26(8), 1857-1874
144. Beekman, A.M. et al. Cytotoxic Payloads for Antibody-Drug Conjugates, Drug Discovery Series no. 71, Ed. D. E. Thurston and P. M. Jackson, 2019, RSC, 187-208
145. Procopiou, G. et al. Cytotoxic Payloads for Antibody-Drug Conjugates, Drug Discovery Series no. 71, Ed. D. E. Thurston and P. M. Jackson, 2019, RSC, 209-240.
146. Mantaj J, Jackson PJM, Rahman KM, Thurston DE. Angew. Chem. Int. Ed. Engl. 2017, 56(2), 462-488
147. Hartley JA Expert Opin. Biol. Ther. 2021, 21(7), 931-943
148. Pillow, T.H and Tercel, M. Cytotoxic Payloads for Antibody-Drug Conjugates, Drug Discovery Series no. 71, Ed. D. E. Thurston and P. M. Jackson, 2019, RSC, 241-258
149. Pyysz, I, et. al. Cytotoxic Payloads for Antibody-Drug Conjugates, Drug Discovery Series no. 71, Ed. D. E. Thurston and P. M. Jackson, 2019, RSC, 137-165
150. Yang Q, Deng Z et al., J. Am. Chem. Soc. 2020, 142, 2532-2540
151. Denny WA Expt. Opin. Ther. Patents 2000, 10(4), 459-474
152. Nicolaou KC Smith AL, Yue EW PNAS 1993, 90(13), 5881-5888
153. Adhikari A, Shen B, Rader C Antibody Therapeutics, 2021, 4(1), 1–15
154. Walker S, Landowitz R, Ding WD PNAS 1992, 89(10), 4608-4612
155. Dushin, R.G. Cytotoxic Payloads for Antibody-Drug Conjugates, Drug Discovery Series no. 71, Ed. D. E. Thurston and P. M. Jackson, 2019, RSC, 259-278
156. Nicolaou KC, Rigol S et al., PNAS 2021, 118(25) e2107042118
157. Venugopal S, Sharma Vet al., Chem. Biol. Drug Des. 2022, 100, 580-598.
158. Robinson DR, Wu YM, Lin SF Oncogene. 2000, 19(49), 5548–57
159. Drake JM, Lee JK, Witte ON Mol. Cell Biol. 2014, 34(10), 1722–32
160. King T, Pardo A Lancet 2011, 378, 1949-1961
161. Wind S, Schmid U et al., Clin. Pharmacokinetics. 2019, 58(9), 1131-1147
162. Bugatti K, Andreucci E et al., ACS Omega 2022, 7, 17658–17669
163. Wang RE, Liu T et al., J. Am. Chem. Soc. 2015, 137, 3229–32
164. Lindell TJ, Weinberg F et al., Science 1970, 170, 447–9
165. Pahl, A. et al. Cytotoxic Payloads for Antibody-Drug Conjugates, Drug Discovery Series no. 71, Ed. D. E. Thurston and P. M. Jackson, 2019, RSC, 398-426
166. Noel P. Trends Pharmacol. Sci. 2019, 40(5), 327-341
167. Subramanyam, C. Cytotoxic Payloads for Antibody-Drug Conjugates, Drug Discovery Series no. 71, Ed. D. E. Thurston and P. M. Jackson, 2019, RSC, 364-379

168. Garcia-Saez I and Skoufias DA Biochem. Pharmacol. 2021, 184, 114364
169. Wei Y, Xiang H, Zhang W Front. Oncol. 2022, 13, 970553
170. Kale J, Osterlund EJ, Andrews DW. Cell Death Differ. 2018, 25, 65-80.
171. Tanaka Y, Aikawa K et al., J. Med. Chem. 2013, 56, 9625-9645
172. Robert C. Nat Commun. 2020;11(1):3801.
173. Demaria O, Cornen S et al., Nature 2019, 574, 45-56
174. McGowan DC Curr. Top. Med. Chem. 2019, 2228-2238
175. Motedayen L, Pease JE et al., J. Med. Chem. 2023, 66(15), 10715-10733
176. Duwall JR, Thomas JD, Bukhalid RA, et al J. Med. Chem. 2023, 66(15), 10715-10733
177. Dragovich PS Chem. Soc. Rev., 2022,51, 3886-3897
178. Hobson A. The Medicinal Chemistry of Glucocorticoid Receptor Modulators, Springer Briefs in Molecular Science, 2023, Springer, 59-97
179. Hobson AD, McPherson MJ et al. J. Med. Chem. 2022, 65, 4500-4533, Hobson AD, McPherson MJ et al. J. Med. Chem. 2022, 65, 15893-15934]
180. Kovalev IS, Zyryanov GV et al. molecules, 2022, 27(19), 6229
181. Hruba L, Das V, Hajduch M, Dzubak P. Biochem. Pharmacol. 2023, 115741
182. Elgemeie GH. Curr. Pharm. Des. 2003, 9(31), 2627-2642
183. Wang H, Xu X, Wang J, Qiao Y Ann. Med. 2023, 55(1), 1422-1430
184. Bargh JD, Isidro-Lobet A et al. Chem. Soc. Rev. 2019, 48, 4361-4374
185. Johannes, S. et al., Chemical Linkers in Antibody-Drug Conjugates (ADCs), Drug Discovery Series no. 81, Ed. F.L van Delft and J. M. Lambert 2022, RSC, 173-212
186. Lyski RD, Bou LB et al., Mol. Can. Ther. 2021, 20(2), 329-339
187. Edupuganti VVSR, Tyndall JDA et al., Rec. Pat Anticancer Drug Disc. 2021, 16, 479-497
188. deGraaf M, Boven E et al. Curr. Pharm. Design 2002, 8(15), 1391-1403
189. Jeffrey SC, Nguyen MT et al., Bioorg. Med. Chem. Lett. 2007, 17(8), 2278-2280
190. Anselmi M, Borbely A et al. Chem. Eur. J. 2021, 27(3), 1015-1022
191. Shin SH, Park YH et al. Adv. Sci. 2021, 8(23), 2102414
192. Lyon RP, Bovee TD et al. Nat. Bio. 2015, 33(7), 733-735
193. Burke PJ, Hamilton JZ et al. Mol. Can. Ther. 2017, 16(1), 116-123
194. Viricel W, Fournet G et al., Chem. Sci. 2019, 14(10), 4048-4053
195. Evans, N. *et al*. Front. Pharmacol. 2022, 13. 764540
196. Jeffrey SC, Brabender JD et al., ACS Med. Chem. Lett. 2010, 1(6), 277-280
197. Tancy-Opalinski I, Legigan T et al. Eur. J. Med. Chem. 2014, 74, 302-313
198. Kern JC, Cancilla M et al. J. Am. Chem. Soc. 2016, 138, 1430-1445
199. Bargh JD, Walsh SJ et al. Chem. Sci. 2020, 11(19), 2375-2380].
200. Dugal-Tessier, J. *et al*. Chemical Linkers in Antibody-Drug Conjugates (ADCs), Drug Discovery Series no. 81, Ed. F.L van Delft and J. M. Lambert 2022, RSC, 136-172.

201. Hermanson, G. (2013) Bioconjugate Techniques, Chapters 2-6, Academic Press
202. Haque M, Forte N, Baker JR. Chem. Comm. 2021, 57, 10689-10702
203. Doppalapudi VR, Huang J et al. Proc. Natl. Acad. Sci. U S A 2010, 107(52), 22611-6
204. Chilamari M, Kalra N, Shukla S, Rai V. Chem. Comm. 2018, 54, 7302–7305
205. Hackenberger CP and Schwarzer D. Angew Chem Int Ed Engl. 2008;47(52) 10030-74.
206. Chalker JM, Bernardes GJL et al. Chem. Asian J. 2009, 4(5), 630-640
207. Ochtrop P and Hackenberger CP. Curr. Opin. Biol. Chem. 2020, 58, 28-36.
208. Patterson JT, Asano S et al. Bioconj. Chem, 2014, 25, 1402-1407]
209. Kondengadan SM, Bansal S et al. Acta Pharmaceutica Sinica B 2023, 13(5), 1990-2016
210. Hitoshi B, Nagano M et al. Bioconjugate Chemistry 2013, 24, 520-532
211. Walsh SJ, Bargh JD et al. Chem. Soc. Rev. 2021, 50, 1305-1353].
212. Fernandez-Fernandez A, Manchanda R et al., Appl. Biochem Biotechnol. 2011, 165, 1628-51
213. Nicolò E, Giugliano F et al. Cancer Treat Rev. 2022;106:102395
214. Müller P, Kreuzaler M et al. Sci Transl Med. 2015;7(315):315ra188.
215. Castle JC, Uduman M,Front Immunol. 2019;10:1856.
216. Antibody Engineering, Edited by Benny Lo, chapter 8, p161-176, 2004
217. Phage display, Edited by Tim Clackson and Henry B. Lowman, chapter 13, p243-288, 2004
218. Antibody Engineering, Edited by Benny Lo, chapter 19, p327-343, 200
219. Main et al., J Pharmacol Exp Ther., 319(3), p1395-404, 2006
220. Cadwell RC & Joyce GF, PCR Methods, Appl 2, p28– 33, 1992
221. Carter, P., Biochem J, 237, p1-7, 1986
222. Sarker, G & Sommer, SS., Biotechniques, 8(4), p404-407, 1990
223. Jeffrey SC, Andreyka JB et al. Bioconj. Chem, 2006,17(3), 831-840
224. Li Y, Gong L et al. Chemm. Comm. 2022, 58, 2568-2571.
225. Hamilton JZ, Pires TA et al. ChemMedChem, 2021, 16(7), 1077-1081
226. Zhang K, Ma Y et al. Molecular Therapy: Oncolytics, 2020, 18, 304-316
227. Quintana JM, Arboleda D et al. Bioconj. Chem. 2022, 33(8), 1474-1484
228. Li W, Veale KH, Qiu Q et al. ACS Med. Chem. Lett. 2019, 10(10, 1386-1392
229. Meyer Y, Richard JA et al. Org. Biomol. Chem. 2010,8, 1777-1780
230. Zhu Q, Yu X et al. Bioorg. Med. Chem. 2018, 26(16), 4706-4715
231. Chan KF, Wong ILK et al. J. Med. Chem. 2012, 55(5), 1999-2014
232. Agren JKM, Billing JF et al. Synthesis 2006, 3141-3145
233. Liao-Chan S, Daine-Matsuoka B et al. PLoS One. 2015;10(4):e0124708.
234. Wang J et al, BMC Cancer 2016; 16:105

235. Park H et al (2016) Lab Anim Res 32:79-86, Reference values of clinical pathology parameters in cynomolgus monkeys (*Macaca fascicularis*) used in preclinical studies.
236. Nair AB, Jacob S. (2016). A simple practice guide for dose conversion between animals and human. J Basic Clin Pharm. 7:27-31
237. Deng R et al. (2011) Projecting human pharmacokinetics of therapeutic antibodies from nonclinical data: what have we learned? Mabs. 3:61-6
238. Mocquot P et al. (2022). The pharmacology of blinatumomab: state of the art on pharmacodynamics, pharmacokinetics, adverse drug reactions and evaluation in clinical trials. J Clin Pharm Ther. 47:1337-1351.

Figure Legends

Figure 1

Binding of scFv 3A2 (left) and 26B5 (right) to cMET and unrelated antigens in phage ELISA

Figure 2a

Binding affinities for 3A2 and affinity optimised variants for human cMET as measured by BIAcore. KDs are shown.

Figure 2b

Binding affinities for 26B5 and affinity optimised variants for human cMET as measured by BIAcore. KDs are shown.

Figure 2c

Binding affinities for (A) 129D5B and (B) 131D5s for human, cynomolgus and rat cMET as measured by BIAcore. KDs are shown.

Figure 3

ELISA of (A) 129D5B and (B) 131D5S, demonstrating specificity of both scFvs for cMET against unrelated antigens.

Figure 4

Epitope binning of 129D5B and 131D5S by BIAcore. (A) 129D5B binding to human cMET blocks further binding by (B) 129D5B as they target the same epitope. However, (C) 131D5S is not blocked by 129D5B indicating it is binding to a different epitope of human cMET

Figure 5

Inhibition of HGF binding to human cMET by scFvs 129D5B and 131D5S by ELISA. Clone 131D5S, but not 129D5B, inhibits HGF ligand binding.

Figure 6

(A) SEC traces of 129D5B (A) and 131D5S (B) showing predominantly monomeric scFv; (C) Duplicate DLS traces for 129D5B (left) and 131D5S (right) showing a uniform and monomeric particle size (2.8-3nm) for both scFvs with no larger particles or aggregation.

Figure 7a

129D5B scFv is highly thermostable. 129D5B scFv melting curve determined by fluorescence change at 330 nm (top, Tm = 76.9°C), and onset of thermal aggregation determined by DLS (bottom, T onset = 62°C).

Figure 7b

131D5S scFv is highly thermostable. 131D5S melting curve determined by fluorescence change at 330 nm (top, Tm = 68.7°C), and onset of thermal aggregation determined by DLS (bottom, T onset = 62°C).

Figure 8

Amino acid sequence of cMET scFv 77F3 (a) VH and (b) VL showing positions of lysines for randomisation (amino acids 13, 23, 74 and 239). Underneath each lysine position are listed the amino acid alternatives that were built into the 77F3 mutant library.

Figure 9

Binding affinities and kinetics of 77F3 and lysine variants 139B2, 139D2 and 139D7 for human cMET as measured by BIAcore. KDs are shown.

Figure 10

(A) Binding affinities of 129D5B and 129D5BTY for human cMET, and (B) Binding specificity of scFv 129D5B and 129D5BTY to cMET and unrelated antigens, demonstrating that 129D5BTY and 129D5B are equivalent cMET scFv clones. KDs are shown.

Figure 11

Biophysical properties of 129D5BTY: (A) SEC trace showing predominantly monomeric scFv; (B) DLS trace showing a uniform particle size with no aggregation; (C) melting curve showing that 129D5BTY scFv is highly thermostable with a T_m of 74°C.

Figure 12

ELISA of parent 129D5BTY scFv and a range of mutations at position VH98 some of which reduce or abolish binding to human cMET and all which abolish binding to mouse cMET demonstrating the importance of Arginine-98.

Figure 13

BIACore binding analyses of selected 129D5BTY mutants at position VH98 on (A) human and (B) mouse cMET demonstrating the importance of Arginine-98.

Figure 14

Characterization of 129D5BTY-MMAE-βGA-brPEG$_8$-PEG$_2$ FDC. (A) AKTA-Superdex-75 purification traces showing a monomeric FDC which was pooled and analysed; (B) SEC-HPLC analyses demonstrating >98% monomeric FDC; (C) SEC-LCMS showing DAR distribution and an average DAR of 5.9; (D) DLS analyses showing uniform and monomeric particle size of this FDC (~3.4nM) with little signs of larger species and aggregates; (E) NanoDSF between room temperature and 85°C showing the onset of unfolding and Tm of unfolding (63.1°C); (F) BIAcore binding analyses measuring high affinity of 2.16nM and associated kinetic constants.

Figure 15

Characterization of 131D5S-MMAE-βGA-brPEG$_8$-PEG$_2$ FDC. (A) SEC-HPLC analyses demonstrating >88% monomeric FDC; (B) SEC-LCMS showing DAR distribution and an average DAR of 5.4; (C) DLS analyses showing uniform and monomeric particle size of this FDC (~3.8-4nM) with little signs of larger species and aggregates; (D) BIAcore binding analyses measuring high affinity of 112pM and associated kinetic constants.

Figure 16

Characterization of 77F3-MMAE-βGA-brPEG$_4$-PEG$_2$ FDC. (A) SEC-HPLC analyses demonstrating >98% monomeric FDC; (B) SEC-LCMS showing DAR distribution and an average DAR of 8.4.

Figure 17

Characterization of 129D5BTY-MMAE-βGA-brPEG$_{12}$-PEG$_4$ FDC. (A) AKTA-Superdex-75 purification traces showing a monomeric FDC which was pooled and analysed; (B) SEC-HPLC analyses demonstrating >98% monomeric FDC; (C) SEC-LCMS showing DAR distribution and an average DAR of 6.4; (D) DLS analyses showing uniform and monomeric particle size of this FDC (~3.4nM) compared with the scFv (3nm) with little signs of larger species and aggregates; (E) NanoDSF between room temperature and 85°C showing the

onset of unfolding and Tm of unfolding (64.9°C); (F) BIAcore binding analyses measuring high affinity of 1.87nM and associated kinetic constants.

Figure 18

Characterization of 129D5B-MMAE-βGA-brPEG$_{12}$-PEG$_7$ FDC. (A) SEC-LCMS showing DAR distribution and an average DAR of 7.5; (B) NanoDSF between room temperature and 85°C showing the onset of unfolding and Tm of unfolding (63.2°C); (C) BIAcore binding analyses measuring high affinity of 4.9nM and associated kinetic constants.

Figure 19

Characterization of 129D5B-MMAE-βGA-brPEG$_8$-PEG$_2$ FDC (A) SEC-HPLC analyses demonstrating >98% monomeric FDC; (B) HIC chromatography showing the resolution of the various DAR species; (C) SEC-LCMS showing DAR distribution and an average DAR of 5.8; (D) NanoDSF between room temperature and 85°C showing the onset of unfolding and Tm of unfolding (64.2°C); (E) BIAcore binding analyses measuring high affinity of 1.7nM and associated kinetic constants.

Figure 20

Characterization of 129D5BTY- MMAE-βGA-brLys(BisPEG$_8$)-PEG$_2$ FDC (A) SEC-HPLC analyses demonstrating >98% monomeric FDC; (B) SEC-LCMS showing DAR distribution and an average DAR of 5.9; (C) DLS analyses showing uniform and monomeric particle size of this FDC (~3.3nM) with little signs of larger species and aggregates; (D) NanoDSF between room temperature and 85°C showing the onset of unfolding and Tm of unfolding (64°C); (E) BIAcore binding analyses measuring high affinity of 1.4nM and associated kinetic constants.

Figure 21

(A) Characterization of 129D5B-DXd-GGFG-PEG$_7$ FDC by SEC-LCMS showing DAR distribution and an average DAR of 7.6; (B) Characterization of 129D5B-Exatecan-βGA-PEG$_7$ FDC by LC-MS showing DAR distribution and an average DAR of 7.9 and a BIACore binding affinity of 254pM (C).

Figure 22

(A) Characterization of 131D5S-DXd-GGFG-brPEG$_8$-PEG$_2$ FDC by SEC-LCMS showing DAR distribution and an average DAR of 9.3; (B) Characterization of 129D5B-N-MeGlucamine-GGFG-PEG$_2$ FDC by LC-MS showing DAR distribution and an average DAR of 4.3

Figure 23

(A) Characterization of 129D5B-Belotecan-βGA-PEG_2 FDC by SEC-LCMS showing DAR distribution and an average DAR of 5.9 and (B) average DAR of 13; (C) SEC-HPLC analyses demonstrating >98% monomeric FDC of the DAR 13 FDC; (D) Characterization of 129D5B-Triptolide-PEG_6 FDC by SEC-LCMS showing DAR distribution and an average DAR of 5.0.

Figure 24

(A) Characterization of N^1-Benzylamino Imidazoquinoline-PEG_7 FDC by SEC-LCMS showing DAR distribution and an average DAR of 1.35; (B) Characterization of 129D5B-Nintedanib α-Galactose-PEG_7 FDC by SEC-LCMS showing DAR distribution and an average DAR of 1.9.

Figure 25

(A) Characterization of 129D5B-GENZ-644282-Val-Ala-brPEG_{12}-PEG_4 FDC by SEC-LCMS showing DAR distribution and an average DAR of 2.4; (B) Characterization of 129D5B-Dexamethasone-dipyrophosphate-PEG_2 FDC by SEC-LCMS showing DAR distribution and an average DAR of 3.74; (C) BIAcore binding analyses of 129D5B-Dexamethasone-dipyrophosphate-PEG_2 FDC measuring high affinity of 298pM and associated kinetic constants.

Figure 26

(A) Characterization of 129D5B Fab by BIAcore binding analyses measuring high affinity of 12.4pM and associated kinetic constants; (B) Characterization of 129D5B Fab-MMAE-βGA-brPEG_8-PEG_2 FDC by BIAcore binding analyses measuring high affinity of 41pM and associated kinetic constants; (C) Characterization of 129D5B Fab-mc-Val-Cit-MMAE FDC by BIAcore binding analyses measuring high affinity of 35pM and associated kinetic constants.

Figure 27

(A) Characterization of 129D5B Fab-MMAE-βGA-brPEG_8-PEG_2 FDC by SEC-LCMS showing DAR distribution and an average DAR of 5.9; (A) Characterization of 129D5B Fab-mc-Val-Cit-MMAE FDC by SEC-LCMS showing DAR distribution and an average DAR of 2.0;
(C) Characterization of 129D5B Fab-MMAE-βGA-brPEG_8-PEG_2 FDC by SEC-HPLC analyses demonstrating >98% monomeric FDC.

Figure 28

(A) Characterization of 107-A01-MMAF-PEG_2 FDC by RP-LCMS showing DAR distribution and an average DAR of 6. The FDC species were separated by LC and individual peaks analysed by mass spectrometry with 2 examples shown (B & C). The 107-A01-MMAF-PEG_2 FDC demonstrated >10% aggregation as analysed by SEC-HPLC (D). The 20F6-MMAF-

PEG_2 conjugated under similar conditions and analysed by LC-MS showed an average DAR of 6.95 and <1% aggregation by SEC-HPLC (F).

Figure 29

Representative flow cytometry plots showing cMET scFv clones 129D5B/129D5BTY and 131D5S when compared to known benchmark IgGs ABT-700 and 5D5. Representative histograms of antibodies binding on the cell surface of high cMET receptor-expressing cell lines Hs746T, SNU5, KATO III and AsPC1 are shown. Binding on moderate to low cMET-expressing cell lines is also illustrated. (1) Histogram represents untreated cell lines; (2) Histogram shows the fluorescence intensity of the secondary antibody when used as a control or the fluorescence intensity of the cMET antibody binding on the cell surface when conjugated to a fluorophore. (3) Represents cMET antibody binding on the cell surface. Percentage binding by fluorescence shift is shown in Table 8.

Figure 30

Quantification for cMET receptors by QIFIT. (A) Fluorescence calibration using provided beads and fluorescently-labelled 5D5 IgG; (B) Calibration of high to low window; (C) Calibration curve determined for fluorescent intensity vs antibody binding capacity (receptor count); (D to I) shows the flow cytometry of the various cell lines using the 5D5 IgG compared to the calibrated beads. The mean fluorescence for each cell line was compared to the calibration curve to determine the receptor count as shown in Table 9.

Figure 31

Cell killing potency of cMET scFvs on Hs746T and T47D cells. (A) 129D5B scFv; (B) 77F3 scFv; (C) 131D5S scFv, demonstrating no killing.

Figure 32

Cell killing potency of 129D5B-MMAE-βGA-brPEG$_8$-PEG$_2$ FDC (DAR 5.9) on (A) Hs746T , SNU5 & KATOIII cells. (B) NUGC4, SNU16 & NCI-N87; (C) SKOV3, NCI-H1975 & AsPC-1 cells; (D) T47D & JIMT-1 cells. IC_{50} values are shown in Table 10.

Figure 33

(A) Cell killing potency of 129D5BTY-MMAE-βGA-brPEG$_8$-PEG$_2$ FDC (DAR 6.1) on Hs746T, T47D & NCI-N87 cells. (B) Cell killing potency of 129D5BTY-MMAE-βGA-brPEG$_8$-PEG$_2$ FDC (DAR 7.4) on Hs746T & T47D cells; (C) Cell killing potency of 129D5B-MMAE-βGA-brPEG$_{12}$-PEG$_7$ FDC (DAR 7.5) on Hs746T & T47D cells; (D) Cell killing potency of 129D5BTY-MMAE-βGA-brPEG$_{12}$-PEG$_4$ FDC (DAR 6.4) on Hs746T & T47D cells. IC_{50} values are shown in Table 10.

Figure 34

Cell killing potency of 131D5S-MMAE-βGA-brPEG$_8$-PEG$_2$ FDC (DAR 5.4) on (A) Hs746T, SNU5 & KATOIII cells. (B) NUGC4, SNU16 & NCI-N87 cells; (C) T47D & JIMT-1 cells; (D) SKOV3, NCI-H1975 & AsPC-1 cells. IC$_{50}$ values are shown in Table 10.

Figure 35

Cell killing potency of (A) 129D5BTY-MMAE-βGA-br(bisPEG$_8$)-PEG$_2$ FDC (DAR 5.3) on Hs746T & T47D cells; (B) 129D5BTY-MMAE-βGA-br(bisPEG$_8$)-PEG$_2$ FDC (DAR 3.8) on Hs746T & T47D cells; (C) 129D5BTY-MMAF-βGA-PEG$_2$ FDC (DAR 7.8) on Hs746T & T47D cells. IC$_{50}$ values are shown in Table 10.

Figure 36

Cell killing potency of (A) 77F3-MMAE-βGA-brPEG$_8$-PEG$_2$ FDC (DAR 5.6) on Hs746T, & T47D cells; (B) 77F3-MMAE-βGA-brPEG$_4$-PEG$_2$ FDC (DAR 8.1) on Hs746T, & T47D cells; (C) (A) 82H8-MMAE-βGA-brPEG$_4$-PEG$_2$ FDC (DAR 6.5) on Hs746T, & T47D cells. IC$_{50}$ values are shown in Table 10.

Figure 37

Cell killing potency of (A) 5D5 IgG on Hs746T, & T47D cells; (B) 5D5-MMAE-βGA-brPEG$_8$-PEG$_2$ ADC (DAR 4) on Hs746T, & T47D cells; (C) ABT-700 IgG on Hs746T, NCI-N87 & T47D cells; (D) telisotuzumab vedotin (ABBV-399) on Hs746T, SNU5, NCI-N87 & T47D cells. IC$_{50}$ values are shown in Table 10.

Figure 38

Representative plots showing cell killing potency from 9/50 cell lines of varying cMET expression level as part of the Omniscreen panel (Crown Biosciences Inc). 129D5B-MMAE-βGA-brPEG$_8$-PEG$_2$ FDC (DAR 5.6) was compared to Cis-Platin. IC$_{50}$ values of all 50 cell lines are shown in Table 10. The FDC is highly potent on tumour cell lines of high, medium and low cMET expression level.

Figure 39

Internalization kinetics over 5h of (A) 129D5B scFv; (B) 129D5B-MMAE-βGA-brPEG$_8$-PEG$_2$ FDC (DAR 5.6); (C) 5D5 IgG and (D) ABT-700 IgG. Internalization half-lives are shown.

Figure 40

Inhibition of cMET receptor phosphorylation of 4 cMET binding antibodies (129D5BTY scFv, 131D5S scFv, ABT-700 IgG and 5D5 IgG and a non-cMET binding IgG4. All 4 cMET binders inhibit with IC_{50} values of 1.4nM, 4.3nM, 1.4nM and 1.5nM respectively.

Figure 41

Pharmacokinetics of various 129D5BTY FDCs after an IV single dose in rats. Different linkers were evaluated and plasma concentrations vs time were plotted for each FDC compared with the scFv. Separate immuno-detection was employed to follow the clearance of the scFv component and the linker payload. The AUC (Area-under-curve) was determined using GraphPad Prism and listed in Table 12. Similar AUCs (Strep-Tag vs MMAE detection) indicated conjugate stability.

Figure 42

Metabolic markers detected in the plasma of rats after 3 cycles of 1mg/kg of 129D5B-MMAE-βGA-brPEG$_8$-PEG$_2$, 1mg/kg of 129D5B-MMAE-βGA-brPEG$_{12}$-PEG$_4$, 4mg/kg of telisotuzumab vedotin or saline doses. (A) Aspartate transaminase; (B) Alaine transaminase; (C) Urea; (D) Creatinine and (E) Bilirubin levels were determined 2 days after each dose and plotted vs time. The three black arrows indicate the dosing event (once/3 weeks).

Figure 43

Metabolic markers detected in the plasma of rats after 3 cycles of 1mg/kg of 129D5B-MMAE-βGA-brPEG$_8$-PEG$_2$, 1mg/kg of 129D5B-MMAE-βGA-brPEG$_{12}$-PEG$_4$, 4mg/kg of telisotuzumab vedotin or saline doses. (A) White Blood Cells-B (WBCB); (B) White Blood Cell-P (WBCP) and (C) Platelets counts were determined 2 days after each dose and plotted vs time. The three black arrows indicate the dosing event (once/3 weeks).

Figure 44

H&E-stained Kidney and liver sections, after the completion of the 3-cycle rat dosing study where animals were treated with 3 cycles of (A+D) Saline; (B+E) 1mg/kg of 129D5B-MMAE-βGA-brPEG$_8$-PEG$_2$ and (C+F) 1mg/kg of 129D5B-MMAE-βGA-brPEG$_{12}$-PEG$_4$. No abnormal pathological features were observed in the FDC treated animals compared to the saline group.

Figure 45

(A) *In vivo* tumour regression efficacy and (B) body weight study of 129D5BTY FDCs compared to a 5D5 IgG-ADC in a SNU5 gastric cancer xenograft (Table 18, Table 19, study Ref S-1). Animals/group (n=6).

Figure 46

(A) *In vivo* tumour regression efficacy and (B) body weight study of 131D5S FDCs compared to a 5D5 IgG-ADC in a SNU5 gastric cancer xenograft (Table 18, Table 19, study Ref S-2). Animals/group (n=6).

Figure 47

(A) *In vivo* tumour regression efficacy and (B) body weight study of 129D5BTY FDCs compared to a 5D5 IgG-ADC in a Hs746T gastric cancer xenograft (Table 18, Table 19, study Ref H-1). Animals/group (n=6).

Figure 48

(A) *In vivo* tumour regression efficacy and (B) body weight study of 131D5S FDCs compared to a 5D5 IgG-ADC in a Hs746T gastric cancer xenograft (Table 18, Table 19, study Ref H-2). Animals/group (n=6).

Figure 49

(A) *In vivo* tumour regression efficacy and (B) body weight study of 129D5BTY FDCs compared to a telisotuzumab vedotin (TV) ADC in a cMET low NCI-N87 gastric cancer xenograft (Table 18, Table 19, study Ref N-1). Animals/group (n=4).

Figure 50

Survival plot of 129D5BTY FDCs compared to a telisotuzumab vedotin (TV) ADC in a cMET low NCI-N87 gastric cancer xenograft (Table 18, Table 19, study Ref N-1). Animals/group (n=4).

Figure 51

In vivo tumour regression efficacy study of 129D5BTY and 131D5S FDCs in Hs746T gastric cancer xenograft of large tumours (~500mm^3), (Table 18, Table 19, study Ref H-3). The v2 FDC was an alternative (129D5B derivative). Animals/group (n=6).

Figure 52

(A) *In vivo* tumour regression efficacy and (B) body weight study of 129D5BTY FDCs compared to a telisotuzumab vedotin (ABBV-399) in a SNU5 gastric cancer xenograft followed out to 100 days (Table 18, Table 19, study Ref S-3). Animals/group (n=8).

Figure 53

(A) *In vivo* tumour regression efficacy and (B) body weight study of 129D5BTY FDCs compared to a telisotuzumab vedotin (ABBV-399) in a Hs746T gastric cancer xenograft followed out to 100 days (Table 18, Table 19, study Ref H-4). Animals/group (n=8).

Figure 54

(A) *In vivo* tumour regression efficacy and (B) body weight study of 129D5BTY FDCs compared to a telisotuzumab vedotin (ABBV-399) and a non-binding (COVID spike protein specific) FDC in a cMET-moderate NUGC-4 gastric cancer xenograft followed out to 65 days (Table 18, Table 19, study Ref NG-1). Animals/group (n=8).

Figure 55

(A) *In vivo* tumour regression efficacy and (B) body weight study of 129D5BTY FDCs compared to a telisotuzumab vedotin (ABBV-399) in a cMET-low NCI-N87 gastric cancer xenograft followed out to 65 days (Table 18, Table 19, study Ref S-2). Animals/group (n=8).

Figure 56

(A) 129D5B-MMAE-βGA-brPEG$_{12}$-PEG$_4$ FDC DAR stability over 7 days after *in vitro* incubation with cynomolgus, human, mouse and rat plasma. The DAR remained constant and similar to the starting DAR of 5.6. The full data set for human plasma is shown in Figure 56b as a representative example.

(B) 129D5B-MMAE-βGA-brPEG$_{12}$-PEG$_4$ FDC DAR stability over 7 days after *in vitro* incubation with human plasma. The DAR distribution and average DAR was determined by SEC-LCMS and DAR 5 and DAR 6 is labelled for clarity. The average DAR and distribution remained constant and similar to the starting average DAR of 5.6. Two technical replicates of duplicate runs are shown for each time point.

Figure 57

Quantification of released MMAE payload uptake (over 3 days) into (A) tumours and (B) normal tissues after a single dose of 1mg/kg 129D5B-MMAE-βGA-brPEG$_8$-PEG$_2$ FDC DAR (6) compared to a single dose of 4mg/kg telisotuzumab vedotin ADC. Peak payload uptake for the FDC was around 24h with peak uptake for the ADC delivered payload beyond 3 days. Normal tissue uptake/accumulation of the payload was very low marginally higher

amounts for the FDC delivered payload in liver and kidney during the first 24h. The quantification is listed in Table 20.

Figure 58

Representative plots showing CD64, CD32a and CD16a binding to 129D5BTY scFvs, FDCs and various reference IgGs. The full set of data with binding affinities and kinetic constants is listed in Table 21.

Figure 59

Cynomolgus monkey haematological analyses. (A) Lymphocytes counts after four 3-weekly doses of (Dose-1), 0.25mg/kg, (Dose-2) 0.375mg/kg, (Dose-3) 0.5mg/kg and (Dose-4) 1mg/kg 129D5BTY-MMAE-βGA-BrPEG$_{12}$-PEG$_4$ FDC (DAR6) over 66 days; (B) Total white blood cells made up of neutrophils and other lymphocytes were also counted. Black arrows indicate each of the 4 doses.

Figure 60

Cynomolgus monkey clinical chemistry analyses (A) Metabolic markers ALT, AST and GLDH determined after four 3-weekly doses of (Dose-1), 0.25mg/kg, (Dose-2) 0.375mg/kg (Dose-3) 0.5mg/kg and (Dose-4) 1mg/kg 129D5BTY-MMAE-βGA-BrPEG$_{12}$-PEG$_4$ FDC (DAR6) over 66 days; (B) Body weights of the cynomolgus monkeys during the four-cycle dosing study.

Figure 61

Clone 129D5B family sequence comparison showing: (A) VH alignment; (B) VL alignment (C) summary of diversity.

Figure 62

Clone 131D5s family sequence comparison showing: (A) VH alignment; (B) VL alignment (C) summary of diversity.

Figure 63

Clones 129D5B and 131D5s sequence comparison.

Figure 64. Haematological measurements from cynomolgus taken pre-dose (1), 48h after dose (2) and 10 days (3)

(a) Average white blood cell count over the entire study (x10^9/L), showing the expected normal range ± 1 standard deviation

(b) Average neutrophil count over the entire study (x10^9/L), showing the expected normal range ± 1 standard deviation
(c) Average lymphocyte count over the entire study (x10^9/L), showing the expected normal range ± 1 standard deviation
(d) Average monocyte, eosinophil, basophil and large unstained cell counts over the entire study (x10^9/mL)
(e) Average platelet count over the entire study (x10^9/L), showing the expected normal range ± 1 standard deviation
(f) Average reticulocyte count over the entire study (x10^9/L), showing the expected normal range ± 1 standard deviation

Figure 65. Clinical Chemistry measurements for key liver markers from cynomolgus taken pre-dose (1), 48h after dose (2) and 10 days (3)
(a) Average alanine aminotransaminase, aspartate transaminase and glutamate dehydrogenase levels over the entire study (U/L)
(b) Average alanine aminotransaminase levels over the entire study (U/L) showing the expected normal range ± 0.5 standard deviation
(c) Average aspartate aminotransaminase levels over the entire study (U/L) showing the expected normal range ± 1 standard deviation
(d) Average alkaline phosphatase levels over the entire study (U/L) showing the expected normal range ± 1 standard deviation
(e) Average bilirubin levels over the entire study ((mmol/L)

Figure 66. Clinical Chemistry measurements for key kidney markers from cynomolgus taken pre-dose (1), 48h after dose (2) and 10 days (3)
(a) Average urine creatinine levels over the entire study (mmol/L) showing the expected normal range ± 1 standard deviation
(b) Average urine total protein levels over the entire study (mg/L)
(c) Average urine total protein:creatinine ratio over the entire study (mg/mmol)
(d) Average urine glucose levels over the entire study (mmol/L) showing the expected normal range ± 1 standard deviation
(e) Average urine glucose:creatinine ratio over the entire study (mmol/mmol)

Figure 67
(a) Average body weights for the entire non-human primate study, before and during the 5 escalating doses
(b) Percentage change in average body weights for the entire non-human primate study, before and during the 5 escalating doses

Figure 68

(a) Pharmacokinetic clearance profile for cMET FDC at all 5 escalating doses detected by ELISA anti-MMAE detection

(b) Pharmacokinetic clearance profile for cMET FDC at all 5 escalating doses detected by ELISA anti-Strep Tag detection

(c) Pharmacokinetic clearance profile for cMET FDC at 1mg/kg dose detected by ELISA anti-MMAE and Strep Tag detection

(d) Bioavailability (AUC) vs Dose plot to illustrate linearity of exposure over the 5 doses with TMDD being observed at the 0.25-0.5mg/kg dose (lower than expected AUC)

Figure 69

Detection of functional, binding cMET FDC by ELISA in urine in the 3 individual animals (M101, M102, M103) after 5 escalating FDC doses, compared to reference quantities.

Figure 70

BIACore binding profiles for the 129D5BTY-MMAE-βGA-brPEG12-PEG4 FDC used in the non-human primate study showing comparable affinities for (a) human and (b) cynomolgus cMET.

Figure 71

BIACore binding analyses of 129D5BTY scFv compared to (a) ABT-700 IgG and (b) 5D5 IgG. All samples were injected at 400nM.

Figure 72

Purification and DAR characterization of 129D5B-Exatecan FDCs

(a) HPLC-SEC profile of FDC showing the pure Exatecan-MA-PEG12-Val-Ala-PEG4 FDC eluting at 25 minutes (fraction A9)

(b) RP-MS analysis of fraction A9 containing the Exatecan-MA-PEG12-Val-Ala-PEG4 FDC of an average DAR of 5.03 (DAR range 3-7).

(c) BIACore SPR binding profile and derived kinetic and affinity constants for fraction A9 containing the Exatecan-MA-PEG12-Val-Ala-PEG4 FDC

(d) HPLC-SEC profile of FDC showing the pure Exatecan-βGA-BrPEG12-PEG4 FDC eluting at 23.81 minutes (fraction A11)

(e) RP-MS analysis of fraction All containing the Exatecan-βGA-BrPEG12-PEG4 FDC of an average DAR of 5.03 (DAR range 4-11).

(f) BIACore SPR binding profile and derived kinetic and affinity constants for fraction All containing the Exatecan-βGA-BrPEG12-PEG4 FDC

(g) HPLC-SEC profile of FDC showing the pure DXd-GGFG-BrPEG8-PEG2 FDC eluting at 25.46 minutes (fraction D4)
(h) RP-MS analysis of fraction D4 containing the DXd-GGFG-BrPEG8-PEG2 FDC of an average DAR of 3.72 (DAR range 2-5).
(i) BIACore SPR binding profile and derived kinetic and affinity constants for DXd-GGFG-BrPEG8-PEG2 FDC

Figure 73
Characterization of the 129D5B scFv-2-(Methylsulphonyl)ethylamino-MMAF-βGA-PEG2 FDC.
(a) Superdex-75 purification of the FDC which elutes as a pure monomer at 168.14 min. Free payload and small molecule contaminants elute after 250 min; **(b)** SEC-MS analyses showing the DAR distribution of the various FDC species; **(c)** BIACore SPR binding analysis on human cMET showing kinetic and binding constants; **(d)** Cell killing potency analysis on Hs746T (cMET-positive) and T47D cells (cMET negative).

Figure 74
Characterization of the 129D5B scFv-Belotecan-βGA-PEG2 FDC.
(a) BIACore SPR binding analysis on human cMET showing kinetic and binding constants; **(b)** Cell killing potency analysis on Hs746T (cMET-positive) and T47D cells (cMET negative). DAR analysis is shown in Figure 23.

Figure 75
DAR characterization of 129D5B-N1-Benzylamino Imidazoquinoline-PEG7 FDC. RP-MS analysis showing an average DAR of 1.81 (DAR range 0-5).

Figure 76.
Evaluation of cMET FDC 129D5BTY-MMAE-βGA-BrPEG12-PEG4 (DAR6) in a cMET-low gastric cancer PDX model. **(a)** SP44-immunohistochemical staining of Crown Biosciences gastric cancer PDX (GA6885) showing high percentage of cMET-negative (IHC 0) and cMET-low (IHC 1+) tumour cells resulting in a low overall cMET IHC score (103.22). **(b)** Early readout after 2 doses of 1mg/kg and 2.5mg/kg FDC compared to 3mg/kg ABBV-399 and saline/untreated controls, showing tumour growth inhibition of the test agents and superior efficacy of the higher FDC dose.

Figure 77.
Evaluation of cMET FDC 129D5BTY-MMAE-βGA-BrPEG12-PEG4 (DAR6) in a cMET-low pancreatic cancer PDX model. **(a)** SP44-immunohistochemical staining of Crown

Biosciences gastric cancer PDX (PA3142) showing high percentage of cMET-negative (IHC 0) and cMET-low (IHC 1+) tumour cells resulting in a low overall cMET IHC score (114.27). **(b)** Early readout after 2 doses of 1mg/kg and 2.5mg/kg FDC compared to 3mg/kg ABBV-399 and saline/untreated controls, showing tumour growth inhibition and superior efficacy of the higher FDC dose.

Examples

Example 1: Discovery of cMET binding scFvs

A non-immune scFv phage display library, $7x10^9$ in size, was generated in-house. This library consisted of an antibody scaffold of human VH5 and VL1 genes, with CDR regions diversified based on sequence diversity observed in natural human antibody sequences. Phage display selections with this scFv library were performed using recombinant purified cMET protein and following published methods [216]. Briefly, phage particles displaying the Antikor VH5-VL1 library were incubated with cMET antigens either immobilised directly on maxisorp plates, or captured via protein G immobilised onto maxisorp plates. For cMET antigens carrying a human Fc domain, undesirable scFvs recognising the Fc region of the fusion protein were removed by the addition of human IgG1 to the selection mixture. After allowing phage binding to occur at room temperature for 2h, unbound phage particles were removed by multiple wash steps, and then specifically bound phage eluted by addition of chaotropic agents such as triethlyamine and/or hydrochloric acid. Eluted phage were then recovered by re-infection into E. coli TG1 cells and plated onto large format 2xTY agar bioassay dishes supplemented with antibiotic.

Following the cMET selections, specific scFv were identified by phage ELISA following published methods [216], or by scFv ELISA using crude bacterial periplasmic extracts [217]. ELISAs were performed against cMET proteins and unrelated antigens to identify specific scFvs. From these selections, two candidate scFvs were isolated, 3A2 and 26B5, that were unique in VH CDR3 sequence and specific for human cMET (Figure 1 and Table 3). Both 3A2 and 26B5 also showed binding to cynomolgus monkey cMET, and 3A2 also showed binding to rat cMET. Both clones have diverse VH CDR3 sequences and both possess 11 framework lysines in total.

Table 3. Summary of 3A2 and 26B5 sequence information.

Clone	Selection antigen	VH			VL	
		VH family	CDR3	Lysines	VL family	Lysines
3A2	Hu cMET-His	VH5	HGGRGRLDV	7	VL1	4
26B5	Hu cMET-HisFc	VH5	ADYDYYRGYYMDI	7	VL1	4

Example 2: Affinity optimisation of cMET binding scFvs

For both 3A2 and 26B5, a number of strategies were employed to increase scFv binding affinity for cMET, using techniques well described in the art. In summary:

Light chain shuffling [218],

Targeted randomisation of VH and VL CDR3 regions using randomised oligonucleotides [219],

Error prone mutagenesis of scFv sequences [220]

Phage display selections for the above strategies were carried out following published methods [216], using solution phase selections with biotinylated human cMET to control antigen concentration and increase selection stringency to favour higher affinity binders. Increased stringency was further applied by lengthening the wash steps to enrich for scFv with slower off rates, and by introducing heat stress to favour scFvs with higher (Tm) melting temperatures.

Binding affinity kinetic constants for scFv preparations of 3A2 and 26B5 and their affinity optimised variants were measured using a BIAcore T200 instrument. Approximately 100-150RU of cMET Fc was captured on a protein G chip by injecting recombinant human, cynomolgus and rat cMET at 2.5μg/mL in HBS buffer for 30s at 30μL/min flow rate. Binding kinetics of anti-cMET scFv were then determined by single-cycle kinetics. ScFv were prepared in dilution series (typically 1:3 dilution series starting with 25-100nM scFv at the highest concentration), and then injected over the antigen coated surfaces and also a blank surface, starting with the lowest concentration of scFv and then working progressively up to the highest concentration. ScFv binding kinetics were then determined from the (blank subtracted) sensorgram traces using 1:1 binding models and BIAevaluation software. Using this approach, affinities for 3A2 and 26B5 and several affinity optimised variants were determined (Figure 2a, 2b, 2c and Table 4).

Table 4. Summary of human, cynomolgus and rat cMET binding affinities for 3A2, 26B5 & affinity matured variants.

Clone	Predecessor	scFv binding kinetics (human cMET)		
		k_a (1/Ms)	k_d (s^{-1})	K_D (nM)
3A2	-	2.04×10^5	2.11×10^{-2}	103
20F6	3A2	2.92×10^5	1.55×10^{-2}	53
49G5	20F6	5.42×10^5	1.08×10^{-3}	2
53D11	20F6	7.88×10^5	9.95×10^{-4}	1.3
59D5	20F6	1.00×10^6	6.99×10^{-4}	0.7

49A6	20F6	5.24×10^{5}	2.60×10^{-3}	5
55G9	20F6	1.56×10^{6}	2.68×10^{-3}	1.7
55A3	20F6	1.02×10^{6}	2.61×10^{-3}	2.6
75G7	20F6	5.03×10^{5}	7.21×10^{-4}	1.4
54E11	20F6	7.07×10^{5}	1.63×10^{-3}	2.3
59D4	20F6	5.77×10^{5}	2.40×10^{-3}	4.2
59A10	20F6	1.59×10^{6}	4.99×10^{-3}	3.1
65C2	20F6	6.43×10^{5}	1.68×10^{-3}	2.6
53G1	20F6	1.01×10^{6}	2.38×10^{-3}	2.4
65A3	20F6	8.48×10^{5}	1.87×10^{-3}	2.2
65G6	20F6	8.79×10^{5}	1.90×10^{-3}	2.2
53G9	20F6	7.46×10^{5}	1.38×10^{-3}	1.8
58H11	20F6	1.04×10^{6}	1.48×10^{-3}	1.4
59E5	20F6	1.05×10^{6}	1.72×10^{-3}	1.6
59H2	20F6	2.47×10^{6}	7.83×10^{-3}	3.2
59A6	20F6	1.02×10^{6}	3.08×10^{-3}	3
59A2	20F6	1.21×10^{6}	4.97×10^{-3}	4
59D10	20F6	7.54×10^{6}	2.12×10^{-2}	2.8
58A9	20F6	8.60×10^{5}	2.28×10^{-3}	2.7
74C3	20F6	5.87×10^{5}	3.76×10^{-4}	0.64
59H6	20F6	5.46×10^{5}	8.90×10^{-4}	1.6
64B2	20F6	3.83×10^{5}	5.27×10^{-4}	1.4
52G1	20F6	2.73×10^{5}	1.05×10^{-3}	3.9
58A2	20F6	7.69×10^{5}	2.75×10^{-3}	3.6
52D5	20F6	1.65×10^{5}	6.18×10^{-4}	3.8
71D4	20F6	4.43×10^{5}	3.09×10^{-4}	0.7
71C2	20F6	5.93×10^{5}	9.55×10^{-4}	1.6
71F11	20F6	6.02×10^{5}	1.30×10^{-3}	2.2
77F3	49G5 + 53D11	8.98×10^{5}	6.37×10^{-5}	0.071
126A8B	77F3	1.39×10^{6}	7.12×10^{-5}	0.051
129D5B	77F3	1.88×10^{6}	4.27×10^{-5}	0.023
26B5	-	8.15×10^{4}	1.01×10^{-1}	1237
83B11D	26B5	2.29×10^{4}	1.15×10^{-1}	505
94C2	83B11D	7.36×10^{6}	7.99×10^{-3}	1.1
94C3	83B11D	1.67×10^{6}	2.81×10^{-3}	1.7
94E6	83B11D	4.19×10^{6}	8.46×10^{-2}	20
112F2	83B11D	2.74×10^{6}	9.19×10^{-3}	3.4

112G4	83B11D	1.26 x10^{7}	3.75 x10^{-3}	0.29
113A3	83B11D	6.57 x10^{6}	1.20 x10^{-2}	1.82
113G8	83B11D	1.81 x10^{7}	7.77 x10^{-3}	0.43
115C7	94C2	3.27 x10^{7}	1.02 x10^{-2}	0.31
116A5	94C3	2.79 x10^{6}	1.71 x10^{-3}	0.61
121H3B	94C3	6.52 x10^{6}	1.76 x10^{-3}	0.27
115D1D	94C2	5.35 x10^{6}	1.03 x10^{-3}	0.192
131D5S	115D1D	4.59 x10^{6}	2.17 x10^{-4}	0.047
Clone	Predecessor	scFv binding kinetics (cynomolgus cMET)		
		k_a (1/Ms)	k_d (s^{-1})	K_D (nM)
129D5B	77F3	1.4 x10^{6}	6.9 x10^{-5}	0.051
131D5S	115D1D	3.0 x10^{6}	2.4 x10^{-4}	0.079
Clone	Predecessor	scFv binding kinetics (rat cMET)		
		k_a (1/Ms)	k_d (s^{-1})	K_D (nM)
129D5B	77F3	8.9 x10^{4}	3.6 x10^{-3}	39.8
131D5S	115D1D	No binding	No binding	No binding

Example 3: Binding characterization of cMET scFvs 129D5B and 131D5S

(a) Specificity for cMET by ELISA

To demonstrate their specificity for cMET, 129D5B and 131D5S were analysed by scFv ELISA against cMET and a range of other unrelated antigens. Each test antigen was immobilised on maxisorb plates (Nunc 443404) by adding 50μL volumes at 2μg/mL in PBS and incubating at 4°C overnight. Following coating, the antigen solution was aspirated and the plates were washed using PBS (prepared from PBS tablets, Oxoid cat no. BR0014G) supplemented with 0.05% Tween 20 (sigma P1379), followed by washes with PBS without added Tween. To block non-specific protein interactions, a solution of 3% skimmed milk powder (Marvel™) in PBS was added to the wells and the plate was incubated for at least 1h at room temperature. Purified 129D5B and 131D5S scFv were prepared in 3% Marvel/PBS at 10μg/mL and incubated for at least 1h at room temperature prior to transfer to the blocked ELISA plate where a further incubation of at least 1h took place. Unbound scFv was then washed away using repetitive washes with PBS/Tween followed by PBS. A solution of HRP-conjugated streptactin (IBA 2-1502-001), prepared at 1:1000 dilution in PBS/3% Marvel was then added to each well and a further incubation at room temperature for at least one hour took place. Unbound streptactin-HRP was removed by repeated washing using PBS/Tween and PBS. The ELISA was then developed using TMB substrate (Sigma cat. no. T0440) and the reaction was stopped after 10 min by the addition of 0.5M

H_2SO_4 solution (Sigma cat. no. 320501). Absorbances were determined by reading at 450nm. Both 129D5B and 131D5S were shown to bind specifically to human cMET and not to any of the other antigens tested (Figure 3). For 129D5B, cross-reactivity with rat and mouse cMET species variants was also observed.

(b) Epitope binning of lead candidates 129D5B and 131D5S

129D5B and 131D5S scFv were shown to bind to unique epitopes of human cMET by Biacore. Human cMET Fc (2.5μg/mL in HBS buffer) was captured onto a protein G chip by injecting for 30s at 30μL/min flow rate. 129D5B scFv, at 1μg/mL in HBS buffer, was then injected over the cMET coupled surface and a blank control surface for 180s, followed immediately by a second injection of 129D5B scFv, at 1μg/mL in HBS buffer, for 180 s. Finally, 131D5S scFv was injected, at 1μg/mL in HBS buffer, for 180 s followed by buffer only for 600 s. Both scFvs were observed to bind simultaneously to human cMET, indicating that they were binding to different epitopes of the protein (Figure 4).

Example 4: Inhibition of Hepatocyte growth factor binding to human cMET by 129D5B and 131D5S

Hepatocyte growth factor (HGF) regulates cell growth, cell motility, and morphogenesis by activating the cMET receptor and both are implicated in oncogenesis [19,22]. To evaluate if 129D5B and 131D5S were capable of blocking this interaction, a ligand:receptor binding assay was developed. In this assay, HGF (Sino Biological 10463-HNAS) was immobilised onto a Nunc maxisorp plates at 0.5μg/mL in PBS buffer overnight at 4°C. Following coating, the HGF solution was aspirated and the plates were washed using PBS (prepared from PBS tablets, Oxoid cat no. BR0014G) supplemented with 0.05% Tween 20 (Sigma P1379), followed by washes with PBS without added Tween. To block non-specific protein interactions, a solution of 3% skimmed milk powder (Marvel™) in PBS was added to the wells and the plate was incubated for at least 1h at room temperature. Dilution series of 129D5B and 131D5S scFv were prepared, starting from 10μg/mL at the highest concentration and diluting 1:4 in 3% Marvel/PBS containing human cMET-Fc HIS (Sino Biological 10692-H03H) at 1ug/ml. Each 129D5B and 131D5S dilution series was incubated for at least 1h at room temperature prior to transfer to the blocked ELISA plate where a further incubation of at least one hour took place. Unbound scFv were then washed away using repetitive washes with PBS/Tween followed by PBS. A solution of HRP-conjugated anti-HIS antibody (Abcam ab1187), prepared at 1:10000 dilution in PBS/3% Marvel was then added to each well and a further incubation at room temperature for at least 1h took place. Unbound anti-HIS-HRP was removed by repeated washing using PBS/Tween and PBS. The ELISA was then developed using TMB substrate (Sigma cat. no.

T0440) and the reaction was stopped after 10 min by the addition of 0.5M H_2SO_4 solution (Sigma cat. no. 320501). Absorbances were determined by reading at 450nm. In this assay, it was shown that 131D5S completely inhibited HGF binding to human cMET whereas 129D5B had little or no effect (Figure 5).

Example 5: Biophysical characterisation of 129D5B and 131D5S

(a) SEC purification of monomeric scFv

129D5B and 131D5S scFvs were expressed overnight in *E.coli* strain TG1 using Terrific autoinduction medium. Supernatant and periplasmic fractions were harvested by centrifugation and loaded onto Strep-Tactin® FPLC cartridges via Cytiva Äkta chromatography systems. Bound scFv were eluted with free biotin and then loaded onto Superdex™ S75 gel filtration column to separate monomeric scFv protein from larger oligomers and impurities (Figure 6a and Figure 6b).

(b) Assessment of aggregation by Dynamic Light Scattering (DLS)

Particle size and distribution of molecules in solution can be obtained by dynamic light scattering (DLS). Molecules scatter light due to Brownian motion. The intensity fluctuations of the scattered light are used to calculate an autocorrelation function which allows determination of the hydrodynamic radius of molecules and dispersity of the solution as well as detection of any aggregates. Clones 129D5B and 131D5S scFvs were assessed by DLS (using a Nanotemper Prometheus Panta) and shown to be highly monodispersed and homogeneous samples with no indication of larger aggregates. Mean particle size was 2.8-3nm consistent with small monomeric proteins (Figure 6c).

(c) Assessment of scFv thermal stability

Nano-differential scanning fluorimetry (NanoDSF) measures changes in intrinsic fluorescence while a thermal ramp is applied, leading to unfolding and/or aggregation of the protein. The melting temperature (Tm) of the protein is defined as the inflection point where half of the protein is still in its folded state. To assess the thermal stability of 129D5B and 131D5S, NanoDSF studies were performed, and both proteins were shown to be highly thermostable, with T onset (initiation of unfolding) in excess of 60°C and Tm values 68-77°C (Figure 7a, 7b).

Example 6: Generation of cMET scFv with reduced lysine content

To facilitate production of cMET FDCs with a more homogenous DAR, the overall lysine content in one cMET scFv (clone 77F3) was reduced from 11 to 7-8 residues.

To determine which lysines residues could be removed, whilst retaining full stability and binding affinity properties, 77F3 was firstly made by bacterial fermentation and purified by affinity chromatography (>95% pure). A cytotoxic payload (MMAE-βGA-BrPEG$_8$-PEG$_2$-NHS Ester) was made in-house and conjugated to the scFv to make 77F3-MMAE-βGA-BrPEG$_8$-PEG$_2$-NHS FDC conjugate (DAR 6) using methods described in Example 39. Using the enzymes trypsin and chymotrypsin, 77F3 FDC was digested into peptide fragments and analysed by mass spectrometry to produce a peptide map and to identify which lysine residues were attached to payload. This analysis identified lysine residues in 77F3 that were rarely coupled to payload, namely at positions 13, 23, 74 and 239. These positions were then targeted for mutagenesis in a new scFv library that aimed to change the lysines to alternative amino acids (Figure 8).

The 77F3 lysine variant library (total diversity 1.2x10^4) was generated by Twist Bioscience Inc and then subcloned into a phagemid vector for phage display selections following standard methods as described in Example 1 [216,217]. Following selections on cMET, specific 77F3 variant scFv were identified by scFv ELISA using crude bacterial periplasmic extracts and by BIAcore following the procedure described in Example 2. From these selections, three candidate scFvs were isolated, 139B2, 139D2 and 139D7, that were of similar affinity and stability to 77F3 and contained well tolerated amino acid variations from lysine at positions 13, 23, 74 and 239 (Figure 9 and Table 5).

Table 5. Summary of human cMET binding affinities for 77F3 and lysine variants 3A2, 26B5 and affinity matured variants.

Clone	**Amino acid at randomised positions**				**Total lysines**	**scFv kinetics**		
						k_a (1/Ms)	k_d (s^{-1})	K_D (nM)
77F3	K13	K23	K74	K239	11	1.21 x10^6	1.33 x10^{-4}	110
139B2	A13	T23	K74	Q239	8	9.93 x10^5	7.99 x10^{-5}	80
139D2	A13	A23	S74	R239	7	1.07 x10^6	1.02 x10^{-4}	96
139D7	L13	T23	S74	R239	7	1.05 x10^6	1.42 x10^{-4}	135

Example 7: Removal of potential deamidation sites in cMET scFv 129D5B

During drug development, it has become standard practice to analyse biologics for developability characteristics. Properties such as expression level, solubility, thermal and colloidal stability have all become common measurements during drug development. In addition, protein sequences are scanned for potential amino acid sequence liabilities. These are common motifs in proteins that could be subjected to chemical or enzymatic modification and potentially affect a drugs structure, stability or function. One example of

this is deamidation, where the amide group in the side chain of asparagine is removed or converted to aspartic acid or isoaspartic acid. The risk of this is dependent on multiple factors such as pH, temperature, buffer formulation, and in particular the amino acid residue neighbouring the asparagine residue, with a C-terminal glycine or serine presenting the highest risk. Biologics that carry these motifs are typically subjected to further mutagenesis to remove the high-risk sites without affecting the drugs biological and biophysical properties.

Two potential deamidation sites were identified in 129D5B: one in VL-CDR2 (NS, Kabat VL51 and VL52); and a second in VL-CDR3 (NS, Kabat VL93 and VL94). These sites were de-risked by converting the motifs to NY in VL-CDR2 and NT in VL-CDR3 using standard mutagenesis techniques [221,222]. The new molecule, named 129D5BTY, was unaffected by these changes and retained the same affinity and specificity for cMET as 129D5B (Figure 10), and also the biophysical properties, i.e., thermal and colloidal stability, were unchanged (Figures 6, 7 and 11).

Example 8: Mutagenesis of 129D5BTY to abolish mouse cMET binding

An arginine residue in 129D5BTY VH-CDR3 (Kabat VH98) was targeted for mutation to investigate the effects on scFv binding to human and mouse cMET. This single amino acid position was converted to other possible residues using standard mutagenesis techniques [221,222], and the mutants assessed for binding to human and mouse cMET by ELISA and BIAcore (Figure 12,13). Binding to human cMET was severely impacted when Arg98 was substituted by other amino acids, with some residues (proline, lysine and valine) virtually abolishing binding. The amino acid change with least impact at this position was Arg98 to Gln98, but binding to human cMET was still reduced by several hundred-fold (Figure 13). Binding to mouse cMET was abolished when Arg98 was changed to any other amino acid (Figure 13).

Abbreviations:

EEDQ	2-Ethoxy-1-ethoxycarbonyl-1,2-dihydroquinoline
DCM	Dichloromethane
AcOH	Acetic acid (glacial)
DIPEA	Diisopropylethyl amine
DMF	Dimethylformamide
THF	Tetrahydrofuran
DBU	1,8-Diazabicyclo 5.4.0 undec-7-ene
EtOAc	Ethyl acetate
$CHCl_3$	Chloroform

^{i}PrOH	*iso*-propyl alcohol
MeCN	Acetonitrile
RT	room temperature
TSTU	N,N,N',N'-Tetramethyl-O-(N-succinimidyl)uronium tetrafluoroborate
TFA	Trifluoroacetic acid
DMTMM	4-(4,6-Dimethoxy-1,3,5-triazin-2-yl)-4-methylmorpholinium chloride
CDI	1,1'-Carbonyldiimidazole
DCC	Dicyclohexylcarbodiimide
DMAP	4-Dimethylamino pyridine
EDC.HCl	(1-ethyl-3-(3-dimethylaminopropyl)carbodiimide hydrochloride)
EDC	(1-ethyl-3-(3-dimethylaminopropyl)carbodiimide
HATU	1,2,3-triazolo[4,5-b]pyridinium 3-oxide hexafluorophosphate
NHS	N-hydroxysuccinimide
NBS	N-bromosuccinimide
HOBt	Hydroxybenzotriazole
TPP	Triphenylphosphine
EtOH	Ethanol
MeOH	Methanol

Experimental:

LCMS were run on an Agilent LCMS6100C SQ system using two main methods:

Method 1: Run time: 6 min, Water (+ 0.1 % formic acid)/ MeCN (+ 0.1 % formic acid), MeCN = 5% - 95%, Flow rate: 0.500 mL/min, Injection: 5uL, Column oven T = 40C, MWD: 210, 250, 284 nm, Fragmentor voltage: 280 V, Polarity: positive

Method 2: Run time: 5.5 min., Water (+ 0.1 % formic acid)/ MeCN (+ 0.1 % formic acid), MeCN = 5% - 95%, Flow rate: 0.500 mL/min, Injection: 5uL, Column oven T = 40C, MWD: 210, 250, 284 nm, Fragmentor voltage: 140 V, Polarity: positive

Example 9: Synthesis of MMAE-βGA-BrPEG$_8$-PEG$_2$-NHS Ester (10)

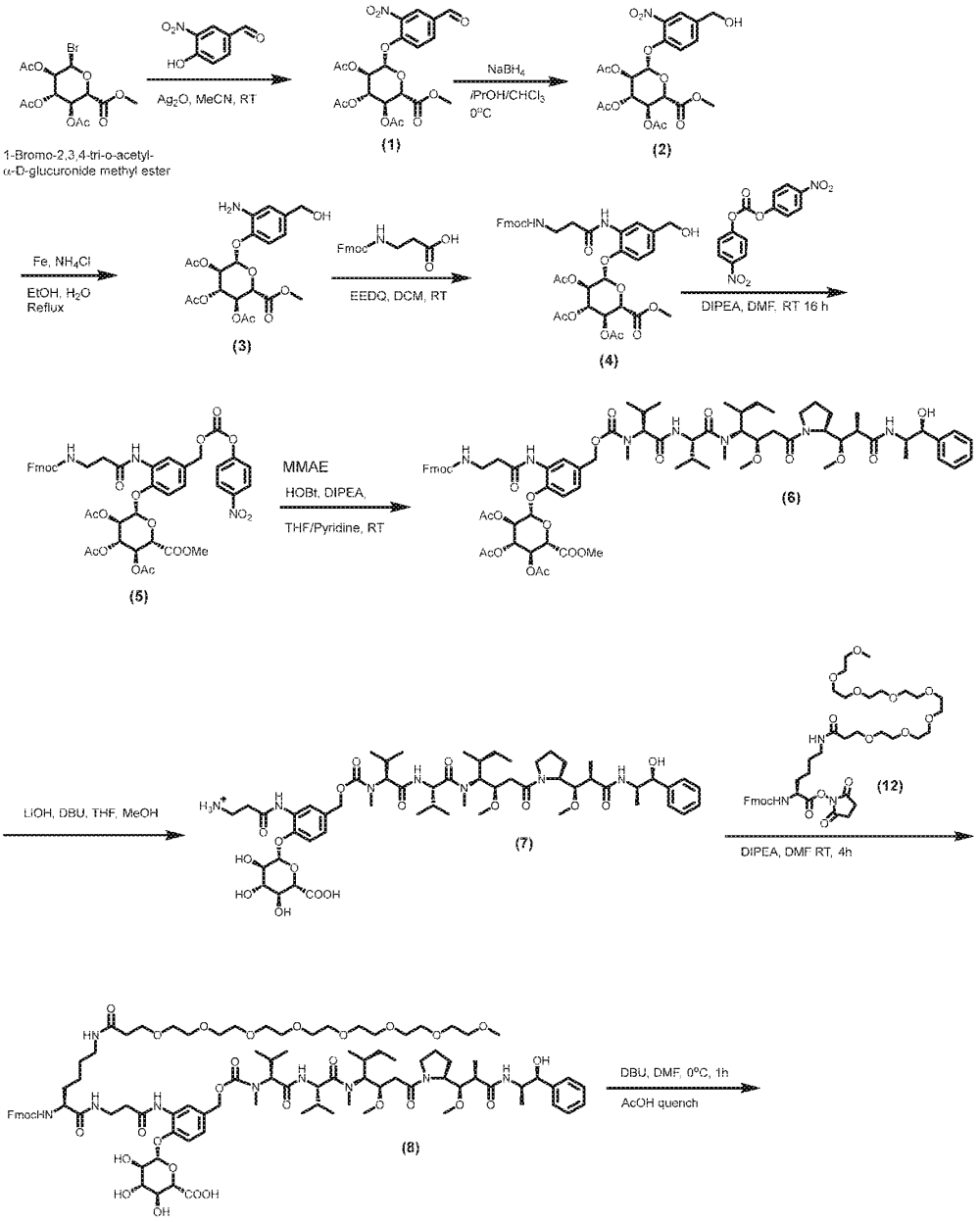

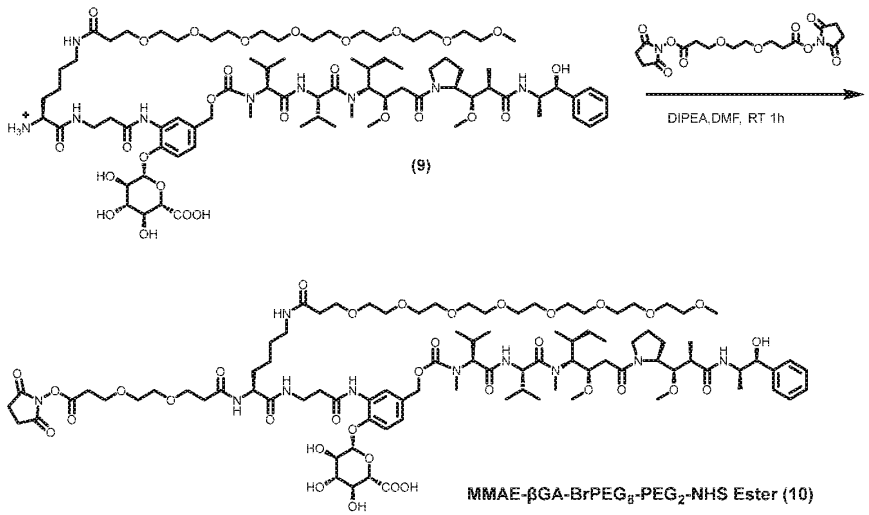

To a solution of the 1-bromo-glucuronide methyl ester (40 g, 100.7 mmol) and 4-hydroxy-3-nitrobenzaldehyde (28.6 g, 171.2 mmol) in dry MeCN (700.0 mL) was added silver oxide (102.7 g, 443.1 mmol) at room temperature. After stirring at RT overnight under N2, the mixture was filtered through celite. The bright yellow solution was then concentrated in vacuo and the residue was redissolved in EtOAc (300 mL). The mixture was washed with sodium bicarbonate (250 mL) saturated solution and the aqueous layer was further extracted with EtOAc (3 x 50 mL). The combined organic layers were dried over Na_2SO_4 and concentrated under reduced pressure to give the desired product **1** as a yellow solid 41.4 g (85.0%) and used in the next step directly without further purification. TLC: R_f = 0.48 (silica gel, PE/EtOAc = 1:1). LCMS m/z calculated for $(M+NH_4)^+$ 501.1.

To a solution of the benzaldehyde-sugar **1** (41.4 g, 85.6 mmol) in IPA/$CHCl_3$ (1:5, 12000 mL) at 0°C was added $NaBH_4$ (9.72 g, 256.9 mmol). After stirring at 0° for 1 h, the reaction solution was quenched with water (150 mL). The organic layer was separated, and the aqueous layer was back extracted with DCM (80 mL x 2). The organic phases were combined, dried over Na_2SO_4, filtered, and then concentrated under vacuo to give the desired product **2** as an off-white solid 38.7 g (93.0%) which was confirmed by LCMS and HNMR and used to next step directly without further purification. TLC: R_f = 0.2 (silica gel, PE/EtOAc 1/1,). LCMS m/z $(M+NH_4)^+$ 503.1.

To a solution of **2** (20 g, 41.2 mmol) in MeOH/water (6/5 v/v, 400 mL) were added NH_4Cl (2.42 g, 45.3 mmol) and iron powder (11.51 g, 206 mmol). After stirring at 80 °C for 3h under a N_2 atmosphere, the mixture was cooled to RT and filtered through celite. The filtrate was quenched with sodium bicarbonate saturated solution and then extracted with EtOAc (3 x 100 mL). The combined organic extracts were dried over Na_2SO_4, filtered and

concentrated in vacuo. The residue was purified by silica gel column chromatography (PE/EA = 1/1, v/v) to give the desired product **3** as an off-white solid 7.7 g (41.0%). TLC: R_f = 0.23 (silica gel, PE/EtOAc 2/3). LCMS m/z (M+1) 456.1

As described in Jeffrey SC et al. [223]. To solution of the amine **3** (7.7 g, 16.9 mmol), Fmoc-β-alanine (5.79 g, 18.6 mmol) in dry DCM (100 ml) EEDQ (8.36 g, 33.8 mmol) was added and the reaction mixture stirred for 24 h under a N_2 atmosphere. The mixture was quenched with sodium bicarbonate saturated solution and the phases separated. The aqueous layer was further back extracted with EtOAc (3 x 50 mL). The organics extracts were combined, dried over $MgSO_4$ and concentrated in vacuo and purified by silica gel column chromatography (DCM:MeOH, 80:1) to give the desired product **4** as an off-white solid 10.97 g (86.7%). TLC: R_f = 0.38 (silica gel, DCM/MeOH 20/1, v/v). LCMS m/z (M+1) 749.9

As described in Jeffrey SC et al. [223]. A mixture of the benzyl alcohol **4** (6.5 g, 8.69 mmol) and pyridine (3.43 g, 43.43 mmol) in dry dichloromethane (80 mL) was cooled to 0°C. To this, a solution of bis-*p*-nitrophenyl carbonate (6.99 g, 34.76 mmol) in 15 ml of dry DCM was then added drop-wise. After addition was complete, the mixture was stirred at 0°C for 2 h under nitrogen after which it was extracted with dichloromethane (30 ml x 3). The combined organic extracts dried over Na_2S0_4, filtered, and concentrated to dryness. The crude product residue was then purified by silica gel column chromatography (DCM:MeOH, 100:1) to give the desired PNP-derivative **5** as an off-white solid 7.4 g (93.2%). TLC: R_f = 0.50 (silica gel, DCM/MeOH 20/1, v/v). LCMS m/z = 914.50 (M+1); 936.40 (M+Na).

As described in Jeffrey SC et al. [223]. To a stirred solution of **5** (5.4 g, 5.91 mmol), and monomethylauristatin E (MMAE, 4.27 g, 5.91 mmol) in dry THF (40 ml) containing pyridine (27.65 mL) DIPEA (903.69 mg, 7.00 mmol) was added followed by HOBt (820.8 mg, 6.09 mmol) which resulted in a faint colour change of the solution from colourless to a faint yellow. The reaction mixture was stirred at RT under nitrogen for 24 h after which the pH was adjusted to pH 6 by the addition of citric acid. The resulting mixture was then extracted with EtOAc (40 ml x 2), the combined organic phases were combined, dried over Na_2SO_4, filtered and concentrated in vacuo. The crude residue was purified by silical gel column chromatography (DCM:MeOH, 30:1) to give the desired MMAE-βGlucuronide **6** as a white solid 6.9 g (78.2%). TLC: R_f = 0.20 (silica gel, DCM/MeOH 20/1, v/v). LCMS m/z 1493.49 (M+1); 1515.50 (M+Na)

As described in Jeffrey SC et al. [223]. To a cooled solution of **6** (6.70 g, 4.490 mmol) in MeOH (50 ml)/THF (50 ml)/H_2O (50 mL) at 0 °C, a solution of $LiOH.H_2O$ (942 mg, 22.450 mmol) and DBU (2.71 g, 17.960 mmol) in water (100 ml) was added dropwise over 1 h.

After the end of the addition, the reaction mixture was removed from the ice/water bath and allowed to stir for one further hour at RT. Glacial acetic acid (3 mL, 50 mmol) was then added, the reaction mixture concentrated in vacuo and purified by automated chromatography [Biotage (water + 0.1% TFA/MeCN, 0-100%)]. The appropriate pure fractions were combined and lyophilized to give the desired globally deprotected derivative MMAE-βGA **7** as a white solid 4.21 g (75% yield). LCMS m/z 1131.19 (M+1); 1153.08 (M + Na); 718.79 (MMAE) 686.71, 506.50 (MMAE fragments)

As described in RP Lyon et al. [192]. To a cooled solution of the MMAE-βA **7** (88.0 mg, 0.0707 mmol) and DIPEA (24.6 µL, 0.1410 mmol) in dry DMF (1 ml) at 0 °C was added a solution of the activated Fmoc-Lys-PEG_8 -NHS ester **12** (76.0 mg, 0.0849 mmol) in dry DMF (1.4 ml) via syringe pump over 1 hour. After the addition was complete, the reaction mixture was warmed back to RT and stirred for further 4 hours. The solvent was then removed under high vacuum and the residue purified by RP automated chromatography [Biotage (water + 0.1%TFA/MeCN + 0.1%TFA, 0-100%)] to give the desired product Lysine-PEG_8 derivative **8** as a white solid after lyophilization 111 mg (84 % yield). LCMS m/z = 1877.70 (M+1); 1898.68 (M + Na); 939.20 (M/2); 719.10 (MMAE); 687.06, 506.77 (MMAE fragments).

The Fmoc-protected derivative **8** (35 mg, 0.0187 mmol) was dissolved in dry DMF (2 ml) and cooled to 0°C in a water/ice bath. A solution of DBU (8.4 µl, 0.0560 mmol) in dry DMF (1 mL) was added dropwise over 1 h. After the DBU addition was complete, the mixture was allowed to stir for one further hour under nitrogen. The reaction was then quenched with AcOH (5.3 µl, 0.0934 mmol), and the mixture concentrated under reduced pressure. The residue was purified by RP automated chromatography [Biotage, (water + 0.1% TFA/MeCN + 0.1% TFA 10-90%) to afford the desired amine **9** as the TFA salt 26.30 mg (98%), as a white powder after lyophilization. LCMS m/z [M+1] 1652.9, (M+1 /2] 827.2.

To a solution of Bis-PEG_2-NHS (53 mg, 0.134 mmol) and DIPEA (7 µl, 0.043 mmol) in DMF (500 µL) under nitrogen was added a solution of MMAE-βGA-BrPEG_8 TFA salt **9** (22.2 mg, 0.0134 mmol) in DMF (840 µl) via syringe pump over 2 h. Upon end of the addition, the solvent was removed on high vacuum and the crude residue purified by RP automated chromatograph [Biotage, (water + 0.1% TFA/MeCN + 0.1% TFA 10-90%) to afford MMAE-βGA-BrPEG_8-PEG_2-NHS ester **10** 35.27 mg (86%) as a white solid after lyophilization. LCMS m/z (M+1) 1940.00, $[1/2M+1]^+$ 970.1.

Example 10: Synthesis of Fmoc-PEG$_8$ lysine-NHS ester (12)

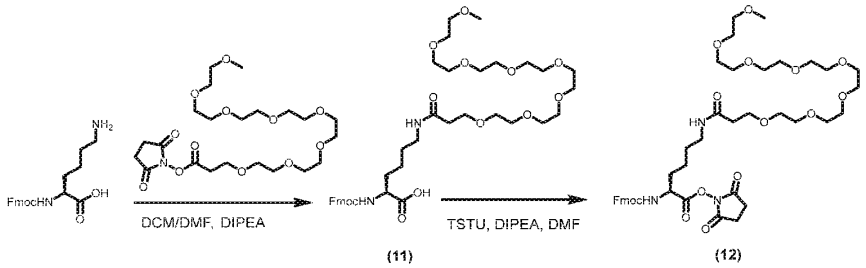

As described in RP Lyon et al. [192]. To a solution of Fmoc-Lys-OH (300 mg, 0.814 mmol) in dry DCM (13.5 ml) was added a solution of dPEG$_8$-NHS ester (300 mg, 0.589 mmol) in dry DMF (4 ml) followed by DIPEA (513 µL, 2.94 mmol) – the mixture is a suspension. The reaction mixture was stirred at RT under nitrogen for 16 h before being quenched with 1M solution NH_4Cl (10 mL). The mixture was separated and extracted with DCM (100 ml x 3). The combined organic phases were concentrated to dryness and the residue purified by RP automated chromatography [Biotage, water + 0.1% TFA/MeCN + 0.1% TFA, 0-100%) to give **11** as a sticky residue 217 mg (48% yield). TLC: R_f = 0.50 (silica gel, DCM/MeOH 10/1). LCMS m/z [M+1] 763.5.

To a solution of the Fmoc-dPEG8 acid **11** (200 mg, 0.262 mmol) and TSTU (158 mg, 0.524 mmol) in dry DMF (3.3 ml) was added DIPEA (229 µl, 1.31 mmol) and the mixture stirred at RT under nitrogen for 4 h. The mixture was concentrated to dryness and the residue purified by RP automated chromatography [Biotage, water + 0.1% TFA/MeCN + 0.1% TFA, 0-100%) to give the desired NHS-ester derivative **12** as a sticky-white solid 182 mg (81%). TLC: R_f = 0.70 (silica gel, CH_2Cl_2/MeOH 10/1). LCMS m/z [M+1] 860.5.

Example 11: Synthesis of MMAE-βGA-BrPEG$_{12}$-PEG$_4$-NHS Ester (15)

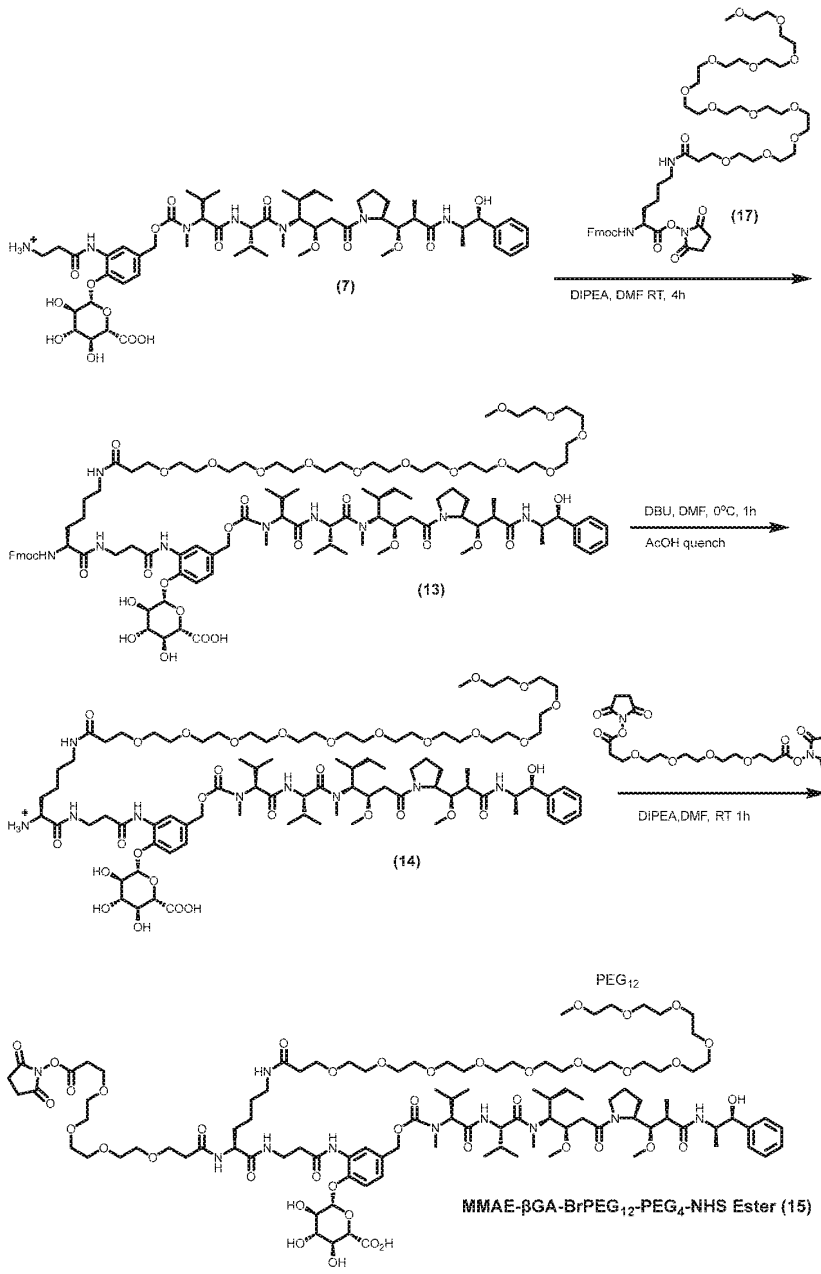

As described in RP Lyon et al. [192]. MMAE-βGA-alanine derivative **7** (88.0 mg, 0.0707 mmol) was dissolved in DMF (1 ml). Fmoc-Lys-PEG$_{12}$ (97.0 mg, 0.0934 mmol) dissolved in DMF (1.4 ml) was then added to the substrate solution, followed by DIPEA (32 µL, 0.184 mmol). The resulting mixture was stirred for 4 h at RT under nitrogen, the solvent was removed under high vacuum and the residue purified by RP automated chromatography [Biotage, (water + 0.1% TFA/ACN + 0.1% TFA, 0-100%)] to give the Fmoc-protected

derivative **13** as a white solid 120 mg (74%) after lyophilisation. LCMS m/z (M+1) 2053.30; (1/2 M+1)1027.13; 718.82 (MMAE), 686.72, 506.51 (MMAE fragments).

The Fmoc-protected derivative **13** (34 mg, 0.0166 mmol) was dissolved in dry DMF (2 ml) and cooled to 0°C in a water/ice bath. To this, a solution of DBU (7.4 µl, 0.0497 mmol) dissolved in dry DMF (0.5 ml) was added dropwise over 1 h, whilst stirring and under nitrogen. After the end of the DBU addition, the mixture was allowed to stir for a further 1.5 h after which the ice bath was removed, and the reaction quenched with AcOH (4.7 µl, 0.0166 mmol). The mixture was then concentrated under reduced pressure and purified by RP automated chromatography [Biotage, (water + 0.1% TFA/MeCN + 0.1% TFA, 10-90%) to give the amine **14** as a white powder 27.0 mg (90%) after lyophilisation. LCMS m/z (M+1) 1831.10; (1/2 M+1) 915.60; 718.82 (MMAE); 686.76, 506.60 (MMAE fragmentation).

To a solution of Bis-PEG_4-NHS (131 mg, 0.268 mmol) and DIPEA (14 µl, 0.080 mmol) in dry DMF (1 mL), a solution of the MMAE-βGA-BrPEG_{12} **14** (49 mg, 0.026 mmol) in dry DMF (1 mL) was added dropwise using a syringe pump over 1 h. After addition was complete, the solvent was removed by high vacuum and the crude purified by RP automated chromatography [Biotage, (water + 0.1% TFA/MeCN + 0.1% TFA, 10-90%) to give the desired compound **15** 31.73 mg (54%) as a white solid after lyophilisation. LCMS m/z (M+1) 2204.50; (1/2 M+1) 1102.58; 718.87 (MMAE), 686.79, 506.61 (MMAE fragmentation).

Example 12: Synthesis of Fmoc-PEG_{12} lysine NHS ester (17)

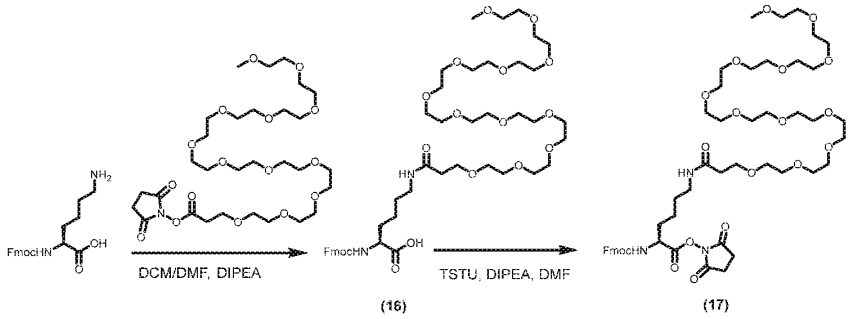

As described RP Lyon et al. [192]. To a solution of Fmoc-Lys-OH (53.7 mg, 0.146 mmol) in dry DCM (3.7 mL) was added a solution of dPEG_{12}-NHS ester (100 mg, 0.146 mmol) in dry DMF (0.37 mL) followed by DIPEA (127 µL, 0.729 mmol) – the mixture is a suspension. The reaction mixture was stirred at RT under nitrogen for 5 h, quenched with 1M solution HCl (5 mL) and stirred for 5 min. The reaction mixture was then extracted with DCM (20 ml), this was dried over $MgSO_4$, filtered, and evaporated. The residue was purified by RP automated chromatography [Biotage, (water + 0.1% TFA/MeCN + 0.1% TFA, 0-100%) to

give the pegylated lysine acid **16** as a sticky oil 140 mg (quantitative yield). LCMS m/z 939.87 (M+1); 961,85 (M+Na).

The pegylated lysine **16** acid (137 mg, 0.1459 mmol) and TSTU (88 mg, 0.2918 mmol) were dissolved in dry acetonitrile (5 mL), DIPEA (127 µL, 1.31 mmol) was added and the mixture stirred for 4 h at RT under nitrogen. The reaction mixture was concentrated under high vacuum and purified by RP automated chromatography [Biotage, (water + 0.1% TFA/ACN + 0.1% TFA, 0-100%) to give the desired activated ester derivative **17** as an off-white oil 138 mg (91%). LCMS m/z 1036.70 (M+1); 1058.72 (M+Na).

Example 13: Synthesis of DXd-GGFG-PEG$_2$-NHS Ester (21)

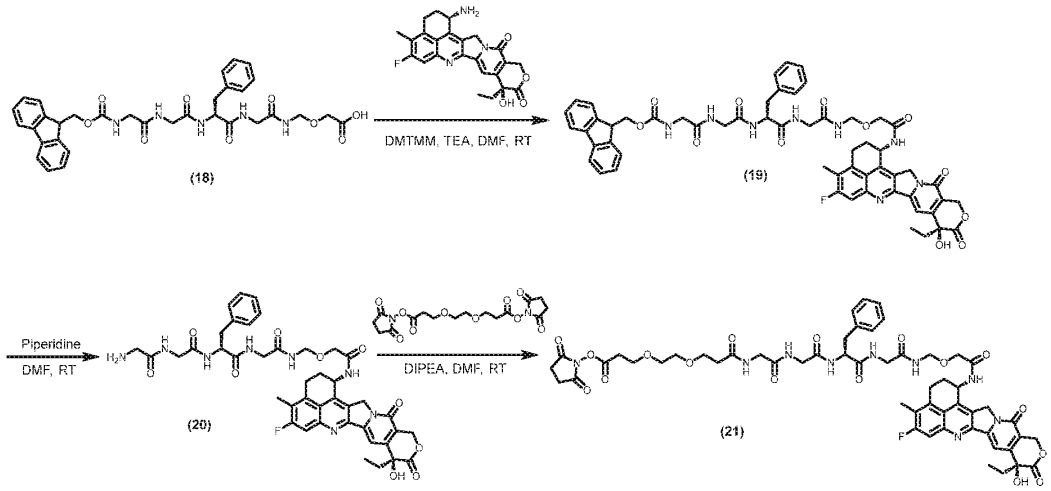

As described in EP3101032, to a stirred solution of Fmoc-GGFG-Glycolic acid **18** (204 mg, 0.316 mmol) and exatecan mesylate (140 mg, 0.263 mmol) in dry DMF (20 mL), triethylamine (36.7 µL, 0.263 mmol) was added followed by DMTMM (156 mg, 0.474 mmol). The resulting solution was was stirred at RT under an inert atmosphere and monitored by LC-MS. Upon complete conversion to **19** (approx. 1h 30 min) piperidine (260 µL, 2.63 mmol) was added, and the reaction mixture was stirred at RT under inert atmosphere for a further 1 hour until the consumption of **19** as determined by LC-MS. The reaction mixture was concentrated *in vacuo* and the crude purified by RP automated chromatography [Biotage (water + 0.1% TFA/ACN + 0.1% TFA, 10-100%)]. The fractions containing the desired product **20** were combined and freeze dried to leave give the de-protected derivative **20** as a yellow solid (214 mg, 97% yield for two steps). LCMS m/z 1063.81 (M+1); 1085.78 (M+Na)

The deprotected exatecan derivative **20** (16 mg, 0.0190 mmol) was dissolved in dry DMF (500 µl) and added dropwise over 1 h (using a syringe pump) to a solution of bis-PEG$_2$

NHS ester (76 mg, 0.190 mmol) dissolved in dry DMF (500 µl) and DIPEA (10 µl, 0.0571 mmol). After addition was complete, the reaction mixture was stirred for a further 1 h at RT, the solvent was then removed and the crude residue purified by RP automated chromatography [Biotage (water + 0.1% TFA/ACN + 0.1% TFA, 10-90%)], to give the desired product **21** as a yellow solid 9.16 mg (48 %). LCMS (M+1) 1126.90; (M+Na) 1149.86

Example 14: Synthesis of DXd-GGFG-PEG$_7$-NHS Ester (22)

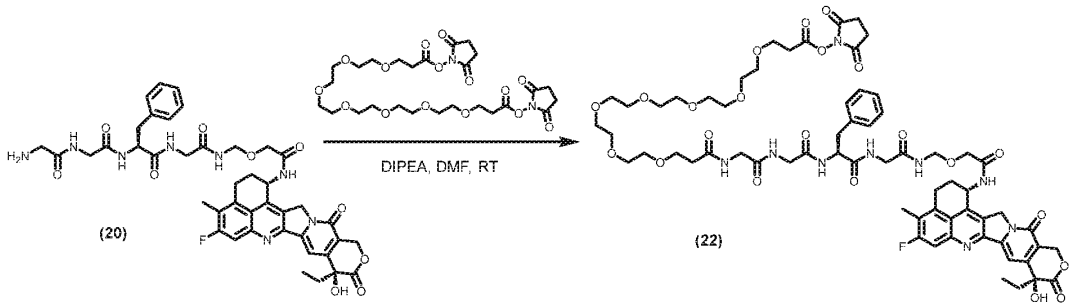

The exatecan derivative **20** (13 mg, 0.0155 mmol) was dissolved in dry DMF (1 ml) and added dropwise over 1 h (using a syringe pump) to a solution of bis-PEG$_7$ NHS ester (96 mg, 0.1546 mmol) dissolved in dry DMF (1 ml) and DIPEA (8.1 µl, 0.0461 mmol). After addition was complete, the reaction mixture was stirred for a further 1 h at RT, the solvent was then removed and the crude residue purified by RP automated chromatography [Biotage (water + 0.1% TFA/ACN + 0.1% TFA, 10-90%)], to give the desired DXd-GGFG-PEG$_7$ derivative **22** as a yellow solid 8.15 mg (39 %). LCMS m/z (M+1) 1347.00

Example 15: Synthesis of DXd-GGFG-BrPEG$_8$-PEG$_2$ NHS Ester (25)

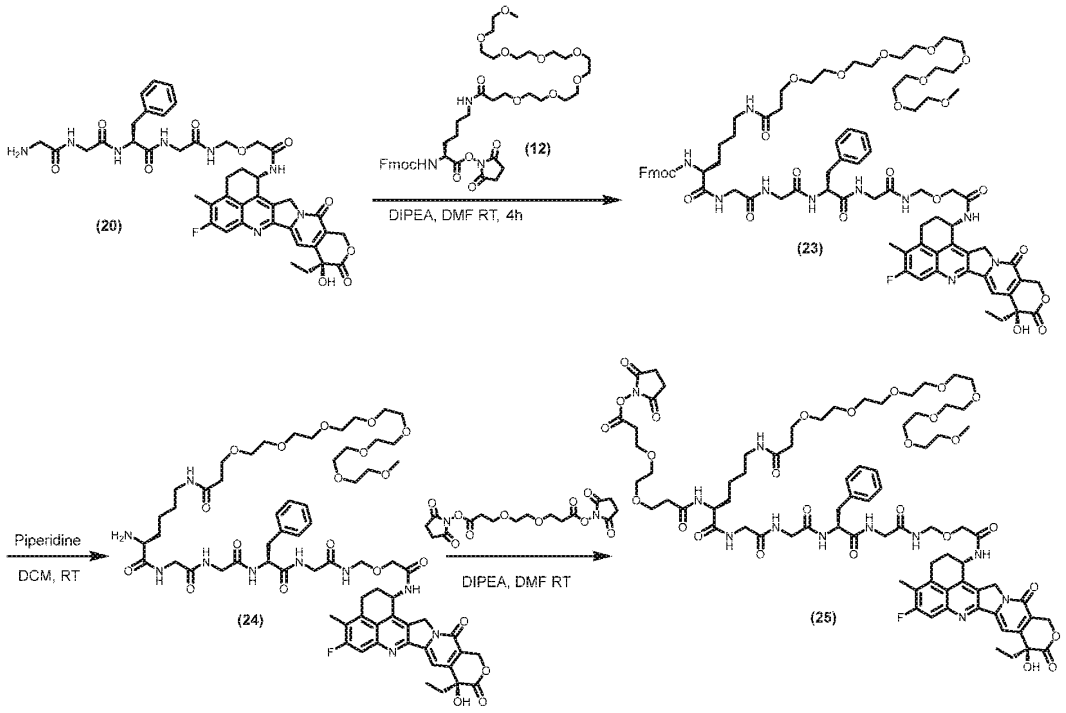

The exatecan derivative **20** (98.50 mg, 0.117 mmol) and the activated lysine branching point **12** (121 mg, 0.141 mmol) were dissolved in dry DMF (10 ml) under nitrogen. DIPEA (49 µl, 0.281) was added and the mixture was stirred at RT under nitrogen for 22 hours after which the reaction mixture was concentrated under high vacuum and the resulting residue purified by automated RP chromatography [Biotage (water + 0.1% TFA/ACN + 0.1% TFA, 0-100%)] to give the branched-Fmoc lysine DXd derivative **23** as a light-yellow solid 71 mg (38%). LCMS m/z (M+1) 1586.50. The Fmoc-deprotected derivative **24** 21 mg (13%) was also isolated. LCMS m/z 1365.20 (M+1).

The Fmoc-derivative **23** (38.70 mg, 24.40 µmol) was dissolved in dry DCM (4 ml) piperidine (53 µL, 0.537 mmol) was added and the mixture stirred at RT under nitrogen for 2 hours. The reaction was was concentrated under high vacuum and the residue purified by RP automated chromatography [Biotage, (water + 0.1% TFA/ACN + 0.1% TFA, 0-100%) to give Fmoc-deprotected derivative **24** as a yellow solid 33 mg (quantitative yield). LCMS m/z (M+1) 1365.20

Bis-PEG$_2$-NHS (38 mg, 0.095 mmol) was dissolved in dry DMF (500 µl), DIPEA (5 µl, 0.029 mmol) was added. Separately, DXd-PEG$_8$ amine **24** (13 mg, 0.095 mmol) was dissolved in dry DMF (500 µl). This was then slowly added (1 h) dropwise using a syringe pump to the stirred solution of the bis-PEG$_2$-NHS and DIPEA. After addition was complete, the

solvent was removed under high vacuum and the crude residue purified by RP automated chromatography [Biotage, (water + 0.1% TFA/ACN + 0.1% TFA, 10-90%)], to give the DXd-GGFG-BrPEG$_8$-PEG$_2$ NHS ester **25** as a yellow solid 3.32 (36%). LCMS (M+1) 1650.09

Example 16: Synthesis of Exatecan-βGA-PEG$_7$ NHS Ester (28)

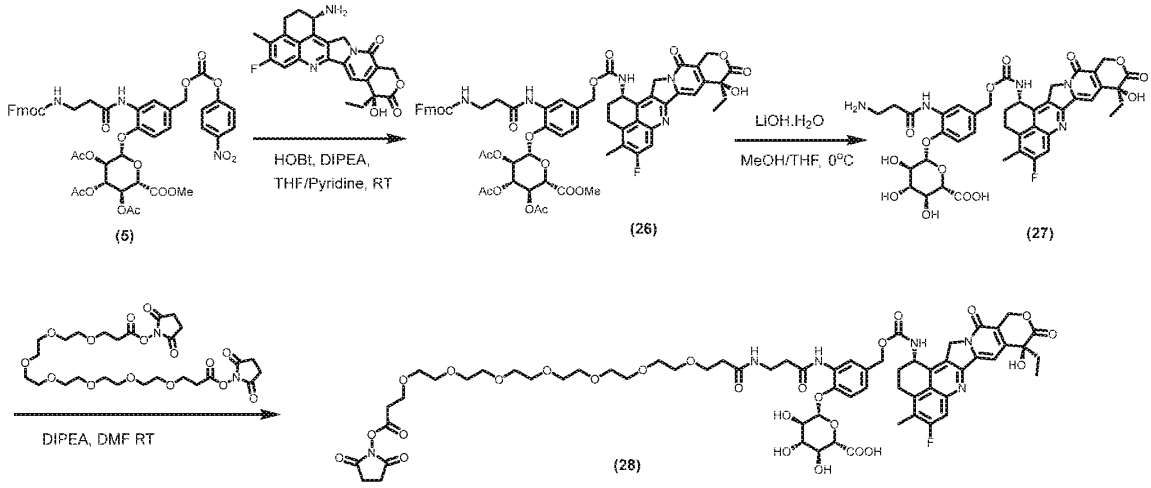

As described in WO2019236954, the PNP-carbonate ester **5** (86 mg, 0.094 mmol), HOBt (13 mg, 0.094 mmol) and exatecan mesylate (50 mg, 0.094 mmol) were stirred in dry THF (2.5 ml) and pyridine (0.5 mL), DIPEA (49 µl, 0.282 mmol) was then added and the reaction mixture stirred at RT under nitrogen for 19 h. The reaction mixture concentrated *in vacuo* and crude purified by RP automated chromatography [Biotage, (water + 0.1% TFA/ACN + 0.1% TFA, 0-100%)]. Combined fractions were concentrated to give the Fmoc-glucuronide exatecan derivative **26** as a yellow solid 71 mg (62% yield). LCMS m/z (M+1) 1210.93, (M+Na) 1234.85

As described in WO2019236954, a stirred solution of the Fmoc-sugar-exatecan **26** (33 mg, 0.0273 mmol) in 1:1 MeOH & THF (4 mL) was cooled with an ice/water bath. To this a solution of LiOH.H$_2$O (6.9 mg, 0.1636 mmol) in 2 mL water was dropwise over 1 h 20 min. The reaction was monitored by LCMS and showed complete consumption of **26**. The reaction mixture was concentrated *in vacuo* and purified by RP automated chromatography [Biotage, (water + 0.1% TFA/ACN + 0.1% TFA, 0-100%)] to give the globally deprotected exatecan-βGA amine derivative **27** as a pale-yellow solid 18 mg (71 %). LCMS (RT = 1.923 min.) m/z (M+1) 848.50. The partially deprotected (Fmoc-alanine) exatecan-βGA was also isolated 7 mg (24 %). LCMS (RT = 2.347 min.) m/z (M+1)1070.70, (M+Na) 1092.68

Bis-PEG$_7$-NHS ester (66 mg, 0.1062 mmol) was dissolved in dry DMF (500 µl) and DIPEA (5.6 µl, 0.0318 mmol) was added. Separately, Exatecan-βGA amine **27** (9 mg, 0.0106 mmol) was dissolved in DMF (500 µl). This was then slowly added (1.5 h) dropwise using a syringe pump to the stirred solution of the bis-PEG$_7$-NHS and DIPEA. After addition was complete, the solvent was removed under high vacuum and the crude residue purified by RP automated chromatography [Biotage, (water + 0.1% TFA/ACN + 0.1% TFA, 10-90%)], to give Exatecan-βGA-PEG$_7$ NHS ester **28** as a pale-yellow sticky solid 1.84 mg (12.8 %). LCMS m/z (M+1) 1354.59, (M+Na) 1376.59.

Example 17: Synthesis of Belotecan-βGA-PEG$_2$ NHS Ester (32)

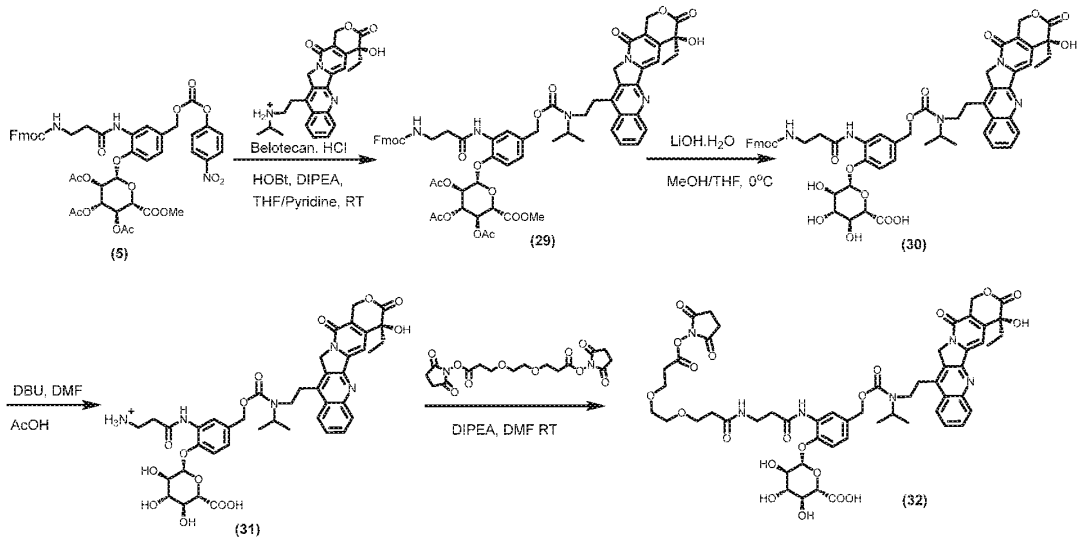

As described in WO2019236954, PNP-carbonate ester **5** (194 mg, 0.213 mmol), HOBt (29 mg, 0.217 mmol) and belotecan hydrochloride (150 mg, 0.213 mmol) were dissolved in dry DMF (5 ml) and dry pyridine (1 ml). DIPEA (44 µl, 0.255 mmol) was then added, and the reaction mixture stirred at RT under nitrogen for 24 h. The reaction mixture was concentrated *in vacuo* and the crude purified by NP automated chromatography [Biotage (DCM/MeOH, 0-20 %)] to give the belotecan-protected sugar derivative **29** as a yellow solid 258 mg (quantitative yield). LCMS m/z (M+1) 1209.99

A stirred solution of the Fmoc-sugar-belotecan derivative **29** (114 mg, 0.0944 mmol) was dissolved in 1:1 MeOH & THF (7 ml) and cooled with an ice/water. To this a solution of LiOH.H$_2$O monohydrate (24 mg, 0.5661 mmol) in water (2 ml) was added dropwise over one hour. The reaction mixture was then allowed to stir whilst reaching RT for 45 minutes, acetic acid (38 µl, 0.6608 mmol) was added, the reaction mixture stirred for a further 2

minutes, and then evaporated to dryness under reduced pressure. The crude **30** was used directly in the next reaction. LCMS m/z (M+1) 1069.00

To a stirred solution of **30** dissolved in dry DMF (6 ml), a solution of DBU (27 µl, 0.1827 mmol) dissolved in dry DMF (6 ml) was added dropwise over 1.5 h under nitrogen and at RT. The reaction was then quenched with acetic acid (35 µl, 0.6090 mmol), allowed to stir for a further 5 minutes, and evaporated to dryness under reduced pressure. The crude was purified RP automated chromatography [Biotage, (water 0.1% TFA/ ACN 0.1% TFA 0-100%)]. The appropriate fractions were combined and lyophilized to give the fully deprotected derivative Belotecan-βGA derivative **31** as a yellow solid 32 mg (40 % overall). LCMS m/z (M+1) 846.50

A solution of Belotecan-βGA derivative **31** (24 mg, 0.0284 mmol) in dry DMF (11 ml) was added dropwise over 3 h via syringe pump into a stirred solution of the bis-PEG_2-NHS (57 mg, 0.1419 mmol) and DIPEA (25 µl, 0.1419 mmol). After addition was complete, the reaction mixture was stirred for an additional 45 minutes then evaporated to dryness under reduced pressure. The crude product was purified via RP automated chromatography [Biotage, (water 0.1% TFA/ ACN 0.1% TFA 0-100%)]. The appropriate fractions were combined and lyophilized to give Belotecan-βGA-PEG_2 NHS ester **32** as a yellow solid 22 mg (69%). LCMS m/z (M+1)1132.60

Example 18: Synthesis of Nintedanib-Val-Ala-PEG$_2$ NHS Ester (37)

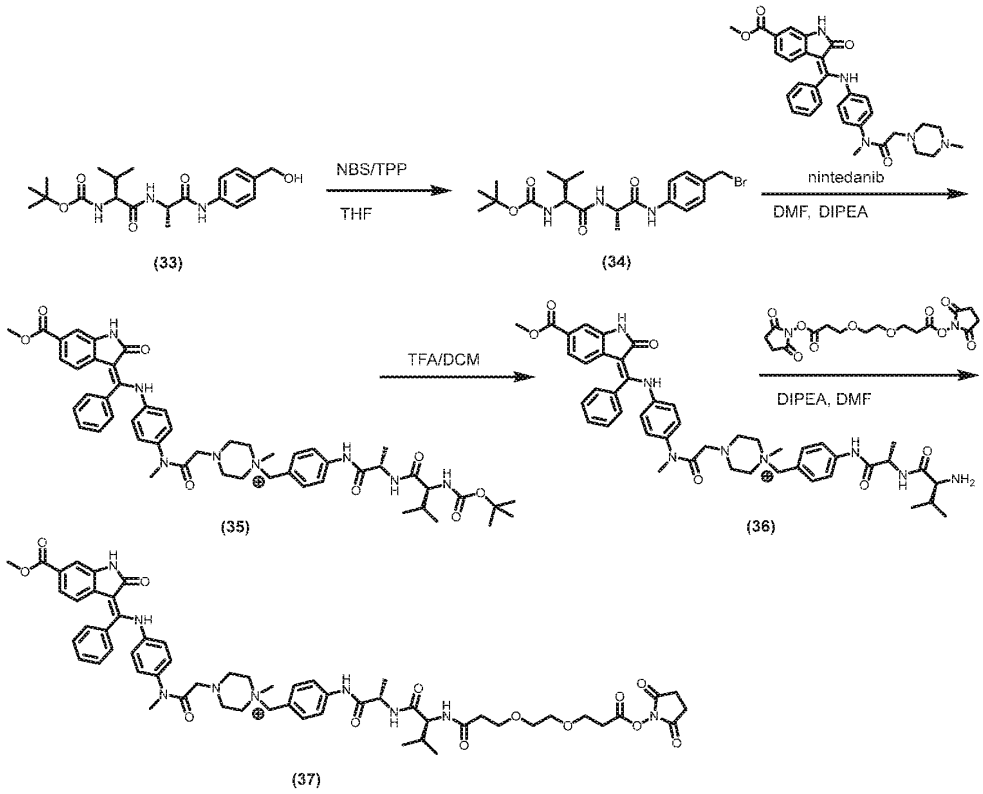

As described in WO2019232449, commercially available Boc-ValAla-PABA **33** (50 mg, 127 µmol) was dissolved in anhydrous THF (5 mL). Triphenylphosphine (40 mg, 152 µmol) and NBS (27 mg, 152 µmol) were then added and the reaction mixture was allowed to stir at RT under nitrogen for 7 hours. The solvent was then removed at reduced pressure, and the resulting crude purified on NP automated chromatography [Biotage, (DCM/MeOH (0-50%)]. Combined fractions were concentrated to give the brominated derivative **34** as a yellow solid 49 mg (84 %). LCMS m/z 469 (M+Na).

[As described in WO2019232449, the brominated Val-Ala derivative **34** (25 mg, 54.8 µmol) and nintedanib (29.5 mg, 54.8 µmol) were dissolved in anhydrous DMF (2 ml), DIPEA (14.3 µl, 82.2 umol) was then added and the reaction mixture stirred at RT under nitrogen for 17 hours. The solvent was removed under vacuum and the resulting crude purified on NP automated chromatography [Biotage, (Hex/EOAc (0-100%)], to give the quaternary ammonium Boc-val-ala **35** as an off-white solid 3 mg (6% yield). LCMS m/z 916 (M+1), 540 (nintedanib fragment), 408 (M-Boc/2).

To the Boc-protected Val-Ala-nintedanib **35** (3 mg, 3.3 µmol), 10% TFA solution in dry DCM (3.3 ml) was added dropwise over 30 minutes and the reaction mixture stirred at RT under nitrogen. After addition was complete, the solvent and TFA were removed under high vacuum. LCMS analysis showed the desired deprotected val-ala-nintedanib-amine **36** as a single peak pure enough to be telescoped into next reaction without further purification. LCMS m/z 816 (M+1), 540 (nintedanib fragment), 408 (M/2).

The deprotected nintedanib-Val-Ala-amine **36** (2.7 mg, 3.3 µmol) was dissolved in dry DMF (1 ml) and added dropwise (syringe pump) over 70 min to a stirred solution of bis-PEG_2-NHS ester (13.1 mg, 32.8 µmol) and DIPEA (1.7 µl, 9.8 µmol) in dry DMF (0.5 ml) at RT under nitrogen. After the addition was completed, the reaction mixture was allowed to stir for a further 35 minutes at RT after which the DMF was removed under high vacuum. The crude was purified on RP automated chromatography [Biotage (water + 0.1% TFA/ACN + 0.1% TFA, 0-100%)] to give the desired nintedanib-val-ala-PEG_2-NHS ester **37** as a bright yellow solid 0.84 mg (23 % overall). LCMS m/z 1101.40 (M+1), 540 (nintedanib fragment).

Example 19: Synthesis of Nintedanib α-Galactose-PEG_7 NHS Ester (46)

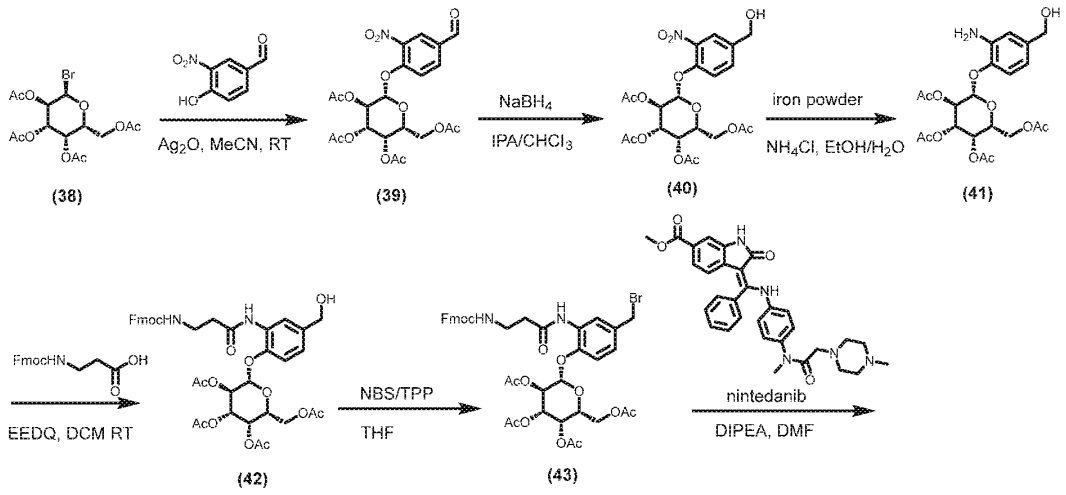

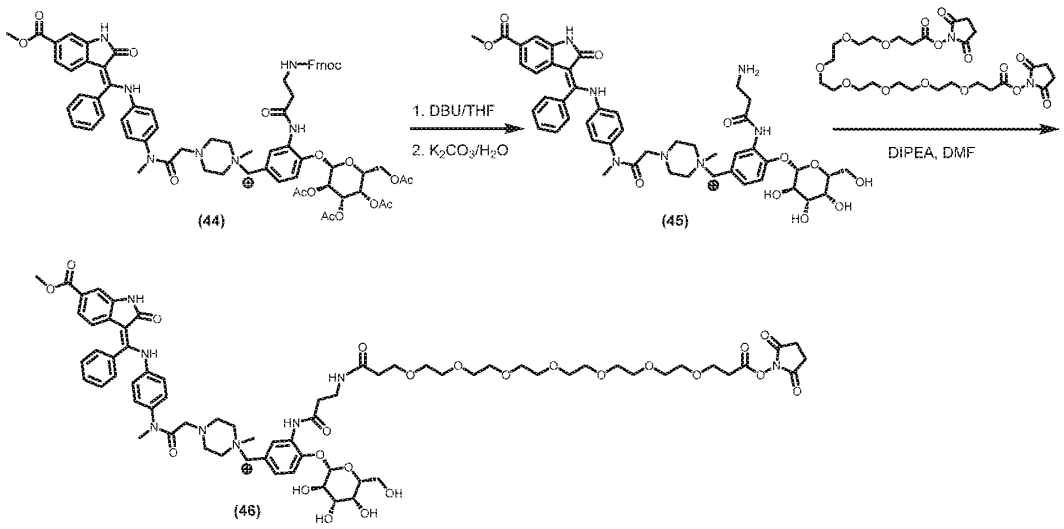

As described in Li Y et al. [224]. α-Galactose tetraacetate bromide **38** (500 mg, 1.22 mmol), 4-hydroxy-3-nitrobenzaldehyde (341 mg, 2.04 mmol) and silver oxide (1.10 g, 4.75 mmol) were stirred in anhydrous MeCN (12 mL) under nitrogen for 3 h at RT after which it was filtered through celite. The bright yellow solution was concentrated *in vacuo* to leave a yellow solid, which was redissolved in EtOAc (10 ml) and washed with sodium bicarbonate saturated solution (15 mL). The aqueous layer was further back extracted with EtOAc (3 x 20 mL). The organic layers were combined, dried over $MgSO_4$ and dried under reduced pressure to give the galactose tetraacetate-benzaldehyde derivative **39** as a light-yellow solid 551 mg (91%). This was used in the next reaction without further purification. Monitored by TLC (H/EA 1:1); Rf = 0.17.

As described in Li Y et al. [224], a solution of the benzaldehyde-galactose tetraacetate **39** (551 mg, 1.11 mmol) was dissolved in in IPA/$CHCl_3$ (1:5, 30 ml) and cooled to 0°C, $NaBH_4$ (125 mg, 3.33 mmol) was then added portion wise, and the reaction mixture stirred under N_2 at 0° for 1 hour. A second portion (125 mg, 3.33 mmol) of $NaBH_4$ was then added and the mixture stirred for a further 2.5 h after which the reaction mixture was quenched by the careful addition of water (30 mL). The organic layer was separated, and the aqueous layer was further extracted with ethyl acetate (3 x 30 mL). The organic phases were combined, dried over $MgSO_4$, filtered, and concentrated under vacuum to give the benzyl alcohol **40** as alight yellow solid 506 mg (91.5% yield). This was used without further purification in the next reaction. Reaction monitored by TLC (H/EA 1:1); Rf = 0.069. LCMS m/z: 517.30 (M + H2O), 522.30 (M + Na)

The galactose tetraacetate-nitrobenzene derivative **40** (506 mg, 1.01 mmol) was dissolved in a 6:5 EtOH/water mixture (13 ml), NH_4Cl (60 mg, 1.11 mmol) and iron powder (283 mg, 5.10 mmol) were then added, and the mixture stirred at 80°C for 3h. The reaction was followed by TLC (silica gel Hexane/EA 1:1, Rf = 0.13), filtered through celite and concentrated *in vacuo* to give the amine derivative **41** as a white solid 226 mg of (48%) which was pure enough to use without further purification. LCMS m/z = 470.30 (M+1), 493.30 (M + Na).

The galactose tetraacetate amine **41** (226 mg, 4.8 µmol), Fmoc-β-alanine (165 mg, 5.3 µmol), and EEDQ (238 mg, 963 µmol) were placed in a round bottom flask and dissolved in dry DCM (12 ml). The reaction mixture was stirred for 21 h under an inert atmosphere after which it was quenched by the addition of sodium bicarbonate saturated solution (15 mL) and the phases separated. The aqueous layer was further back extracted with EtOAc (3 x 20 mL), the organics were then combined, dried over $MgSO_4$ and concentrated *in vacuo*. The crude was purified by NP automated chromatography [Biotage, Hexane/EA (10-100%)] to give galactose tetraacetate Fmoc-β-alanine derivative **42** as a white solid 188 mg (51 %). LCMS m/z = 763.50 (M+1), 785.46 (M+Na).

As described in Hamilton JZ et al. [225]. The galactose tetraacetate benzyl alcohol derivative **42** (88 mg, 115.4 µmol) was dissolved in dry THF (2 ml), triphenylphosphine (45 mg, 173 µmol) and NBS (31 mg, 173 µmol) were then added sequentially to the solution, and the mixture allowed to stir at RT under nitrogen for 24 h. The reaction mixture was then concentrated *in vacuo* and crude purified by NP automated chromatography [Biotage, Hex/EtOAc (30-70%)]. Combined fractions were concentrated to give the benzyl galactose tetraacetate benzyl bromide derivative **43** as a white solid (25 mg (26 %). LCMS m/z = 827.40 (M+1), 849.33 (M+Na).

To a solution of the galactose tetraacetate benzyl bromide **43** (25 mg, 30 µmol) and nintedanib (16.3 mg, 30 µmol) in dry DMF (2 ml) DIPEA (7.9 µL, 45 µmol) was added and the resulting mixture was allowed to stir under nitrogen at RT for 3h. The reaction mixture was then concentrated *in vacuo* and the crude purified on RP automated chromatography [Biotage (water + 0.1% TFA/ACN + 0.1% TFA, 0-100%)]. Combined fractions were concentrated to give the nintedanib-galactose tetraacetate **44** as a white solid 21 mg (54 %). m/z = 1286.00 (M+1), 540.42 (nintedanib fragment).

To a stirred solution of the nintedanib-galactose tetraacetate **44** (15 mg, 117 µmol) in 5 mL of a 1:1 mixture of MeOH and THF, DBU (8.7 µL, 58 µmol) was added and the mixture stirred at RT for 5 min after which a solution of potassium carbonate (16 mg, 117 µmol) dissolved in 2.5 ml water was added at RT and the reaction mixture stirred for a further 25 more min. after which it was purified by RP automated chromatography [Biotage (water

+ 0.1% TFA/ACN + 0.1% TFA, 0-100%)] to give the globally deprotected derivative nintedanib-galactose **45** as a white solid 10 mg (96 %). LCMS m/z = 894.70 (M+1), 540.40 (nintedanib fragment).

To a stirred solution of bis-PEG$_7$-NHS ester (83 mg, 134 µmol) in dry DMF (1 ml) and DIPEA (7 µL, 40 µmol) under nitrogen, a solution of nintedanib-galactose amine **45** (12 mg, 13.4 µmol) dissolved in dry DMF (1 ml) was added dropwise over 1 h using a syringe pump. After the addition was complete, the mixture was allowed to stir for a further 30 min. The solvent was then removed under high vacuum and the crude purified by RP automated chromatography [Biotage (water + 0.1% TFA/ACN + 0.1% TFA, 10-100%)] to give nintedanib α-Galactose-PEG$_7$ NHS Ester **46** as pale-yellow solid 5.8 mg (31 %) after lyophilisation. LCMS m/z = 1400.20 (M+1), 540.40 (nintedanib fragment).

Example 20: Synthesis of Dexamethasone-dipyrophosphate-PEG$_2$ TFP Ester (50)

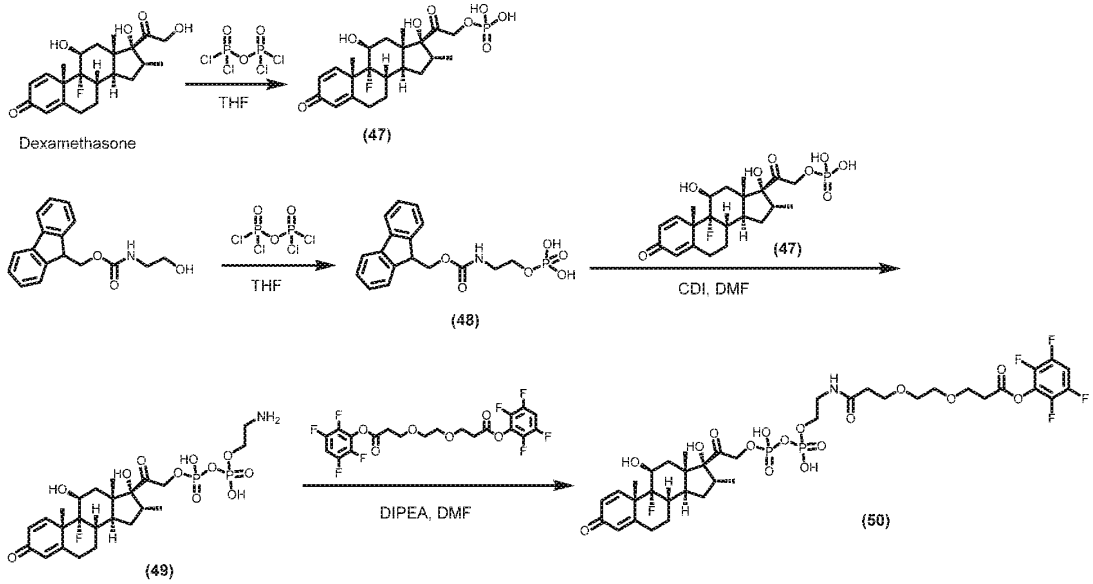

As described in Kern JC et al. [198], to a solution of dexamethasone (2 g, 5.1 mmol) in THF (2 ml) at -40°C was added diphosphoryl chloride (1.8 mL, 12.7 mmol). The reaction mixture was stirred at -40°C for 2 h, quenched with water and treated with saturated sodium bicarbonate solution unti pH~8. The solution was then made acidic by the drop wise addition of 1N HCl solution and extracted with EtOAc (300 mL). The combined organic layers were washed with brine, dried over Na_2SO_4, filtered and concentrated to afford dexamethasone dihydrogen phosphate **47** as a yellow solid 2.09 g (86%) LCMS *m/z* = 473.4 $[M+H]^+$, ^1H NMR (400 MHz, DMSO-d_6) δ 7.29 (d, *J* = 10.2 Hz, 1H), 6.22 (dd, *J* = 10.2, 1.8 Hz, 1H), 6.01 (s, 1H), 4.97 – 4.87 (m, 1H), 4.55 – 4.46 (m, 1H), 4.15 (dd, *J* = 10.4, 3.2 Hz, 1H), 3.85 – 3.58 (m, 2H), 2.99 – 2.86 (m, 1H), 2.68 – 2.57 (m, 1H), 2.43

– 2.26 (m, 2H), 2.20 – 2.05 (m, 2H), 1.82 – 1.72 (m, 1H), 1.69 – 1.54 (m, 2H), 1.51 – 1.48 (m, 7H), 1.46 – 1.41 (m, 1H), 1.38 – 1.27 (m, 1H), 1.12 – 1.03 (m, 1H), 0.79 (d, *J* = 7.2 Hz, 3H).

As described in Kern JC et al. [198], to a solution of (9H-fluoren-9-yl)methyl (2-hydroxyethyl)carbamate (2 g, 7.06 mmol) in THF (2 ml) at -40°C was added diphosphoryl chloride (2.4 mL, 17.65 mmol). The reaction mixture was stirred at -40°C for 2 h. The reaction was quenched with water and treated with saturated sodium bicarbonate solution unti pH~8. The solution was made acidic by the addition of 1N HCl solution and extracted with EtOAc (300 mL). The combined organic layers were washed with brine, dried over Na_2SO_4, filtered and concentrated to afford (9H-fluoren-9-yl)methyl (2-(phosphonooxy)ethyl)carbamate **48** as a white solid 2.6 g (100%). LCMS *m/z* = 364.3 $[M+H]^+$, ^1H NMR (400 MHz, DMSO-d_6) δ 7.89 (d, *J* = 7.6 Hz, 2H), 7.69 (d, *J* = 7.4 Hz, 2H), 7.43 – 7.39 (m, 2H), 7.36 – 7.31 (m, 2H), 4.29 (d, *J* = 6.2 Hz, 2H), 4.21 (t, *J* = 7.0 Hz, 1H), 3.80 (q, *J* = 6.4 Hz, 2H), 3.21 (q, *J* = 6.0 Hz, 2H).

As described in Kern JC et al. [198], to a stirred solution of (9H-fluoren-9-yl)methyl (2-(phosphonooxy)ethyl)carbamate **48** (500 mg, 1.38 mmol) in DMF (5 mL) was added triethylamine (348 mg, 3.44 mmol) and CDI (223 mg, 1.38 mmol). The resulting solution was stirred at room temperature for 30 min. To this mixture were added dexamethasone dihydrogen phosphate **47** (520 mg, 1.1 mmol), the mixture was allowed to stir at room temperature overnight. The reaction was diluted with 1 N HCl to pH-7 and purified by RP preparative chromatography (25% MeCN/water with 0.1% HCOOH) to give the Fmoc-deprotected dexamethasone ethylamino-dihydrogen pyrophosphate **49** as a white solid 200 mg (24%). LCMS *m/z* = 596.4 $[M+H]^+$, ^1H NMR (400 MHz, DMSO-d_6) δ 8.27 (s, 2H), 7.29 (d, *J* = 10.2 Hz, 1H), 6.21 (dd, *J* = 10.2, 1.8 Hz, 1H), 6.00 (s, 1H), 4.83 – 4.72 (m, 1H), 4.67 – 4.56 (m, 1H), 4.15 (d, *J* = 11.6 Hz, 1H), 4.11 – 4.03 (m, 2H), 3.88-3.67 (m, 3H), 3.37 – 3.32 (m, 1H), 3.06 – 2.87 (m, 3H), 2.68 – 2.55 (m, 1H), 2.42 – 2.26 (m, 2H), 2.17 – 1.95 (m, 2H), 1.80 – 1.67 (m, 2H), 1.61 (q, *J* = 11.6 Hz, 1H), 1.49 (s, 3H), 1.41 – 1.28 (m, 1H), 1.11 – 1.01 (m, 1H), 0.88 (s, 3H), 0.78 (d, *J* = 7.2 Hz, 3H).

To a solution of dexamethasone ethylamino-dihydrogen pyrophosphate **49** (120 mg, 0.2 mmol) in DMF (2 mL) was added bis-PEG_2-(2,3,5,6-tetrafluorophenyl) ester (111 mg, 0.22 mmol) and DIPEA (78 mg, 0.6 mmol). The reaction mixture was stirred at room temperature for 1.5 h and purified by RP prep-HPLC (water + 0.1% TFA: MeCN) to give the dexamethasone dihydrogen pyrophosphate 2,3,5,6-tetrafluorophenyl PEG_2 ester as a brown solid 16 mg (8%). LCMS m/z = 932.5 $[M+H]^+$, ^1H NMR (400 MHz, DMSO-d_6) δ 8.17 (d, *J* = 5.6 Hz, 1H), 7.99 – 7.86 (m, 1H), 7.29 (d, *J* = 10.2 Hz, 1H), 6.21 (dd, *J* = 10.2, 1.8 Hz, 1H), 6.00 (s, 1H), 4.98 (dd, *J* = 17.8, 8.8 Hz, 1H), 4.63 (dd, *J* = 17.8, 7.8 Hz, 1H), 4.14 (d, *J* = 10.2 Hz, 1H), 3.91 (q, *J* = 6.2 Hz, 2H), 3.76 (t, *J* = 6.0 Hz, 2H), 3.62 –

3.57 (m, 9H), 3.27 (q, *J* = 5.8 Hz, 2H), 3.01 (t, *J* = 5.8 Hz, 2H), 2.96 – 2.87 (m, 1H), 2.67 – 2.57 (m, 1H), 2.46 – 2.37 (m, 1H), 2.36 – 2.27 (m, 4H), 2.17 – 2.04 (m, 2H), 1.80 – 1.72 (m, 1H), 1.68 – 1.50 (m, 2H), 1.48 (s, 3H), 1.44 – 1.28 (m, 1H), 1.10 – 1.02 (m, 1H), 0.88 (s, 3H), 0.78 (d, *J* = 7.2 Hz, 3H).

Example 21: Synthesis of N^1-Benzylamino Imidazoquinoline-PEG_7 NHS Ester (54)

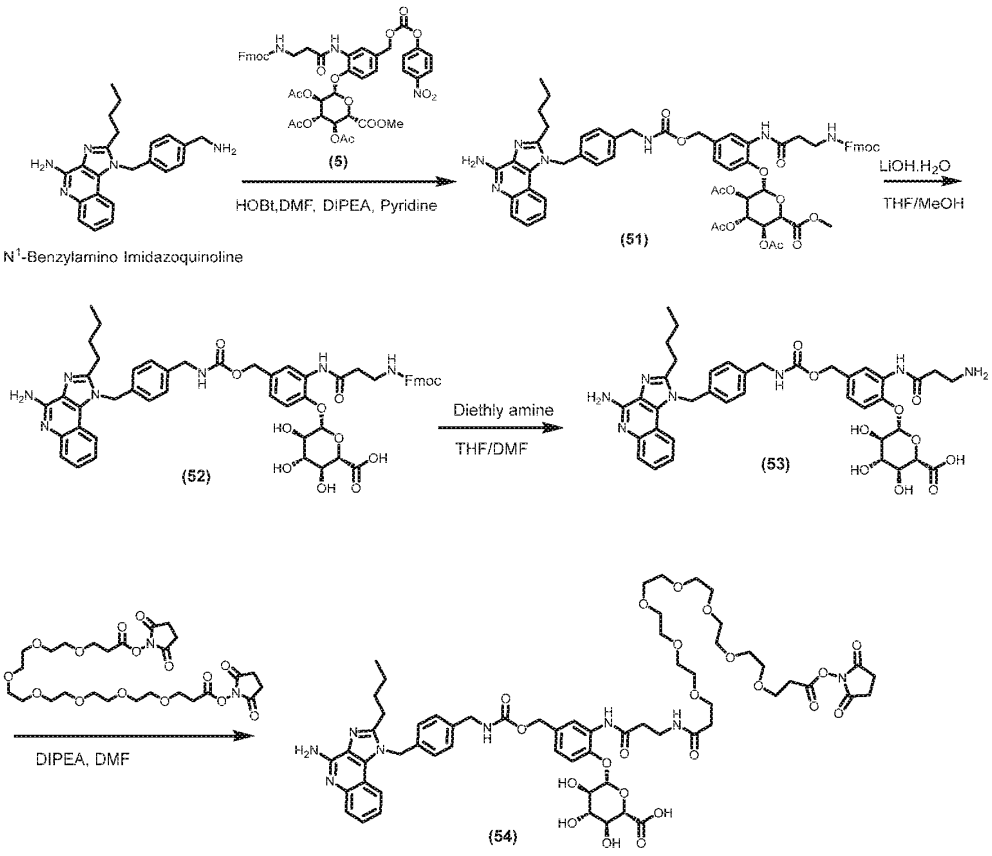

To a stirred solution of N^1-benzylamino imidazoquinoline hydrochloride (20.3 mg, 0.047 mmol) in dry DMF (0.5 ml) DIPEA (32.8 µl, 0.188 mmol) was added, and the solution was allowed to stir for 15 minutes at RT under inert atmosphere. In another flask, the PNP-carbonate ester **7** (43 mg, 0.047 mmol) and HOBt (7 mg, 0.052 mmol) were dissolved in dry DMF 1 ml and pyridine 0.3 ml at RT under nitrogen. The latter solution was then added to the imidazoquinoline/DIPEA solution and the reaction mixture was stirred at RT for 2h 40 min. The reaction mixture was concentrated *in vacuo* and the crude purified by NP automated chromatography [Biotage, DCM/MeOH (0-40%)]. The combined fractions were concentrated to the glucuronide-imidazoquinoline derivative **51** as an off-white solid 31 mg (62 %). LCMS m/z 1134.68 (M+1), 1162.70 (M+Na), 739.60

The glucuronide-imidazoquinoline derivative **51** (10 mg, 0.0088 mmol) was dissolved in a mixture of a MeOH/THF 1:1 (2 ml), this was cooled with an ice/water bath and a solution of $LiOH.H_2O$ (2.2 mg, 0.053 mmol) dissolved in 1 ml water added dropwise over 1 h. The reaction mixture was stirred for a further 45 further min. after which it was quenched with acetic acid (3 µL, 0.0053 mmol), and concentrated *in vacuo*. The crude deprotected βGA-Fmoc derivative **52** was used without further purification. LCMS m/z 994.60 (M+1); 497.93 (M/2).

The Fmoc-protected imidazoquinoline-βGA **52** (8.8 mg, 0.0088 mmol) was dissolved in dry DMF (1 ml)and DIPEA (31 µL, 0.301 mmol) was added. The reaction mixture was stirred for 50 minutes under nitrogen and concentrated *in vacuo*. The crude was purified by RP automated chromatography [Biotage (water + 0.1% TFA/ACN + 0.1% TFA, 10-100%)] and appropriate fractions combined and lyophilised to give the desired fully-deprotected imidazoquinoline-βGA amine **53** as a white solid (quantitative yield). LCMS m/z 772.50 (M+1); 386.81 (M/2); 377.81 (M – payload).

To a stirred solution of bis-PEG_7-NHS (28.1 mg, 0.045 mmol) dissolved in dry DMF (1 ml) and DIPEA (2.4 µL, 0.0136 mmol) a solution of the Imidazoquinoline-βGA-amine **53** (3.5 mg, 0.0045 mmol) dissolved in dry DMF (1 ml) was added dropwise over 1 h using a syringe pump. Once addition was complete the solvent was removed on high vacuum and the crude purified by RP automated chromatography [Biotage (water + 0.1% TFA/ACN + 0.1% TFA, 0-100%)] to give the desired N^1-Benzylamino Imidazoquinoline-PEG_7 NHS ester **54** as white powder after lyophilisation 3 mg (52%). LCMS m/z = 1278.20 (M+1); 386.81 (M/2); 1300.18 (M+Na).

Example 22: Synthesis of Triptolide-PEG$_6$ NHS Ester (58)

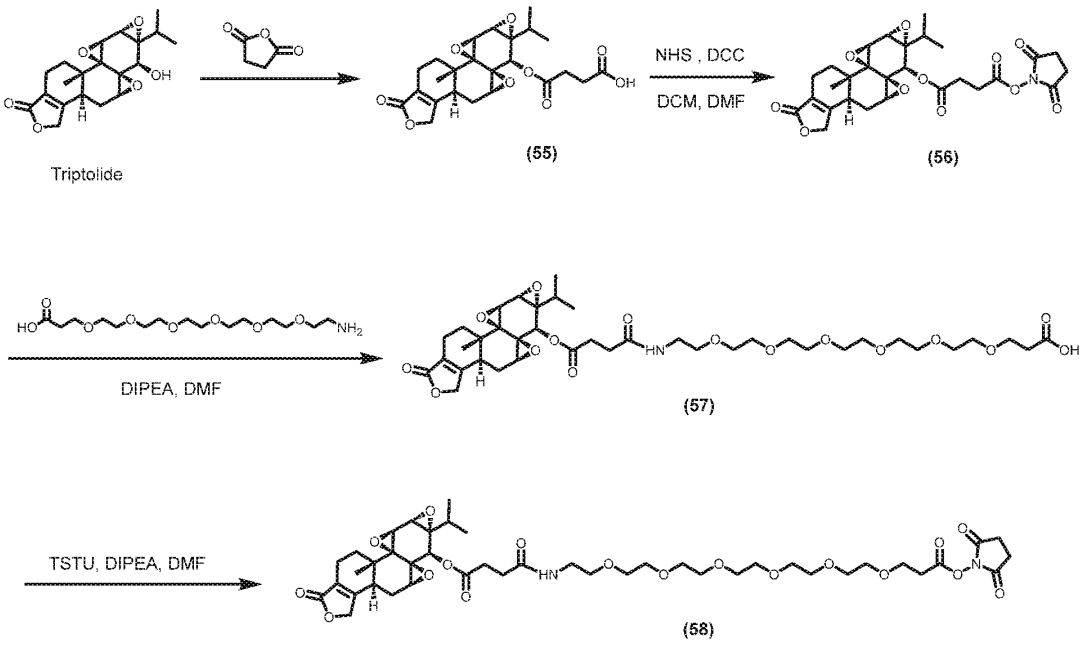

As described in Zhang K et al. [226], succinic anhydride (11 mg, 111 µmol), DMAP (0.7 mg, 5.6 µmol) and triptolide (10 mg, 28 µmol) were dissolved in 0.6 ml of dry pyridine and allowed to stir at RT under inert atmosphere for 26h.The mixture was diluted with ethyl acetate (5 ml) and washed with saturated copper sulphate solution (5 ml), water (5 ml), and brine (5 ml). The organic phase was separated, dried over sodium sulphate and the solvent was removed under reduced pressure. The crude was purified by NP automated chromatography [Biotage (DCM/MeOH 0-20%)] to give the triptolide succinate **55** as a white solid 6 mg (47%). Monitored by TLC (H/EA, 3:1). Rf = 0.25. LCMS m/z = 461.27 (M+1), 483.30 (M+Na), 361.27 (triptolide fragment).

As described in Zhang K et al. [226], triptolide succinate **55** (3 mg, 6.5 µmol) was dissolved in dry DMF (0.2 ml) and dry DCM (1.6 ml), DCC (1.6 mg, 7.8µmol) and n-hydroxysuccinimide (0.83 mg, 7.2 µmol) were sequentially added and the mixture was allowed to stir at RT under an inert atmosphere for 24 hours. The mixture was concentrated under a vacuum and the residue purified by RP automated chromatography [Biotage (water + 0.1% TFA/ACN + 0.1% TFA, 10-90%)] to give NHS-activated ester triptolide derivative **56** 2.57 mg (71%). m/z: 558.39 (M+1), 558.40 (M+Na), 1115.81 (dimer), 361.22 (triptolide fragment).

The triptolide succinic acid NHS ester **56** (1.2 mg, 2.2 µmol) was dissolved in dry DMF (1 ml) and DIPEA (1.1 µL, 6.5 µmol) was added followed by the addition of the amino-PEG_6-COOH. The mixture was allowed to stir at RT under inert atmosphere for 2 hours after which the solvent was removed under a vacuum to give triptolide-succinate-PEG_6-acid **57** which was used directly in the next step without purification. LCMS m/z = 796.61 (M+1), 818.64 (M+ Na).

Triptolide-succinate-PEG_6 acid **57** (1.71 mg, 2.2 µmol) was stirred with TSTU (1.3 mg, 4.3 µmol) and DIPEA (1.9 µl, 10.7 µmol) in dry DMF (1 ml) for two hours under nitrogen. The solvent was removed at high vacuum and the residue was purified by RP automated chromatography [Biotage (water + 0.1% TFA/ACN + 0.1% TFA, 0-90%)] to give the triptolide-succinate-PEG_6 NHS ester **58** as a white solid after lyophilisation 0.5 mg. LCMS m/z = 893.70 (M+1), 915.70 (M+Na).

Example 23: Synthesis of Maleimidocaproly-GGFG-Exatecan (59)

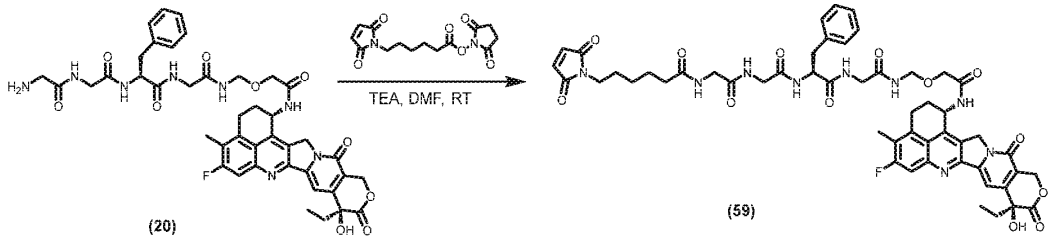

As described in EP3101032, DXd-GGFG **20** (50 mg, 59.46 µmol) was dissolved in dry DMF, maleimidocaproyl-NHS hexanoate (20.16 mg, 65.41 µl) was then added followed by TEA (5.42 mg, 53.52 µl) and the reaction mixture stirred under nitrogen for 2 h. The solvent was removed under high vacuum and the residue purified by RP automated chromatography to give Maleimidocaproly-GGFG-Exatecan **59** as a yellow solid 6.42 mg (10.5%). LCMS m/z 1034.80 (M+1), 1056.78 (M+Na)

Example 24: Synthesis of Maleimidocaproly-Val-Cit-MMAE (61)

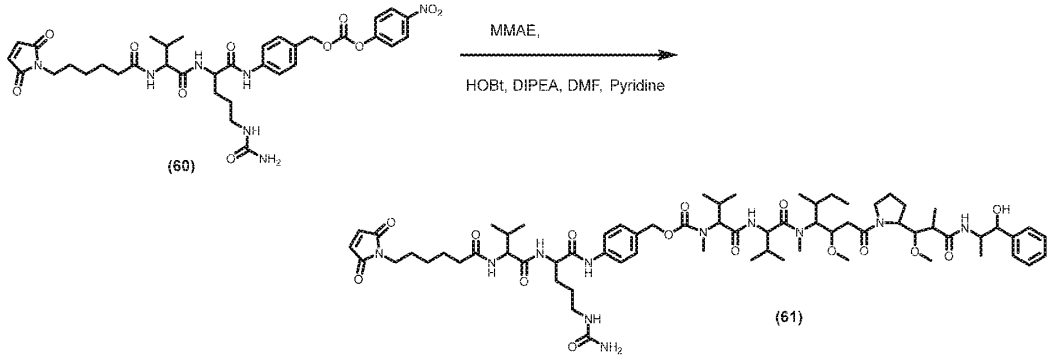

MMAE (40 mg, 55.71 µmol), commercially available maleimidocaproyl-Val-Cit-PAB-PNP **60** (49.32 mg, 66.85 µl), HOBt (7.68 mg, 56.83 µl) and DIPEA (10.67 µl, 61.28 µmol) was stirred in dry DMF with a drop of pyridine under nitrogen for 19 h. The solvent was removed under high vacuum and the residue purified by RP automated chromatography to give the desired MMAE derivative **61** as a white solid after lyophilisation 17.7 mg. m/z = 1317.50 (M+1), 659.40 (M/2), 1341.47 (M+Na).

Example 25: Synthesis of MMAE-Val-Ala-Oligosaccharide-PEG2-TFP Ester (69)

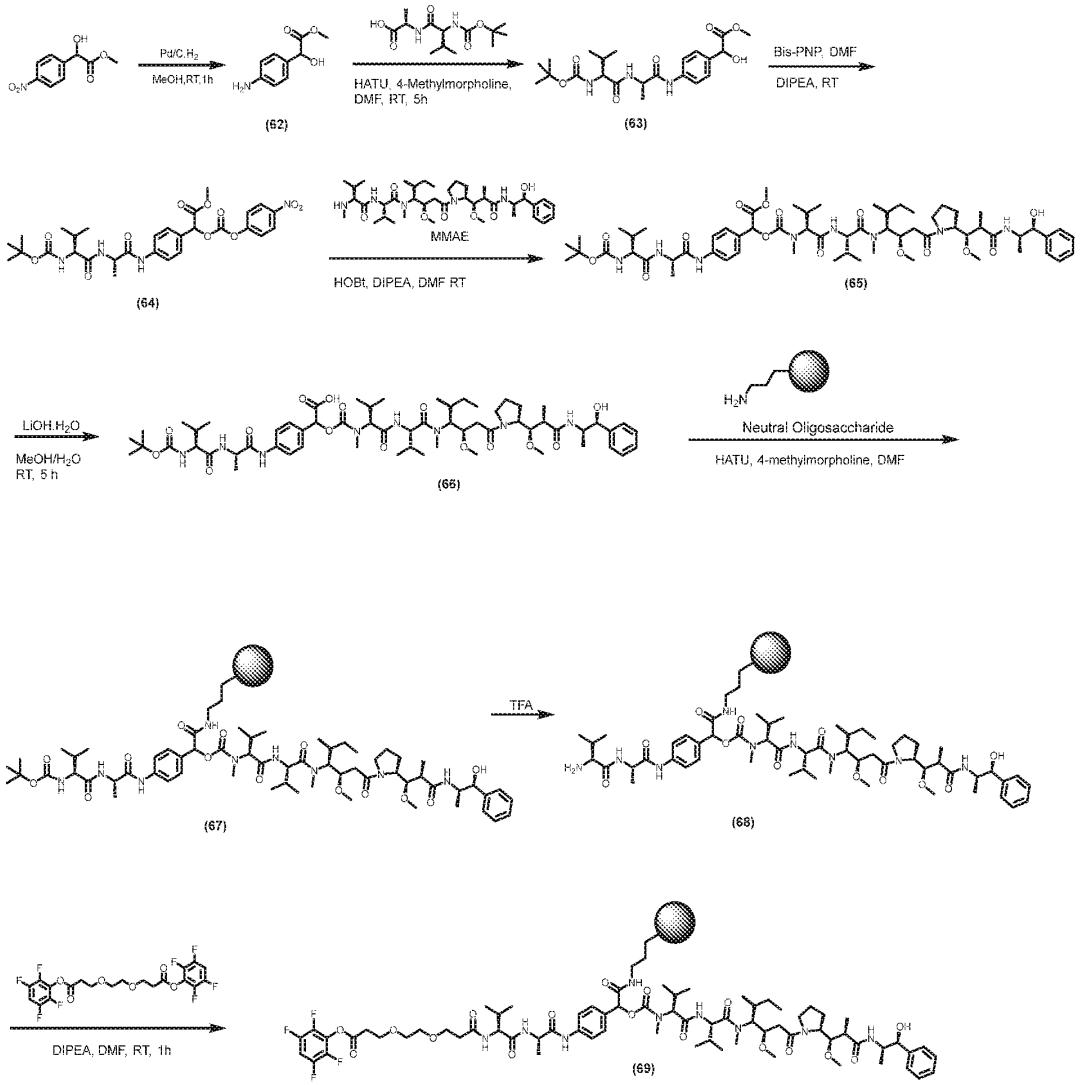

As described in Quintana JM et al. [227], to a solution of methyl 2-hydroxy-2-(4-nitrophenyl)acetate (1.5 g, 7.1 mmol) in MeOH (12 ml) was added 10% Pd/C (300 mg). The reaction mixture was stirred at room temperature for 3 h under hydrogen. The reaction was filtered through Celite washed with with EtOAc and concentrated to afford methyl 2-(4-aminophenyl)-2-hydroxyacetate **62** as a yellow solid 760 mg (59%). LCMS *m/z* = 182.2 $[M+H]^+$, ^1H NMR (400 MHz, DMSO-d_6) δ 7.01 (d, *J* = 8.4 Hz, 2H), 6.50 (m, 2H), 5.67 (d, *J* = 5.4 Hz, 1H), 5.07 (s, 2H), 4.90 (d, *J* = 5.2 Hz, 1H), 3.57 (s, 3H).

To a solution of (tert-butoxycarbonyl)-L-valyl-L-alanine (1.21 g, 4.19 mmol) in DMF (15 ml) was added dropwise 4-Methylmorpholine (637 mg, 6.29 mmol) at 0 °C, then HATU (1.75 g, 4.61 mmol) was added, followed by the addition of a solution of methyl 2-(4-

aminophenyl)-2-hydroxyacetate **62** (760 mg, 4.19 mmol) in DMF (6 ml), the ice bath was removed and the reaction mixture was stirred at room temperature for 5 h. The reaction was quenched with H_2O and extracted with EtOAc (30 ml× 3). The combined organic layers were washed with brine, dried over Na_2SO_4, filtered and concentrated, purified by column chromatography on silica gel (DCM/MeOH 50: 1) to afford methyl 2-(4-((S)-2-((S)-2-((tert-butoxycarbonyl)amino)-3-methylbutanamido)propanamido)phenyl)-2-hydroxyacetate **63** as a yellow solid 1.4 g (74%). LCMS *m/z* = 474.3 $[M+Na]^+$,^{1}H NMR (400 MHz, DMSO-d_6) δ 9.90 (d, *J* = 75.0 Hz, 1H), 8.14 (dd, *J* = 71.8, 7.4 Hz, 1H), 7.56 (dd, *J* = 16.0, 8.4 Hz, 2H), 7.34 – 7.29 (m, 2H), 6.75 (dd, *J* = 40.6, 8.6 Hz, 1H), 6.01 – 5.98 (m, 1H), 5.11 – 5.05 (m, 1H), 4.48 – 4.38 (m, 1H), 3.87 – 3.75 (m, 1H), 3.59 (s, 3H), 2.02 – 1.87 (m, 1H), 1.37 (d, *J* = 5.8 Hz, 9H), 1.29 (dd, *J* = 7.2, 1.8 Hz, 3H), 0.87 – 0.80 (m, 6H).

To a stirred solution of methyl 2-(4-((S)-2-((S)-2-((tert-butoxycarbonyl)amino)-3-methylbutanamido)propanamido)phenyl)-2-hydroxyacetate **63** (500 mg, 1.11 mmol) in dry DMF (8 ml) was added DIPEA (215 mg, 1.66 mmol) and bis(4-nitrophenyl) carbonate (674 mg, 2.21 mmol) at 0 °C. The resulting solution was stirred at room temperature for 4h, quenched with H_2O and extracted with EtOAc (30 mL× 3). The combined organic layers were washed with brine, dried over Na_2SO_4, filtered and concentrated, purified by column chromatography on silica gel (DCM/MeOH 60: 1) to afford methyl 2-(4-((S)-2-((S)-2-((tert-butoxycarbonyl)amino)-3-methylbutanamido)propanamido)phenyl)-2-(((4-nitrophenoxy)carbonyl)oxy)acetate **64** as a yellow solid 580 mg (85%). LCMS *m/z* = 639.4 $[M+Na]^+$,^{1}H NMR (400 MHz, DMSO-d_6) δ 10.07 (d, *J* = 71.4 Hz, 1H), 8.34 (d, *J* = 9.2 Hz, 2H), 8.13 – 8.07 (m, 1H), 7.72 – 7.64 (m, 2H), 7.58 (d, *J* = 9.2 Hz, 2H), 7.45 (d, *J* = 8.2 Hz, 2H), 6.09 (d, *J* = 2.4 Hz, 1H), 4.48 – 4.38 (m, 1H), 3.88 – 3.76 (m, 1H), 3.71 (s, 3H), 2.01 – 1.88 (m, 1H), 1.37 (d, *J* = 6.0 Hz, 9H), 1.30 (dd, *J* = 7.2, 2.4 Hz, 3H), 0.88 – 0.80 (m, 6H).

To a solution of methyl 2-(4-((S)-2-((S)-2-((tert-butoxycarbonyl)amino)-3-methylbutanamido)propanamido)phenyl)-2-(((4-nitrophenoxy)carbonyl)oxy)acetate **64** (181 mg, 0.29 mmol) in dry DMF (2 ml) was added DIPEA (114 mg, 0.88 mmol), HOBt (60 mg, 0.44 mmol) and MMAE (253 mg, 0.35 mmol). The mixture was stirred at rt overnight under nitrogen. The mixture was diluted with water (100 ml) and extracted with EtOAc (50 ml × 3). The combined organic layers were washed with brine (150 ml), dried over Na_2SO_4, filtered and concentrated. The residue was purified by chromatography on silica gel (DCM/MeOH 100:1 to 20:1) to afford the MMAE derivative **65** as a white solid 270 mg (77%). LCMS *m/z* = 1195.9 $[M+H]^+$,^{1}H NMR (400 MHz, DMSO-d_6) δ 10.16 – 9.87 (m, 1H), 8.32 – 8.03 (m, 2H), 7.87 (d, *J* = 8.4 Hz, 1H), 7.67 – 7.59 (m, 2H), 7.54 – 7.39 (m, 2H), 7.33 – 7.13 (m, 5H), 6.74 (dd, *J* = 36.4, 8.4 Hz, 1H), 5.87 – 5.77 (m, 1H), 5.42

– 5.31 (m, 1H), 4.79 – 4.19 (m, 5H), 4.06 – 3.90 (m, 2H), 3.85 – 3.75 (m, 1H), 3.63 – 3.58 (m, 3H), 3.26 – 3.09 (m, 8H), 3.08 – 2.84 (m, 5H), 2.45 – 2.20 (m, 2H), 2.17 – 1.67 (m, 7H), 1.59 – 1.42 (m, 2H), 1.37 (d, *J* = 7.8 Hz, 9H), 1.32 – 1.22 (m, 5H), 1.07 – 0.70 (m, 32H), 0.66 – 0.56 (m, 1H).

To a solution of the MMAE derivative **65** (760 mg, 0.64 mmol) in MeOH (3 ml) was added a solution of LiOH.H_2O (86 mg, 2.03 mmol) in H_2O (3 ml) dropwise at 0 °C, and the mixture stirred at rt for 2h. The mixture was acidified with 1N HCl to pH-2, filtered with H_2O and concentrated to afford the MMAE-mandelic acid derivative **66** as a white solid 700 mg (93%). LCMS *m/z* = 1182.6 $[M+H]^+$,^{1}H NMR (400 MHz, DMSO-d_6) δ 10.14 – 9.84 (m, 1H), 8.28 – 8.03 (m, 1H), 8.01 – 7.84 (m, 1H), 7.67 – 7.56 (m, 2H), 7.54 – 7.37 (m, 2H), 7.36 – 7.10 (m, 6H), 6.85 – 6.62 (m, 1H), 5.69 (d, *J* = 12.6 Hz, 1H), 5.43 – 5.30 (m, 1H), 4.74 – 4.24 (m, 4H), 4.07 – 3.90 (m, 2H), 3.85 – 3.74 (m, 1H), 3.63 – 3.52 (m, 1H), 3.26 – 3.15 (m, 9H), 3.11 (d, *J* = 6.4 Hz, 1H), 3.01 – 2.92 (m, 3H), 2.30 – 2.07 (m, 3H), 2.00 – 1.69 (m, 6H), 1.55 – 1.44 (m, 2H), 1.37 (d, *J* = 6.8 Hz, 9H), 1.29 (d, *J* = 6.8 Hz, 5H), 1.05 – 0.74 (m, 33H).

To a solution of the MMAE-mandelic acid derivative **66** (11 mg, 0.009 mmol) in dry DMF (1 ml) was added HATU (4.3 mg, 0.01 mmol), the mixture was stirred at rt for 0.5h, then 4-Methylmorpholine (2 mg, 0.02 mmol) and the neutral oligosaccharide (10 mg, 0.009 mmol) were added, the mixture was stirred at rt under nitrogen for 2h and directly purified by prep-HPLC to afford the MMAE-Oligosaccharide derivative **67** as a white solid 3 mg (14%).

To a solution of the MMAE-Oligosaccharide derivative **67** (3 mg, 0.001 mmol) in H_2O (1 ml) was added TFA (0.3 mg, 0.003 mmol), the mixture was stirred at 50°C for 2h after which it was lyophilized to afford the Boc-deprotected derivative **68** which was used directly for the next step.

To a solution of the Boc-deprotected derivative **68** (2.86 mg, 0.001 mmol) in dry DMF (0.5 ml) was added bis(2,3,5,6-tetrafluorophenyl) 3,3'-(ethane-1,2-diylbis(oxy))dipropionate (0.7 mg, 0.001 mmol) and DIPEA (0.5 mg, 0.003 mmol). The reaction mixture was stirred at room temperature for 1 h under nitrogen after which it was directly purified by prep-HPLC to afford the tetrafluorophenyl ester derivative **69** as a white solid 1 mg (30%).

Example 26: Synthesis of Exatecan-MA-PEG$_{12}$-Val-Ala-PEG$_4$-NHS Ester (74)

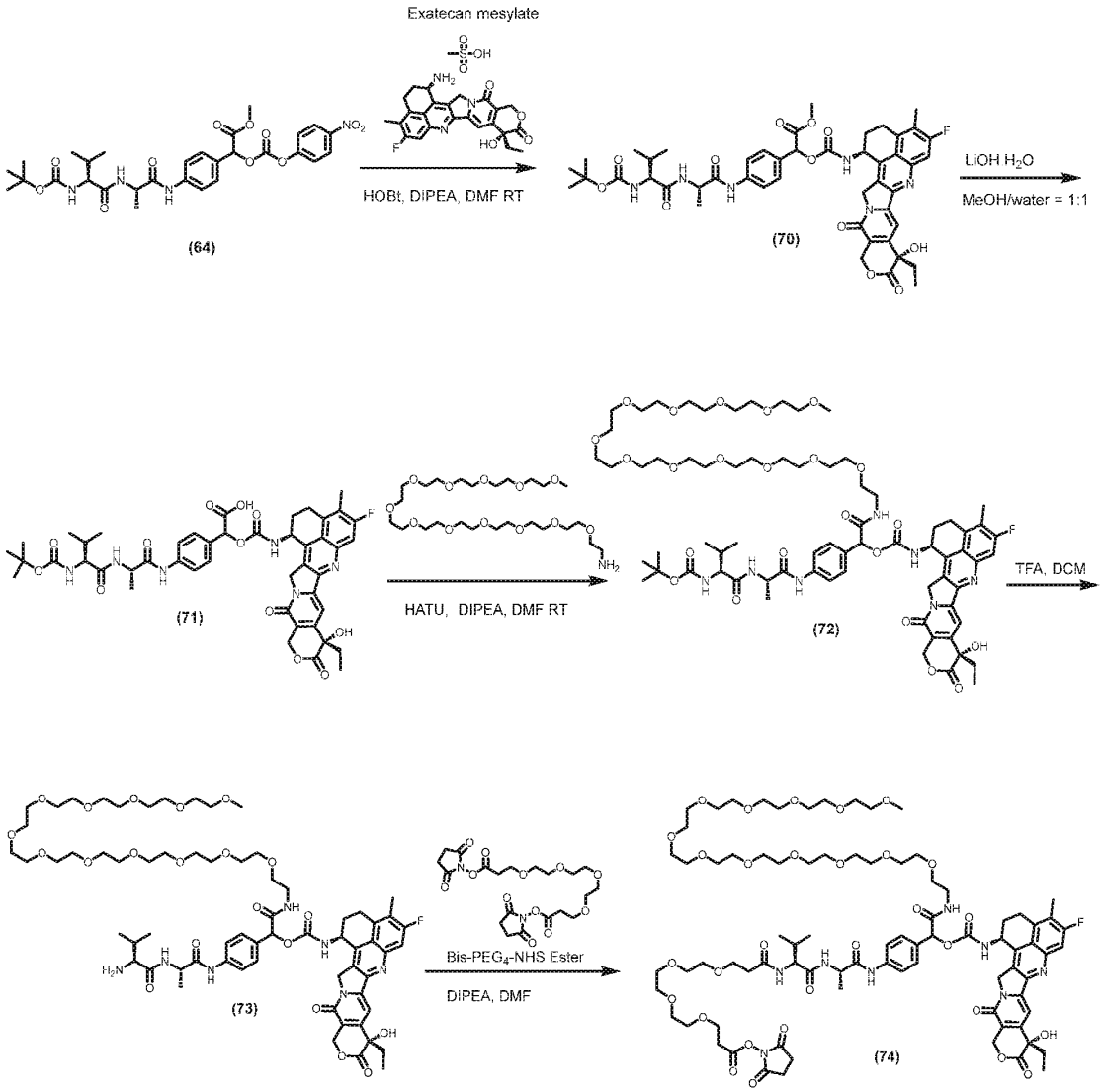

To a solution of methyl 2-(4-((S)-2-((S)-2-((tert-butoxycarbonyl)amino)-3-methylbutanamido)propanamido)phenyl)-2-(((4-nitrophenoxy)carbonyl)oxy)acetate **64** (500 mg, 0.811 mmol) and Exatecan mesylate (331 mg, 0.624 mmol) in dry DMF (10 ml) was added DIPEA (241 mg, 1.87 mmol). The reaction mixture was stirred at RT overnight under nitrogen. The reaction mixture was diluted with water (100 ml), filtered. The filter cake was purified by trituration with Et_2O to afford methyl 2-(4-((S)-2-((S)-2-((tert-butoxycarbonyl)amino)-3-methylbutanamido)propanamido)phenyl)-2-((((1S,9S)-9-ethyl-5-fluoro-9-hydroxy-4-methyl-10,13-dioxo-2,3,9,10,13,15-hexahydro-1H,12H-benzo[de]pyrano[3',4':6,7]indolizino[1,2-b]quinolin-1-yl)carbamoyl)oxy)acetate **70** as a yellow solid 500 mg (67.5%). LCMS *m/z* = 913.60 $[M+H]^+$. ^1H NMR (400 MHz, DMSO-d6)

δ 10.07 (s, 1H), 8.36 (t, J = 9.8 Hz, 1H), 8.07 (s, 1H), 7.80 – 7.73 (m, 1H), 7.62 (t, J = 11.4 Hz, 2H), 7.41 (t, J = 8.6 Hz, 2H), 7.31 (d, J = 11.8 Hz, 1H), 6.68 (d, J = 8.8 Hz, 1H), 6.51 (d, J = 5.6 Hz, 1H), 5.86 (d, J = 4.4 Hz, 1H), 5.43 (d, J = 6.2 Hz, 2H), 5.32 – 5.24 (m, 2H), 4.41 (s, 1H), 3.82 (s, 1H), 3.68 (d, J = 12.4 Hz, 3H), 3.15 (s, 1H), 2.37 (s, 3H), 2.21 (m, 2H), 1.87 (m, 2H), 1.36 (s, 9H), 1.28 (m, 3H), 0.85 (m, 9H).

To a stirred solution of methyl 2-(4-((S)-2-((S)-2-((tert-butoxycarbonyl)amino)-3-methylbutanamido)propanamido)phenyl)-2-((((1S,9S)-9-ethyl-5-fluoro-9-hydroxy-4-methyl-10,13-dioxo-2,3,9,10,13,15-hexahydro-1H,12H-benzo[de]pyrano[3',4':6,7]indolizino[1,2-b]quinolin-1-yl)carbamoyl)oxy)acetate **70** (100 mg, 0.109 mmol) in a mixture of THF (2 mL) and MeOH (1 mL) was added a solution of LiOH (5.25 mg, 0.219 mmol, 2.0 eq.) in water (1 mL) at 0 °C. The resulting solution was stirred at 0 °C for 30 min. then diluted with 1 N HCl to pH7 and then concentrated in vacuo. The crude was purified by prep-TLC (DCM/MeOH 10:1) to give the exatecan-madelic acid derivative **71** as a yellow solid 30 mg (30.6%). LCMS *m/z* = 899.20 $[M+H]^+$. ^{1}H NMR (400 MHz, DMSO-d6) δ 9.98 (d, J = 75.2 Hz, 1H), 8.29 – 8.02 (m, 2H), 7.78 (d, J = 10.8 Hz, 1H), 7.59 (m, 2H), 7.44 – 7.28 (m, 3H), 6.75 (m, 1H), 6.52 (d, J = 4.2 Hz, 1H), 5.68 (s, 1H), 5.50 – 5.19 (m, 5H), 4.42 (q, J = 7.2 Hz, 1H), 3.80 (dt, J = 16.4, 7.8 Hz, 1H), 3.10 – 2.97 (m, 4H), 2.39 – 2.35 (m, 3H), 2.27 – 2.08 (m, 2H), 1.91 (m, 4H), 1.36 (m, 10H), 1.33 – 1.27 (m, 4H), 0.85 (m, 9H).

To a solution of the exatecan-mandelic acid derivative **71** (60 mg, 0.067 mmol) in DMF (2 ml) was added HATU (45 mg, 0.134 mmol) and DIPEA (26 mg, 0.202 mmol). The reaction mixture was stirred at room temperature for 15 min. after which the PEG_{12}-amine was added (75 mg, 0.134 mmol) and the mixture and stirred at RT overnight under nitrogen. The reaction was diluted with water (50 ml) and extracted with EtOAc (50 ml x 2). The combined organic layers were washed with brine, dried over Na_2SO_4, filtered and concentrated. The crude was purified by prep-TLC (DCM/MeOH 10:1) to give the exatecan-PEG derivative **72** as a yellow solid 20 mg (20.8%). LCMS *m/z* = 1440.55 $[M+H]^+$.

To a solution of the exatecan-PEG derivative **72** (20 mg, 0.0139 mmol) in DCM (2 ml) was added TFA (2 ml). The reaction mixture was stirred at room temperature for 1.5 h. The reaction mixture was concentrated in vacuo to afford the Boc-deprotected derivative **73** as the TFA salt (20 mg, crude). LCMS *m/z* = 1340.85 $[M+H]^+$.

A solution of **73** (20 mg, 0.139 mmol) in dry DMF (1 ml) was added dropwise to a solution of bis(2,5-dioxopyrrolidin-1-yl) 4,7,10,13-tetraoxahexadecanedioate (40 mg, 0.83 mmol) and DIPEA (5.3 mg, 0.417 mmol) at 10 °C. The reaction mixture was stirred at 10 °C for 0.5 h. after which the mixture was purified by prep-HPLC to give the desired Exatecan-

MA-PEG$_{12}$-Val-Ala-PEG$_4$-NHS ester activated **74** as a white solid 4.6 mg (19.3%). LCMS *m/z* = 1713.90 $[M+H]^+$, 857.75 $[1/2M+H]^+$.

Example 27: Synthesis of GENZ-644282-Val-Ala-BrPEG$_8$-PEG$_2$-NHS Ester (80)

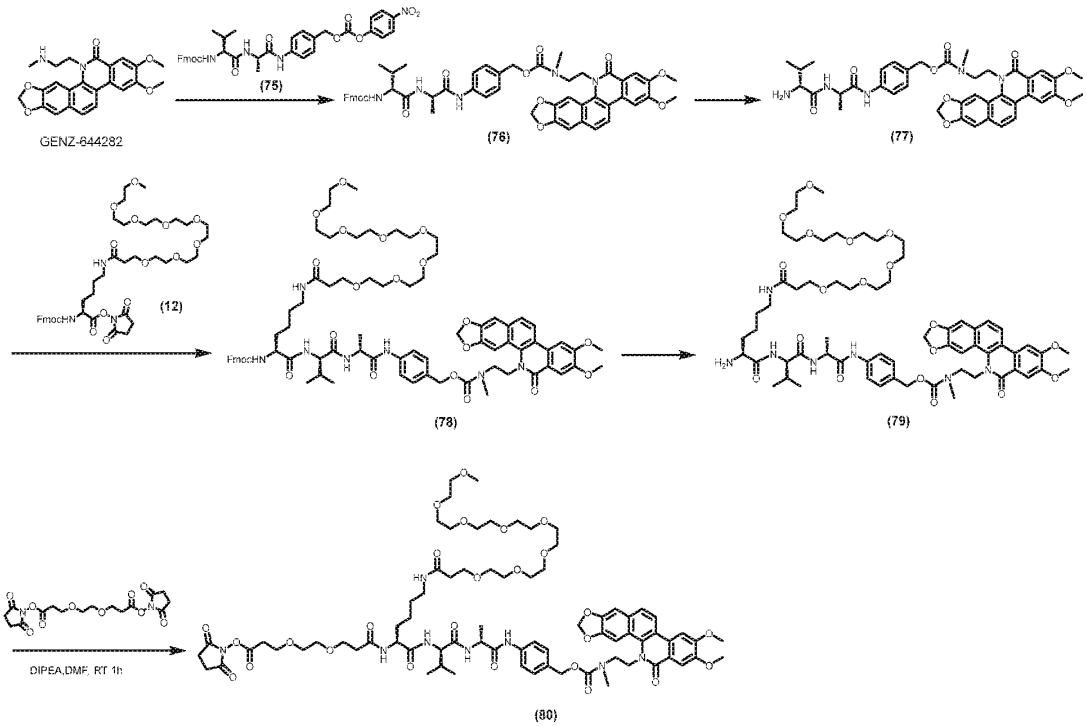

GENZ-644282 (50 mg, 0.123 mmol), Fmoc-ValAla-PNP ester **75** (84 mg, 0.123 mmol) and HOBt (33 mg, 0.246 mmol) were dissolved in a mixture of anhydrous DMF (2 ml) and pyridine (0.4 mL), and DIPEA (21 µl, 0.123 mmol) was added. The mixture was stirred for 3 h at RT, dried under reduced pressure and the crude purified by NP automated chromatography [Biotage, Hex/EtOAc 0-100%) to give 0.12 mg (quantitative yield) of the desired Fmoc-val-ala-GENZ-644282 derivative **76** as a yellow oil. LCMS m/z: 949.79 (M + 1); 950.79 (M + 2); 972.87 (M+Na).

The Fmoc-protected GENZ-644282 derivative **76** (117 mg, 0.123 mmol) was dissolved in 10 ml of a 4% (v/v) solution of diethylamine in anhydrous DMF and the mixture was stirred at RT over 2 h. The reaction mixture was concentrated *in vacuo* and the crude purified by RP automated chromatography [Biotage (water + 0.1% TFA/ACN + 0.1% TFA, 0-100%)]. Combined fractions were concentrated to give the desired deprotected derivative **77** as an off-white solid 89 mg (quantitative yield). LCMS m/z: 727.60 (M + 1); 749.54 (M+Na).

To a solution of GENZ-644282-val-ala amine **77** (20 mg, 0.028 mmol) dissolved in dry DMF (1 ml). Fmoc-Lys-PEG_8 (24 mg, 0.028 mmol) dissolved in dry DMF (1.4 ml) was added followed by the addition of DIPEA (20 µL, 0.056 mmol). The resulting mixture was stirred for 4 h at RT after which the solvent was removed under high vacuum and the crude purified by RP automated chromatography [Biotage (water + 0.1% TFA/ACN + 0.1% TFA, 0-100%)] to give the Fmoc-GENZ-644282-val-ala-PEG_8 derivative **78** 21 mg (53 % yield). LCMS m/z: 1472.40 (M + 1); 1494.39 (M+Na).

The Fmoc-GENZ-644282-val-ala-PEG_8 derivative **78** (36 mg, 0.025 mmol) was dissolved in dry DMF (3 ml) and cooled to 0°C in a water/ice bath. To this stirred solution under nitrogen, a solution of DBU (7.3 µL, 0.049 mmol) dissolved in dry DMF (2 mL) was slowly added dropwise over 1 h. After the end of the DBU addition, the mixture was quenched with AcOH (4.1 µL, 0.025 mmol), and concentrated under reduced pressure. The crude was purified by RP automated chromatography [Biotage (water + 0.1% TFA/ACN + 0.1% TFA, 0-0%)] and fractions combined and freeze dried to give the deprotected amine derivative **79** as a white solid 25 mg (68 % yield). LCMS m/z: 1250.20 (M + 1); 1272.11 (M+Na); 625.71 (M/2).

To a stirred solution of bis-NHS-PEG_2 (80 mg, 0.20 mmol) in dry DMF (2 ml), DIPEA (10.5 µL, 0.060 mmol) was added. In a separate flask, GENZ-val-ala-PEG_8 amine **79** (25 mg, 0.020 mmol) was dissolved in dry DMF (1 ml), this was then added dropwise to the stirred solution of the bis-NHS-PEG_2 solution over 1 h. Once addition was complete, the solvent was removed on high vacuum and the crude purified by RP automated chromatography [Biotage (water + 0.1% TFA/ACN + 0.1% TFA, 10-90%)]. to give the desired GENZ-644282-Val-Ala-BrPEG_8-PEG_2-NHS ester derivative **80** as a white solid 12 mg (39 %). LCMS m/z: 1535.40 (M + 1); 1557.40 (M+Na).

Example 28: Synthesis of Exatecan N-MeGlucamine-GGFG-PEG$_2$-NHS Ester (86)

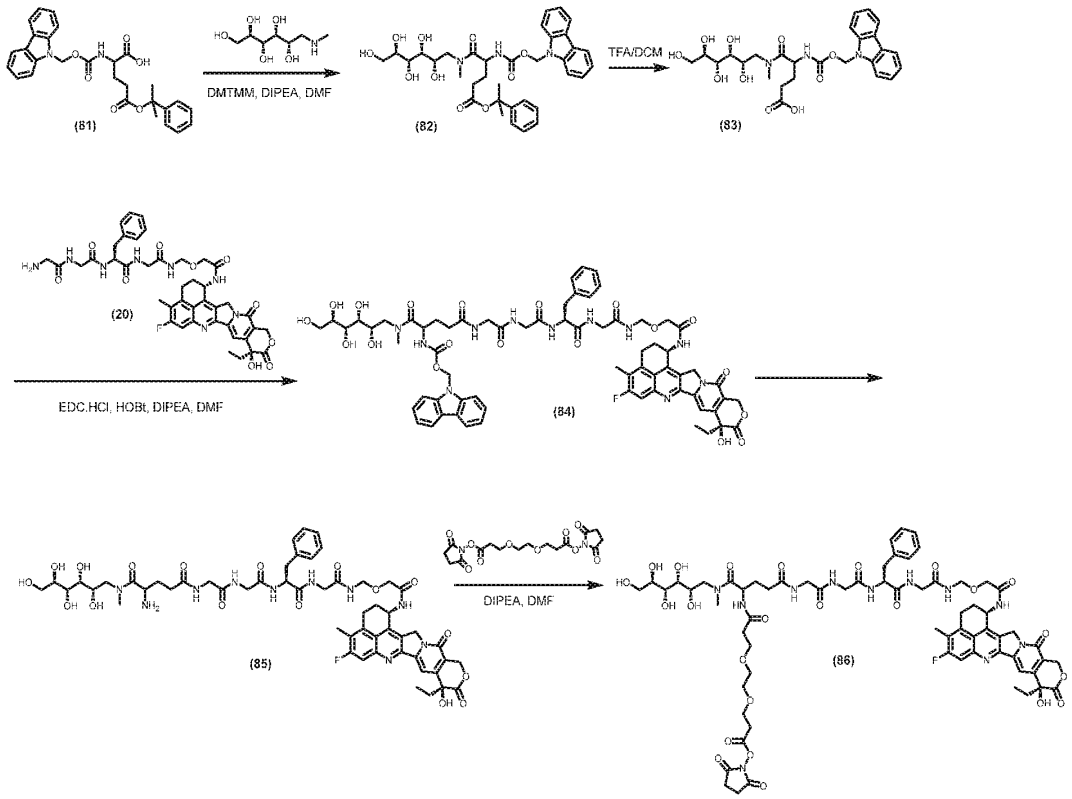

As described in Li W [228], Fmoc-L-Glu-(2-phenylisopropyloxy)-OH **81** (100 mg, 204.69 µmol) and N-methyl-D-glucamine (60 mg, 307.04 µmol) were weighed in a round bottom flask to which was added DMF (5 ml) and DIPEA (35.6µl, 204.69 µmol), followed by DMTMM dissolved in a mixture of DMF (5 ml) and distilled water (1.25 ml). The mixture was allowed to stir at RT for 2h 25 min. The reaction mixture was concentrated *in vacuo* and the crude purified by RP automated chromatography [Biotage (water + 0.1% TFA/ACN + 0.1% TFA, 10-100%)]. The appropriate fractions were combined and lyophlised to give the N-methyl-D-glucamine glutamic acid derivative **82** as a white solid 118 mg of **(**87%). LCMS m/z 687.49 (M+Na), 547.40

iPrPhFmocGlu-N-methyl-D-glucamine **82** (108 mg, 162.23 µmol) was dissolved in a TFA in DCM solution (16 ml, 1% v/v) and stirred in in an ice bath. After 10 min, the reaction mixture was concentrated *in vacuo* and the deprotected derivative **83** used without purification in the next step, assuming full conversion. LCMS m/z 547.40 (M+1), 569.34 (M+Na).

N-methylglucamine-Glu-OH-Fmoc **83** (60 mg, 109.58 µmol), exatecan-GGFG-amine **4** (92 mg, 109.58 µmol), EDC (25 mg, 131.49 µmol), HOBt (14.8 mg, 109.58 µmol), and DIPEA (38.2 µl, 219.15 µmol) were dissolved in 6 ml DMF and allowed to stir for 20h at RT under nitrogen atmosphere. The reaction mixture was concentrated *in vacuo* and crude purified by RP automated chromatography [Biotage (water + 0.1% TFA/ACN + 0.1% TFA, 0-100%)]. The combined fractions were lyophilised to give Fmoc-GluOH-N-methyl-D-glucamine-GGFG-Exatecan derivative **84** as a yellow solid. 83 mg (55 %). LCMS m/z 1371.89 (M+1), 1393.85 (M+Na)

Fmoc-GluOH-N-methyl-D-glucamine-GGFG-Exatecan **84** (41.5 mg, 30.28 µmol) was dissolved in dry DMF (1.5 ml) containing DIEA (106 µl, 1.03 mmol). The mixture was stirred at RT under inert atmosphere for 1.5 h. The reaction mixture was concentrated *in vacuo* and crude purified RP automated chromatography [Biotage (water + 0.1% TFA/ACN + 0.1% TFA, 0-100%)]. The combined fractions were freeze dried to give the deported glutamic acid derivative **85** as a yellow solid 18 mg (52 %). LCMS m/z 1148 (M+1), 1170 (M+Na)

N-methyl-D-glucamine-GluOH-GGFG-exatecan **85** (18 mg, 16.59 µmol) was dissolved in dry DMF (1 ml) and added dropwise over one hour (syringe pump), to a stirred solution of bis-PEG_2-NHS ester(62.9 mg, 165.90 µmol) and DIPEA (8.2 µl, 47.07 µmol) at RT under inert atmosphere. After addition was complete, the reaction mixture was concentrated *in vacuo* and the crude purified RP automated chromatography [Biotage (water + 0.1% TFA/ACN + 0.1% TFA, 0-100%)]. The combined fractions were lyophilised to give the N-methyl-D-glucamine-GluOH-GGFG-exatecan-PEG_2-NHS ester derivative **86** as a light-yellow solid 4.23 mg (34%). LCMS m/z1433.70 (M+1), 1455.72 (M+Na)

Example 29: Synthesis of MMAE-βGA-BrPEG_{12}-PEG_2-NHS Ester (87)

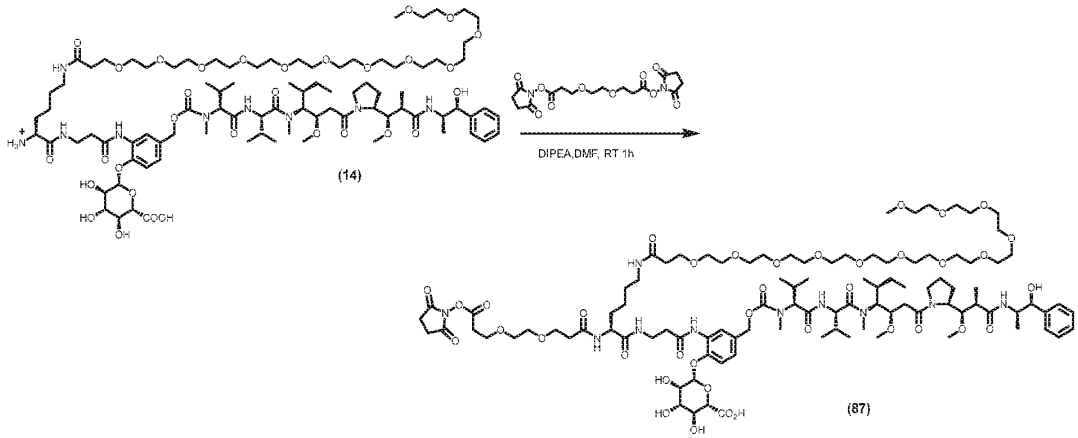

To a stirred solution of bis-NHS-PEG$_2$ (53 mg, 0.134 mmol) dissolved in dry DMF (500 µl) and DIPEA (7 µl, 0.0403 mmol), MMAE-βGA-BrPEG$_{12}$-amine **14** (22.2 mg, 0.0134 mmol) dissolved in dry DMF (840 µl) was added dropwise over 1 h using a syringe pump. Afre addition was complete, the solvent was removed on high vacuum and the crude purified by RP automated chromatography [Biotage (water + 0.1% TFA/ACN + 0.1% TFA, 10-90%)] to give MMAE-βGA-BrPEG$_{12}$-PEG$_2$-NHS Ester **87** as a white solid after lyophilisation 35.27 mg (86%). LCMS m/z = 2116.50 (M+1); 1058.50 (M/2); 718.90 (MMAE); 506.59 (MMAE fragment).

Example 30: Synthesis of MMAE-βGA-BrPEG$_{12}$-PEG$_7$-NHS Ester (88)

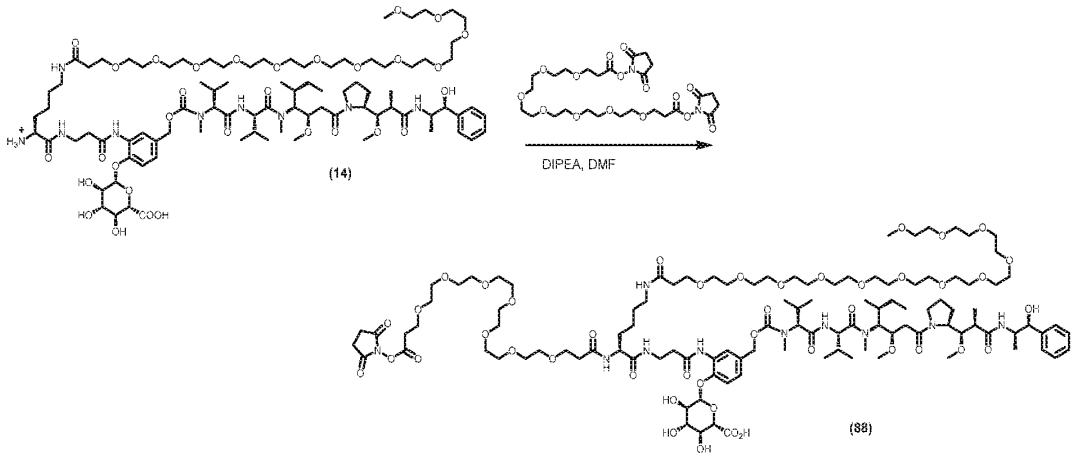

Bis-PEG$_7$-NHS (78 mg, 0.126 mmol) was dissolved in dry DMF (1 ml), DIPEA (6.6 µl, 0.038 mmol) was then added. To this stirred solution, MMAE-βGA-BrPEG$_{12}$-amine **14** (23 mg, 0.0126 mmol) dissolved in dry DMF (1 ml) was then added dropwise via syringe pump over 1 h. After addition was complete, the solvent was removed on a high vacuum and the crude purified by RP automated chromatography [Biotage (water + 0.1% TFA/ACN + 0.1% TFA, 10-90%)] to give MMAE-βGA-BrPEG$_{12}$-PEG$_7$-NHS Ester **88** as a white solid after lyophilisation 11.48 mg (39%). m/z = 2335.87 (M+1), 1167.46 (doubly charged ion), 718.40 (MMAE), 506.19 (MMAE fragmentation).

Example 31: Synthesis of SN38-βGA-DMEDA-PEG$_2$-NHS Ester (95)

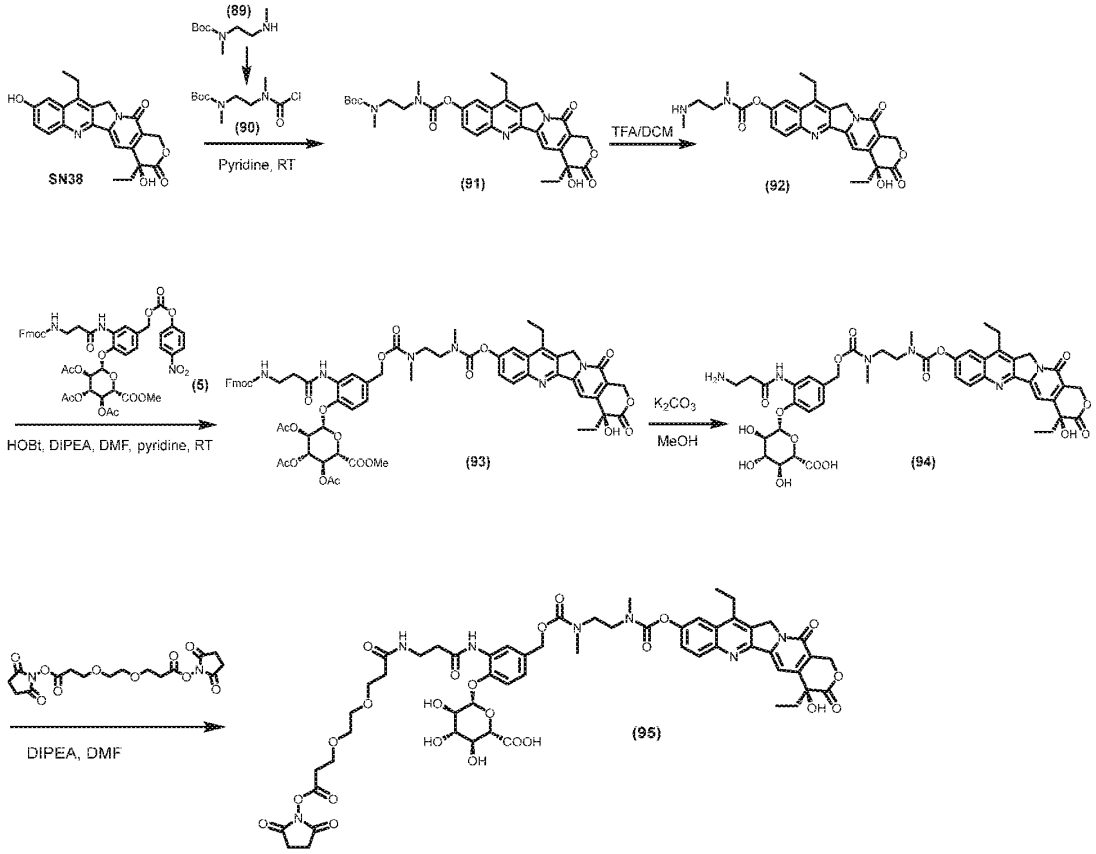

As described in Meyer Y et al [229], Phosgene solution (370 µl, 15% in toluene) was placed in a round bottom flask and cooled in an ice bath under nitrogen. In a separate flask, the starting N-Boc-diethylamine **89** (95 mg, 0.505 mmol) and triethylamine (77 µl, 0.555 mmol) were dissolved in dry toluene (1 ml). The solution of the amine **90** was then added dropwise to the phosgene solution over 15 minutes, then allowed to stir for 20 hours under nitrogen. The reaction mixture was evacuated and the crude containing the chlorocarbonyl **90** was used directly in the next reaction without further purification.

SN38 (99 mg 0.2525 mmol) was added to the chlorocarbonyl-boc-amine **90**, pyridine (1 ml) was then added, and the resulting mixture allowed to stir at RT under inert atmosphere for 21 hours. The reaction was quenched with water (5 ml) and extracted with ethyl acetate (3 x 5 ml). The organic phases were combined, washed with brine, dried over magnesium sulphate, and evaporated to dryness under reduced pressure. The residue was purified on NPB [Biotage (DCM/MeOH, 0-20 %)] to afford the desired SN-38-Boc-DMEDA derivative **91** as a transparent oil 71 mg (46 %).

SN-38-Boc-DMEDA **91** (71 mg, 0.117 mmol), was dissolved a 1:1 solution of DCM and trifluoroacetic acid (2 ml), the reaction mixture was stirred in an ice/water bath for 2h under nitrogen. The reaction mixture was concentrated *in vacuo* and the crude deprotected SN-38-DMEDA **92** used in the next reaction without any further purification.

The PNP-carbonate ester **5** (107 mg, 0.117 mmol), HOBt (16 mg, 0.119 mmol) and crude SN-38-DMEDA **92** (59 mg, 0.117 mmol, quantitative yield assumed) stirred in dry THF (3.3 ml), pyridine (0.65 ml) DIPEA (422 µL, 0.129 mmol) were then added and the reaction mixture stirred at RT under nitrogen for 20 h. Reaction mixture was then concentrated *in vacuo* and crude purified on NP automated chromatography [Biotage (DCM/MeOH, 0-20 %)]. Fractions were combined and concentrated to give the SN-38-DMEDA-glucuronide **93** as a yellow solid 98 mg (65%), found m/z = 1210.93 (M + 1), 1234.85 (M + Na)

The SN-38-DMEDA-sugar **93** (48 mg, 0.0375 mmol) was dissolved in MeOH (4.3 ml) and potassium carbonate (26 mg, 6.1873 mmol) was added to the solution. The reaction mixture was stirred for 2 hours, and then neutralised with HCl 0.1 M solution. The solvent was removed under high vacuum and the crude purified by RP automated chromatography [Biotage (water + 0.1% TFA/ACN + 0.1% TFA, 0-100%)]. to give globally deprotected SN-38-DMEDA-βGA **94** as a yellow solid 15 mg (44 %).

To a stirred solution of bis- PEG_2-NHS ester (15 mg, 0.0163 mmol), and DIPEA (14 µl, 0.0816 mmol) in dry DMF (3 ml,) SN-38-DMEDA-βGA **94** dissolved in DMF (6 ml) was added dropwise to the solution over 1h 40 min under nitrogen atmosphere using a syringe pump. The reaction mixture was then stirred for a further 45 min. The solvent was removed using high vacuum and the crude purified by RP automated chromatography [Biotage (water + 0.1% TFA/ACN + 0.1% TFA, 0-100%)] to give SN38-βGA-DMEDA-PEG_2-NHS Ester **95** as a pale-yellow solid**,**9 mg (29 %).

Example 32: Synthesis of SN38-BA-Val-Ala-PEG$_2$-NHS Ester (101)

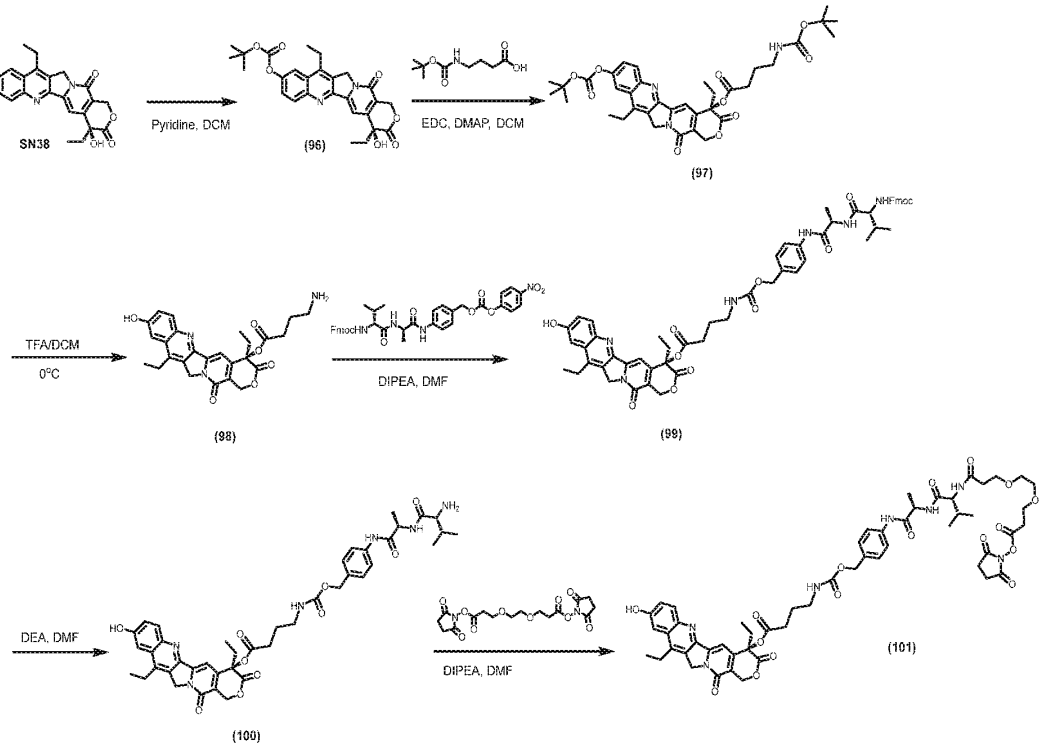

As described in Zhu Q et al. [230], Di-^{t}butyl-dicarbonate (47 mg, 0.2153 mmol) and pyridine (401 µL, 4.9693 mmol) were added to a suspension of SN-38 (65 mg, 0.1656 mmol) in dry DCM (3 ml). The mixture was stirred at room temperature overnight under an inert atmosphere. The solution was washed with 1 N HCl (5 ml), saturated $NaHCO_3$ solution (5 ml), brine (5 ml) and dried over Na_2SO_4. The solvent was removed under vacuum to give the crude Boc-SN-38 **96** which was used without further purification. LCMS m/z = 493.30 $(M+1)^+$

As described in Zhu Q et al. [230], Boc-SN-38 **96** (89 mg, 0.1807 mmol), 4-tert-Butoxycarbonylaminobutyric acid (73 mg, 0.3600 mmol), EDCI (0.034 g, 0.21 mmol) and DMAP (0.033g, 0.27 mmol) were dissolved in dry DCM (4 ml) and stirred overnight at room temperature under nitrogen. The solution was washed with water (10 ml), brine (10 ml) dried over Na2SO4 and the solvent was removed under vacuum. The residue was purified by RP automated chromatography [Biotage (water + 0.1% TFA/ACN + 0.1% TFA, 0-100%)] to give Boc-SN-38-Fmoc-butylamine derivative **97** as a yellow powder 27.00 mg (22 %).

Boc-SN-38-Fmoc-butylamine derivative **97** (26.6 mg, 0.050 mmol) was placed in an oven-dried flask under nitrogen and dissolved in dry DCM (1.0 ml). This solution was placed in an ice/water bath and 0.5 ml (7.651 mmol) of TFA in 0.5 ml of dry DCM was added

dropwise at 0°C using a syringe pump. After 1 h the cold bath was removed and the reaction mixture stirred for a further 30 minutes. The reaction mixture was then concentrated under reduced pressure, providing a dark yellow oily residue as the double-deprotected SN-38-butylamine derivative **98** which was used in the next step without any further purification. LCMSm/z = 478.30 $(M+1)^+$

To a solution of Fmoc-Val-Ala-PAB-PNP (25 mg, 0.0367 mmol) and the crude SN-38-butylamine derivative **98** in dry DMF (1.5 ml), DIPEA (32 µL, 0.1836 mmol) was added, the flask was then covered with aluminium foil and the reaction stirred under nitrogen for 1 h at 4 °C. The reaction mixture was then allowed to warm up and stirred for a further 5 hours at RT. The DMF was evaporated, and the crude purified by RP automated chromatography [Biotage (water 0.1% TFA/ ACN 0.1% TFA 0-100%)] to give SN-38-BA-Fmoc-val-ala **99** as pale-yellow powder 11 mg (30%). LCMS m/z = 1019.72 (M+1)

SN-38-BA-Fmoc-val-ala **99** was dissolved in a round bottom flask containing diethylamine (50 µl) in dry DMF (0.25 mL). After 1 h, the reaction mixture was concentrated, dried under high vacuum to give SN-38-val-ala-amine **100** which was used in the next step without further purification. LCMS m/z = 797.60 $(M+1)^+$

SN-38-val-ala-amine **100** (7 mg, 0.0088 mmol) in dry DMF (1 ml) was added via syringe pump over 1 hour into a stirred solution of bis-PEG_2-NHS ester (40 mg, 0.1004 mmol) and DIPEA (5.2 uL, 0.0301 mmol) in DMF (0.5 ml) and under nitrogen.The reaction mixture was stirred for one further hour, and then evaporated to dryness under reduced pressure. The crude was purified via RP automated chromatography [Biotage (water 0.1% TFA/ ACN 0.1% TFA 0-100%)], fractions were combined and lyophilized to give SN38-BA-Val-Ala-PEG_2-NHS ester **101** as pale-yellow powder. LCMS m/z = 1082.8 (M+1)

Example 33: Synthesis of MMAE-βGA-BrPEG$_4$-PEG$_2$-NHS Ester (104)

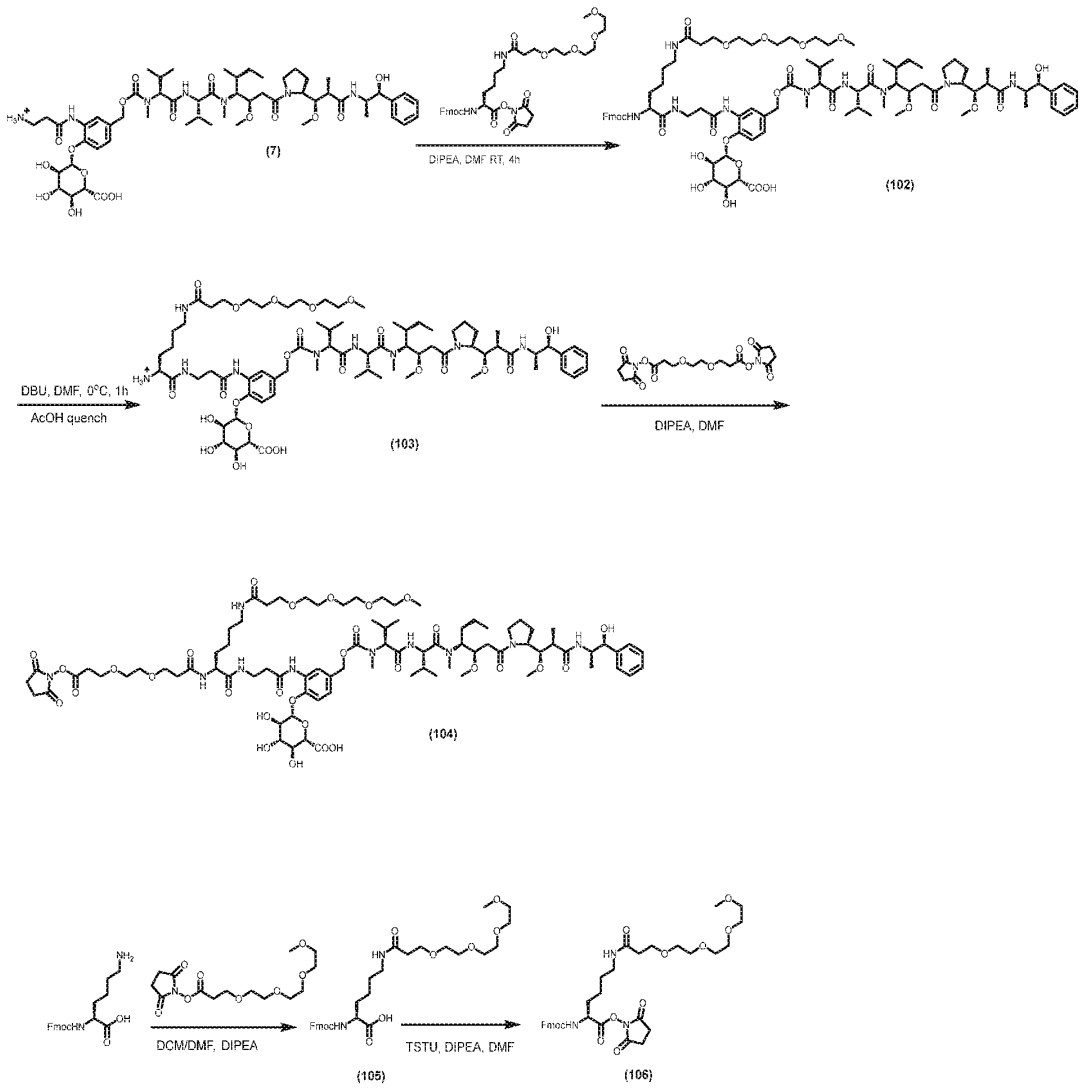

As described in RP Lyon et al. [192]. To a stirred solution of MMAE-βGA-alanine derivative **7** (62 mg, 0.0498 mmol) dissolved in dry DMF (0.7 ml) and DIPEA (17.4 µl, 0.0996 mmol), a solution of the activated Fmoc-Lys-PEG$_4$-NHS ester **106** (40.9 mg, 0.0598 mmol) dissolved in DMF (1 ml) was added. The reaction mixture was stirred for 4 h after which the solvent was removed under high vacuum and the oily residue purified by RP automated chromatography [Biotage: H_2O (0.1% TFA)/CH_3CN (0.1% TFA), 10-90%] to give the Fmoc-lysine-PEG$_4$ derivative **102** as a white solid 80 mg (94 % yield) after lyophilisation. LCMS m/z = 1699.00 (M+1), 850.00 (1/2 M+1).

To a stirred solution of Fmoc-lysine-PEG_4 derivative **102** (80 mg, 0.0471 mmol) was dissolved in dry DMF (3 ml) and cooled to 0°C in a water/ice bath, DBU (21.2 µL, 0.141 mmol) dissolved in dry DMF (1.7 mL) was added dropwise over 1 h under nitrogen. After addition was complete, the mixture was allowed to stir for a further 30 min. the ice bath was then removed and the reaction was quenched with AcOH (19 µl, 0.3325 mmol), and concentrated. The residue was purified by RP automated chromatography [Biotage: H_2O (0.1% TFA)/CH_3CN (0.1% TFA), 30-100%] to give the deprotected lysine-PEG_4 derivative **103** 64.2 mg (92 %).

To a solution of Bis-PEG_2-NHS (203 mg, 0.0508 mmol) and DIPEA (26.5 µl, 0.1520 mmol) in dry DMF (3 ml) a solution of the MMAE-βGA-BrPEG_4 **103** (75 mg, 0.0508 mmol) in dry DMF (2.1 ml) was added drop wise over 1 h using a syringe pump. After addition was complete the mixture was allowed to stir for further 30 min. after which the solvent was removed on high vacuum and the crude purified by RP automated chromatography [Biotage (water + 0.1% TFA/ACN + 0.1% TFA, 10-90%)] to give the desired MMAE-βGA-BrPEG_4-PEG_2-NHS Ester **104** as a white solid after lyophilisation 65.0 mg (73%). LCMS (M+K) 1800.74, ((1/2 M+K) 901.33.

To Fmoc-Lys-OH (300 mg) in dry DCM (16 mL) was added a solution of the PEG_4-NHS ester in dry DCM (4 mL) followed by DIPEA (710 µL) – mixture is a suspension, so dry DMF (2 ml) was added and the mixture stirred, becoming clear after 1.5 h. The clear reaction mixture was stirred at RT under nitrogen overnight after which it was quenched with 1M NH_4Cl solution (20 mL). The phases were separated, and the aqueous layer was further extracted with DCM (3 x 10 ml). The organic phases were combined, dried over $MgSO_4$, filtered and concentrated to dryness under reduced pressure to give a colourless oil that was purified by NP automated chromatography [Biotage (DCM/MeOH 0-10%)] to give the lysine-PEG_4 **105** as an oil 449 mg (94%). TLC, DCM/MeOH (25 %). Rf = 0.064. LCMS m/z = 587.00 (M+1).

Fmoc-Lys-PEG_4 **105** (140 mg, 0.239 mmol) was dissolved in dry DMF (3 ml), TSTU (143.7 mg, 0.477 mmol) and DIPEA (207.3 µL, 1.19 mmol) were added, and the mixture stirred at RT under nitrogen. After 2.5 h, the solvent was removed under high vacuum and the crude purified by NP automated chromatography [Biotage (DCM/MeOH 5-10%)], to give the lysine-PEG_4-NHS ester **106** 152 mg (93%). TLC (DCM/MeOH, 5%). Rf = 0.18. LCMS m/z = 685.00 (M+1).

Example 34: Synthesis of MMAE-βGA-BrLys(BisPEG$_8$)-PEG$_2$-NHS Ester (112)

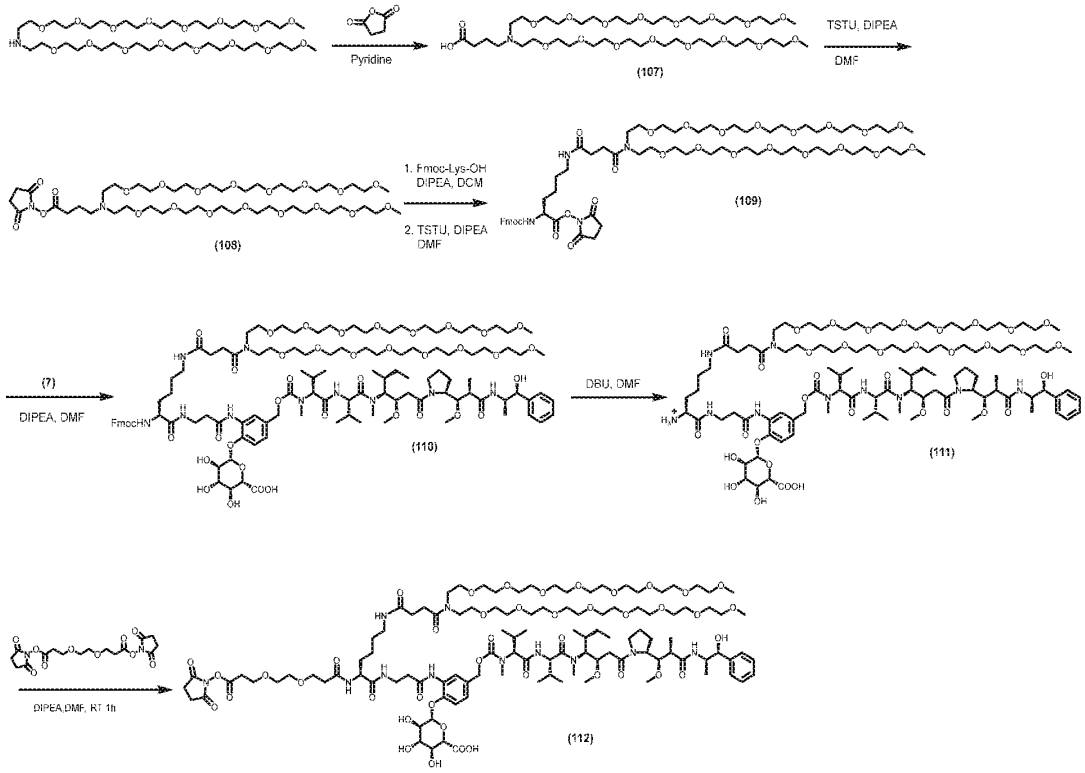

As described in Chan KF et al. [231], in a round bottom flask, di(2,5,8,11,14,17,20,23-octaoxapentacosan-25-yl)amine (131 mg, 0.175 mmol) and succinic anhydride (35 mg, 0.349 mmol) were dissolved in 10 ml of pyridine and stirred at RT, under nitrogen for 3 hours. The reaction mixture was then poured into a separating funnel containing 1 M hydrochloric acid solution and the mixture continuously extracted with DCM. The combined organic layers were dried over MgSO4, filtered, and evaporated to give the Bis-PEG$_8$-amine butanoic acid **107** light brown oil (assumed quantitative yield) that was used without further purification. LCMS m/z: 850.70 (M+1); 872.70 (M+Na); 425.90 (1/2 M+1).

Bis-PEG$_8$-amine butanoic acid **107** (140 mg, 0.174 mmol), DIPEA (162 uL, 0.152 mmol) and TSTU (105 mg, 0.348 mmol) were dissolved in dry DMF (5 ml) and stirred under nitrogen at RT for 5 hours. The solvent was removed on high vacuum and the crude activated ester **108** used without further purification. LCMS m/z: 947.72 (M+1); 964.80 (M+H2O; 474.43 (1/2 M+1).

To Fmoc-Lys-OH (63.8 mg, 0.173 mmol) in dry DCM (3 ml) was added a solution of the bis-(PEG)$_8$ activated ester **108** (164 mg, 0.173 mmol) dissolved in dry DCM 0.5 ml) followed by DIPEA (151 µL, 0.866 mmol). The mixture was stirred at RT under nitrogen for 5 hours and quenched with 1M NH_4Cl solution (5 ml). Phases were separated, and the

aqueous layer was further extracted with DCM (3 x 10 mL). The organic phases were combined, dried over $MgSO_4$, filtered and concentrated to dryness under reduced pressure to give a colourless oil that was purified by RP automated chromatography [Biotage (water + 0.1% TFA/ACN + 0.1% TFA, 10-90%)] to give the Fmoc-Lys-Bis-$(PEG)_8$-acid as an off-white oil 60 mg (29 %). LCMS m/z = 1200.96 (M+1); 601.14 (M/2). The Fmoc-Lys-Bis-$(PEG)_8$-acid (60 mg, 0.050 mmol), DIPEA (43,5 uL, 0.250 mmol) and TSTU (30.1 mg, 0.100 mmol) were dissolved in dry DMF (3 ml) and stirred under nitrogen at RT for 5 hours. The solvent was removed on high vacuum and the crude purified by RP aoutomated chromatography [Biotage (water + 0.1% TFA/ACN + 0.1% TFA, 0-100%)] to give Fmoc-Lys-Bis-$(PEG)_8$-NHS ester **109** as a clear viscous oil 51 mg (80 %). LCMS m/z: 1299.99 (M+1); 649.61 (1/2 M+1).

To a stirred solution of MMAE-βA **7** (11 mg, 0.0097 mmol) was dissolved in anhydrous DMF (2 ml), Fmoc-Lys-Bis-$(PEG)_8$-NHS ester **109** (12.6 mg, 0.0097 mmol) was added followed by DIPEA (5.1 µl, 0.029 mmol). After 3 h of stirring at RT under nitrogen atmosphere, the solvent was removed under high vacuum and the crude purified in RP automated chromatography [Biotage (water + 0.1% TFA/ACN + 0.1% TFA, 10-100%]) and appropriate fractions combined and lyophilised to give the Fmoc-bis-(PEG_8)-MMAE-glucuronide derivative **110** 20 mg (89 % yield) as a white solid. LCMS m/z: 2314.50 (M+1); 1157.45 (1/2 M+1); 718.80 (MMAE).

The Fmoc-bis-(PEG_8)-MMAE-glucuronide derivative **110** (20 mg, 0.0087 mmol) was dissolved in anhydrous DMF (2 ml) and cooled in an ice bath. DBU (3.9 µL, 0.026 mmol) dissolved in anhydrous DMF (1 ml) was added dropwise over one hour under inert atmosphere. After the end of the addition, the mixture was allowed to stir for further 20 min, the solvent was removed under high vacuum and the crude purified by RP automated chromatography [Biotage (water + 0.1% TFA/ACN + 0.1% TFA, 10-100%)] to give bis-(PEG_8)-MMAE-glucuronide amine derivative **111** 214 mg (78 % yield) as a white solid after lyophilisation. LCMS m/z: 2093.30 (M+1); 1047.20 (1/2 M+1).

To a stirred solution of bis-PEG_2-NHS ester (3.8 mg, 0.0010 mmol) dissolved in DMF (1 ml), and DIPEA (0.5 µL, 0.003 mmol, bis-(PEG_8)-MMAE-glucuronide amine **111** (2 mg, 0.001 mmol) dissolved in DMF (1 m) was added dropwise over 35 min. using a syringe pump. Once addition was complete, the mixture was allowed to stir for further 1 hour after which the solvent was removed on high vacuum and the crude purified by RP automated chromatography [Biotage (water + 0.1% TFA/ACN + 0.1% TFA, 10-90%)] to give MMAE-βGA-BrLys(BisPEG_8)-PEG_2-NHS ester **112** as a white solid after lyophilisation 120.91 mg (40 %). LCMS m/z = 2376.60 (M+1), 1188.90 (1/2 M+1), 2398.36 (M+Na).

Example 35: Synthesis of MMAE-βGA-BrGlu(BisPEG$_8$)-PEG$_2$-NHS Ester (118)

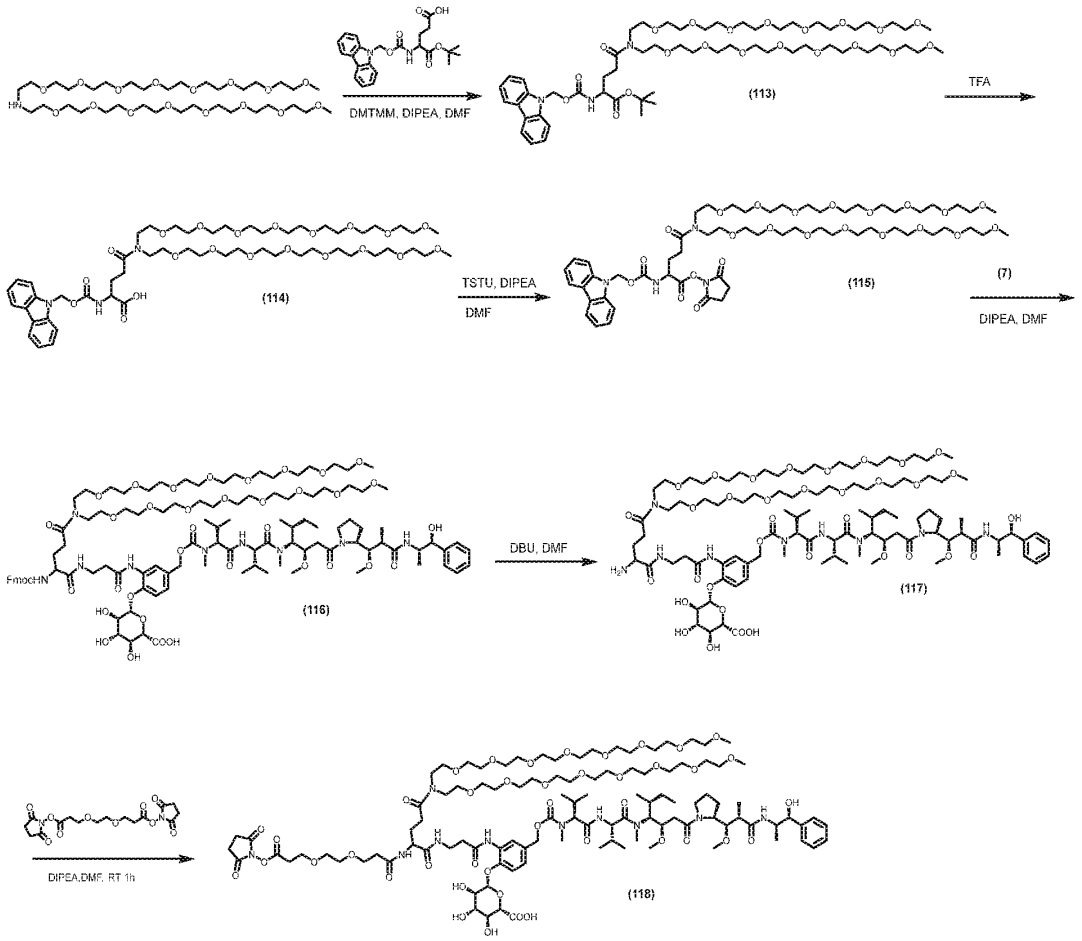

As described in Agren JKM et al. [235], Di(2,5,8,11,14,17,20,23-octaoxapentacosan-25-yl)amine (10 mg, 0.013 mmol), FmocGluOtBu (5.7 mg, 0.013 mmol), EDC (3 mg, 0.026 mmol), HOBt (1.8 mg, 0.013 mmol) and DIPEA (4. µL, 0.027 mmol) were dissolved in 1 ml dry THF. The mixture was stirred under nitrogen at RT for 21 hours. The solvent was removed on high vacuum and the crude was purified by RP automated chromatography [Biotage (water + 0.1% TFA/ACN + 0.1% TFA, 0-100%)] to give PEGylated glutamic acid derivative **113** 15 mg (97 %) as a white powder. LCMS m/z 1159.20 (M+1); 1182.21 (M+Na).

The starting double-protected PEGylated glutamic acid derivative **113** (15 mg, 0.013 mmol) was dissolved in 1 ml neat TFA and the mixture stirred for 30 min. under nitrogen. The excess TFA was removed on high vacuum and the crude Fmoc-bis(PEG$_8$)-glutamic acid **114** was used without further purification. LCMS m/z: 1103.10 (M+1); 1125.12 (M+Na).

Fmoc-bis(PEG_8)-glutamic acid **114** (88 mg, 0.080 mmol) and TSTU (48 mg, 0.161 mmol) were dissolved in dry DMF (1 ml); DIPEA (70 µl, 0.401 mmol) was added and the mixture stirred for 5 h at RT after which it was under high vacuum. The residue was purified by RP automated chromatography [Biotage (water + 0.1% TFA/ACN + 0.1% TFA, 0-100%)] to give Fmoc-bis(PEG_8)-glutamic acid NHS ester **115** as a clear oil 80 mg (83%). LCMS m/z 1200.90 (M+1); 1122.90 (M+Na).

To a stirred solution of MMAE-βA **7** (41 mg, 0.036 mmol) dissolved in dry DMF (6 ml). NHS-activated Fmoc-Glu-bis(PEG_8) (43.50 mg, 0.036 mmol) dissolved in dry DMF (1 ml) was added solution followed by DIPEA (19 µl, 0.109 mmol). The reaction mixture was stirred for 4 h at RT after which the solvent was removed under high vacuum and crude purified by RP automated chromatography [Biotage (water + 0.1% TFA/ACN + 0.1% TFA, 15-100%)] to give the MMAE-Fmoc-bis(PEG8)-βGA **116** 5 mg (31%) as a sticky white solid. LCMS m/z 2215.40 (M+1); 2237.30 (M+Na); 718.83 (MMAE); 506.49 (MMAE fragment).

MMAE-Fmoc-bis(PEG8)-βGA **116** (5 mg, 0.0023 mmol) was dissolved in dry DMF (1 ml) and DBU (1.1 µL, 0.0068 mmol) was added in one portion. The reaction mixture was stirred at RT under nitrogen. After 1.5 h, the solvent was removed under high vacuum and the crude purified by RP automated chromatography [Biotage (water + 0.1% TFA/ACN + 0.1% TFA, 0-100%)] to give MMAE- bis(PEG8)-βGA amine **117** 3 mg (67 %) as a white solid were obtained. LCMS m/z 1992.20 (M+1); 996.84 (1/2 M+1); 718.80 (MMAE); 506.60 (MMAE fragment).

MMAE- bis(PEG8)-βGA amine **117** (8 mg, 0.004 mmol) was dissolved in dry DMF (1 mL) and added dropwise to a solution of bis-PEG_4-NHS ester (16.1 mg, 0.040 mmol) and DIPEA (2.1 µL, 0.012 mmol) in 1mL DMF over one hour using a syringe pump. After the addition, was complete, the reaction mixture was stirred at RT under inert atmosphere for 1 further hour. The solvent was then removed under high vacuum and the crude purified by RP automated chromatography [Biotage (water + 0.1% TFA/ACN + 0.1% TFA, 0-100%)] to give the desired MMAE-βGA-BrGlu(BisPEG_8)-PEG_2-NHS Ester **118** as a white solid after lyophilisation 3.58 mg (67%). LCMS m/z 2217.39 (M+1); 1139.67 (1/2 M+1); 718.80 (MMAE); 686.79, 506.56 (MMAE fragment).

Example 36: Synthesis of MMAE-Val-Ala-BrPEG$_8$-PEG$_2$-NHS Ester (123)

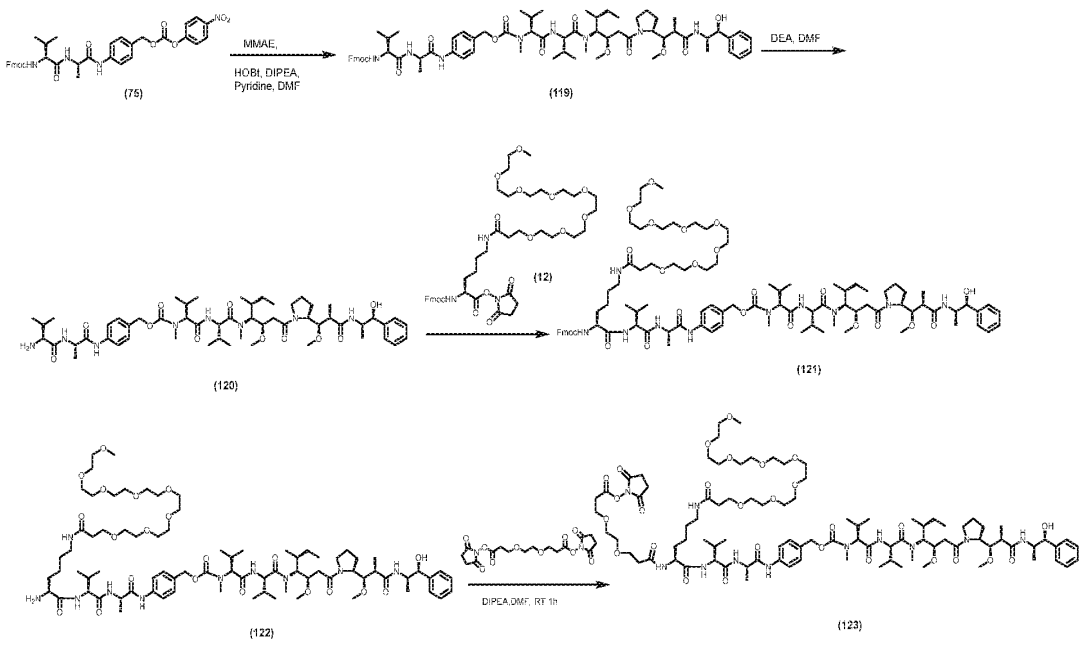

MMAE (100 mg, 0.139 mmol), Fmoc-ValAla-PAB-PNP (104 mg, 0.153 mmol) and HOBt (38 mg, 0.279 mmol) were placed in a round bottom flask and dissolved in a mixture of DMF (2 ml) and pyridine (0.4 ml). DIPEA (24 µL, 0.139 mmol) was added and the solution was allowed to stir at RT under nitrogen for 24 h. The mixture was dried under high vacuum and the crude was washed with ethyl acetate (3 x) to afford Fmoc-val-ala-MMAE **119** as a solid pure enough to carry on with the synthesis without any further purification, 127 mg (74%). LCMS m/z 1260.90 (M+1); 718.80 (MMAE)

Fmoc-ValAla-MMAE **119** (90 mg, 0.071 mmol) was dissolved in dry DMF (10 ml) and diethylamine (370 µL, 3.573 mmol) was added. The solution was allowed to stir at RT under nitrogen for 2 h and then dried under high vacuum. The crude was purified by RP automated chromatography [Biotage (water + 0.1% TFA/ACN + 0.1% TFA, 0-100%)], fractions combine and concentrated to afford the H_2N-val-ala-MMAE **120** as a white solid 74 mg (quantitative yield). LCMS m/z 1038.10 (M+1), 1060.06 M+Na), 718.80 (MMAE).

H_2N-ValAla-MMAE **120** (81 mg, 0.0781 mmol) and Fmoc-Lys-PEG$_8$-NHS **12** (81 mg, 0.0937 mg) were dissolved in DMF (5 mL) and DIPEA (33 µL, 0.1874 mmol) was added. The solution was allowed to stir at RT under nitrogen for 5 h. and then a further amount (0.0698 mmol) of Fmoc-Lys-PEG$_8$-NHS **12** was added to the reaction mixture, and stirring

continued for a further 18 h. The reaction mixture was evaporated under high vacuum and the crude residue purified by RP automated chromatography [Biotage (water + 0.1% TFA/ACN + 0.1% TFA, 0-100%)]. Fractions were combined and evaporated to give the Fmoc-branched lysine MMAE derivative **121** as an off-white solid 50 mg (36%). LCMS m/z 1783.00 (M+1); 1805.96 (M+Na); 718.84 (MMAE).

DBU (23.4 µL, 0.157 mmol) was dissolved in dry DMF (5 ml) and added dropwise over 1 hour, to a stirred solution of Fmoc-branched lysine MMAE **121** (93 mg, 0.052 mmol) dissolved in dry DMF (5 ml) at ^{0}C and under nitrogen. Once addition was complete the reaction mixture was quenched with acetic acid (14.7 µL, 0.261 mmol) and concentrated to dryness under high vacuum. The crude was purified by RP automated chromatography [Biotage (water + 0.1% TFA/ACN + 0.1% TFA, 15-100%)]. Fractions were combined and lyophilised to give the deprotected derivative **122** as a white powder (quantitative yield) LCMS m/z 1560.70 (M+1); 1582.70 (M+Na); 718.81 (MMAE).

Bis-PEG_2-NHS ester (110 mg, 0.275 mmol) was dissolved in dry DMF (2 ml) and DIPEA (14.4 uL, 0.083 mmol) was added. To this stirred solution under nitrogen, MMAE-val-ala-Lys-PEG_8-NH2 **122** (43 mg, 0.0276 mmol) dissolved in dry DMF (2 ml) was added dropwise over 1 h with a syringe pump. Once addition was complete the solvent was removed on high vacuum and the crude purified by RP automated chromatography [Biotage (water + 0.1% TFA/ACN + 0.1% TFA, 10-90%)] to give MMAE-Val-Ala-BrPEG_8-PEG_2-NHS ester **123** as a white solid after lyophilisation 21 mg (41 %). LCMS m/z 1846.90 (M+1); 923.97 (M/2); 718.70 (MMAE); 686.60 (MMAE fragment).

Example 37: Synthesis of MMAE-Val-Ala- BrLys(BisPEG$_8$)-PEG$_4$-NHS Ester (126)

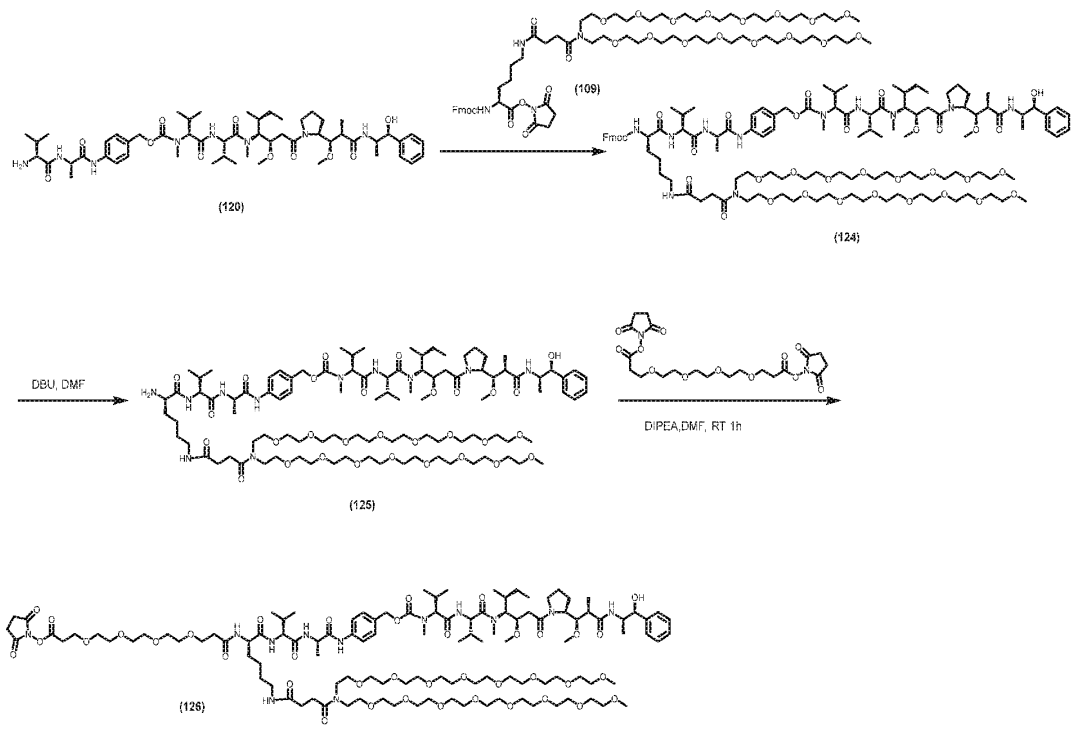

H_2N-ValAla-MMAE **120** (33 mg, 0.032 mmol), the NHS-activated bis-PEG$_8$ linker **109** (38 mg, 0.032 mmol), and HATU (24.1 mg, 0.063 mmol) were dissolved in dry DMF (3 ml) and DIPEA (16.6 µl, 0.095 mmol) was added. The mixture was stirred under nitrogen at RT for 2.5 hours. The solvent was removed on high vacuum and the crude was purified by RP automated chromatography [Biotage (water + 0.1% TFA/ACN + 0.1% TFA, 0-100%)] to give the Fmoc-val-ala-MMAE-bisPEG$_8$ derivative **124** as a white powder 45 mg (64 %). LCMS m/z 2221.40 (M+1); 2243.37 (M+Na); 1111.18 (1/2 M+1); 718.80 (MMAE); 506.52 (MMAE fragment).

DBU (4.5 µl, 0.030 mmol) was dissolved in dry DMF (1 ml) and added dropwise over 1 hour, to a stirred solution of Fmoc-ValAla-MMAE-bisPEG$_8$ **124** (22 mg, 0.010 mmol) in dry DMF (1 ml) at ^{0}C and under nitrogen. Once addition was complete, the mixture was quenched with acetic acid (1.80 µL, 0.061 mmol) and concentrated to dryness under high vacuum to give the crude deprotected derivative MMAE-val-ala-bisPEG$_8$ amine **125**. This was used without further purification. LCMS m/z 1999.28 (M+1); 1000.10 (1/2 M+1); 718.80 (MMAE); 506.50 (MMAE fragment).

Bis-PEG_4-NHS ester (9.8 mg, 0.020 mmol) was dissolved in dry DMF (0.5 ml) and DIPEA (1.1 µL, 0.006 mmol) was added. To this stirred solution under nitrogen, MMAE-val-ala-Lys-bisPEG_8-NH2 **125** (4 mg, 0.002 mmol) dissolved in dry DMF (1 ml) was added dropwise over 1 h with a syringe pump. Once addition was complete, the solvent was removed on high vacuum and the crude purified by RP automated chromatography [Biotage (water + 0.1% TFA/ACN + 0.1% TFA, 10-90%)] to give MMAE-Val-Ala-BrLys(bisPEG_8)-PEG_4-NHS Ester **126** as a white solid after lyophilisation 2.16 mg (45 %). LCMS m/z 2372.60 (M+1); 1186.56 (M/2); 1208.88 (M/2, Na adduct); 718.85 (MMAE); 506.59 (MMAE fragment).

Example 38: Summary of cMET scFv linker-payload conjugates

Table 6 describes disclosed FDCs using a wide range of auristatin and non-auristatin based linker-payloads. Specific examples are described in Examples 39 to 57. Similar FDCs incorporating the 129D5B and 129D5BTY scFvs are described to demonstrate equivalence. The synthesis of the MMAF-PEG_2 linker payload is described in WO2016046574.

Example 39: Conjugation of 129D5BTY scFv to MMAE-βGA-brPEG_8-PEG_2-NHS Ester (10)

129D5BTY scFv was conjugated to linker-payload **10** to obtain a DAR 5.9 as per conditions described in WO2016046574. Specifically, a stock solution of pure scFv (>95%) was diluted to 4.3mg/ml into a pre-equilibrated solution of 20% DMSO in bicarbonate buffer pH9.2. Linker-Payload (25mM in DMSO) was added starting with 5 equivalents before adding more paylaod every 90-120 min and the reaction mixture incubated at 20°C, 300rpm until the desired DAR was achieved. The reaction progress was monitored by size-exclusion chromatography mass spectrometry (SEC-MS, Agilent AdvanceBio SEC 120A 1.9mm 2.1x150mm PEEK isocratic run in 75mM Ammonium Acetate, 10% IPA on an Agilent QTOF 6545XT). A total of 19.2 equivalents (5 additions) were required.

The crude reaction mixture was pH neutralized with 1M NaH_2PO_4 (1.5%) and purified on an AKTA Pure through a Superdex 75 26/600 isocratic run eluting with 10% IPA/PBS (Figure 14a). The monomeric fractions were combined, and buffer exchanged into Histidine/NaCl buffer pH7.5. The concentrated sample was filtered through a sterile 0.2µm PES filter, flash frozen in liquid nitrogen and stored at -80°C. The sample was analysed by SEC HPLC (Sepax Zenix C 150 7.8 x 300mm), SEC and RP-LCMS, UV/Vis spectroscopy, DLS and nanoDSF before being used for further studies. The sample was pure and monomeric (>98.5%, Figure 14b), with a DAR distribution of 3-9 (~80% within 5-7, Figure 14c) with a cumulative radius of ~3.4nm (Figure 14d). The NanoDSF data (Figure 14e) showed a decrease in thermal stability compared to the unconjugated parent antibody

129D5BTY but maintained a highly thermal stable folded structure with a Tm of 64.1°C and a binding affinity (K_d) of 2.16nM (Figure 14f), Table 6.

Example 40: Conjugation of 131D5S scFv to MMAE-βGA-brPEG$_8$-PEG$_2$-NHS Ester (10)

131D5S scFv was conjugated to linker-payload **10** to obtain a DAR 5.4 as per conditions described in Example 39. Specifically, a stock solution of pure scFv (>95%) was diluted to 1mg/ml into a pre-equilibrated solution of 20% DMSO in bicarbonate buffer pH9.2. Linker-Payload (25mM in DMSO) was added in 5 equivalents every 90-120 min and the reaction mixture incubated at 20°C, 300rpm. The reaction progress was monitored by size-exclusion chromatography mass spectrometry (SEC-MS, Agilent AdvanceBio SEC 120A 1.9mm 2.1x150mm PEEK isocratic run in 75mM Ammonium Acetate on an Agilent QTOF 6545XT. A total of 21 equivalents (5 additions) were required.

The crude reaction mixture was pH neutralized with 0.1M NaH_2PO_4 (10%) and purified on an AKTA Avant through a Superdex 75 26/600 isocratic run eluting with 10% IPA/PBS. The monomeric fractions (Figure 15a) were combined and buffer exchanged into Histidine/NaCl buffer pH7.5. The concentrated sample was filtered through a sterile 0.2μm PES filter, flash frozen in liquid nitrogen and stored at -20°C. The sample was analysed by SEC HPLC (Sepax Zenix C 150 7.8 x 300mm), SEC-LCMS (Figure 15b, UV/Vis spectroscopy, DLS (Figure 15c) and nanoDSF before being used for further studies. The binding affinity was 112pM (Figure 15d; Table 6).

Example 41: Conjugation of 77F3 scFv to MMAE-βGA-brPEG$_4$-PEG$_2$-NHS Ester (104)

77F3 scFv was conjugated to Linker-Payload **104** to obtain a DAR 8.4 as per conditions described in Example 39. Specifically, a stock solution of pure scFv (>95%) was diluted to 1mg/ml into a pre-equilibrated solution of 20% DMSO in bicarbonate buffer pH9.2. Linker-Payload (25mM in DMSO) was added in 5 equivalents every 90-120 min and the reaction mixture incubated at 20°C, 300rpm. A total of 60 equivalents (12 additions) were required.

The crude reaction mixture was pH neutralized with 1M NaH_2PO_4 (10%) and purified on an AKTA Avant through a Superdex 75 26/600 isocratic run eluting with 10% IPA/PBS. The monomeric fractions (Figure 16a) were combined and buffer exchanged into PBS. The concentrated sample was filtered through a sterile 0.2μm PES filter and stored at 4°C. The sample was analysed by SEC HPLC (Sepax Zenix C 150 7.8 x 300mm), amino acid analyses, SEC-LCMS (Figure 16b), UV/Vis spectroscopy, DLS and SEC-MALS before being used for further studies. The binding affinity was 10.4nM (Table 6).

Example 42: Conjugation of 129D5BTY scFv to MMAE-βGA-brPEG$_{12}$-PEG$_4$-NHS Ester (15)

129D5BTY scFv was conjugated to Linker-Payload **15** to obtain a DAR 6.4 as per conditions described in Example 39. Specifically, a stock solution of pure scFv (>95%) was diluted to 4.8mg/ml into a pre-equilibrated solution of 20% DMSO in bicarbonate buffer pH9.2. Linker-Payload (25mM in DMSO) was added starting with 5 equivalents every 90-120 min and the reaction mixture incubated at 20°C, 300rpm. The reaction progress was monitored by size-exclusion chromatography mass spectrometry (SEC-MS, Agilent AdvanceBio SEC 120A 1.9mm 2.1x150mm PEEK isocratic run in 75mM Ammonium Acetate, 10% IPA on an Agilent QTOF 6545XT). A total of 8.3 equivalents (2 additions) were required.

The crude reaction mixture was pH neutralized with 1M NaH_2PO_4 (1.5%) and purified on an AKTA Avant through a Superdex 75 26/600 isocratic run eluting with 10% IPA/PBS (Figure 17a). The monomeric fractions were combined and buffer exchanged into Histidine/NaCl buffer pH7.5. The concentrated sample was filtered through a sterile 0.2μm PES filter, flash frozen in liquid nitrogen and stored at -80°C. The sample was analysed by SEC HPLC (Sepax Zenix C 150 7.8 x 300mm) showing 99% monomeric FDC (Figure 17b), SEC-LCMS DAR 6.4 (Figure 17c), UV/Vis spectroscopy, DLS monomeric particle size (Figure 7d), nanoDSF showing Tm ~64.9 °C (Figure 17e) and binding affinity of 1.8nM (Figure 17f) before being used for further studies (Table 6).

Example 43: Conjugation of 129D5B scFv to MMAE-βGA-brPEG$_{12}$-PEG$_7$-NHS Ester (88)

129D5B scFv was conjugated to Linker-Payload **88** to obtain a DAR 7.5 as per conditions described in Example 39. Specifically, a stock solution of pure scFv (>95%) was diluted to 1mg/ml into a pre-equilibrated solution of 20% DMSO in bicarbonate buffer pH9.2. Linker-Payload (25mM in DMSO) was added in 5 equivalents every 90-120 min and the reaction mixture incubated at 20°C, 300rpm. The reaction progress was monitored by size-exclusion chromatography mass spectrometry (SEC-MS, Agilent AdvanceBio SEC 120A 1.9mm 2.1x150mm PEEK isocratic run in 75mM Ammonium Acetate, 10% IPA on an Agilent QTOF 6545XT). A total of 25 equivalents (5 additions) were required.

The crude reaction mixture was pH neutralized with 1M NaH_2PO_4 (1.5%) and purified on an AKTA Avant through a Superdex 75 26/600 isocratic run eluting with 10% IPA/PBS. The monomeric fractions were combined and buffer exchanged into Histidine/NaCl buffer pH7.5. The concentrated sample was filtered through a sterile 0.2μm PES filter, flash frozen in liquid nitrogen and stored at -20°C. The sample was analysed by SEC-LCMS (Figure 18a), UV/Vis spectroscopy, DLS and nanoDSF (Figure 18b) before being used for further studies. The binding affinity was 4.9nM (Figure 18c; Table 6).

Example 44: Conjugation of 129D5B scFv to MMAE-βGA-brPEG$_8$-PEG$_2$-NHS Ester (10)

129D5B scFv was conjugated to linker-payload **10** to obtain a DAR 5.8 as per conditions described in Example 39. Specifically, a stock solution of pure scFv (>95%) was diluted to 1mg/ml into a pre-equilibrated solution of 20% DMSO in bicarbonate buffer pH9.2. Linker-Payload (25mM in DMSO) was added in 5 equivalents every 90-120 min and the reaction mixture incubated at 20°C, 300rpm. The reaction progress was monitored by size-exclusion chromatography mass spectrometry (SEC-MS, Agilent AdvanceBio SEC 120A 1.9mm 2.1x150mm PEEK isocratic run in 75mM Ammonium Acetate, 10% IPA on an Agilent QTOF 6545XT). A total of 20 equivalents (4 additions) were required.

The crude reaction mixture was pH neutralized with 1M NaH_2PO_4 (1.5%) and purified on an AKTA Avant through a Superdex 75 26/600 isocratic run eluting with 10% IPA/PBS. The monomeric fractions were combined and buffer exchanged into Histidine/NaCl buffer pH7.5. The concentrated sample was filtered through a sterile 0.2μm PES filter, flash frozen in liquid nitrogen and stored at -20°C. The sample was analysed by SEC HPLC (Sepax Zenix C 150 7.8 x 300mm) (Figure 19a, HIC-UV (Figure 19b), SEC-LCMS (Figure 19c), UV/Vis spectroscopy, DLS and nanoDSF (Figure 19d) before being used for further studies. The binding affinity was 1.7nM (Figure 19e; Table 6).

Example 45: Conjugation of 129D5BTY scFv to MMAE-βGA-brLys(BisPEG$_8$)-PEG$_2$-NHS Ester (112)

129D5BTY scFv was conjugated to linker-payload **112** to obtain a DAR 5.9 as per conditions described in Example 39. Specifically, a stock solution of pure scFv (>95%) was diluted to 1mg/ml into a pre-equilibrated solution of 20% DMSO in bicarbonate buffer pH9.2. Linker-Payload (25mM in DMSO) was added in 5 equivalents every 90-120 min and the reaction mixture incubated at 20°C, 300rpm. The reaction progress was monitored by size-exclusion chromatography mass spectrometry (SEC-MS, Agilent AdvanceBio SEC 120A 1.9mm 2.1x150mm PEEK isocratic run in 75mM Ammonium Acetate, 10% IPA on an Agilent QTOF 6545XT). A total of 20 equivalents (4 additions) were required.

The crude reaction mixture was pH neutralized with 1M NaH_2PO_4 (1%) and purified on an Agilent 1200 BioInert through a Zenix C150 10mmx300mm column using an isocratic run eluting with 10% IPA/PBS. The monomeric fractions were combined and buffer exchanged into Histidine/NaCl buffer pH7.5. The concentrated sample was filtered through a sterile 0.2μm PES filter, flash frozen in liquid nitrogen and stored at -20°C. The sample was analysed by SEC HPLC (Sepax Zenix C 150 7.8 x 300mm) (Figure 20a, SEC-LCMS (Figure

20b), UV/Vis spectroscopy, nanoDSF (Figure 20c) and DLS (Figure 20d) before being used for further studies. The binding affinity was 1.4nM (Figure 20e; Table 6).

Example 46: Conjugation of 129D5B to DXd-GGFG-PEG$_7$-NHS Ester (22)

129D5B scFv was conjugated to linker-payload **22** to obtain a DAR 7.6 as per conditions described above. Specifically, a stock solution of pure scFv (>95%) was diluted to 1mg/ml into a pre-equilibrated solution of 20% DMSO in bicarbonate buffer pH9.2. Linker-Payload (25mM in DMSO) was added in 5 equivalents every 90-120 min and the reaction mixture incubated at 20°C, 300rpm. The reaction progress was monitored by size-exclusion chromatography mass spectrometry (SEC-MS, Agilent AdvanceBio SEC 120A 1.9mm 2.1x150mm PEEK isocratic run in 75mM Ammonium Acetate, 10% IPA on an Agilent QTOF 6545XT). A total of 25 equivalents (5 additions) were required.

The crude reaction mixture was pH neutralized with 0.1M NaH_2PO_4 (10%) and purified on an Agilent 1200 BioInert through a Zenix C150 10mmx300mm column using an isocratic run eluting with 10% IPA/PBS. The monomeric fractions were combined and buffer exchanged into Histidine/NaCl buffer pH7 and analysed by SEC-LCMS (Figure 21a; Table 6).

Example 47: Conjugation of 129D5B to Exatecan-βGA-PEG$_7$ NHS Ester (28)

129D5B scFv was conjugated to linker-payload **28** to obtain a DAR 7.9 as per conditions described above. Specifically, a stock solution of pure scFv (>95%) was diluted to 1mg/ml into a pre-equilibrated solution of 20% DMSO in bicarbonate buffer pH9.2. Linker-Payload (25mM in DMSO) was added in 5 equivalents every 90-120 min and the reaction mixture incubated at 20°C, 300rpm. The reaction progress was monitored by size-exclusion chromatography mass spectrometry (SEC-MS, Agilent AdvanceBio SEC 120A 1.9mm 2.1x150mm PEEK isocratic run in 75mM Ammonium Acetate, 10% IPA on an Agilent QTOF 6545XT). A total of 25 equivalents (5 additions) were required.

The crude reaction mixture was pH neutralized with 1M NaH_2PO_4 (1.5%) and purified on an Agilent 1200 BioInert through a Zenix C150 10mmx300mm column using an isocratic run eluting with 10% IPA/PBS. The monomeric fractions were combined and buffer exchanged into Histidine/NaCl buffer pH7.5. The concentrated sample was filtered through a sterile 0.2μm PES filter, flash frozen in liquid nitrogen and stored at -20°C. The sample was analysed by SEC HPLC (Sepax Zenix C 150 7.8 x 300mm), SEC-LCMS (Figure 21b) and UV/Vis spectroscopy before being used for further studies. The affinity was 254pM (Figure 21c; Table 6).

Example 48: Conjugation of 131D5S to DXd-GGFG-brPEG$_8$-PEG$_2$ NHS Ester (25)

131D5S scFv was conjugated to linker-payload **25** to obtain a DAR 9.3 as per conditions described above. Specifically, a stock solution of pure scFv (>95%) was diluted to 1mg/ml into a pre-equilibrated solution of 20% DMSO in bicarbonate buffer pH9.2. Linker-Payload (25mM in DMSO) was added starting with 5 equivalents every 90-120 min and the reaction mixture incubated at 20°C, 300rpm. The reaction progress was monitored by size-exclusion chromatography mass spectrometry (SEC-MS, Agilent AdvanceBio SEC 120A 1.9mm 2.1x150mm PEEK isocratic run in 75mM Ammonium Acetate on an Agilent QTOF 6545XT). A total of 45 equivalents (9 additions) were required (Figure 22a; Table 6).

Example 49: Conjugation of 129D5B to Exatecan N-MeGlucamine-GGFG-PEG$_2$-NHS Ester (86)

129D5B scFv was conjugated to linker-payload **86** to obtain a DAR 4.3 as per conditions described above. Specifically, a stock solution of pure scFv (>95%) was diluted to 1mg/ml into a pre-equilibrated solution of 20% DMSO in bicarbonate buffer pH9.2. Linker-Payload (25mM in DMSO) was added in 5 equivalents every 90-120 min and the reaction mixture incubated at 20°C, 300rpm. The reaction progress was monitored by size-exclusion chromatography mass spectrometry (SEC-MS, Agilent AdvanceBio SEC 120A 1.9mm 2.1x150mm PEEK isocratic run in 75mM Ammonium Acetate, 10% IPA on an Agilent QTOF 6545XT. A total of 30 equivalents (6 additions) were required.

The crude reaction mixture was pH neutralized with 1M NaH_2PO_4 (10%) and purified on an Agilent 1200 BioInert through a Zenix C150 10mmx300mm column using an isocratic run eluting with 10% IPA/PBS. The monomeric fractions were combined and buffer exchanged into Histidine/NaCl buffer pH7.5. The concentrated sample was filtered through a sterile 0.2μm PES filter, flash frozen in liquid nitrogen and stored at -20°C. The sample was analysed by, SEC-LCMS (Figure 22b) and UV/Vis spectroscopy before being used for further studies (Table 6).

Example 50: Conjugation of 129D5B scFv to Belotecan-βGA-PEG$_2$ NHS Ester (32)

129D5B scFv was conjugated to linker-payload **32** to obtain a DAR 5.9 as per conditions described above. Specifically, a stock solution of pure scFv (>95%) was diluted to 1mg/ml into a pre-equilibrated solution of 20% DMSO in bicarbonate buffer pH9.2. Linker-Payload (25mM in DMSO) was added in 20 equivalents every 90-120 min and the reaction mixture incubated at 20°C, 300rpm. The reaction progress was monitored by size-exclusion chromatography mass spectrometry (SEC-MS, Agilent AdvanceBio SEC 120A 1.9mm 2.1x150mm PEEK isocratic run in 75mM Ammonium Acetate, 10% IPA on an Agilent QTOF 6545XT). A total of 25 equivalents (5 additions) were required.

The crude reaction mixture was purified/buffer exchanged in a single step using a Zeba column into PBS with 4% trehalose and flash frozen in liquid nitrogen and stored at -20°C. The sample was analysed by SEC-LCMS (Figure 23a), UV/Vis spectroscopy, SEC-HPLC (Figure 23c) before being used for further studies (Table 6). Higher reactive equivalents (40) produced FDCs with a DAR of 13 as shown by SEC-LCMS (Figure 23b) with no aggregation.

The binding affinity was 12.2nM (Figure 74a, Table 6). Cell killing potency on cMET-expressing Hs746T cells was 733.7pM (Figure 74b, Table 10).

Example 51: Conjugation of 129D5B scFv to Triptolide-PEG$_6$ NHS Ester (58)

129D5B scFv was conjugated to linker-payload **58** to obtain a DAR 5.0 as per conditions described above. Specifically, a stock solution of pure scFv (>95%) was diluted to 1mg/ml into a pre-equilibrated solution of 20% DMSO in bicarbonate buffer pH9.2. Linker-Payload (25mM in DMSO) was added in 5 equivalents every 90-120 min and the reaction mixture incubated at 20°C, 300rpm. The reaction progress was monitored by size-exclusion chromatography mass spectrometry (SEC-MS, Agilent AdvanceBio SEC 120A 1.9mm 2.1x150mm PEEK isocratic run in 75mM Ammonium Acetate, 10% IPA on an Agilent QTOF 6545XT). A total of 20 equivalents (5 additions) were required to obtain a DAR 5 by SEC-LCMS (Figure 23d; Table 6).

Example 52: Conjugation of 129D5B scFv to N^1-Benzylamino Imidazoquinoline-PEG$_7$ NHS Ester (54)

129D5B scFv was conjugated to linker-payload **54** to obtain a DAR 1.35 as per conditions described above. Specifically, a stock solution of pure scFv (>95%) was diluted to 1mg/ml into a pre-equilibrated solution of 20% DMSO in bicarbonate buffer pH 9.2. Linker-Payload (25mM in DMSO) was added in 5 equivalents every 90-120 min and the reaction mixture incubated at 20°C, 300rpm. The reaction progress was monitored by size-exclusion chromatography mass spectrometry (SEC-MS, Agilent AdvanceBio SEC 120A 1.9mm 2.1x150mm PEEK isocratic run in 75mM Ammonium Acetate on an Agilent QTOF 6545XT (Figure 24a, Table 6). A total of 15 equivalents (3 additions) were required. The sample was neutralized with 1M NaH_2PO_4 (1.5% v/v) and stored at 4°C.

A modified conjugation reaction based on Example 77 yielded a slightly higher DAR (1.81). A stock solution of pure scFv (>95%) was diluted to 50µM (1.4mg/mL) into a pre-equilibrated solution of 100mM sodium phosphate pH 8.0, 10% DMA. Linker-Payload (25mM in DMSO) was added starting with 1 molar equivalent (compared to scFv lysines) before adding more payload every 60 min and the reaction mixture incubated at 22°C, 500rpm until the DAR was achieved (3 molar equivalents required) (Figure 75).

Example 53: Conjugation of 129D5B scFv to Nintedanib α-Galactose-PEG$_7$ NHS Ester (46)

129D5B scFv was conjugated to linker-payload **46** to obtain a DAR 1.9 as per conditions described above. Specifically, a stock solution of pure scFv (>95%) was diluted to 1mg/ml into a pre-equilibrated solution of 20% DMSO in bicarbonate buffer pH9.2. Linker-Payload (25mM in DMSO) was added starting with 10 equivalents every 90-120 min and the reaction mixture incubated at 20°C, 300rpm. The reaction progress was monitored by reverse-phase chromatography mass spectrometry (RP-MS, Agilent PLRP) eluting with a gradient of 0.1%FA/water/MeCN in in 75mM Ammonium Acetate on an Agilent QTOF 6545XT. A total of 40 equivalents (4 additions) were required. The crude reaction mixture was analysed by LCMS (Figure 24b; Table 6) and HIC-UV chromatography.

Example 54: Conjugation of 129D5B scFv to GENZ-644282-Val-Ala-brPEG$_{12}$-PEG$_4$-NHS Ester (80)

129D5B scFv was conjugated to linker-payload **80** to obtain a DAR 2.4 as per conditions described above. Specifically, a stock solution of pure scFv (>95%) was diluted to 1mg/ml into a pre-equilibrated solution of 20% DMSO in bicarbonate buffer pH9.2. Linker-Payload (25mM in DMSO) was added starting with 5 equivalents every 90-120 min and the reaction mixture incubated at 20°C, 300rpm. The reaction progress was monitored by RP-MS, (RPMS C4 Phenomenex column (100x2.1mm) gradient run in 0.1%FA/water/MeCN on an Agilent QTOF 6545XT). A total of 20 equivalents (4 additions) were required. The crude reaction mixtures were pH neutralized with 1M NaH_2PO_4 (10%) before being used for further studies (Figure 25a; Table 6).

Example 55: Conjugation of 129D5B scFv to Dexamethasone-dipyrophosphate-PEG$_2$ TFP Ester (50)

129D5B scFv was conjugated to linker-payload **50** to obtain a DAR 3.74 as per conditions described above. Specifically, a stock solution of pure scFv (>95%) was diluted to 1mg/ml into a pre-equilibrated solution of 20% DMSO in bicarbonate buffer pH9.2. Linker-Payload (25mM in DMSO) was added in 10 equivalents every 90-120 min and the reaction mixture incubated at 20°C, 300rpm. The reaction progress was monitored by size-exclusion chromatography mass spectrometry (SEC-MS, Agilent AdvanceBio SEC 120A 1.9mm 2.1x150mm PEEK isocratic run in 75mM Ammonium Acetate, 10% IPA on an Agilent QTOF 6545XT). A total of 10 equivalents (1 addition) were required (Figure 25b). The binding affinity was 298nM (Figure 25c; Table 6).

Example 56: Conjugation of 129D5B Fab to MMAE-βGA-brPEG$_8$-PEG$_2$-NHS Ester (10)

A Fab version of the 129D5B scFv was constructed by BioIntron Inc by fusing the VH gene to the CH1 gene from a rabbit IgG1 and the VL gene to the rabbit CL gene and expressed and purified from CHO cells. The binding affinity was confirmed by BIAcore as 30pM (Figure 26a). This was conjugated to linker-payload **10** to obtain a DAR 5.9 as per conditions described in Example 39. Specifically, a stock solution of pure scFv (>95%) was diluted to 1mg/ml into a pre-equilibrated solution of 20% DMSO in bicarbonate buffer pH9.2. Linker-Payload (25mM in DMSO) was added starting with 5 equivalents every 90-120 min and the reaction mixture incubated at 20°C, 300rpm. The reaction progress was monitored by RP chromatography mass spectrometry RP-MS, RPMS C4 phenomenex column (100x2.1mm) gradient run in 0.1%FA/water/MeCN on an Agilent QTOF 6545XT. A total of 15 equivalents (2 additions) were required (Figure 27a, Figure 27c; Table 6). The binding affinity was 41pM (Figure 26b).

Example 57: Conjugation of 129D5B Fab to Maleimidocaproly-Val-Cit-MMAE (61)

129D5B Fab (example 53) was conjugated to linker-payload 61 to obtain a DAR 2. Under nitrogen, in a round bottomed flask, the antibody was diluted into PBS to a final 1mg/ml before adding the EDTA (50mM) and TCEP (1mM) and degassing for 10mins at RT before incubating at 4°C overnight. Degassed Payload diluted in anhydrous DMSO were added to the antibody solution at RT and incubated with gentle stirring for 1hr. The reaction was monitored by RP-Mass spectrometry (RPMS C4 Phenomenex column (100x2.1mm) gradient run in 0.1%FA/water/MeCN on an Agilent QTOF 6545XT). The reaction was quenched with acetyl cysteine (1.8 equivalents to the payload) at 20°C at RT. The crude reaction mixture was purified by HIC chromatography on an AKTA Pure, on a 1ml Butyl HP column eluting with a gradient of ammonium sulphate in sodium sulphate pH7.4.

The required fractions were combined, and buffer exchanged into Histidine/NaCl buffer pH7.5. The concentrated sample was filtered through a sterile 0.2μm PES filter, flash frozen in liquid nitrogen and stored at -20°C. The sample was analysed by RP-LCMS (Figure 22B) SEC HPLC (Sepax Zenix C 150 7.8 x 300mm), Figure 27b; Table 6). The binding affinity was 35pM (Figure 26c).

Table 6: Summary of FDC biophysical properties (ND-Not determined)

FDC (Lysine conjugation unless stated)	**Ave. DAR**	**Tm (°C)**	% mono-mer (HPLC-SEC)	**DLS**		Binding association rate, k_a ($M^{-1}s^{-1}$)	Binding dissociation rate, k_d (s^{-1})	**Binding affinity**
				Cumu-lant	PDI			K_d (M)

				radius (nm)				
129D5BTY-MMAE-βGA-brPEG8-PEG2	6.3	64.1	99.4	3.6	0.19	4.8×10^{4}	2.2×10^{-4}	4.5×10^{-9}
129D5BTY-MMAE-βGA-brPEG8-PEG2	5.9	64.1	98.5	3.4	0.12	5.9×10^{4}	1.3×10^{-4}	2.2×10^{-9}
129D5BTY-MMAE-βGA-brPEG8-PEG2	7.3	62.9	93.2	4.3	0.36	3.6×10^{4}	1.9×10^{-4}	5.3×10^{-9}
129D5BTY-MMAE-βGA-brPEG$_{12}$-PEG$_4$	6.4	64.9	99	3.9	0.14	7.4×10^{4}	1.4×10^{-4}	1.8×10^{-9}
129D5BTY-MMAE-βGA-brLys(BisPEG$_8$)-PEG$_2$	5.9	64.1	96.3	3.7	0.17	1.0×10^{5}	1.4×10^{-4}	1.4×10^{-9}
129D5B-MMAE-βGA-brPEG$_8$-PEG$_2$	5.8	64.1	98	3.4	0.16	1.1×10^{5}	1.8×10^{-4}	1.7×10^{-9}
129D5B-MMAE-βGA-brPEG$_8$-PEG$_2$	5.9	63.6	98.4	ND	ND	1.2×10^{5}	1.9×10^{-4}	1.6×10^{-9}
129D5B-MMAE-βGA-brPEG$_{12}$-PEG$_7$	7.5	63.2	ND	3.73	0.14	5.7×10^{4}	2.8×10^{-4}	4.9×10^{-9}
129D5B-MMAF-PEG$_2$	7.8	ND	ND	ND	ND	ND	ND	ND
77F3-MMAE-βGA-brPEG$_8$-PEG$_2$	5.6	ND	99.3	3.51	0.21	6.6×10^{4}	3.2×10^{-4}	4.8×10^{-9}
77F3-MMAE-βGA-brPEG$_4$-PEG$_2$	8.4	ND	98.9	3.44	0.13	3.7×10^{4}	3.9×10^{-4}	1.0×10^{-8}
94C2-MMAE-βGA-brPEG$_4$-PEG$_2$	5.8	75.48	98.2	6.2555	ND	4.5×10^{6}	1.0×10^{-2}	2.3×10^{-9}
82H8-MMAE-βGA-brPEG$_4$-PEG$_2$	6.5	ND	ND	ND	ND	4.4×10^{4}	2.9×10^{-4}	6.7×10^{-9}
131D5S-MMAE-βGA-brPEG$_8$-PEG$_2$	5.4	53.4	88	3.9	0.17	5.1×10^{6}	5.8×10^{-4}	1.1×10^{-10}
20F6-MMAF-PEG$_2$	6.95	ND	98	ND	ND	2.0×10^{4}	2.7×10^{-2}	1.35×10^{-6}
20F6L18R-MMAF-PEG$_2$	8.5	ND	96.9	ND	ND			
129D5B-MMAE-Val-Ala-Lys-bisPEG$_8$-PEG$_4$	6.6	46.4	ND	4.45	0.51	5.7×10^{4}	1.5×10^{-4}	2.6×10^{-9}
129D5B-Belotecan-βGA-PEG$_2$	5.9	ND	94	ND	ND	8.6×10^{4}	2.1×10^{-4}	2.5×10^{-9}

129D5B-Belotecan-βGA-PEG$_2$	13	ND	ND	ND	ND	1.65 x10^4	2.0 x10^{-4}	1.22 x 10^{-8}
129D5B-Exatecan-βGA-PEG$_7$	7.9	ND	97.2	ND	ND	1.2 x10^5	9.9 x10^{-5}	8.1 x 10^{-10}
129D5B-Exatecan-βGA-PEG$_7$	7.0	ND	ND	ND	ND	4.9 x10^5	1.3 x10^{-5}	2.5 x 10^{-10}
129D5B-DXd-GGFG-PEG$_7$	7.6	ND	ND	ND	ND	ND	ND	ND
129D5B-DXd-GGFG-brPEG$_8$-PEG$_2$	3.7	ND	ND	ND	ND	2.69 x10^5	9.1 x10^{-5}	3.39 x 10^{-10}
131D5S-DXd-GGFG-brPEG$_8$-PEG$_2$	9.3	ND	ND	ND	ND	ND	ND	ND
129D5B-Gluc-BrPEG$_8$-Exatecan	2.7	ND	ND	ND	ND	ND	ND	ND
129D5B-Exatecan N-MeGlucamine-GGFG-PEG$_2$	4.3	ND	ND	ND	ND	ND	ND	ND
129D5B-Dexamethasone-dipyrophosphate-PEG$_2$-TFP	3.74	ND	ND	ND	ND	3.2 x10^5	9.7 x10^{-5}	2.9 x 10^{-10}
129D5B Fab-MMAE-βGA-BrPEG$_8$-PEG$_2$	5.89	ND	ND	ND	ND	1.2 x10^6	5.0 x10^{-5}	4.1 x 10^{-11}
129D5B Fab-Maleimidocaproly-Val-Cit-MMAE (Cys-thiol conjugate)	2	ND	99.5	ND	ND	6.9 x10^5	2.4 x10^{-5}	3.5 x 10^{-11}
129D5B-Triptolide-PEG$_6$	5	ND	ND	ND	ND	ND	ND	ND
129D5B-Nintedanib α-Galactose-PEG$_7$	1.9	ND	ND	ND	ND	ND	ND	ND
129D5B-N1-Benzylamino Imidazoquinoline-PEG7	1.35	ND	ND	ND	ND	ND	ND	ND
129D5B-N1-Benzylamino Imidazoquinoline-PEG7	1.81	ND	ND	ND	ND	ND	ND	ND

129D5B-GENZ-644282-Val-Ala-BrPEG$_8$-PEG$_2$	0.38	ND	ND	ND	ND	ND	ND	ND
129D5B-Exatecan-MA-PEG$_{12}$-Val-Ala-PEG$_4$	5.03	57.05	ND	ND	ND	2.64×10^5	9.8×10^{-5}	3.69×10^{-10}
129D5B-Exatecan-βGA-BrPEG$_{12}$-PEG$_4$	7.9	ND	ND	ND	ND	4.16×10^4	1.9×10^{-4}	4.51×10^{-9}
129D5B-2-(Methylsulphonyl) ethyl amino-MMAF-βGA-PEG$_2$	5.15	ND	ND	ND	ND	1.61×10^5	1.2×10^{-4}	7.18×10^{-10}

Example 58: Conjugation to cMET scFv described in WO2013/079973

Phage display is a common method for scFv discovery but even for those skilled in the art, scFvs against the cMET target may not be suitable for bioconjugation unless following the disclosures herein. For example DiCara DM et al (WO2013079973) described anti-cMET scFvs, discovered from human phage libraries which bind with to cMET with high affinity. Two clones, 107-A07 and 107-A01 are noted.

ScFv clone 107-A01 was constructed and produced as described in WO2013079973 and was conjugated to MMAF-PEG2 Linker-Payload (WO2016046574) to obtain a DAR 6 using the same conditions as described in WO2016046574. Specifically, a stock solution of pure scFv (>95%) was diluted to 1mg/ml into a pre-equilibrated solution of 20% DMSO in bicarbonate buffer pH9.2. Linker-Payload (25mM in DMSO) was added in 6 equivalents every 90-120 min and the reaction mixture incubated at 20°C, 300rpm. A total of 12 equivalents (2 additions) were required.

The crude reaction mixture was pH neutralized with 0.1M NaH_2PO_4 (10%) and purified on an Agilent 1200, on a Zenix-C 150 10mmx 300mm, using an isocratic run eluting with 10% IPA/PBS. The monomeric fractions were combined and buffer exchanged into PBS pH7.5. The concentrated sample was filtered through a sterile 0.2μm PES filter and stored at 4°C. The sample was analysed by SEC-LCMS (Figure 28a-c), UV/Vis spectroscopy, SDS-PAGE and SEC-HPLC (Figure 28d) before being used for further studies. A parallel conjugation reaction was carried out using the 20F6 cMET scFv described herein (Example 2) and analysed similarly. The sample was analysed by SEC-LCMS (Figure 28e), UV/Vis spectroscopy, SDS-PAGE and SEC-HPLC (Figure 28f) before being used for further studies. The 107-A01-MMAF-PEG2 FDC demonstrated significant levels of aggregation (>10%) and poor biophysical properties compared to the 20F6-MMAF-PEG2 FDC (<1% aggregation),

even though the latter FDC had a similar or higher DAR. A similar observation was also seen when scFv clone 107-A07 was used. This demonstrated that scFvs disclosed in this invention display unexpectedly superior bioconjugation and biophysical properties when compared to other human anti-cMET scFvs.

Example 59: Flow cytometry of cMET FDCs on low, medium and high cMET expressing cell lines

A list of cell lines analysed is shown in Table 7, with estimated cMET receptor levels from the literature [57]. For cell surface binding, 50-70% confluent cells were harvested from flasks using cell dissociation buffer (Gibco). Cells were washed and resuspended in PBS, 0.5% BSA, 0.8mM EDTA and 0.02% NaN_3. Cells were transferred to a 96-well microplate and incubated with primary antibodies (129D5B/129D5BTY scFvs, 131D5S scFv, ABT-700 IgG and 5D5 IgG) or controls for 1h on ice. Cells were washed and incubated for 1h on ice and in the dark with appropriate detection antibodies (labelled with a fluorophore) except for untreated cells. After incubation, cells were washed, re-suspend in flow buffer and analysed on a Guava EasyCyte HT flow cytometer (Cytek Biosciences).

Table 7: Properties of cell lines used in flow cytometry analyses

Cell line	**Tissue of Origin**	**cMET expression** (High >100k receptors/cell, Moderate 30-100k/cell, Low <30k/cell)
Hs746T	Gastric	High
SNU5	Gastric	High
KATO III	Gastric	High
NUGC-4	Gastric	Moderate-Low
SNU16	Gastric	Moderate
NCI-N87	Gastric	Low
T47D	Breast	Negative
JIMT1	Breast	Low
AsPC-1	Pancreas	High
NCI-H1975	Lung	Moderate
SKOV3	Ovary	Moderate

The results showed that cMET scFv clones 129D5B/129D5BTY and 131D5S bound to Hs746T, SNU5 and other cMET-expressing cell lines from different tissue origins, when compared to known benchmark IgGs ABT-700 and 5D5 (Table 8, Figure 29). Significant binding was also seen in cell lines expressing moderate to low cMET levels.

Table 8: Properties of cell lines used in flow cytometry analyses		
Cell line	**Sample analysed**	**Percentage binding by fluorescence shift**
Hs746T	129D5BTY scFv	92
	131D5S scFv	26
	ABT-700 IgG	99
SNU5	129D5BTY scFv	73
	129D5B scFv	97
	131D5S scFv	83
	ABT-700 IgG	99
	5D5 IgG	99
KATO III	129D5B scFv	87
	ABT-700 IgG	99
	5D5 IgG	99
NUGC-4	129D5B scFv	48
SNU16	129D5B scFv	5
NCI-N87	129D5B scFv	36
T47D	129D5B scFv	0
JIMT1	129D5B scFv	21
AsPC-1	129D5B scFv	77
NCI-H1975	129D5B scFv	16
SKOV3	129D5B scFv	32

In a more detailed analyses, cMET receptor cell surface density (antigen-binding capacity per cell) was determined by indirect immunofluorescence staining of cell surface antigens using the QIFIKIT (DAKO-K0078) on 6 cell lines. Anti-cMET 5D5 IgG1 (5D5.11.6) hybridoma was purchased from the ATCC. All cell lines were acquired from ATCC (UK-LGC) and were grown in the recommended media and conditions. Cells were treated with cMET 5D5 mouse antibody at saturating concentration (5mg/ml). Surface binding was detected by treating cells with QIFIKIT-provided FITC-conjugated antibody at saturating concentration (Figure 30).

For the construction of the calibration curve, calibration beads were treated with QIFIKIT-provided FITC-conjugated antibody – individual markers are used to determine the MFI (Mean Fluorescence Intensity) of each bead population (Fig 30a). The Set-Up beads were used to establish the window of analysis, as it comprises a mixture of blank and high-level

beads (Fig 30b). Indirect immunofluorescence staining data of the QIFIKIT beads was acquired on a Guava EasyCyte HT flow cytometer (Cytek Biosciences) using standard operating procedures. The standard curve (Fig 30c) was used to assign ABC (antibody-binding capacity) or the number of monoclonal antibody binding sites/cell per cell or microbeads to each of the cell lines tested (Table 9).

Table 9: cMET receptor count by calibrated flow cytometry analyses

Cell line	Mean Fluorescent Intensity (MFI)	cMET receptors/cell
SNU5	2544.83	402,641
Hs746T	1491.54	230,120
NUGC-4	294.21	34,005
NCI-H1975	291.71	33,596
NCI-N87	134.00	7,764
T47D	1.56	~0

Example 60: Cell-killing Potency Assays

Cell lines were obtained from commercial depositaries and grown according to the recommended conditions, harvested during the logarithmic growth period and counted. The cell concentration was adjusted to the optimal conditions for each cell line. Cell suspension (in the range of 1000-10,000 cells/well) was added to three 96-well plates and incubated overnight in a humidified incubator at 37° C with 5% CO_2. FDC, ADC and unconjugated antibodies at high working concentrations were prepared in media with 10 (x3) and 100 (x2) fold serial dilutions to achieve 6-8 dose levels. Cells are treated with diluted compounds (x5 replicates for each drug concentration). Control plates are treated with either medium or triton-X100 and incubated for 96h in a humidified incubator at 37°C with 5% CO_2. Celltiter-96 Aqueous One Solution (Promega G5381) reagent is added to each well. After 4 hours incubation at 37° C with 5% CO_2 optical density at 490nm is recorded. The data is analysed to calculate relative IC_{50}, and a dose-response curve is fitted using a nonlinear regression model with a sigmoidal dose-response using GraphPad Prism. The cell killing potency is summarised in Table 10 with representative plots shown in Figures 31 to 37. FDC potency was in the range of 0.1 to 2nM IC_{50} with cMET-negative cell lines showing no or low sensitivity to the FDC. Surprisingly, FDCs were potent against cMET low cell lines (e.g. NCI-N87) whereas telisotuzumab vedotin ADC was much less effective (reported threshold for efficacy is ~100,000 receptors/cell [57] suggesting that

high-DAR FDCs can kill tumour cells with as low as ~8000 receptors/cell.

Table 10: In vitro cell killing potency.

FDC	DAR	Cell Line	Origin	cMET expression	Potency IC50 (nM)
129D5B scFv	0	Hs746T	Gastric	High	No effect
		T47D	Breast	Negative	No effect
		SNU-5	Gastric	High	No effect
		Kato III	Gastric	High	No effect
		NUGC-4	Gastric	Moderate	No effect
		JIMT-1	Breast	Low	No effect
		SKOV-3	Ovary	Moderate	No effect
		NCI-N87	Gastric	Low	No effect
		SNU-16	Gastric	Moderate	No effect
		NCI-H1975	Lung	Moderate	No effect
		AsPC-1	Pancreas	High	No effect
131D5S scFv	0	Hs746T	Gastric	High	No effect
		T47D	Breast	Negative	No effect
		SNU-5	Gastric	High	No effect
		Kato III	Gastric	High	No effect
		NUGC-4	Gastric	Moderate	No effect
		JIMT-1	Breast	Low	No effect
		SKOV3	Ovary	Moderate	No effect
		NCI-N87	Gastric	Low	No effect
		SNU-16	Gastric	Moderate	No effect
		NCI-H1975	Lung	Moderate	No effect
		AsPC-1	Pancreas	High	No effect
77F3 scFv	0	Hs746T	Gastric	High	No effect
		T47D	Breast	Negative	No effect
129D5B-MMAE-βGA-brPEG$_8$-PEG$_2$	5.9	Hs746T	Gastric	High	0.258
		T47D	Breast	Negative	No effect
		SNU-5	Gastric	High	0.436
		Kato III	Gastric	High	0.527
		NUGC-4	Gastric	Moderate	0.184
		JIMT-1	Breast	Low	2.7

		SKOV-3	Ovary	Moderate	1.9
		NCI-N87	Gastric	Low	1.8
		SNU-16	Gastric	Moderate	1.0
		NCI-H1975	Lung	Moderate	0.665
		AsPC-1	Pancreas	High	1.3
129D5BTY-MMAE-βGA-brPEG$_8$-PEG$_2$	6.1	Hs746T	Gastric	High	0.120
		T47D	Breast	Negative	No effect
		NCI-N87	Gastric	Low	1.3
129D5BTY-MMAE-βGA-brPEG$_8$-PEG$_2$	7.3	Hs746T	Gastric	High	0.285
		T47D	Breast	Negative	>72
131D5S-MMAE-βGA-brPEG$_8$-PEG$_2$	5.4	Hs746T	Gastric	High	0.110
		T47D	Breast	Negative	No effect
		SNU-5	Gastric	High	0.107
		Kato III	Gastric	High	0.051
		NUGC-4	Gastric	Moderate	0.039
		JIMT-1	Breast	Low	0.612
		SKOV-3	Ovary	Moderate	0.470
		NCI-N87	Gastric	Low	1.2
		SNU-16	Gastric	Moderate	0.810
		NCI-H1975	Lung	Moderate	0.110
		AsPC-1	Pancreas	High	0.114
129D5B-MMAE-βGA-brPEG$_{12}$-PEG$_7$	7.5	Hs746T	Gastric	High	1.05
		T47D	Breast	Negative	No effect
129D5BTY-MMAE-βGA-brPEG$_{12}$-PEG$_4$	6.4	Hs746T	Gastric	High	0.394
		T47D	Breast	Negative	115
129D5BTY-MMAE-βGA br(Lys-BisP$_8$)-PEG$_2$	3.8	Hs746T	Gastric	High	0.245
		T47D	Breast	Negative	No effect
129D5BTY-MMAE-βGA br(Lys-BisP$_8$)-PEG$_2$	5.3	Hs746T	Gastric	High	0.138
		T47D	Breast	Negative	No effect
129D5B-MMAF-βGA-PEG$_2$	7.8	Hs746T	Gastric	High	0.010
		T47D	Breast	Negative	>129
129D5B-2-(Methylsulphonyl)ethylamino-MMAF-βGA-PEG2	5.2	Hs746T	Gastric	High	0.093
		T47D	Breast	Negative	No effect

129D5B-Belotecan-βGA-PEG2	13.0	Hs746T	Gastric	High	0.734
		T47D	Breast	Negative	5.4
77F3-MMAE-βGA-brPEG$_8$-PEG$_2$	5.6	Hs746T	Gastric	High	0.919
		T47D	Breast	Negative	No effect
77F3-MMAE-βGA-brPEG$_4$-PEG$_2$	8.1	Hs746T	Gastric	High	1.7
		T47D	Breast	Negative	No effect
82H8-MMAE-βGA-brPEG$_4$-PEG$_2$	6.5	Hs746T	Gastric	High	1.3
		T47D	Breast	Negative	> 182
5D5 IgG	0	Hs746T	Gastric	High	No effect
		BT474	Breast	Low	No effect
		NCI-N87	Gastric	Low	No effect
		T47D	Breast	Negative	No effect
5D5-MMAE-βGA-brPEG$_8$-PEG$_2$	4	Hs746T	Gastric	High	0.008
		LNcaP	Prostate	Negative	No effect
ABT700 IgG	0	Hs746T	Gastric	High	No effect
		NCI-N87	Gastric	Low	No effect
		T47D	Breast	Negative	No effect
ABT700-vcMMAE	3.1	Hs746T	Gastric	High	0.005
		T47D	Breast	Negative	No effect
		NCI-N87	Gastric	Low	113
		SNU-5	Gastric	High	0.114

Example 61: Cell-killing Potency on 50 cell-line Omniscreen™ panel

Crown Biosciences (UK) run independent cell potency screens across cell lines with known genetic properties. Fifty cell lines were selected on the basis of cMET RNA expression to include tumours from 9 tissues of origin with high, medium and low cMET expression (as determined by Crown Biosciences). 129D5B-MMAE-βGA-BrPEG$_8$-PEG$_2$ FDC (DAR 6.75) was incubated at a range of concentrations for 72h and cell viability determined using CellTiter-Glo® Luminescent Cell Viability Assay (Promega). The potency was determined as IC$_{50}$ and compared to reference drug cisplatin. A summary of the FDC's potency against these cell lines is shown in Table 11 and representative plots shown in Figure 38.

Table 11: Omniscreen cell killing potency					
No	**Cell Line**	**Tissue**	**cMET Levels**	**cMET FDC**	**CisPlatin**

			cMET exp-ression	Log2 cMET (Crown)	mRNA exp-ression (Log2)	IC50 (mM)	IC50 (mM)
1	SNU-620	Stomach	High	10.02	11.74	0.002	58.4
2	Hs746T	Stomach	High		11.87	0.01	22.5
3	SNU5	Stomach	High	9.83	11.88	0.007	2.5
4	NUGC-4	Stomach	High	8.06	11.09	0.006	2.6
5	EBC1	NSCLC	High	9.62	11.89	0.004	18.3
6	NCI-H820	NSCLC	High	8.57		0.008	2.3
7	NCI-H1573	NSCLC	High	8.01	10.24	0.015	13.3
8	AsPC-1	Pancreas	High	7.62	10.78	0.01	3.5
9	Capan-2	Pancreas	High	7.43	10.37	0.014	>100
10	KP4	Pancreas	High	7.11	9.69	0.014	4.8
11	BxPC-3	Pancreas	High	6.96	9.51	0.011	2.4
12	HCC38	TNBC	High	6.69	9.32	0.016	9.4
13	KMRC-20	Kidney	High	8.36	10.71	0.017	3.8
14	Caki-1	Kidney	High	6.84	10.06	0.016	2.2
15	786-O	Kidney	High	6.54	9.72	0.017	1.9
16	Detroit 562	HN/Pharynx	High	8.14	11.12	0.007	2.2
17	CAL27	HN/Tongue	High	6.32	9.18	0.018	3.3
18	SCC-4	HN/Tongue	High	6.15	9.17	>0.1	4.8
19	HT-29	Large intestine/ colorectum	High	6.21	9.03	0.01	11.1
20	MHCC97-H	Liver	High	10.97		0.004	21.7
21	KATOIII	Stomach	Medium	6.82	9.63	0.005	7.756
22	SNU16	Stomach	Medium	5.08	8.23	0.008	6.158
23	NCI-H1650	NSCLC	Medium	6.26	8.81	0.043	8.909
24	A549	NSCLC	Medium	6.05	9.18	0.054	6.34
25	HPAF-II	Pancreas	Medium	6.47	9.08	0.007	8.179
26	Capan-1	Pancreas	Medium	6.13	8.79	0.059	0.57
27	PANC-1	Pancreas	Medium	6.03	8.82	0.114	13.312
28	Hs 578T	TNBC	Medium	5.51	9.18	0.021	11.462
29	HCC 1806	TNBC	Medium	5.53		0.04	2.441

30	HCC 1187	TNBC	Medium	5.26	8.25	>0.5	4.27
31	KYSE-410	HN/Esophagus	Medium	5.97	8.85	0.022	8.511
32	KYSE-270	HN/Esophagus	Medium	5.20	8.48	0.109	4.83
33	OE19	HN/Esophagus	Medium	5.14	7.39	>0.5	11.796
34	FaDu	HN/Pharynx	Medium	5.29	8.12	0.079	3.202
35	SW-48	Large intestine/ colorectum	Medium	5.45	7.77	0.048	9.332
36	MKN74	Stomach	Low	4.72	7.65	0.042	14.0
37	NCI-N87	Stomach	Low	4.66	7.85	0.171	4.2
38	IM95m	Stomach	Low	4.47	8.21	0.027	23.7
39	AGS	Stomach	Low	4.46	7.84	0.027	11.0
40	HGC-27	Stomach	Low	3.32	6.30	0.644	3.4
41	NCI-H1975	NSCLC	Low	5.66	9.45	0.014	4.3
42	NCI-H460	NSCLC	Low	4.69	7.85	0.111	0.7
43	NCI-H1703	NSCLC	Low	4.19	7.75	0.031	13.2
44	NCI-H520	NSCLC	Low	3.03	5.98	0.303	7.8
45	SW-1990	Pancreas	Low	5.21	8.47	>1	4.1
46	MIA PaCa-2	Pancreas	Low	1.22	5.94	0.344	7.3
47	BT-549	TNBC	Low	5.01		>1	10.4
48	HCC 1395	TNBC	Low	5.00	8.19	0.034	4.3
49	RKO	Large intestine/ colorectum	Low	4.00	7.38	0.028	3.9
50	Hep G2	Liver	Low	4.51	8.00	>1	7.4

The cMET FDC was potently cytotoxic to a range of solid tumour cell lines including gastric/stomach, lung, pancreas, triple-negative breast, kidney, head & neck, colon, oesophagus and liver at a range of cMET-expression levels (high, medium and low).

Example 62: cMET FDC internalization

Cell surface internalization experiments were conducted as described by [236]. Briefly, SNU5 cells ($2x10^5$/well) were incubated in the dark on ice for 1h with Alexa Fluor 488 labelled antibodies/conjugates (0.15 to 2 mg/mL) in cold medium containing FBS. After washing, cells were resuspended in warm medium containing FBS and incubated at 37°C, 5% CO_2 for the indicated intervals to promote internalisation of surface fluorescence (0, 15, 30, 45, 60, 120, 180, 240 & 300 min). At each time point cells were rapidly chilled in the dark. Once all time points have been collected, cells were incubated on ice/protected from light for 30 minutes with either, quenching ab (10μg/ml) or unlabelled antibody (10mg/mL). Cells were washed and resuspended in flow buffer (PBS/0.5% BSA). The mean fluorescence intensity of 10,000 cells was quantified by flow cytometry (Guava Flow Cytometer). Internalised fluorescence was calculated from quenched and non-quenched sample data by correcting for incomplete surface quenching. Internalised fluorescence was plotted, and a curve fit was obtained in Prism by nonlinear regression with the one-phase association equation: Y = Y0 + (Plateau—Y0) _ (1—exp(-K_x)) with Y0 = 0 when X (time) is zero and Plateau = 100. The summary statistic half-life ($t_{1/2}$) is the time at which internalised fluorescence is equal to fifty per cent and enabled comparison of internalisation for the different dye-conjugated cMET Abs. Half-time is in the time units on the X-axis and is computed as the reciprocal of ln (2)/K. For each curve fit the 95% confidence interval for half-time is reported. The t1/2 for internalization for the 129D5B scFv, 129D5B FDC, 5D5 IgG and ABT-700 IgG was 85, 81, 81 and 64 minutes respectively. Linker-payload conjugation did not appear to affect the rate of internalization which itself was similar to bivalent IgGs (Figure 39).

Example 63: Inhibition of cMET phosphorylation by scFvs

Non-small cell lung cancer cell line A549 was obtained from the American Type Culture Collection. (ATCC-CRM-CLL-185). Phosphorylation inhibition was determined according to [237]. A549 cells were seeded at $4.0x10^4$ per well in a 96-well plate in complete growth medium [F12K+10% FCS]. Twenty-four hours later, cells were pretreated with antibodies in duplicate wells for one hour at 37°C, and then stimulated with 1nM (~100ng/ml) recombinant human HGF (R&D Systems) for 10 min at 37 °C. Cells were wash with PBS and incubated on ice with 100ul/well of Cell Lysis Buffer (Cell Signalling Technology) supplemented with PMSF protease inhibitor. Cell lysates were collected by centrifugation at 13000 rpm for 10 min at 4°C. and correspond to the supernatant phase. Protein content was quantified using a Pierce 660nm protein assay (Pierce).

The phosphorylation status of c-Met was quantified by ELISA. Briefly, a goat anti-cMET antibody (R&D Systems, ref AF276) was used as a capture antibody. After a saturation

step with a TBS-BSA 5% buffer, 7 mg protein lysates were added to each well of the coated 96-well plate and incubated for 90 min at room temperature (RT). The plates were washed with 0.1% TBS-Tween and the anti-phospho-c-Met Mab, directed against the phosphorylated Tyr residues at position 1230, 1234 and 1235 - Invitrogen) was added. After an additional 1-hour incubation and 4 washes, an anti-rabbit-antibody coupled to HRP was added and incubated for 45 minutes at RT. The plates were washed before SuperSignal ELISA Pico Chemiluminescent Substrate (ThermoScientific) was added and the luminescence was measured using a ClarioSTAR Microplate reader. The data shown in Figure 40 shows that 129D5BTY and 131D5S scFvs inhibit phosphorylation (IC_{50} 1.4nM and 4.3nM respectively) as well as reference IgG antibodies 5D5 and ABT-700 (IC_{50} 1.4nM and 1.5nM respectively). An irrelevant IgG4 antibody does not inhibit.

Example 64: Pharmacokinetics of cMET FDCs after single dose

The pharmacokinetic clearance for a range of FDCs (DAR ~6) was measured after a single IV dose of 1mg/kg in Sprague-Dawley rats, immuno-detecting the scFv component by anti-StrepTag ELISA and the payload component by anti-MMAE ELISA on cMET protein coated ELISA plates (Table 12; Figure 41). The data was plotted using GraphPad (Prism) and the bioavailability (plasma exposure) was determined as the area under the curve (AUC) of plasma concentration vs time (Table 12). The AUC for the unmodified 129D5B scFv was 2.7 $mgmL^{-1}hr$ and conjugates all had greater plasma exposure due to the presence of the linker payload with the increase in exposure exceeding 20x with the longest PEG-chain containing linker. FDCs with a greater plasma exposure are expected to be more efficacious whilst retaining the benefits of superior penetration compared to ADCs. The pharmacokinetic profile and AUC were very similar whether detected by anti-StrepTag immuno-detection or anti-MMAE immunodetection confirming that the FDCs were stable with no significant payload deconjugation occurring.

Table 12: Summary of single cycle pharmacokinetics for 129D5BTY FDCs				
		Bioavailability AUC ($mgmL^{-1}hr$)		**Mean AUC increase vs scFv**
Payload	**DAR (Ave)**	**Anti-scFv**	**Anti-MMAE**	
First study				
None (scFv only)	0	2.70 ± 0.37	N/A	N/A
Glucuronide-Branched-PEG_8-MMAE-PEG_2	6.35	18.24 ± 0.58	19.34 ± 0.45	x 6.96

Glucuronide-Branched-PEG_8-MMAE-PEG4	6.50	25.04 ± 1.47	24.16 ± 0.53	x 9.11
Glucuronide-Branched-PEG_{12}-MMAE-PEG_2	6.30	26.72 ± 0.94	37.07 ± 1.33	x 11.81
Glucuronide-Branched-PEG_{12}-MMAE-PEG_4	6.50	50.36 ± 2.97	42.07 ± 3.29	x 17.12
Glucuronide-Branched-(Bis)PEG_8-MMAE-PEG_2	6.50	38.22 ± 1.54	39.49 ± 1.28	x 14.39
Second study				
Glucuronide-Branched-PEG_8-MMAE-PEG_2	6.1	44.79 ± 8.49	42.88 ± 4.32	x 16.23
Glucuronide-Branched-PEG_{12}-MMAE-PEG_4	6.4	52.57 ± 2.29	65.30 ± 4.39	x 21.82

Example 65: Toxicological measurements in rats of cMET FDCs after single dose

The clinical chemistry toxicological parameters for a range of FDCs (DAR 6.4 ± 0.1) was measured after a single IV dose of 1mg/kg in Sprague-Dawley rats, compared to carrier/saline buffer treated controls. The peak value for liver markers aspartate transaminase (AST) and alanine transaminase (ALT) was previously determined to occur at 48-72h, post-IV injection therefore this was selected as the sampling timepoint. The data is shown in Table 13. Rapid elimination of high-DAR FDCs are expected to trigger a transient spike in AST and ALT liver markers, which was observed. ALT levels were elevated 42-64% and AST levels increased 175-233% compared to untreated control animals. Immunohistochemical staining of liver and kidneys one week post-IV dosing showed no significant pathological damage compared to untreated control animals.

Table 13: Summary of single dose toxicology for 129D5BTY FDCs

Sample	**DAR (Ave)**	**ALT (U/L)**	**AST (U/L)**
First study			
Saline carrier	N/A	60 ± 2.52	81 ± 2.64
scFv only	0	58.5 ± 2.72	78.75 ± 3.9
Glucuronide-Branched-PEG_8-MMAE-PEG_2	6.35	98.25 ± 5.25	243 ± 7.27

Glucuronide-Branched-PEG_8-MMAE-PEG4	6.50	85.5 ± 2.87	222.5 ± 9.77
Glucuronide-Branched-PEG_{12}-MMAE-PEG_2	6.30	96.50 ± 6.91	238.5 ± 14.59
Glucuronide-Branched-PEG_{12}-MMAE-PEG_4	6.50	92.0 ± 10.62	252.5 ± 10.24
Glucuronide-Branched-(Bis)PEG_8-MMAE-PEG_2	6.50	86.25 ± 8.38	269.5 ± 18.52

Example 66: Toxicological measurements in rats of cMET FDCs after multiple doses

The clinical chemistry and haematological toxicological parameters for two FDCs (DAR 6.1-6.36) was measured after three IV doses of 1mg/kg in Sprague-Dawley rats in 3-week cycles, compared to carrier/saline buffer treated controls. AST, ALT, bilirubin, urea, creatine, white blood cells, red blood cells and platelets were measure 48h after each dose. Also compared was experimental ADC telisotuzumab vedotin (DAR 3.1) at 4mg/kg which contains the same MMAE payload type as the FDCs at a similar conjugate molar ratio. The data is shown in Tables 14-17 and plotted in Figures 42-43.

Table 14: Summary of multiple dose clinical chemistry toxicology for 129D5BTY FDCs

	Ave. ALT (U/L)	**SEM ALT**	**Ave. AST (U/L)**	**SEM AST**
Glucuronide-Branched-PEG_8-MMAE-PEG_2 (DAR 6.1)				
48h after 1st dose (t=48h)	94.75	7.26	260.5	9.84
48h after 2nd dose (t=216h)	76.25	7.65	162.25	9.29
48h after 3rd dose (t=384h)	72.5	3.06	263.75	10.52
Glucuronide-Branched-PEG_{12}-MMAE-PEG_4 (DAR 6.4)				
48h after 1st dose (t=48h)	93.75	9.93	244	6.36
48h after 2nd dose (t=216h)	82.5	11.29	214.25	3.75
48h after 3rd dose (t=384h)	60.75	5.29	246.5	9.74
Telisotuzumab vedotin (DAR 3.1)				
48h after 1st dose (t=48h)	52.67	2.96	84.33	6.89
48h after 2nd dose (t=216h)	49	1.53	85.67	3.28

48h after 3rd dose (t=384h)	50.67	4.67	88.33	13.37
Saline				
48h after 1st dose (t=48h)	80	4.12	79.75	4.8
48h after 2nd dose (t=216h)	61.75	3.2	80	2.61
48h after 3rd dose (t=384h)	55.25	4.39	110.5	20.43

Table 15: Summary of multiple dose clinical chemistry toxicology for 129D5BTY FDCs

	Ave. Urea (mmol/L)	**SEM Urea**	**Ave. Bilirubin (µmol/L)**	**SEM Billirubin**	**Ave. Creatinine (µmol/L)**	**SEM Creatinine**
Glucuronide-Branched-PEG$_8$-MMAE-PEG$_2$						
48h after 1st dose (t=48h)	4.45	0.28	2.55	0.32	18.925	0.63
48h after 2nd dose (t=216h)	3.975	0.37	2.375	0.22	22.8	1.03
48h after 3rd dose (t=384h)	3.95	0.15	2.525	0.46	24.375	0.70
Glucuronide-Branched-PEG$_{12}$-MMAE-PEG$_4$						
48h after 1st dose (t=48h)	4.125	0.11	2.85	0.32	18.85	0.366
48h after 2nd dose (t=216h)	3.875	0.08	2.55	0.31	23.12	0.81
48h after 3rd dose (t=384h)	4.475	0.19	2.525	0.24	25.075	1.15
Telisotuzumab vedotin (DAR 3.1)						
48h after 1st dose (t=48h)	4.37	0.29	3.47	0.23	21.87	0.49
48h after 2nd dose (t=216h)	4.47	0.33	2.80	0.12	22.40	0.42
48h after 3rd dose (t=384h)	4.37	0.09	2.80	0.06	23.63	1.13
Saline						
48h after 1st dose (t=48h)	4.65	0.19	2.675	0.24	15.92	0.60

48h after 2nd dose (t=216h)	3.375	0.13	3.125	0.28	20.725	0.30
48h after 3rd dose (t=384h)	3.925	0.13	5.05	1.5	21.35	1.19

Table 16: Summary of multiple dose haematology toxicology for 129D5BTY FDCs

	Ave. Platelets	**SEM PLT**	**Ave. Lg Platelets**	**SEM Lg PLT**
Glucuronide-Branched-PEG$_8$-MMAE-PEG$_2$ (DAR 6.1)				
48h after 1st dose (t=48h)	871.50	18.91	13.75	1.89
48h after 2nd dose (t=216h)	876.00	123.42	19.00	4.62
48h after 3rd dose (t=384h)	868.25	22.23	11.00	0.91
Glucuronide-Branched-PEG$_{12}$-MMAE-PEG$_4$ (DAR 6.4)				
48h after 1st dose (t=48h)	819.75	42.15	13.75	0.63
48h after 2nd dose (t=216h)	882.33	93.82	23.00	6.66
48h after 3rd dose (t=384h)	845.25	88.35	13.00	1.08
Telisotuzumab vedotin (DAR 3.1)				
48h after 1st dose (t=48h)	566.00	272.84	9.00	2.00
48h after 2nd dose (t=216h)	913.67	23.95	10.00	1.53
48h after 3rd dose (t=384h)	481.00	23.86	20.33	2.33
Saline				
48h after 1st dose (t=48h)	657.25	143.28	9.00	0.82
48h after 2nd dose (t=216h)	796.00	101.46	14.50	1.19
48h after 3rd dose (t=384h)	503.00	485.00	6.00	1.00

Table 17: Summary of multiple dose haematology toxicology for 129D5BTY FDCs

	Ave. WBCP	**SEM WBCP**	**Ave. WBCB**	**SEM WBCB**	**Ave. RBC**	**SEM RBC**
Glucuronide-Branched-PEG$_8$-MMAE-PEG$_2$						

48h after 1st dose (t=48h)	10.22	0.90	11.06	0.93	7.09	0.10
48h after 2nd dose (t=216h)	12.76	0.98	13.95	1.22	7.74	0.14
48h after 3rd dose (t=384h)	11.57	1.34	12.29	1.41	7.81	0.20
Glucuronide-Branched-PEG$_{12}$-MMAE-PEG$_4$						
48h after 1st dose (t=48h)	10.76	0.32	11.57	0.36	7.31	0.11
48h after 2nd dose (t=216h)	11.53	0.15	12.54	0.03	7.58	0.09
48h after 3rd dose (t=384h)	10.32	0.79	11.05	0.79	7.69	0.12
Telisotuzumab vedotin (DAR 3.1)						
48h after 1st dose (t=48h)	11.50	4.65	12.34	5.18	7.18	0.93
48h after 2nd dose (t=216h)	14.87	2.61	16.56	3.23	7.96	0.27
48h after 3rd dose (t=384h)	14.28	2.23	15.38	2.90	7.82	0.23
Saline						
48h after 1st dose (t=48h)	11.66	0.83	12.63	0.97	7.38	0.11
48h after 2nd dose (t=216h)	15.60	1.90	16.69	2.14	7.84	0.10
48h after 3rd dose (t=384h)	7.15	6.74	7.84	7.30	5.02	3.01

The more rapid elimination of the high DAR FDCs led to an increase in AST levels after each dose, but this was a transient rise and approximately 2-3x higher than untreated controls. This rise was as expected considering the 2x higher DAR, 5x lower molecular weight and 4x lower conjugate mass injected. ALT increases were more moderate with no significant increase after the 3rd dose compared to untreated controls or the ADC. No

significant changes were observed with other metabolic markers. Considering the haematological measurements, there was no significant increase in red or white blood cells or platelet count. At the end of the study 7 days after the 3rd dose, formalin fixed liver and kidney tissues were collected, transferred to 70% isopropanol and paraffin-embedded in order to section into slides for immunohistochemical staining. Consecutive sections 4μm thick were stained with haematoxylin and eosin and digitally scanned at x20 objective using the Hamamatsu Nanozoomer (Histologix Ltd, UK). The images were assessed by a Board certified veterinary pathologist (PathCelerate, UK). There were no pathological findings in FDC vs saline treated animals. Representative images from 12 sections are shown in Figure 44.

Example 67: *In vivo* tumour regression and cure efficacy in human tumour xenograft models

cMET FDCs were evaluated in human tumour xenograft models. Hs746T gastric and NCI-N87 gastric tumour cells were implanted into BALB/c nude mice, SNU5 gastric tumour cells were implanted into CB17 SCID mice and NUGC4 gastric tumour cells were implanted into NOD-SCID mice. Approximately 1-10x10^6 cells were implanted in 1:1 mixture of media/matrigel and implanted subcutaneously into the animal flank. When the tumours had reached the required size (150mm^3 to 500mm^3), dosing commenced by intravenous injection into the tail vein. Tumours were measured by calipers and tumour volume calculated as Length x $width^2$ and body weights recorded every 2-3 days. Independent Contract Research Organizations (Crown Bio, UK/China and Pharmidex UK) carried out the studies adhering to local veterinary/ethical guidelines. Test agents are described in Table 18.

Table 18: *In vivo* efficacy test agents

Test agent	**Antibody**	**Linker-payload (synthesis reference)**	**DAR (average)**
5D5-ADC	5D5 IgG	MMAE-βGA-BrPEG$_8$-PEG$_2$ **(10)**	4
Telisotuzumab vedotin (TV), ABBV-399 ADC	ABT-700 IgG	Valine-Citrulline-MMAE **(61)**	3.1
129D5B-FDC2	129D5B scFv	MMAE-βGA-BrPEG$_8$-PEG$_2$ **(10)**	6
129D5BTY-FDC1	129D5DTY scFv	MMAE-βGA-BrPEG$_{12}$-PEG$_4$ **(15)**	6
129D5BTY-FDC2	129D5DTY scFv	MMAE-βGA-BrPEG$_8$-PEG$_2$ **(10)**	6
131D5B-FDC2	131D5S scFv	MMAE-βGA-BrPEG$_8$-PEG$_2$ **(10)**	6

NB FDC	COV scFv	MMAE-βGA-BrPEG$_8$-PEG$_2$ **(10)**	6

The tumour growth inhibition/cure data is summarised in Table 19 and illustrated in Figures 45 to 55 with *p*-values for comparing groups.

Table 19: *In vivo* tumour regression and cure studies

Study Ref	**Tumour model**	**Mice/ group**	**No of Doses**	**Dosing Frequency from day-1**	**Test agents and dose**	**Tumour Growth Inhibition (TGI)* % at (day) compared to carrier**	**Body weight change % at end of dosing**
S-1	SNU5	4	4	Once/week	Carrier buffer	N/A	3.33
					5D5-ADC 4mg/kg	+4.1 (62)	1.85
					129D5B-FDC2 0.6mg/kg	100 (62)	7.53
					129D5B-FDC2 1mg/kg	100 (62)	8.69
					129D5B-FDC2 2mg/kg	100 (62)	11.57
S-2	SNU5	4	4	Once/week	Carrier buffer	N/A	3.33
					5D5-ADC 4mg/kg	54.3 (48)	1.85
					131D5S-FDC2 0.6mg/kg	-108 (48)	6.66
					131D5S -FDC2 1mg/kg	100 (48)	5.80
					131D5S -FDC2 2mg/kg	100 (48)	10.0
H-1	Hs746T	6	4	Once/week	Carrier buffer	N/A	8.01
					5D5-ADC 4mg/kg	15.5 (40)	0.03
					129D5B-FDC2 0.6mg/kg	100 (40)	2.52
					129D5B-FDC2 1mg/kg	100 (40)	4.83
					129D5B-FDC2 2mg/kg	100 (40)	2.35
H-2	Hs746T	6	4	Once/week	Carrier buffer	N/A	8.01
					5D5-ADC 4mg/kg	15.5 (40)	0.03
					131D5S-FDC2 0.6mg/kg	-57.3 (40)	1.98

					131D5S -FDC2 1mg/kg	100 (40)	1.96
					131D5S -FDC2 2mg/kg	100 (40)	6.92
N-1	NCI-N87	4	6	Once/week	Carrier buffer	N/A	0.08
					TV/ABBV399-ADC 4mg/kg	42.0 (42)	-0.63
					129D5B-FDC2 0.6mg/kg	44.6 (42)	2.01
					129D5B-FDC2 1mg/kg	65.1 (42)	5.51
					129D5B-FDC2 2mg/kg	87.1 (42)	-1.35
					129D5B scFv 2mg/kg	12.3 (42)	3.85
H-3	Hs746T	6	4	Once/week	Carrier buffer	N/A	2.35
					5D5-ADC 4mg/kg	54.2 (35)	1.65
					129D5B-FDC2 2mg/kg	100 (35)	2.78
					129D5B(2)-FDC2 2mg/kg	100 (35)	3.43
					131D5S-FDC2 2mg/kg	100 (35)	2.94
S-3	SNU5	8	6	Once/week	Carrier buffer	N/A	0.19
					TV/ABBV399-ADC 4mg/kg	100 (53)	6.32
					129D5BTY-FDC2 0.5mg/kg	100 (53)	5.73
					129D5BTY-FDC2 1mg/kg	100 (53)	8.36
					129D5BTY-FDC2 1.5mg/kg	100 (53)	9.22
					129D5BTY-FDC1 1mg/kg	100 (53)	7.71
					129D5BTY scFv 1.5mg/kg	0.05 (53)	5.5
H-4	Hs746T	8	4	Once/week	Carrier buffer	N/A (17)	20.29
					TV/ABBV399-ADC 4mg/kg	100 (34)	5.96
					129D5BTY-FDC2 0.5mg/kg	XX (34)	7.47
					129D5BTY-FDC2 1mg/kg	100 (34)	6.69

					129D5BTY-FDC2 1.5mg/kg	100 (34)	6.37
					129D5BTY-FDC1 1mg/kg	100 (34)	7.43
					129D5BTY scFv 1.5mg/kg	>-1000 (17)	40.36
NG-1	NUGC-4	8	4	Once/week	Carrier buffer	N/A (17)	4.69
					129D5BTY-FDC1 0.25mg/kg	-624 (31)	0.3
					129D5BTY-FDC1 0.5mg/kg	100 (52)	5.91
					129D5BTY-FDC1 1mg/kg	100 (38)	6.46
					129D5BTY-FDC1 1.5mg/kg	100 (38)	4.33
					129D5BTY-FDC2 0.5mg/kg	-9 (38)	6.32
					129D5BTY-FDC2 1mg/kg	100 (35)	9.13
					COV-FDC 1mg/kg	>-1000 (35)	0.06
N-2	NCI-N87	8	4	Once/week	Carrier buffer	N/A (17)	9.37
					TV/ABBV399-ADC 4mg/kg	-97 (31)	9.30
					129D5BTY-FDC1 0.5mg/kg	-447 (31)	11.96
					129D5BTY-FDC1 1mg/kg	-76 (31)	8.07
					129D5BTY-FDC1 2.5mg/kg	100 (31)	9.14
					129D5BTY-FDC2 0.5mg/kg	-556 (31)	9.66
					129D5BTY-FDC2 1mg/kg	-315 (31)	8.09

** TGI: 100% TGI is a complete cure from the tumour size at start of treatment, -100% represents a doubling of tumour size*

The data shows that the 129D5B(TY) and 131D5S-based cMET FDCs are efficacious in a range of tumour xenograft models with the 129D5BTY FDC being the most potent and 129D5BTY FDC with a MMAE-βGA-BrPEG$_{12}$-PEG$_4$ linker payload being consistently more active in models compared to MMAE-βGA-BrPEG$_8$-PEG$_2$. In many cases FDCs were equally

or significantly more potent, causing similar or greater tumour inhibition when compared on a similar payload or similar conjugate molar concentration. In many cases, the FDCs were equally or better tolerated (by body weight measurements) than similar ADCs with equal or more MMAE payload content. FDCs were also highly active in tumour models as low as 33,000 (NUGC4) and 8,000 receptors (NCIN87) per cell, unlike telisotuzumab vedotin (ABBV-399) [57].

Example 68: Plasma stability of cMET FDCs

cMET FDC 129D5BTY- MMAE-βGA-BrPEG$_{12}$-PEG$_4$ (DAR6) (140pmol, 1μl) was incubated in duplicate in plasma (K2-EDTA treated from individual snap frozen aliquots thawed on ice) at 37°C in a thermomixer. Plasma from four species was used: Cynomologus monkey, mouse, human and Sprague-Dawley rat. Plasma was centrifuged at 17000g for 10 minutes to remove precipitate prior to use. After incubation for the desired time, pre-equilibrated MagStrep "type3" XT beads (IBA; catalogue number 2-4090-002- 1μl of packed beads in 50μl of PBS containing 1mM EDTA) were added to the plasma-conjugate samples. The T-zero samples were prepared by adding conjugate to a mixture of plasma and beads and then immediately incubated at 6°C with mixing. The samples with beads were incubated on a thermomixer set to 6°C and 1200rpm for 45 minutes. After incubation the beads were recovered on a magnetic rack and were subjected to three rounds of washing with 200ul of PBSE. The washed beads were then eluted with 50μl of 50mM biotin in PBSE for 20 minutes on a thermomixer at 6°C with mixing speed 1200 rpm. Eluates were recovered using the magnetic stand and were filtered using spin filters (0.22μm) for 2 minutes at 10,000 rpm. Filtered samples were subjected to LCMS as described above. Eluates (10-15 μl) were separated on C4 column (Phenomenex Biozen 2.1mmx 10cm, 1.7μm bead size) connected to an Agilent 6345 XT QTOF. The column was eluted with a gradient of 0.1% aqueous formic acid, 10% IPA and acetonitrile containing 0.1% formic acid. Duplicate technical replicates were run in duplicate on the system. The resulting mass spectra were deconvoluted using Agilent Masshunter software. The deconvoluted spectra were manually integrated and mean DAR calculated from the four runs (duplicate runs of two technical replicates) for each species timepoint. Figure 56a shows the plot of average DAR over 1 week in all 4 species and Figure 56b shows a representative example of the LC-MS DAR analyses for the human plasma stability study. In all four species, the cMET FDC has a similar and stable DAR profile demonstrating that the FDC is stable to degradation and linker-payload release.

Example 69: Uptake of MMAE payload delivered by cMET FDC

Subcutaneous SNU5 tumours were grown to ~500mm^3 and single doses of 1mg/kg cMET FDC (129D5B-MMAE-βGA-BrPEG$_8$-PEG$_2$, DAR 6) or 4mg/kg cMET ADC (telisotuzumab

vedotin, DAR 3.1) was administered IV. Tumours and normal tissues were collected at various time points and snap frozen in liquid nitrogen. Approximately 100mg of tumour/tissue was weighed and extracted in 20% methanol with homegenizer beads and homogenized. The extract was centrifuged and the supernatant was lyophilised and redissolved in 10% methanol, 0.1% formic acid for LC-MS analyses. MMAE calibrations and an internal standard of MMAF were used. Analyses was carried out in a Waters TQ-X triple quadrupole (column Waters HSS T3 and mobile phase 0.1% Formic acid in a water/methanol gradient) following and quantifying the MMAE mass of 718.5 Da. The data is shown in Table 20 and plotted in Figure 57.

Table 20: MMAE payload uptake in SNU5 tissues

	cMET FDC, MMAE uptake pg/mg tissue			**cMET ADC, MMAE uptake pg/mg tissue**		
	2h	24h	72h	2h	24h	72h
Tumour	9.9 ± 1.0	72.74 ± 2.8	43.81 ±0.8	3.84 ±0.5	33.76 ±2.3	65.61 ±3.9
Lung	0.0036	0.0045	0.0035	0.0047	0.0038	0.004
Heart	0.002	0.001	0.0009	0.0008	0.0008	0.0006
Liver	0.05	0.0056	0.0009	0.0014	0.0017	0.0019
Kidney	0.225	0.082	0.0009	0.006	0.0068	0.0035

The FDC and ADC were administered at equimolar concentrations but despite the more rapid plasma clearance, surprisingly more MMAE payload was delivered to the tumour when conjugated as an FDC compared to an ADC during the first 24-48h and surprisingly low normal tissue uptake over 72h.

Example 70: FcR binding of cMET FDCs

The BIACore T200 was used for surface plasmon resonance to measure molecular interactions in real-time. CM5 series S sensor chip (Cytiva BR100530) was used to immobilise ligand (human CD16a/FCGR3A protein (176 val – Sino Biological 10389-H08H1), Human CD32a/FCGR2A protein (167 His – Sino Biological 10374-H08C1) and Human CD64/FCGR1A protein (Sino Biological 10256-H0H8) proteins) on the surface through covalent coupling. 1000 RU were immobilized.

To measure kinetic parameters, varying concentrations of the cMET scFvs, antibodies, Fragment Drug Conjugate (FDC) and control antibodies ('analytes') were flowed over the immobilised CD16a, CD32a and CD64 sensor chips. Real-time measurements are made of the association phase, as analyte is flowed, and of the dissociation phase, as buffer is flowed. The k_{on} (association), k_{off} (dissociation), and equilibrium binding constants

(affinity, K_a = 1/Kd) were determined using the BIAevaluation software. The chip surface was regenerated using 3M MgCl. The data (representative data shown in Figure 58) shows that the scFvs and corresponding FDC do not cross-react to Fc-Gamma receptors where IgG-based antibodies and conjugates have observable binding summarised in Table 21.

Table 21. Summary of Fc-Gamma binding affinities

Ligand	Analyte-Clone	scFv binding affinity and kinetics		
		k_a (1/Ms)	k_d (s^{-1})	K_D (nM)
CD64 (Fc-gamm-RI)	129D5BTY scFv	NB	NB	NB
	129D5BTY FDC	NB	NB	NB
	TCT (HER2) scFv	NB	NB	NB
	Trastuzumab IgG	1.8×10^5	1.8×10^{-3}	9.7
	ABT-700 IgG	1.6×10^5	1.6×10^{-3}	10.1
	IgG4	4.7×10^4	6.2×10^{-4}	13.2
	Anti-CD64 IgG	3.8×10^5	1.4×10^{-5}	0.036
	5D5 IgG	9.1×10^4	1.1×10^{-3}	12.6
CD32a (Fc-gamma-RII)	129D5BTY scFv	NB	NB	NB
	129D5BTY FDC	NB	NB	NB
	TCT (HER2) scFv	NB	NB	NB
	Trastuzumab IgG	2.7×10^6	1.4×10^0	547
	ABT-700 IgG	3.9×10^5	8.4×10^{-3}	21.7
	IgG4	7.2×10^4	2.0×10^{-3}	27.6
	Anti-CD64 IgG	1.1×10^5	7.0×10^{-5}	0.06
	5D5 IgG	9.1×10^4	7.5×10^{-3}	83.1
CD16a (Fc-gamma-RIII)	129D5BTY scFv	NB	NB	NB
	129D5BTY FDC	NB	NB	NB
	TCT (HER2) scFv	NB	NB	NB
	Trastuzumab IgG	2.8×10^5	1.3×10^{-2}	445
	ABT-700 IgG	5.8×10^2	2.3×10^{-3}	3953
	IgG4	2.8×10^4	8.6×10^{-4}	31.1
	Anti-CD64 IgG	2.9×10^6	6.7×10^{-3}	2.3
	5D5 IgG	3.6×10^4	2.3×10^{-3}	63.2

Example 71: Toxicological evaluation in non human primates

A non-GLP pilot study to understand the toxicological profile of cMET FDC 129D5BTY-MMAE-βGA-BrPEG_{12}-PEG_4 (DAR6) in cynomolgus non-human primates (*Macaca*

fascicularis, females, 2.5-3 years old, 2.5-3kg weight) was undertaken. Studies were carried out at CRO Aptuit (Italy). Standard animal housing, lighting and diet (altromin 6024 supplemented with fruit and vegetables) was used. Escalating doses (intravenous bolus) of FDC were administered into 3 animals and a range of metabolic, clinical chemistry and haematological parameters were measured at pre-dose, 2 days post-dose, 7 days post-dose and one day before the 2nd and subsequent doses. Each dose cycle was for 3 weeks. Dose-1 was 0.25mg/kg, dose-2 was 0.375mg/kg, dose-3 was 0.5mg/kg and dose-4 was 1mg/kg. Based on an ADC of DAR3, the equivalent MMAE dose on an ADC is 2.5mg/kg, 3.75mg/kg, 5mg/kg and 10mg/kg. The FDC was prepared as in Example 42 with additional checks to ensure an endotoxin level of <1 EU/mg. Haematological measurements are show in Figure 59, clinical chemistry measurements associated with liver metabolism is shown in Figure 60a and body weights shown in Figure 60b. During the study there were no adverse clinical observations, the body weights were normal and the animals did not show signs of toxicity. Lymphocytes were generally in the normal (pre-dose) range except there was a small reduction in neutrophils after the 1st dose which did not worsen with subsequent doses (mild neutropenia) and fully recovered by the 4th dose. There was no significant increase in aspartate or alanine amino-transaminases (normally associated with liver toxicity). Overall, the cMET FDC was well tolerated indicating that higher doses were possible. A dose of 1mg/kg FDC has the same amount of MMAE payload as telisotuzumab vedotin at 10mg/kg (5-times larger, 2x lower DAR) and 10mg/kg exceeds the range where toxicity is seen in non-human primate models [97]. Therefore this cMET FDC was surprisingly well tolerated.

Example 72: Synthesis of Exatecan-βGA-BrPEG$_{12}$-PEG$_4$ NHS Ester (133)

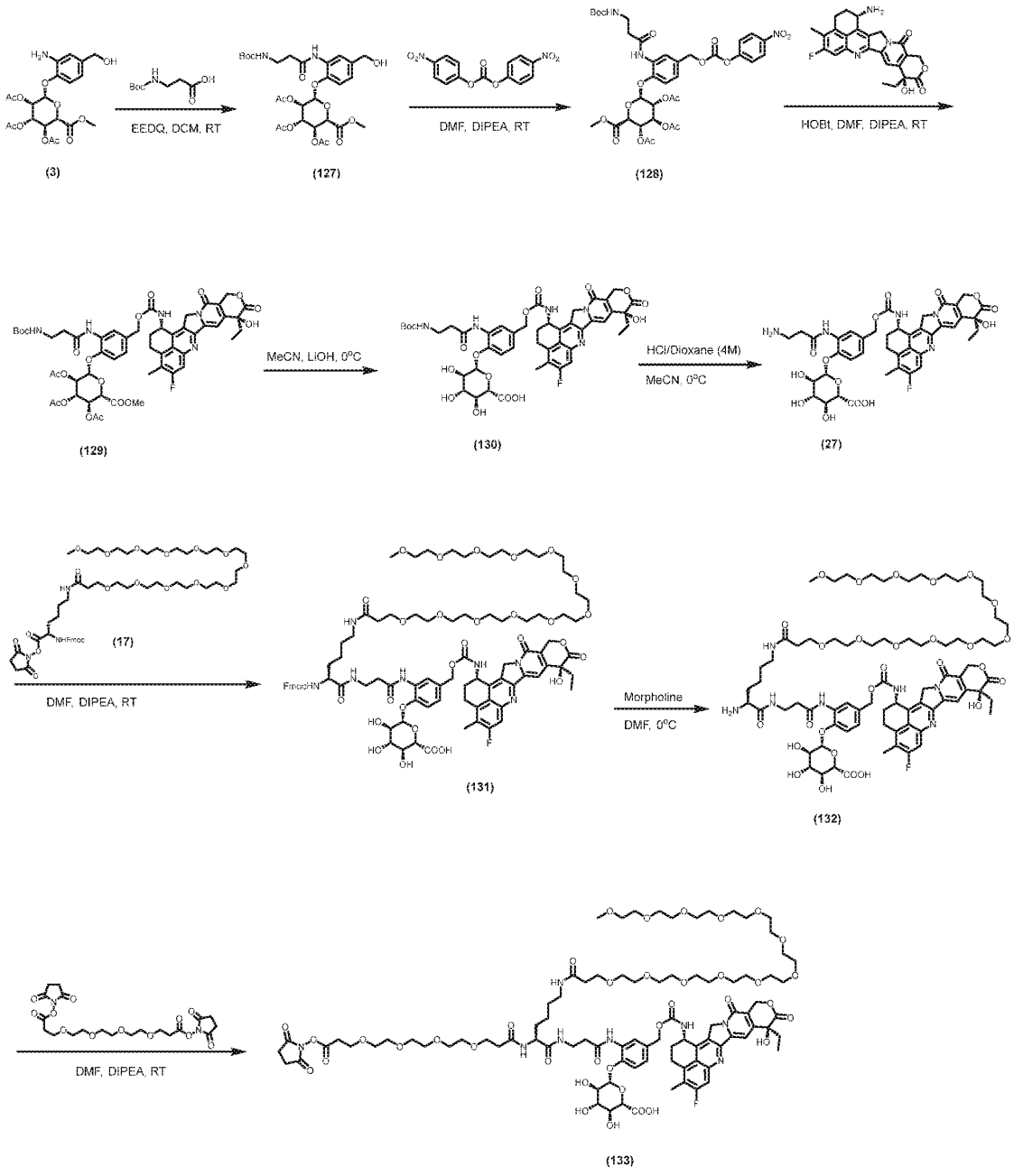

To a solution of (2S,3R,4S,5S,6S)-2-(2-amino-4-(hydroxymethyl)phenoxy)-6-(methoxycarbonyl)tetrahydro-2H-pyran-3,4,5-triyl triacetate **3** (500 mg, 1.10 mmol) in dry DCM (5 mL) was added 3-((tert-butoxycarbonyl)amino)propanoic acid (249.28 mg, 1.32 mmol) and EEDQ(543.01 mg, 2.20 mmol). The mixture was stirred at room

temperature overnight, diluted with DCM (100 mL) and washed with water (50 mL × 3). The organic phase was dried over Na_2SO4, filtered, concentrated and the resulting residue purified by silica gel chromatography (PE:EtOAc 2:1) to afford (2S,3R,4S,5S,6S)-2-(2-(3-((tert-butoxycarbonyl)amino)propanamido)-4-(hydroxymethyl)phenoxy)-6-(methoxycarbonyl)tetrahydro-2H-pyran-3,4,5-triyl triacetate **127** as a yellow solid (383 mg, 55.6%). LCMS m/z =627.10$[M+H]^+$. ^{1}H NMR (400 MHz, DMSO-d6) δ 8.67 (s, 1H), 7.82 (s, 1H), 7.02 (d, J = 2.8 Hz, 2H), 6.80 (s, 1H), 5.61 – 5.39 (m, 2H), 5.27 – 4.97 (m, 3H), 4.71 (d, J = 9.6 Hz, 1H), 4.40 (d, J = 5.6 Hz, 2H), 3.64 (d, J = 4.8 Hz, 3H), 3.22 (t, J = 6.4 Hz, 2H), 2.09 – 1.90 (m, 9H), 1.38 (d, J = 5.0 Hz, 9H).

To a solution of (2S,3R,4S,5S,6S)-2-(2-(3-((tert-butoxycarbonyl)amino)propanamido)-4-(hydroxymethyl)phenoxy)-6-(methoxycarbonyl)tetrahydro-2H-pyran-3,4,5-triyl triacetate **127** (200 mg, 0.32 mmol) in DMF (5 mL) was added bis(4-nitrophenyl) carbonate (194.20 mg, 0.62 mmol) and DIPEA(123.76 mg, 0.96 mmol). The resulting mixture was stirred at room temperature for 16 hours, diluted with water (100 mL), and extracted with EtOAc (50 mL × 3). The combined organic phases were dried over Na_2SO4, filtered and concentrated. The residue was purified by silica gel chromatography (PE:EtOAc=2:1) to afford (2S,3R,4S,5S,6S)-2-(2-(3-((tert-butoxycarbonyl)amino)-propanamido)-4-((((4-nitrophenoxy)carbonyl)oxy)methyl)phenoxy)-6-(methoxycarbonyl)tetrahydro-2H-pyran-3,4,5-triyl triacetate **128** (140 mg, 55.3%) as a yellow solid. LCMS m/z =814.40$[M+Na]^+$. ^{1}H NMR (400 MHz, DMSO-d6) δ 8.78 (s, 1H), 8.36 – 8.25 (m, 2H), 7.99 (s, 1H), 7.62 – 7.50 (m, 2H), 7.23 (d, J = 8.6 Hz, 1H), 7.12 (d, J = 8.6 Hz, 1H), 6.81 (s, 1H), 5.75 (s, 2H), 5.63 (d, J = 7.8 Hz, 1H), 5.50 (t, J = 9.6 Hz, 1H), 5.22 (d, J = 8.4 Hz, 2H), 5.07 (t, J = 9.8 Hz, 1H), 4.74 (d, J = 10.0 Hz, 1H), 3.64 (s, 3H), 3.22 (d, J = 6.6 Hz, 2H), 3.17 (d, J = 5.2 Hz, 2H), 2.07 – 1.97 (m, 9H), 1.38 (s, 9H).

To a solution of (2S,3R,4S,5S,6S)-2-(2-(3-((tert-butoxycarbonyl)amino)propanamido)-4-((((4-nitrophenoxy)carbonyl)oxy)methyl)phenoxy)-6-(methoxycarbonyl)tetrahydro-2H-pyran-3,4,5-triyl triacetate **128** (300 mg, 379 μmol), HOBt (4.0 mg, 31.6 μmol) and Exatecan mesylate (167 mg, 316 μmol) in DMF (5 mL) was added DIPEA (122 mg, 948 μmol). The reaction mixture was stirred at room temperature overnight under N_2 after which the reaction mixture was diluted with water (50 mL) and extracted with EtOAc (40 mL x 2). The combined organic phases were dried with Na_2SO_4, concentrated *in vacuo*. The crude was purified by silica gel chromatography (DCM: MeOH=30:1) to afford (2S,3R,4S,5S,6S)-2-(2-(3-((tert-butoxycarbonyl)amino)propanamido)-4-(((((1S,9S)-9-ethyl-5-fluoro-9-hydroxy-4-methyl-10,13-dioxo-2,3,9,10,13,15-hexahydro-1H,12H-benzo[de]pyrano[3',4':6,7]indolizino[1,2-b]quinolin-1-yl)carbamoyl)oxy)methyl)phenoxy)-6-(methoxycarbonyl)tetrahydro-2H-pyran-3,4,5-triyl triacetate **129** (260 mg, 63.1%) as a yellow solid. LCMS *m/z* = 1088.15 $[M+H]^+$. ^{1}H NMR

(400 MHz, DMSO) δ 8.73 (s, 1H), 8.06 (d, J = 8.8 Hz, 1H), 7.88 (s, 1H), 7.77 (d, J = 10.8 Hz, 1H), 7.31 (s, 1H), 7.18 (d, J = 8.4 Hz, 1H), 7.10 (d, J = 8.6 Hz, 1H), 6.78 (s, 1H), 6.51 (s, 1H), 5.59 (d, J = 7.8 Hz, 1H), 5.53 – 5.41 (m, 3H), 5.27 (s, 3H), 5.17 (dd, J = 9.8, 7.8 Hz, 1H), 5.11 – 5.02 (m, 3H), 4.72 (d, J = 9.8 Hz, 1H), 3.62 (s, 3H), 3.41 – 3.36 (m, 2H), 3.17 (q, J = 6.8 Hz, 4H), 2.46 (d, J = 6.8 Hz, 2H), 2.40 – 2.35 (m, 3H), 2.18 (s, 2H), 2.08 – 1.97 (m, 9H), 1.88 (m, 2H), 1.36 (s, 9H), 0.88 (t, J = 7.4 Hz, 3H).

To a solution of (2S,3R,4S,5S,6S)-2-(2-(3-((tert-butoxycarbonyl)amino)propanamido)-4-(((((1S,9S)-9-ethyl-5-fluoro-9-hydroxy-4-methyl-10,13-dioxo-2,3,9,10,13,15-hexahydro-1H,12H-benzo[de]pyrano[3',4':6,7]indolizino[1,2-b]quinolin-1-yl)carbamoyl)oxy)methyl)phenoxy)-6-(methoxycarbonyl)tetrahydro-2H-pyran-3,4,5-triyl triacetate **129** (100 mg, 91.6 μmol) in MeCN (2 mL) at 0 °C was added a solution of LiOH (8 mg, 0.335 mmol) in water (2 mL). The reaction mixture was stirred at 0 °C for 1 h after which the reaction mixture was quenched with AcOH (10.5 mg) and concentrated *in vacuo* to afford (2S,3S,4S,5R,6S)-6-(2-(3-aminopropanamido)-4-((5S,8S,11S,12R)-11-((S)-sec-butyl)-12-(2-((S)-2-((1R,2R)-3-(((1S,2R)-1-hydroxy-1-phenylpropan-2-yl)amino)-1-methoxy-2-methyl-3-oxopropyl)pyrrolidin-1-yl)-2-oxoethyl)-5,8-diisopropyl-4,10-dimethyl-3,6,9-trioxo-2,13-dioxa-4,7,10-triazatetradecyl)phenoxy)-3,4,5-trihydroxytetrahydro-2H-pyran-2-carboxylic acid **130** (100 mg, crude) as a yellow solid, which was used into next step directly. LCMS *m/z* = 948.10 $[M+H]^+$. ^{1}H NMR (400 MHz, DMSO) δ 9.12 (s, 1H), 8.20 – 8.01 (m, 2H), 7.77 (d, J = 10.8 Hz, 1H), 7.31 (s, 1H), 7.11 (t, J = 7.2 Hz, 2H), 6.77 (t, J = 5.8 Hz, 1H), 6.50 (s, 1H), 5.82 – 5.73 (m, 1H), 5.44 (s, 2H), 5.27 (d, J = 13.8 Hz, 4H), 5.06 (s, 2H), 4.77 (d, J = 6.8 Hz, 1H), 3.72 (d, J = 9.0 Hz, 1H), 3.21 – 3.09 (m, 4H), 2.38 (s, 3H), 2.18 (m, 2H), 1.87 (m, 2H), 1.36 (s, 9H), 0.88 (t, J = 7.2 Hz, 3H).

To a solution of (2S,3S,4S,5R,6S)-6-(2-(3-((tert-butoxycarbonyl)amino)propanamido)-4-(((((1S,9S)-9-ethyl-5-fluoro-9-hydroxy-4-methyl-10,13-dioxo-2,3,9,10,13,15-hexahydro-1H,12H-benzo[de]pyrano[3',4':6,7]indolizino[1,2-b]quinolin-1-yl)carbamoyl)oxy)methyl)phenoxy)-3,4,5-trihydroxytetrahydro-2H-pyran-2-carboxylic acid **130** (100 mg, 105 μmol) in MeCN (2 mL) at 0°C was added HCl/dioxane (4M, 2 mL). The reaction mixture was stirred at 0°C for 1 h then concentrated. The crude residue was purified by prep-HPLC to afford (2S,3S,4S,5R,6S)-6-(2-(3-aminopropanamido)-4-(((((1S,9S)-9-ethyl-5-fluoro-9-hydroxy-4-methyl-10,13-dioxo-2,3,9,10,13,15-hexahydro-1H,12H-benzo[de]pyrano[3',4':6,7]indolizino[1,2-b]quinolin-1-yl)carbamoyl)oxy)methyl)phenoxy)-3,4,5-trihydroxytetrahydro-2H-pyran-2-carboxylic acid **27** (10 mg, 12.8% two steps) as a white solid. LCMS *m/z* = 848.10 $[M+H]^+$.

^{1}H NMR (400 MHz, DMSO) δ 9.61 (brs, 1H), 8.16 – 8.02 (m, 2H), 7.74 (d, J = 10.8 Hz, 1H), 7.30 (s, 1H), 7.22 – 7.12 (m, 2H), 6.60 – 6.47 (m, 1H), 5.43 (s, 2H), 5.30 – 5.18

(m, 3H), 5.13 – 4.99 (m, 2H), 4.59 (d, J = 6.8 Hz, 1H), 3.15 – 2.97 (m, 6H), 2.91 – 2.81 (m, 1H), 2.74 – 2.63 (m, 1H), 2.36 (s, 3H), 2.24 – 2.14 (m, 2H), 1.93 – 1.81 (m, 2H), 0.88 (t, J = 7.4 Hz, 3H).

To a solution of (2S,3S,4S,5R,6S)-6-(2-(3-aminopropanamido)-4-(((((1S,9S)-9-ethyl-5-fluoro-9-hydroxy-4-methyl-10,13-dioxo-2,3,9,10,13,15-hexahydro-1H,12H-benzo[de]pyrano[3',4':6,7]indolizino[1,2-b]quinolin-1-yl)carbamoyl)oxy)methyl) phenoxy)-3,4,5-trihydroxytetrahydro-2H-pyran-2-carboxylic acid (300.0 mg, 353 µmol) in DMF (5 mL) was added 2,5-dioxopyrrolidin-1-yl (S)-44-((((9H-fluoren-9-yl)methoxy)carbonyl)amino)-38-oxo-2,5,8,11,14,17,20,23,26,29,32,35-dodecaoxa-39-azapentatetracontan-45-oate **17** (439 mg, 425 µmol) and DIPEA (136 mg, 1.06 mmol). The mixture was stirred at RT overnight then directly purified RP-column chromatography (40% MeCN in water) and prep-HPLC [SHIMADZU LC 20Column: Agilent 10 Prep-C18, 250*21.2mm, 10 um Mobile Phase A: 0.1% HCOOH in water (v/v)Mobile Phase B: MeCN] to afford (2S,3S,4S,5R,6S)-6-(2-((S)-44-((((9H-fluoren-9-yl)methoxy)carbonyl)amino)-38,45-dioxo-2,5,8,11,14,17,20,23,26,29,32,35-dodecaoxa-39,46-diazanonatetracontan-49-amido)-4-(((((1S,9S)-9-ethyl-5-fluoro-9-hydroxy-4-methyl-10,13-dioxo-2,3,9,10,13,15-hexahydro-1H,12H-benzo[de]pyrano [3',4':6,7]indolizino[1,2-b]quinolin-1-yl)carbamoyl)oxy)methyl)phenoxy)-3,4,5-trihydroxytetrahydro-2H-pyran-2-carboxylic acid **131** (90 mg, 14.4%) as a yellow oil. LCMS m/z = 893.70 $[M+H_3O+H]^+/2$. ^1H NMR (400 MHz, DMSO) δ 9.42 (d, J = 10.4 Hz, 1H), 8.49 (s, 6H), 8.29 – 8.05 (m, 3H), 7.86 (m, 5H), 7.81 – 7.66 (m, 3H), 7.45 – 7.24 (m, 7H), 7.19 – 7.05 (m, 2H), 6.60 (d, J = 42.0 Hz, 1H), 6.28 (s, 1H), 5.44 (d, J = 3.6 Hz, 2H), 5.32 – 5.22 (m, 4H), 5.03 (m, 2H), 4.58 (d, J = 6.8 Hz, 1H), 4.24 – 4.15 (m, 2H), 3.89 (m, 1H), 3.56 (m, 8H), 3.45 – 3.06 (m, 41H), 2.95 – 2.89 (m, 2H), 2.37 (d, J = 5.6 Hz, 4H), 2.27 (m, 2H), 2.21 – 2.15 (m, 2H), 1.86 (m, 2H), 1.59 – 1.44 (m, 2H), 1.27 (m, 6H), 0.86 (d, J = 7.2 Hz, 3H).

To a solution of (2S,3S,4S,5R,6S)-6-(2-((S)-44-((((9H-fluoren-9-yl)methoxy)carbonyl) amino)-38,45-dioxo-2,5,8,11,14,17,20,23,26,29,32,35-dodecaoxa-39,46-diazanonatetracontan-49-amido)-4-(((((1S,9S)-9-ethyl-5-fluoro-9-hydroxy-4-methyl-10,13-dioxo-2,3,9,10,13,15-hexahydro-1H,12H-benzo[de]pyrano[3',4':6,7] indolizino[1,2-b]quinolin-1-yl)carbamoyl)oxy)methyl)phenoxy)-3,4,5-trihydroxytetrahydro-2H-pyran-2-carboxylic acid **131** (70 mg, 39.5 µmol) in dry DMF (3 mL) at 0°C was added drop-wise a solution of morpholine (30 mg) in dry DMF (0.5 mL). The mixture was allowed to warm to room temperature and stirred overnight after which it was purified by Biotage automated chromatography (40% MeCN in water) to afford (2S,3S,4S,5R,6S)-6-(2-((S)-44-amino-38,45-dioxo-2,5,8,11,14,17,20,23,26,29,32,35-dodecaoxa-39,46-diazanonatetracontan-49-amido)-4-(((((1S,9S)-9-ethyl-5-fluoro-9-hydroxy-4-methyl-10,13-dioxo-2,3,9,10,13,15-hexahydro-1H,12H-benzo[de]pyrano

[3',4':6,7]indolizino[1,2-b]quinolin-1-yl)carbamoyl)oxy)methyl)phenoxy)-3,4,5-trihydroxytetrahydro-2H-pyran-2-carboxylic acid **132** (40 mg, 64.5%) as a white solid. LCMS m/z = 774.05 $[M+2H]^+/2$. ^{1}H NMR (400 MHz, MeOD) δ 8.16 (brs, 1H), 7.63 (s, 1H), 7.26 – 7.19 (m, 1H), 7.17 – 7.08 (m, 1H), 5.59 (d, J = 16.4 Hz, 1H), 5.39 – 5.25 (m, 4H), 5.19 – 5.09 (m, 3H), 4.41 – 4.16 (m, 3H), 3.77 – 3.49 (m, 56H), 3.35 (s, 3H), 3.26 – 3.00 (m, 3H), 2.75 – 2.49 (m, 2H), 2.45 – 2.27 (m, 7H), 2.02 – 1.91 (m, 2H), 1.80 – 1.55 (m, 2H), 1.40 – 1.22 (m, 6H), 1.01 (t, J = 7.4 Hz, 3H).

A solution of bis(2,5-dioxopyrrolidin-1-yl) 4,7,10,13-tetraoxahexadecanedioate (149 mg, 226 μmol) and DIPEA (17 mg, 135 μmol) in DMF (1 mL) at 10°C was added a solution of (2S,3S,4S,5R,6S)-6-(2-((S)-44-amino-38,45-dioxo-2,5,8,11,14,17,20,23,26,29,32,35-dodecaoxa-39,46-diazanonatetracontan-49-amido)-4-(((((1S,9S)-9-ethyl-5-fluoro-9-hydroxy-4-methyl-10,13-dioxo-2,3,9,10,13,15-hexahydro-1H,12H-benzo[de]pyrano[3',4':6,7]indolizino[1,2-b]quinolin-1-yl)carbamoyl)oxy)methyl) phenoxy)-3,4,5-trihydroxytetrahydro-2H-pyran-2-carboxylic acid **132** (70 mg, 45.2 μmol) in DMF (1 mL) drop-wise. The mixture was stirred at 10°C for 1.0 h and purified directly by prep-HPLC [Instrument: SHIMADZU LC 20Column: Agilent 10 Prep-C18, 250*21.2mm, 10 um Mobile Phase A: 0.1% HCOOH in water (v/v) Mobile Phase B: MeCN]. The appropriate fractions were combined and extracted with DCM (100 mL x 3). The combined organic phase were dried over Na_2SO4 and concentrated to afford (2S,3S,4S,5R,6S)-6-(2-((S)-44-(16-((2,5-dioxopyrrolidin-1-yl)oxy)-16-oxo-4,7,10,13-tetraoxahexadecanamido)-38,45-dioxo-2,5,8,11,14,17,20,23,26,29,32,35-dodecaoxa-39,46-diazanonatetracontan-49-amido)-4-(((((1S,9S)-9-ethyl-5-fluoro-9-hydroxy-4-methyl-10,13-dioxo-2,3,9,10,13,15-hexahydro-1H,12H-benzo[de]pyrano[3',4':6,7] indolizino[1,2-b]quinolin-1-yl)carbamoyl)oxy)methyl)phenoxy)-3,4,5-trihydroxytetrahydro-2H-pyran-2-carboxylic acid **133** (22 mg, 25.3%) as a white solid. LCMS m/z = 1919.65 $[M+H]^+$. ^{1}H NMR (400 MHz, DMSO) δ 12.82 (s, 1H), 9.08 (s, 1H), 8.25 – 8.16 (m, 1H), 8.05 (d, J = 8.4 Hz, 1H), 7.93 (d, J = 7.2 Hz, 2H), 7.82 – 7.70 (m, 2H), 7.31 (s, 1H), 7.10 (s, 2H), 6.50 (s, 1H), 5.85 (d, J = 3.8 Hz, 1H), 5.49 – 5.35 (m, 3H), 5.34 – 5.24 (m, 4H), 5.11 – 5.01 (m, 2H), 4.91 – 4.82 (m, 1H), 4.22 – 4.13 (m, 1H), 3.88 (d, J = 9.6 Hz, 1H), 3.71 (t, J = 6.0 Hz, 2H), 3.59 – 3.44 (m, 62H), 3.44 – 3.41 (m, 3H), 3.39 – 3.35 (m, 2H), 3.23 (s, 4H), 3.17 – 3.07 (m, 1H), 3.00 – 2.88 (m, 4H), 2.80 (s, 3H), 2.42 – 2.33 (m, 5H), 2.27 (t, J = 6.6 Hz, 2H), 2.23 – 2.15 (m, 2H), 1.93 – 1.81 (m, 2H), 1.64 – 1.40 (m, 2H), 1.37 – 1.27 (m, 2H), 1.27 – 1.18 (m, 2H), 0.88 (t, J = 7.2 Hz, 3H).

Example 73: Synthesis of 2-(Methylsulphonyl)ethylamino-MMAF-βGA-PEG$_2$ NHS Ester (138)

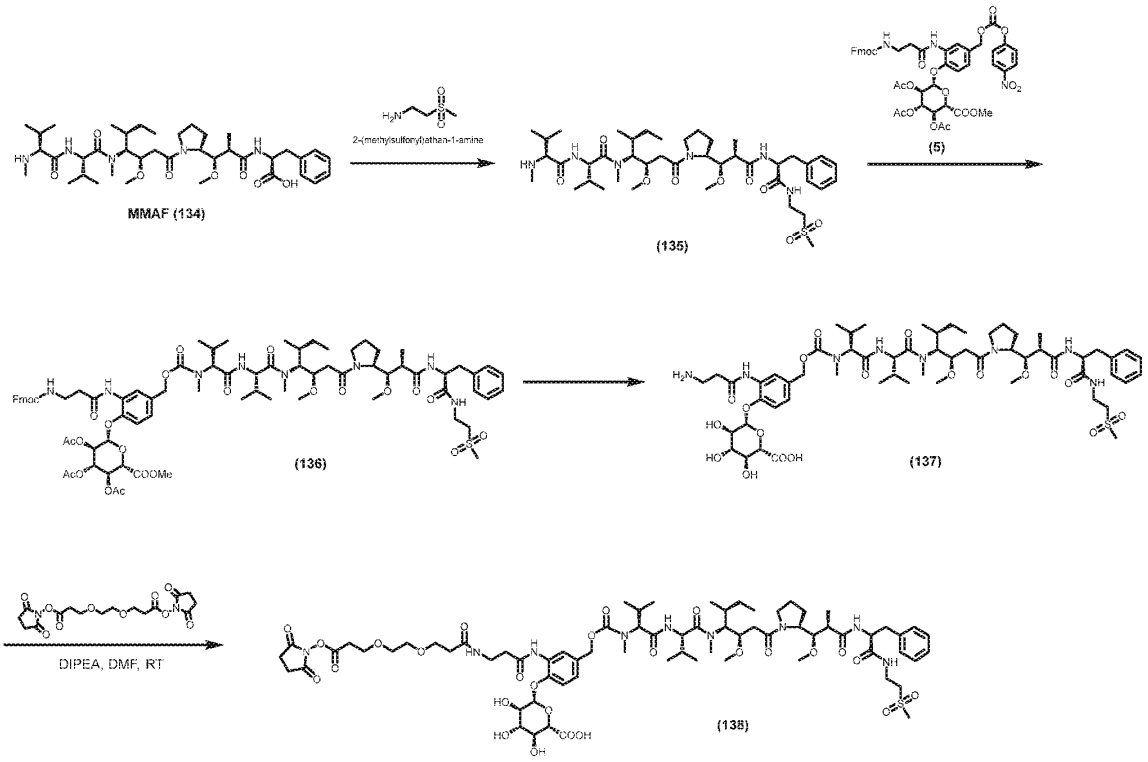

MMAF **134** MMAF (100 mg, 0.137 mmol), HATU (103.6 mg, 0.273 mmol), 2-methanesulfonylethan-1-amine (18.5 mg, 0.159 mmol) and triethylamine (45.7 µL, 0.328 mmol) were dissolved in dry DMF (10 mL) and stirred at RT under inert atmosphere for 18 hours. The reaction mixture was concentrated *in vacuo* and the remaining crude purified on RP chromatography [Biotage (water + 0.1% TFA/ACN + 0.1% TFA, 0-100%)]. The combined fractions were lyophilised to to give the MMAF-methylsulphonyl derivative **135** as an off-white solid (65 mg, 57% yield). RT = 2.534 min. LCMS m/z = 837.70 (M+1); 838.70 (M+2), 859.60 (M + Na); 731.69 (loss of methanesulfonylethane).

PNP-carbonate ester **5** (30.1 mg, 0.033 mmol), HOBt (4.1 mg, 0.030 mmol) and MMAF sulfonamide **135** (23 mg mg, 0.027 mmol) were dissolved in a mixture of dry DMF (2 mL), pyridine (400 µL) and DIPEA (14.4 µL, 0.824 mmol. The reaction mixture was stirred at rt under N_2 for 3 h and then concentrated *in vacuo*. The was crude was purified on RP chromatography [Biotage (water + 0.1% TFA/ACN + 0.1% TFA, 0-100%)]. The combined fractions were freeze dried to give the MMAF-sugar derivative **136** as an off-white solid (18 mg, 41% yield). RT = 4.259 min. LCMS m/z 1612.59 (M+1); 1634.63 (M+Na); 837.88 (MMAF sulfonamide fragment)

A solution pf the MMAF-(acetate-protected) sugar **136** (18 mg, 0.0112 mmol) dissolved in a 1:1 mixture of THF/MeOH (1 mL) was cooled with an ice/water bath. To this, a solution of $LiOH.H_2O$ (2.81 mg, 0.067 mmol) dissolved in water (1 mL) was added dropwise over 1 h. After the end of the addition, the mixture was allowed to stir while reaching RT for 5h. After LCMS showed incomplete deprotection, a second portion of $LiOH.H_2O$ (2.81 mg, 0.067 mmol) dissolved in water (1 mL) was added to the reaction mixture and stirred for a further 3 h at RT, which led to complete deprotection. The reaction was quenched by the addition of Glacial acetic acid (3.8 µL, 0.067 mmol) and the reaction mixture was concentrated *in vacuo*. The residue was purified by RP automated chromatography [Biotage (water + 0.1% TFA/ACN + 0.1% TFA, 0-100%)] to give the globally deprotected MMAF-glucuronic acid **137** derivative as a white solid 9 mg (64 %). RT = 2.247 min. LCMS m/z = 1250.24 (M+1); 1272.21 (M + Na); 837.86 (MMAF-sulfonamide fragment); 625.66 (MMAF fragment).

To a stirred solution of bis-PEG_2-NHS (29.0 mg, 0.0721 mmol) and DIPEA (3.8 µl, 21.63 µmol) in dry DMF (1 mL), a solution of the MMAF-βGA **137** (9.0 mg, 7.21 µmol) dissolved in dry DMF (1 mL) was added dropwise using a syringe pump over 1 h. After addition was complete, the solvent was removed by high vacuum and the crude purified by RP automated chromatography [Biotage, (water + 0.1% TFA/MeCN + 0.1% TFA, 10-90%)] to give the desired NHS-ester derivative **138** 7.0 mg (64%) as a white solid after lyophilisation. RT 2.387 min. LCMS m/z = 1535.50 (M+1); 1536.50 (M+2); 1557.50 (M+Na); 837.89 (MMAF-sulfonamide fragment); 625.70 (MMAF fragment).

Example 74: Toxicological evaluation in non-human primates at higher doses

The non-GLP pilot study to understand the toxicological profile of cMET FDC 129D5BTY-MMAE-βGA-BrPEG_{12}-PEG_4 (DAR6) in cynomolgus non-human primates (see Example 71) was continued with 2 further doses. Each additional dose cycle was for 3 weeks. Dose-4 was 1mg/kg, dose-5 was 2mg/kg. Based on an ADC of DAR3, the equivalent MMAE dose on an ADC is 10mg/kg and 20mg/kg respectively. The FDC was prepared as in Example 42 with additional checks to ensure an endotoxin level of <1 EU/mg. As the same animals were used, the cumulative dose at the end of the study was 4.125mg/kg over 12 weeks.

Haematological measurements are shown in Figure 64, clinical chemistry measurements associated with liver metabolism is shown in Figure 65 and kidney metabolism in Figure 66 and final body weights shown in Figure 67. All tissues were examined by a qualified pathologist (DVM, Dip.RCPath, FRCPath) and any histological observations are described below. All reference (normal) values were derived from Park et al [235].

The following tissues were examined macroscopically: Adrenals, Aorta (thoracic), Brain, Caecum, Colon, Duodenum, Eyes, Femur (femoral head), Gall bladder, Heart, Ileum, Injection sites, Jejunum, Kidneys, Larynx, Liver, Lung (all lobes), Lymph node mandibular, Lymph node mesenteric, Lymph node inguinal, Mammary gland (thoracic), Oesophagus (distal portion), Optic nerves, Ovaries, Pancreas, Parathyroids, Pituitary, Rectum, Salivary glands (mandibular, parotid), Sciatic nerve, Skeletal muscle (hindlimb), Skin, Spinal cord (cervical region, thoracis region, lumbar region), Spleen, Sternum with bone marrow, Stomach, Thymus, Thyroids, Tongue, Tonsils, Trachea, Trachea bifurcation (with main-stem bronchi), Urinary bladder, Uterus and Vagina with no test item related abnormalities detected in any animal.

The following tissues were examined microscopically: Brain, Caecum, Colon, Duodenum, Eyes, Gall bladder, Heart, Ileum, Injection sites, Jejunum, Kidneys, Liver, Lung (all lobes), Lymph node mesenteric, Ovaries, Pancreas, Sciatic nerve, Skeletal muscle (hindlimb), Spleen, Sternum with bone marrow, Stomach and Urinary bladder. No test item abnormalities were observed in the majority of animals other (a) minimal inflammatory cell infiltrate in the bladder mucosa of one animal and (d) minimal to mild observations (oedema, inflammation, basophilia) related to a mild obstructive nephropathy (outflow obstruction) in the renal medulla and collecting tubules in the cortex.

By the 5th and final dose (2mg/kg, cumulative dose of 4.125mg/kg), the cMET FDC was well tolerated by a number of different measures. Haematologically, white blood cells, neutrophils and lymphocytes (Figure 64a-d) remained in the normal range indicating the absence of neutropenia. Platelet counts were also normal indicating the absence of thrombocytopenia (Figure 64e). From clinical chemistry analyses after the final dose, liver enzymes (Figure 65a-d), notably alanine and aspartate aminotransferase (ALT and AST) were in the normal range, indicating no significant liver damage. This correlated with normal levels of bilirubin (Figure 65e). This was surprising given the high quantity of MMAE administered (at least 4x higher than generally tolerated [97]) with the liver being a major organ for MMAE metabolism. Clinical chemistry markers for kidney function were also in the normal range (Figure 66). However, there was evidence of protein in the urine after the highest dose, indicative of abnormal kidney function. This was reversible/recoverable.

During the entire study, there were no adverse clinical observations other than a moderate but reversible loss in body weight after the 5th dose (Figure 67). This was related to the fluid loss caused by the abnormal kidney function and corelates to the mild microscopic findings seen in the kidney histopathology.

The final dose of 2mg/kg was tolerated and the data can be used to make the following conclusions:

- The maximum tolerated dose (MTD) in cynomolgus was not reached and represents at least 4x higher MMAE payload delivery than comparable ADCs [97].
- This is equivalent to 8mg/kg (mouse) [236] and together with a minimum efficacious dose of ~0.25mg/kg (Example 67), this equates to a therapeutic index of at least 32.
- cMET FDC clearance involves the kidneys.
- The human equivalent dose would be in the region of 0.67mg/kg [236].

Example 75: Pharmacokinetic analyses in non-human primates

Plasma samples were collected over 72h for each dosing cycle and the pharmacokinetic clearance was detected by anti-MMAE and anti-StrepTag detection, as described for the rodent studies (Example 66). The clearance profiles are plotted in Figure 68a-c and the kinetic parameters are listed in Table 22. At each escalating dose, the plasma exposure (bioavailability) as determined by the area-under-curve (AUC) calculation increased and this increase was linear from the 3rd dose onwards. This indicates that there was no cMET-target mediated tissue deposition/clearance (TMDD) at the higher doses. The bioavailability as detected by anti-MMAE/payload (intact conjugate) and anti-Strep tag (scFv only) was similar indicating that there was no significant payload deconjugation in the plasma. There was some evidence of clipping of the Strep tag at the lower doses, but the pharmacokinetic profile was very similar when detecting either component as exemplified in Figure 68c. The half-life of the intact conjugate was 7-9h at the higher doses. A plot of AUC vs FDC dose (Figure 68d) illustrates the linearity of the pharmacokinetics at the higher dose and the TMDD at the lower doses.

Urine samples were collected and cMET FDC binding was analysed to see if any intact conjugate was present (Figure 69). Although not quantitative due to the nature of the collections, significant quantities (~1000g) of functional, binding FDC were detected at around 4-48 hours but not 10 days suggesting the FDC clears, at least in part, as an intact molecule via the kidney excretion route.

These data can be used to make the following conclusions:

- The bioavailability and half-life of the cMET FDC is surprisingly long given the small format size (~40kDa) and kidney clearance. Blinatumomab is a scFv-based protein (~55kDa) with a faster half-life of 1-2.5h in non-human primates [238].

- The cMET FDC binds to cynomolgus cMET with a very similar high affinity (3.48nM vs 9.72nM, Figure 70) and one would have expected a small format with rapid clearance pharmacokinetics to be subject to significant TMDD and poor bioavailability in non-human primates. Unexpectedly, this was not observed.
- The half-life of the cMET FDC would translate to ~12h in humans [237] and is surprisingly close to that of IgG-based ADCs such as telisotuzumab vedotin (NHP half-life ~18-24h, human half-life 36-48h) [57,58].

Table 22. Pharmacokinetic analyses of cMET FDC in non-human primates

	Bioavailability (AUC) (mghr/mL) anti-MMAE	Bioavailability (AUC) (mghr/mL) anti-Strep	Elimination Half-Life (h) anti-MMAE
Dose-1, 0.25 mg/kg	10.62	8.28	4.29
Dose-2, 0.375 mg/kg	35.99	19.64	7.06
Dose-3, 0.50 mg/kg	47.16	36.68	7.22
Dose-4, 1.00 mg/kg	76.80	74.56	7.01
Dose-5, 2.00 mg/kg	125.45	138.9	9.09

Example 76: Binding of 129D5BTY scFv and 129D5BTY-MMAE-βGA-brPEG12-PEG4 FDC

Binding of the 129D5BTY scFv was compared to the ABT-700 IgG (antibody component of tesilotuzumab vedotin) by BIACore SPR as described in Example 2. Two injections (400nM) of the 129D5BTY scFv were used to saturate the sensor chip surface. A further injection of ABT-700 (400nM) for 5 minutes showed an increased sensorgram response indicating that ABT-700 was able to access cMET epitopes that were non-overlapping and different to that bound by 129D5BTY scFv (Figure 71a). A similar study was carried out to compare binding with the 5D5 IgG (a precursor to Roche's MetMab) where 400nM of 129D5BTY scFv was compared to 400nM of 5D5 IgG. The sensorgrams indicated non-overlapping epitopes (Figure 71b).

BIACore SPR binding analyses was also used to determine the binding affinities and kinetic constants for the 129D5BTY-MMAE-βGA-brPEG12-PEG4 FDC on human and cynomolgus cMET. The binding association rate, dissociation rate and affinity were similar across the two species indication excellent species cross-reactivity (Figure 70, Table 23).

Table 23. Binding kinetic constants for 129D5BTY-MMAE-βGA-brPEG12-PEG4 FDC			
	k_{on} ($M^{-1}s^{-1}$)	k_{off} (s^{-1})	K_d (M^{-1})
Human cMET	4.48×10^{4}	1.56×10^{-4}	3.47×10^{-9}
Cynomolgus cMET	2.79×10^{4}	2.71×10^{-4}	9.71×10^{-9}

Example 77: Conjugation of 129D5B scFv to Exatecan-MA-PEG$_{12}$-Val-Ala-PEG$_4$-NHS Ester (74)

129D5B scFv was conjugated to linker-payload **74** to obtain a DAR 5.03 as follows. A stock solution of pure scFv (>95%) was diluted to 50μM (1.4mg/mL) into a pre-equilibrated solution of 100mM sodium phosphate pH 8.0, 10% DMA. Linker-Payload (25mM in DMSO) was added starting with 1 molar equivalent (compared to scFv lysines) before adding more payload every 60 min and the reaction mixture incubated at 22°C, 500rpm until the desired DAR was achieved. The reaction progress was monitored by reverse-phase mass spectrometry (reaction stopped by the addition of Tris-HCl pH 7.5 (final concentration 10mM, 50% of 0.1% formic acid in water was added, the sample was filtered through 0.2mm spin filters and applied to a C4 reverse phase column (Phenomenex bioZen 2.6mm widepore 100x2.1mm) on an Agilent QTOF 6545XT run in 10% IPA/10% acetonitrile in 0.1% fomic acid/water) and. A total of 1.5 molar equivalents (over 11 lysines) was required.

The sample was purified by SEC HPLC (Sepax Zenix C 150 3μm 10 x 300mm). Sample quality was analysed by RP-LCMS, UV/Vis spectroscopy, DLS and nanoDSF before being used for further studies. The sample was pure and monomeric (>98%, Figure 72a), with a DAR distribution of 3-7 (~88% within 4-6) (Figure 72b). The NanoDSF showed a small decrease in thermal stability compared to the unconjugated parent antibody 129D5BTY but maintained a highly thermal stable folded structure with a Tm of 57.05°C and a high binding affinity (K_d) of 0.37nM (Figure 72c), Table 6.

Example 78: Conjugation of 129D5B scFv to Exatecan-βGA-BrPEG$_{12}$-PEG$_4$ NHS Ester (133)

129D5B scFv was conjugated, purified and analysed according to the method described in Example 77 to linker-payload **133** to obtain a conjugate. The sample was pure and monomeric (>98%, Figure 72d) with a DAR 7.9 (Figure 72e) with >70% DAR 6-10. A stock solution of pure scFv (>95%) was diluted to 50μM (1.4mg/mL) into a pre-equilibrated solution of 100mM sodium phosphate pH 8.0, 10% DMA. Linker-Payload (25mM in DMSO) was added starting with 1 molar equivalent (compared to scFv lysines) before adding more payload every 60 min and the reaction mixture incubated at 22°C,

500rpm until the desired DAR was achieved (2 molar equivalents required). A high binding affinity was retained (K_d) of. 4.5nM (Figure. 72f, Table 6).

Example 79: Conjugation of 129D5B scFv to DXd-GGFG-BrPEG$_8$-PEG$_2$ NHS Ester (25)

129D5B scFv was conjugated, purified and analysed according to the method described in Example 77 to linker-payload **25** to obtain a DAR 3.7 (Figure 72g). The sample was pure and monomeric (>98%, Figure 69h). A stock solution of pure scFv (>95%) was diluted to 50µM (1.4mg/mL) into a pre-equilibrated solution of 100mM sodium phosphate pH 8.0, 10% DMA. Linker-Payload (25mM in DMSO) was added starting with 1 molar equivalent (compared to scFv lysines) before adding more payload every 60 min and the reaction mixture incubated at 22°C, 500rpm until the desired DAR was achieved (1.6 molar equivalents required). A high binding affinity was retained (K_d) of. 0.34nM (Figure 72i, Table 6).

Example 80: Conjugation of 129D5B scFv 2-(Methylsulphonyl)ethylamino-MMAF-βGA-PEG$_2$ NHS Ester (138)

129D5B scFv was conjugated, purified and analysed according to the method described in Example 39 to linker-payload **138** to obtain a DAR 5.15. Specifically, a stock solution of pure scFv (>95%) was diluted to 1mg/ml into a pre-equilibrated solution of 20% DMSO in bicarbonate buffer pH9.2. Linker- Payload (25mM in DMSO) was added in 5 molar equivalents every 90-120 min and the reaction mixture incubated at 20°C, 300rpm. The reaction progress was monitored by size- exclusion chromatography mass spectrometry (SEC-MS, Agilent AdvanceBio SEC 120A 1.9mm 2.1x150mm PEEK isocratic run in 75mM Ammonium Acetate, 10% IPA on an Agilent QTOF 6545XT). A total of 30 equivalents (6 additions) were required (~2.7 equivalents over the lysines).

The crude reaction mixture was pH neutralized with 1M NaH2PO4 (1.5%) and purified on an AKTA Avant through a Superdex 75 26/600 isocratic run eluting with 10% IPA/PBS. The monomeric fractions were combined and buffer exchanged into Histidine/NaCl buffer pH7.5 (Figure 73a). The concentrated sample was filtered through a sterile 0.2µm PES filter, flash frozen in liquid nitrogen and stored at -20°C. The sample was analysed by SEC (Sepax Zenix C 150 7.8 x 300mm), SEC-LCMS (Figure 73b). The binding affinity was high at 719pM (Figure 73c; Table 6). Cell killing potency on cMET-expressing Hs746T cells was 96.3pM with no significant activity against cMET-negative T47D cells (Figure 73d, Table 10).

Example 81: FDC efficacy in cMET low gastric and pancreatic cancer patient-derived xenograft (PDX) tumour models

A selection of 16 PDX models (supplied by Crown Bioscience, China) for 5 solid tumours (gastric, pancreatic, breast, lung and head & neck) were evaluated by immunohistochemistry (IHC) for cMET protein expression and cMET gene expression. IHC was carried out using the validated SP44 anti-cMET antibody by Crown Bioscience. Two PDX models were chosen based on low gene expression and IHC score (gastric model GA6885, IHC score 103.22 and pancreatic model PA3142, IHC score 114.27, Figure 76a and Figure 77a) that were not expected to demonstrate tumour growth inhibition efficacy when treated with ABBV399 (telisotuzumab vedotin) as disclosed in EP3626273B1 (In Champions NSCLC PDX model CTG-0363, IHC score 105.52, ABBV399 treatment of 6 doses, weekly at 3mg/kg was ineffective and not significantly different to the vehicle-treated group).

The human patient derived tumours were implanted subcutaneously in BALB/c nude mice in 2-3mm^3 pieces and groups of 5 animals randomized into 4 groups of tumour sizes 150-200mm^3 and treated with ABBV399 (3mg/kg), cMET FDC 129D5BTY-MMAE-βGA-BrPEG$_{12}$-PEG$_4$ (DAR6) at 1mg/kg and 2.5mg/kg and a vehicle/saline control which were prepared as described for other animal studies (Examples 67, 69, 71).

After 2 doses (of the planned 6 doses) for all test agents at one dose/week, the higher dose of FDC demonstrated clear tumour growth inhibition in both the gastric and pancreatic cancer PDX models compared to ABBV399 with excellent tolerability as measured by body weight changes (Figure 76b and Figure 77b, Table 24). In the gastric PDX model, all test agents demonstrated tumour growth inhibition, but in the more challenging pancreatic PDX model, only the higher FDC dose demonstrated any observable tumour growth inhibition (Table 24). PDX models, notably gastric and pancreatic are known to better represent the heterogeneity and physiological properties (e.g. drug resistance and dense stroma) of human cancers compared to cell-line models. The observed superior efficacy of the cMET FDC 129D5BTY-MMAE-βGA-BrPEG$_{12}$-PEG$_4$ supports the premise of improved penetration and enhanced payload delivery whilst being well tolerated.

Table 24

	Mean tumour growth inhibition (%) at day 14 (*negative number indicates growth)	
Test agent (dose)	**Pancreatic PDX PA3142**	**Gastric PDX GA6885**
FDC (1mg/kg) x 2	-1.02*	49.93
FDC (2.5mg/kg) x 2	63.86	79.98
ABBV-399 (3mg/kg) x2	-11.61*	48.48

Amino acid sequences

SEQ ID NO	Clones	Sequence
1	129D5B/129D5BTY VH	EVQLVQSGAEVKKPGESLKISCKGSGYSF TTYWIGWVRQMPGKGLEWMGIINPADSN TRYNPGFQGQVTISADKSISTAYLQWSSL KASDTAVYYCARHSGRGRLWPWGQGTLV TVSS
196	129D5BTY VL	QPVLTQPPSVSAAPGQKVTISCSGSSSNI GSNYVSWYQQLPGTAPKLLIYSN**Y**NRPSG VPDRFSGSKSGTSASLAISGLQSEDEADY YCAAWDN**T**VAGWVFGGGTKLTVL
2	129D5B VL	QPVLTQPPSVSAAPGQKVTISCSGSSSNI GSNYVSWYQQLPGTAPKLLIYSNSNRPSG VPDRFSGSKSGTSASLAISGLQSEDEADY YCAAWDNSVAGWVFGGGTKLTVL
3	3A2, 20F6, 59D5, 54E11, 59D4, 59A10, 65C2, 53G1, 65A3, 65G6, 53G9, 58H11, 59E5, 59H2, 59A6, 59A2, 59D10, 58A9, 59H6, 52G1, 58A2, 52D5, 75G7, 71C2, 71F11 and 53D11 VH	EVQLVQSGAEVKKPGESLKISCKGSGYSF TTYWIGWVRQMPGKGLEWMGIINPADSN TRYNPSFQGQVTISADKSISTAYLQWSSL KASDTAVYYCARHGGRGRLDVWGQGTLV TVSS
4	3A2 VL	QSVLTQPPSVSAAPGQKVTISCSGSSSNI GNYYVSWYQQLPGTAPKLLIYRNSNRPSG VPDRFSGSKSGTSASLAISGLQSEDEADY YCAAWDDSLSGWVFGGGTKLTVL
5	49G5 VH	EVQLVQSGAEVKKPGESLKISCKGSGYSF TTYWIGWVRQMPGKGLEWMGIINPADSN TRYNPSFQGQVTISADKSISTAYLQWSSL KASDTAVYYCARHGGRGRLWPWGQGTLV TVSS
6	20F6, 49A6, 55G9, 55A3 and 49G5 VL	QSVLTQPPSVSAAPGQKVTISCSGSSSNI GSNYVSWYQQLPGTAPKLLIYSNSNRPSG VPDRFSGSKSGTSASLAISGLQSEDEADY YCAAWDDSLSGWVFGGGTKLTVL
7	77F3 VH	EVQLVQSGAEVKKPGESLKISCKGSGYSF TTYWIGWVRQMPGKGLEWMGIINPADSN TRYNPSFQGQVTISADKSISTAYLQWSSL KASDTAVYYCARHGGRGRLWPWGQGTLV TVSS
8	53D11, 126A8B and 77F3 VL	QSVLTQPPSVSAAPGQKVTISCSGSSSNI GSNYVSWYQQLPGTAPKLLIYSNSNRPSG

		VPDRFSGSKSGTSASLAISGLQSEDEADY YCAAWDNSVAGWVFGGGTKLTVL
9	139B2 VH	EVQLVQSGAEVAKPGESLKISCTGSGYSF TTYWIGWVRQMPGKGLEWMGIINPADSN TRYNPSFQGQVTISADKSISTAYLQWSSL KASDTAVYYCARHGGRGRLWPWGQGTLV TVSS
10	139B2 VL	QSVLTQPPSVSAAPGQKVTISCSGSSSNI GSNYVSWYQQLPGTAPKLLIYSNSNRPSG VPDRFSGSKSGTSASLAISGLQSEDEADY YCAAWDNSVAGWVFGGGTQLTVL
11	139D2 VH	EVQLVQSGAEVAKPGESLKISCAGSGYSF TTYWIGWVRQMPGKGLEWMGIINPADSN TRYNPSFQGQVTISADSSISTAYLQWSSL KASDTAVYYCARHGGRGRLWPWGQGTLV TVSS
12	139D2 and 139D7 VL	QSVLTQPPSVSAAPGQKVTISCSGSSSNI GSNYVSWYQQLPGTAPKLLIYSNSNRPSG VPDRFSGSKSGTSASLAISGLQSEDEADY YCAAWDNSVAGWVFGGGTRLTVL
13	139D7 VH	EVQLVQSGAEVLKPGESLKISCTGSGYSF TTYWIGWVRQMPGKGLEWMGIINPADSN TRYNPSFQGQVTISADSSISTAYLQWSSL KASDTAVYYCARHGGRGRLWPWGQGTLV TVSS
14	26B5 VH	EVQLVQSGAEVKKPGESLKISCKGSGYTF ATYWIGWVRQMPGKGLEWMGIINPGDS DTRYNPSFQGQVTISADKSISTAYLQWSS LKASDTAVYYCARADYDYYRGYYMDIWG QGTLVTVSS
15	26B5 VL	QSVLTQPPSVSAAPGQKVTISCSGSSSNI GSYVVYWYQQLPGTAPKLLIYDNTNRPSG VPDRFSGSKSGTSASLAISGLQSEDEADY YCATWDDSLNGPVFGGGTKLTVL
16	83B11D VH	EVQLVQSGAEVKKPGESLKISCKGSGYTF DTYWIGWVRQMPGKGLEWMGIINPGDS DTRYNPSFQGQVTISADKSISTAYLQWSS LKASDTAVYYCARADYDYYRGYYMDIWG QGTLVTVSS
17	83B11D, 94C3, 94E6, 112F2, 112G4 and 94C2 VL	QSVLTQPPSVSAAPGQKVTISCSGSSSNI GSYVVYWYQQLPGTAPKLLIYDNNQRPSG VPDRFSGSKSGTSASLAISGLQSEDEADY YCASWDDSLNGPVFGGGTKLTVL
18	94C2 VH	EVQLVQSGAEVKKPGESLKISCKGSGYTF DTYWIGWVRQMPGKGLEWMGIINPGDS DTRYNPSFQGQVTISADKSISTAYLQWSS LKASDTAVYYCARVDDFYYRGYYMDIWG QGTLVTVSS
19	115D1D VH	EVQLVQSGAEVKKPGESLKISCKGSGYAF DTYWIGWVRQMPGKGLEWMGIINPGDS DTRYNPSFQGQVTISADKSISTAYLQWSS LKASDTAVYYCARVDDYYYRGYYMDIWG QGTLVTVSS
20	115D1D, 121H3B and 116A5 VL	QSVLTQPPSVSAAPGQKVTISCSGSSSNI GPYVVYWYQQLPGTAPKLLIYDNNQRPSG

		VPDRFSGSKSGTSASLAISGLQSEDEADY YCATWDDSLNGPVFGGGTKLTVL
21	131D5S VH	EVQLVQSGAEVKKPGESLKISCKGSGYAF DTYWVGWVRQMPGKGLEWMGIINPGDS DTRYNPSFQGQVTISADKSISTAYLQWSS LKASDTAVYYCARVDDYYYRGYYMDIWG QGTLVTVSS
22	131D5S VL	QSVLTQPPSVSAAPGQKVTISCSGSSSNI GPYVVYWYQQLPGSAPKLLIYDNNQRPTG VPDRFSGSKSGTSASLAISGLQSEDEADY YCATWDDSLNGPVFGGGTKLTVL

SEQ ID NO	Clones	Sequence
71	49A6 VH	EVQLVQSGAEVKKPGESLKISCKGSGYSF TTYWIGWVRQMPGKGLEWMGIINPADSN TRYNPSFQGQVTISADKSISTAYLQWSSL KASDTAVYYCARHGGRGRLAYWGQGTLV TVSS
72	55G9 VH	EVQLVQSGAEVKKPGESLKISCKGSGYSF TTYWIGWVRQMPGKGLEWMGIINPADSN TRYNPSFQGQVTISADKSISTAYLQWSSL KASDTAVYYCARHGGRGRLERWGQGTLV TVSS
73	55A3 VH	EVQLVQSGAEVKKPGESLKISCKGSGYSF TTYWIGWVRQMPGKGLEWMGIINPADSN TRYNPSFQGQVTISADKSISTAYLQWSSL KASDTAVYYCARHGGRGRLPYWGQGTLV TVSS
74	74C3 VH	EVQLVQSGAEVKKPGESLKISCKGSGYSF TTYWIGWMRQMPGKGLEWMGIINPADSN TRYNPSFQGQVTISADKSISTAYLQWSSL KASDTAVYYCARHGGRGRLDVWGQGTLV TVSS
75	64B2 VH	EVQLVQSGAEVKKPGESLKISCEGSGYSF TTYWIGWVRQMPGKGLEWMGIINPADSN TRYNPSFQGQVTISADKSISTAYLQWSSL KASDTAVYYCARHGGRGRLDVWGQGTLV TVSS
76	71D4 VH	EVQLVQSGAEVKKPGESLKISCKGSGYSF TTYWVGWVRQMPGKGLEWMGIINPADS NTRYNPSFQGQVTISADKSISTAYLQWSS LKASDTAVYYCARHGGRGRLDVWGQGTL VTVSS
77	126ABB VH	EVQLVQSGAEVKKPGESLKISCKGSGYSF TTYWIGWVRQMPGKGLEWMGIINPADSN TRYSPSFQGQVTISADKSISTAYLQWSSL KASDTAVYYCARHSGRGRLWPWGQGTLV TVSS
78	59D5 VL	QSVLTQPPSVSAAPGQKVTISCSGSSSNI GSNYVSWYQQLPGTAPKLLIYSNSNRPSG VPDRFSGSKSGTSASLAISGLQSEDEADY YCAAWDNPSGGWVFGGGTKLTVL
79	54E11 VL	QSVLTQPPSVSAAPGQKVTISCSGSSSNI GSNYVSWYQQLPGTAPKLLIYSNSNRPSG

		VPDRFSGSKSGTSASLAISGLQSEDEADY YCAAWDQISGGWVFGGGTKLTVL
80	59D4 VL	QSVLTQPPSVSAAPGQKVTISCSGSSSNI GSNYVSWYQQLPGTAPKLLIYSNSNRPSG VPDRFSGSKSGTSASLAISGLQSEDEADY YCAAWDQEFGGWVFGGGTKLTVL
81	59A10 VL	QSVLTQPPSVSAAPGQKVTISCSGSSSNI GSNYVSWYQQLPGTAPKLLIYSNSNRPSG VPDRFSGSKSGTSASLAISGLQSEDEADY YCAAWDQGYNGWVFGGGTKLTVL
82	65C2 VL	QSVLTQPPSVSAAPGQKVTISCSGSSSNI GSNYVSWYQQLPGTAPKLLIYSNSNRPSG VPDRFSGSKSGTSASLAISGLQSEDEADY YCAAWDQSTDGWVFGGGTKLTVL
83	53G1 VL	QSVLTQPPSVSAAPGQKVTISCSGSSSNI GSNYVSWYQQLPGTAPKLLIYSNSNRPSG VPDRFSGSKSGTSASLAISGLQSEDEADY YCAAWSNYAAGWVFGGGTKLTVL
84	65A3 VL	QSVLTQPPSVSAAPGQKVTISCSGSSSNI GSNYVSWYQQLPGTAPKLLIYSNSNRPSG VPDRFSGSKSGTSASLAISGLQSEDEADY YCAAWENYAAGWVFGGGTKLTVL
85	65G6 VL	QSVLTQPPSVSAAPGQKVTISCSGSSSNI GSNYVSWYQQLPGTAPKLLIYSNSNRPSG VPDRFSGSKSGTSASLAISGLQSEDEADY YCAAWENWEAGWVFGGGTKLTVL
86	53G9 VL	QSVLTQPPSVSAAPGQKVTISCSGSSSNI GSNYVSWYQQLPGTAPKLLIYSNSNRPSG VPDRFSGSKSGTSASLAISGLQSEDEADY YCAAWDLTEAGWVFGGGTKLTVL
87	58H11 VL	QSVLTQPPSVSAAPGQKVTISCSGSSSNI GSNYVSWYQQLPGTAPKLLIYSNSNRPSG VPDRFSGSKSGTSASLAISGLQSEDEADY YCAAWDTDQAGWVFGGGTKLTVL
88	59E5 VL	QSVLTQPPSVSAAPGQKVTISCSGSSSNI GSNYVSWYQQLPGTAPKLLIYSNSNRPSG VPDRFSGSKSGTSASLAISGLQSEDEADY YCAAWDSEEAGWVFGGGTKLTVL
89	59H2 VL	QSVLTQPPSVSAAPGQKVTISCSGSSSNI GSNYVSWYQQLPGTAPKLLIYSNSNRPSG VPDRFSGSKSGTSASLAISGLQSEDEADY YCAAWDSSYGGWVFGGGTKLTVL
90	59A6 VL	QSVLTQPPSVSAAPGQKVTISCSGSSSNI GSNYVSWYQQLPGTAPKLLIYSNSNRPSG VPDRFSGSKSGTSASLAISGLQSEDEADY YCAAWDSANAGWVFGGGTKLTVL
91	59A2 VL	QSVLTQPPSVSAAPGQKVTISCSGSSSNI GSNYVSWYQQLPGTAPKLLIYSNSNRPSG VPDRFSGSKSGTSASLAISGLQSEDEADY YCAAWDSSAAGWVFGGGTKLTVL
92	59D10 VL	QSVLTQPPSVSAAPGQKVTISCSGSSSNI GSNYVSWYQQLPGTAPKLLIYSNSNRPSG VPDRFSGSKSGTSASLAISGLQSEDEADY YCAAWDGNDDGWVFGGGTKLTVL
93	58A9 VL	QSVLTQPPSVSAAPGQKVTISCSGSSSNI GSNYVSWYQQLPGTAPKLLIYSNSNRPSG

		VPDRFSGSKSGTSASLAISGLQSEDEADY YCAAWDNHQASWVFGGGTKLTVL
94	74C3 VL	QSVLTQPPSVSAAPGQKVTISCSGSSSNI GSNYVSWYQQLPGTAPKLLIYSNSNRPSG VPDRFSGSKSGTSASLAISGLQSEDEADY YCAAWDNPEAGWVFGGGTKLTVL
95	59H6 VL	QSVLTQPPSVSAAPGQKVTISCSGSSSNI GSNYVSWYQQLPGTAPKLLIYSNSNRPSG VPDRFSGSKSGTSASLAISGLQSEDEADY YCAAWDQDWSGWVFGGGTKLTVL
96	64B2 VL	QSVLTQPPSVSAAPGQKVTISCSGSSSNI GSNYVSWYQQLPGTAPKLLIYSNSNRPSG VPDRFSGSKSGTSASLAISGLQSEDEADY YCAAWDQQFAGWVFGGGTKLTVL
97	52G1 VL	QSVLTQPPSVSAAPGQKVTISCSGSSSNI GSNYVSWYQQLPGTAPKLLIYSNSNRPSG VPDRFSGSKSGTSASLAISGLQSEDEADY YCAAWDSIAHNWVFGGGTKLTVL
98	58A2 VL	QSVLTQPPSVSAAPGQKVTISCSGSSSNI GSNYVSWYQQLPGTAPKLLIYSNSNRPSG VPDRFSGSKSGTSASLAISGLQSEDEADY YCAAWDSNPSHWVFGGGTKLTVL
99	52D5 VL	QSVLTQPPSVSAAPGQKVTISCSGSSSNI GSNYVSWYQQLPGTAPKLLIYSNSNRPSG VPDRFSGSKSGTSASLAISGLQSEDEADY YCAAWDIASANWVFGGGTKLTVL
100	71D4 VL	QSVLTQPPSVSAAPGQKVTISCSGSSSNI GSNYVSWYQQLPGTAPKLLIYSNSNRPSG VPDRFSGSKSGTSASLAISGLQSEDEADY YCAAWDQISAGWVFGGGTKLTVL
101	75G7 VL	QSVLTQPPSVSAAPGQKVTISCSGSSSNI GSNYVSWYQQLPGTAPKLLIYSNSNRPSG VPDRFSGSKSGTSASLAISGLQSEDEADY YCAAWDNHYAGWVFGGGTKLTVL
102	71C2 VL	QSVLTQPPSVSAAPGQKVTISCSGSSSNI GSNYVSWYQQLPGTAPKLLIYSNSNRPSG VPDRFSGSKSGTSASLAISGLQSEDEADY YCAAWDNTSAGWVFGGGTKLTVL
103	71F11 VL	QSVLTQPPSVSAAPGQKVTISCSGSSSNI GSNYVSWYQQLPGTAPKLLIYSNSNRPSG VPDRFSGSKSGTSASLAISGLQSEDEADY YCAAWDNSLAGWVFGGGTKLTVL
104	94C3 and 116A5 VH	EVQLVQSGAEVKKPGESLKISCKGSGYTF DTYWIGWVRQMPGKGLEWMGIINPGDS DTRYNPSFQGQVTISADKSISTAYLQWSS LKASDTAVYYCARTDDYYYRGYYMDIWG QGTLVTVSS
105	94E6 VH	EVQLVQSGAEVKKPGESLKISCKGSGYTF DTYWIGWVRQMPGKGLEWMGIINPGDS DTRYNPSFQGQVTISADKSISTAYLQWSS LKASDTAVYYCARTNDEYYRGYYMDIWG QGTLVTVSS
106	112F2 and 113A3 VH	EVQLVQSGAEVKKPGESLKISCKGSGYTF DTYGIGWVRQMPGKGLEWMGIINPGDSD TRYNPSFQGQVTISADKSISTAYLQWSSL

		KASDTAVYYCARVDDFYYRGYYMDIWGQ GTLVTVSS
107	112G4 and 113G8 VH	EVQLVQSGAEVKKPGESLKISCKGSGYTF DTYGIGWVRQMPGKGLEWMGTIDPGDS DTRYNPSFQGQVTISADKSISTAYLQWSS LKASDTAVYYCARTDDYYYRGYYMDIWG QGTLVTVSS
108	115C7 VH	EVQLVQSGAEVKKPGESLKISCKGSGYTF DTYQIGWVRQMPGKGLEWMGIINPGDSD TRYNPSFQGQVTISADKSISTAYLQWSSL KASDTAVYYCARVDDFYYRGYYMDIWGQ GTLVTVSS
109	121H3B VH	EVQLVQSGAEVKKPGESLKISCKGSGYTF DTYWIGWVRQMPGKGLEWMGIINPGDS DARYNPSFQGQVTISADKSISTAYLQWSS LKASDTAVYYCARADDYYYRGYYMDIWG QGTLVTVSS
110	113A3 VL	QSVLTQPPSVSAAPGQKVTISCSGSSSNI GSYVVYWYQQLPGTAPKLLIYDNNQRPSG VPDRFSGSKSGTSASLAISGLQSEDEADY YCASWDDVDSAPVFGGGTKLTVL
111	113G8 VL	QSVLTQPPSVSAAPGQKVTISCSGSSSNI GSYVVYWYQQLPGTAPKLLIYDNNQRPSG VPDRFSGSKSGTSASLAISGLQSEDEADY YCASWDDPNNAPVFGGGTKLTVL
112	115C7 VL	QSVLTQPPSVSAAPGQKVTISCSGSSSNI GSYVVYWYQQLPGTAPKLLIYDNNQRPSG VPDRFSGSKSGTSASLAISGLQSEDEADY YCATWDDPSQQPVFGGGTKLTVL

The CDR sequences described herein are defined according to the Kabat system.

CDR-H1:

Sequence	Clones	SEQ ID NO
TYWIG	3A2 20F6 49G5 53D11 77F3 129D5B 139B2 139D2 139D7 126A8B 59D5 49A6 55G9 55A3 54E11 59D4 59A10 65C2 53G1 65A3	23/24/25/26

	65G6 53G9 58H11 59E5 59H2 59A6 59A2 59D10 58A9 74C3 59H6 64B2 52G1 58A2 52D5 75G7 71C2 71F11 26B5 83B11D 94C2 115D1D 94C3 94E6 116A5 121H3B	
TYWVG	131D5s 71D4	27

Sequence	Clones	SEQ ID NO
TYGIG	112F2 112G4 113A3 113G8	113
TYQIG	115C7	114

CDR-H2:

Sequence	Clones	SEQ ID NO
IINPADSNTRYNPGFQG	129D5B	28
IINPGDSDTRYNPSFQG	26B5 83B11D 94C2 115D1D 131D5s 94C3 94E6 112F2 113A3 115C7 116A5	29

Sequence	Clones	SEQ ID NO
IINPADSNTRYNPSFQG	3A2	115

	20F6 49G5 53D11 77F3 139B2 139D2 139D7 59D5 49A6 55G9 55A3 54E11 59D4 59A10 65C2 53G1 65A3 65G6 53G9 58H11 59E5 59H2 59A6 59A2 59D10 58A9 74C3 59H6 64B2 52G1 58A2 52D5 71D4 75G7 71C2 71F11	
IINPADSNTRYSPSFQG	126A8B	116
TIDPGDSDTRYNPSFQG	112G4 113G8	117
IINPGDSDARYNPSFQG	121H3B	118

CDR-H3:

Sequence	Clones	SEQ ID NO
HGGRGRLDV	3A2 20F6 53D11 59D5 54E11 59D4 59A10 65C2 53G1 65A3 65G6 53G9	30

	58H11 59E5 59H2 59A6 59A2 59D10 58A9 74C3 59H6 64B2 52G1 58A2 52D5 71D4 75G7 71C2 71F11	
HGGRGRLWP	49G5 77F3 139B2 139D2 139D7	31
HSGRGRLWP	129D5B 126A8B	32
ADYDYYRGYYMDI	26B5 83B11D	33
VDDFYYRGYYMDI	94C2 112F2 113A3 115C7	34
VDDYYYRGYYMDI	115D1D 131D5s	35

Sequence	Clones	SEQ ID NO
HGGRGRLAY	49A6	119
HGGRGRLER	55G9	120
HGGRGRLPY	55A3	121
TDDYYYRGYYMDI	94C3 112G4 113G8 116A5	122
TNDEYYRGYYMDI	94E6	123
ADDYYYRGYYMDI	121H3B	124

CDR-L1:

Sequence	Clones	SEQ ID NO
SGSSSNIGNYYVS	3A2	36
SGSSSNIGSNYVS	20F6 49G5 53D11 77F3 129D5B 139B2 139D2	37

	139D7 126A8B 59D5 49A6 55G9 55A3 54E11 59D4 59A10 65C2 53G1 65A3 65G6 53G9 58H11 59E5 59H2 59A6 59A2 59D10 58A9 74C3 59H6 64B2 52G1 58A2 52D5 71D4 75G7 71C2 71F11	
SGSSSNIGSYVVY	26B5 83B11D 94C2 94C3 94E6 112F2 112G4 113A3 113G8 115C7	38
SGSSSNIGPYVVY	115D1D 131D5s 116A5 121H3B	39

CDR-L2:

Sequence	Clones	SEQ ID NO
RNSNRPS	3A2	40
SNSNRPS	20F6 49G5 53D11 77F3 129D5B 139B2	41

	139D2 139D7 126A8B 59D5 49A6 55G9 55A3 54E11 59D4 59A10 65C2 53G1 65A3 65G6 53G9 58H11 59E5 59H2 59A6 59A2 59D10 58A9 74C3 59H6 64B2 52G1 58A2 52D5 71D4 75G7 71C2 71F11	
DNTNRPS	26B5	42
DNNQRPS	83B11D 94C2 115D1D 94C3 94E6 112F2 112G4 113A3 113G8 115C7 116A5 121H3B	43
DNNQRPT	131D5s	44
SNYNRPS	129D5BTY	197

CDR-L3:

Sequence	Clones	SEQ ID NO
AAWDDSLSGWV	3A2 20F6 49G5 49A6 55G9	45

	55A3	
AAWDNSVAGWV	53D11 77F3 129D5B 139B2 139D2 139D7 126A8B	46
ATWDDSLNGPV	26B5 115D1D 131D5s 116A5 121H3B	47
ASWDDSLNGPV	83B11D 94C2 94C3 94E6 112F2 112G4	48

Sequence	Clones	SEQ ID NO
AAWDNPSGGWV	59D5	125
AAWDQISGGWV	54E11	126
AAWDQEFGGWV	59D4	127
AAWDQGYNGWV	59A10	128
AAWDQSTDGWV	65C2	129
AAWSNYAAGWV	53G1	130
AAWENYAAGWV	65A3	131
AAWENWEAGWV	65G6	132
AAWDLTEAGWV	53G9	133
AAWDTDQAGWV	58H11	134
AAWDSEEAGWV	59E5	135
AAWDSSYGGWV	59H2	136
AAWDSANAGWV	59A6	137
AAWDSSAAGWV	59A2	138
AAWDGNDDGWV	59D10	139
AAWDNHQASWV	58A9	140
AAWDNPEAGWV	74C3	141
AAWDQDWSGWV	59H6	142
AAWDQQFAGWV	64B2	143
AAWDSIAHNWV	52G1	144
AAWDSNPSHWV	58A2	145
AAWDIASANWV	52D5	146
AAWDQISAGWV	71D4	147
AAWDNHYAGWV	75G7	148
AAWDNTSAGWV	71C2	149
AAWDNSLAGWV	71F11	150
ASWDDVDSAPV	113A3	151
ASWDDPNNAPV	113G8	152
ATWDDPSQQPV	115C7	153
AAWDNTVAGWV	129D5BTY	198

Nucleotide sequences

>3A2 VH (same for 20F6, 59D5, 54E11, 59D4, 59A10, 65C2, 53G1, 65A3, 65G6, 53G9, 58H11, 59E5, 59H2, 59A6, 59A2, 59D10, 58A9, 59H6, 52G1, 58A2, 52D5, 75G7, 71C2, 71F11 and 53D11) (SEQ ID NO. 49)

GAGGTTCAGCTGGTTCAGAGCGGTGCCGAAGTTAAAAAACCGGGTGAAAGCCTGAAAATTTCAT
GTAAAGGTAGCGGCTATTCTTTCACTACTTATTGGATCGGTTGGGTGCGCCAGATGCCTGGTAAA
GGTCTGGAATGGATGGGCATCATCAACCCCGCTGACAGCAACACTCGTTATAACCCGAGCTTCC
AGGGTCAAGTTACCATTAGCGCGGATAAAAGCATTAGCACCGCATATCTGCAGTGGTCTAGCCT
GAAAGCGAGCGACACCGCCGTGTATTACTGTGCCCGTCATGGTGGTCGTGGTCGTCTGGACGTT
TGGGGTCAGGGCACCCTGGTCACCGTCTCGAGT

>49G5 VH (SEQ ID NO. 50)

GAGGTTCAGCTGGTTCAGAGCGGTGCCGAAGTTAAAAAACCGGGTGAAAGCCTGAAAATTTCAT
GTAAAGGTAGCGGCTATTCTTTCACTACTTATTGGATCGGTTGGGTGCGCCAGATGCCTGGTAAA
GGTCTGGAATGGATGGGCATCATCAACCCCGCTGACAGCAACACTCGTTATAACCCGAGCTTCC
AGGGTCAAGTTACCATTAGCGCGGATAAAAGCATTAGCACCGCATATCTGCAGTGGTCTAGCCT
GAAAGCGAGCGACACCGCCGTGTATTACTGTGCCCGTCATGGTGGTCGTGGGCGTTTGTGGCC
GTGGGGTCAGGGCACCCTGGTCACCGTCTCGAGT

>77F3 VH (SEQ ID NO. 51)

GAGGTTCAGCTGGTTCAGAGCGGTGCCGAAGTTAAAAAACCGGGTGAAAGCCTGAAAATTTCAT
GTAAAGGTAGCGGCTATTCTTTCACTACTTATTGGATCGGTTGGGTGCGCCAGATGCCTGGTAAA
GGTCTGGAATGGATGGGCATCATCAACCCCGCTGACAGCAACACTCGTTATAACCCGAGCTTCC
AGGGTCAAGTTACCATTAGCGCGGATAAAAGCATTAGCACCGCATATCTGCAGTGGTCTAGCCT
GAAAGCGAGCGACACCGCCGTGTATTACTGTGCCCGTCATGGCGGTCGTGGGCGTTTGTGGCC
GTGGGGTCAGGGCACCCTGGTCACCGTCTCGAGT

>129D5B VH (SEQ ID NO. 52)

GAGGTTCAGCTGGTTCAGAGCGGTGCCGAAGTTAAAAAACCGGGTGAAAGCCTGAAAATTTCAT
GTAAAGGTAGCGGCTATTCTTTCACTACTTATTGGATCGGTTGGGTGCGCCAGATGCCTGGTAAA
GGTCTGGAATGGATGGGCATCATCAACCCCGCTGACAGCAACACTCGTTATAACCCGGGCTTCC
AGGGTCAAGTTACCATTAGCGCGGATAAAAGCATTAGCACCGCATATCTGCAGTGGTCTAGCCT
GAAAGCGAGCGACACCGCCGTGTATTACTGTGCCCGTCATAGCGGTCGTGGGCGTTTGTGGCC
GTGGGGTCAGGGCACCCTGGTCACCGTCTCGAGT

>139B2 VH (SEQ ID NO. 53)

GAGGTTCAGCTGGTTCAGAGCGGTGCCGAAGTTGCGAAACCGGGTGAAAGCCTGAAAATTTCAT
GTACGGGTAGCGGCTATTCTTTCACTACTTATTGGATCGGTTGGGTGCGCCAGATGCCTGGTAAA
GGTCTGGAATGGATGGGCATCATCAACCCCGCTGACAGCAACACTCGTTATAACCCGAGCTTCC
AGGGTCAAGTTACCATTAGCGCGGATAAAAGCATTAGCACCGCATATCTGCAGTGGTCTAGCCT
GAAAGCGAGCGACACCGCCGTGTATTACTGTGCCCGTCATGGCGGTCGTGGGCGTTTGTGGCC
GTGGGGTCAGGGCACCCTGGTCACCGTCTCGAGT

>139D2 VH (SEQ ID NO. 54)

GAGGTTCAGCTGGTTCAGAGCGGTGCCGAAGTTGCGAAACCGGGTGAAAGCCTGAAAATTTCAT
GTGCGGGTAGCGGCTATTCTTTCACTACTTATTGGATCGGTTGGGTGCGCCAGATGCCTGGTAA
AGGTCTGGAATGGATGGGCATCATCAACCCCGCTGACAGCAACACTCGTTATAACCCGAGCTTC
CAGGGTCAAGTTACCATTAGCGCGGATAGTAGCATTAGCACCGCATATCTGCAGTGGTCTAGCC
TGAAAGCGAGCGACACCGCCGTGTATTACTGTGCCCGTCATGGCGGTCGTGGGCGTTTGTGGCC
GTGGGGTCAGGGCACCCTGGTCACCGTCTCGAGT

>139D7 VH (SEQ ID NO. 55)

GAGGTTCAGCTGGTTCAGAGCGGTGCCGAAGTTCTGAAACCGGGTGAAAGCCTGAAAATTTCAT
GTACGGGTAGCGGCTATTCTTTCACTACTTATTGGATCGGTTGGGTGCGCCAGATGCCTGGTAAA
GGTCTGGAATGGATGGGCATCATCAACCCCGCTGACAGCAACACTCGTTATAACCCGAGCTTCC
AGGGTCAAGTTACCATTAGCGCGGATAGTAGCATTAGCACCGCATATCTGCAGTGGTCTAGCCT
GAAAGCGAGCGACACCGCCGTGTATTACTGTGCCCGTCATGGCGGTCGTGGGCGTTTGTGGCC
GTGGGGTCAGGGCACCCTGGTCACCGTCTCGAGT

>26B5 VH (SEQ ID NO. 56)

GAGGTTCAGCTGGTTCAGAGCGGTGCCGAAGTTAAAAAACCGGGTGAAAGCCTGAAAATTTCAT
GTAAAGGTAGCGGCTATACTTTCGCTACTTATTGGATCGGTTGGGTGCGCCAGATGCCTGGTAA
AGGTCTGGAATGGATGGGCATCATCAACCCCGGTGACAGCGACACTCGTTATAACCCGAGCTTC
CAGGGTCAAGTTACCATTAGCGCGGATAAAAGCATTAGCACCGCATATCTGCAGTGGTCTAGCCT
GAAAGCGAGCGACACCGCCGTGTATTACTGTGCCCGTGCTGACTACGACTACTACCGTGGTTAC
TACATGGACATCTGGGGTCAGGGCACCCTGGTCACCGTCTCGAGT

>83B11D VH (SEQ ID NO. 57)

GAGGTTCAGCTGGTTCAGAGCGGTGCCGAAGTTAAAAAACCGGGTGAAAGCCTGAAAATTTCAT
GTAAAGGTAGCGGCTATACTTTCGATACTTATTGGATCGGTTGGGTGCGCCAGATGCCTGGTAA
AGGTCTGGAATGGATGGGCATCATCAACCCCGGTGACAGCGACACTCGTTATAACCCGAGCTTC
CAGGGTCAAGTTACCATTAGCGCGGATAAAAGCATTAGCACCGCATATCTGCAGTGGTCTAGCCT
GAAAGCGAGCGACACCGCCGTGTATTACTGTGCCCGTGCTGACTACGACTACTACCGTGGTTAC
TACATGGACATCTGGGGTCAGGGCACCCTGGTCACCGTCTCGAGT

>94C2 VH (SEQ ID NO. 58)

GAGGTTCAGCTGGTTCAGAGCGGTGCCGAAGTTAAAAAACCGGGTGAAAGCCTGAAAATTTCAT
GTAAAGGTAGCGGCTATACTTTCGATACTTATTGGATCGGTTGGGTGCGCCAGATGCCTGGTAA
AGGTCTGGAATGGATGGGCATCATCAACCCCGGTGACAGCGACACTCGTTATAACCCGAGCTTC
CAGGGTCAAGTTACCATTAGCGCGGATAAAAGCATTAGCACCGCATATCTGCAGTGGTCTAGCCT
GAAAGCGAGCGACACCGCCGTGTATTACTGTGCCCGTGTTGATGATTTTTATTACCGTGGTTACT
ACATGGACATCTGGGGTCAGGGCACCCTGGTCACCGTCTCGAGT

>115D1D VH (SEQ ID NO. 59)

GAGGTTCAGCTGGTTCAGAGCGGTGCCGAAGTTAAAAAACCGGGTGAAAGCCTGAAAATTTCAT
GTAAAGGTAGCGGCTATGCTTTCGATACTTATTGGATCGGTTGGGTGCGCCAGATGCCTGGTAA
AGGTCTGGAATGGATGGGCATCATCAACCCCGGTGACAGCGACACTCGTTATAACCCGAGCTTC
CAGGGTCAAGTTACCATTAGCGCGGATAAAAGCATTAGCACCGCATATCTGCAGTGGTCTAGCCT
GAAAGCGAGCGACACCGCCGTGTATTACTGTGCCCGTGTTGATGATTATTATTACCGTGGTTACT
ACATGGACATCTGGGGTCAGGGCACCCTGGTCACCGTCTCGAGT

>131D5S VH (SEQ ID NO. 60)

GAGGTTCAGCTGGTTCAGAGCGGTGCCGAAGTTAAAAAACCGGGTGAAAGCCTGAAAATTTCAT
GTAAAGGTAGCGGCTATGCTTTCGATACTTATTGGGTCGGTTGGGTGCGCCAGATGCCAGGTAA
AGGTCTGGAATGGATGGGCATCATCAACCCCGGTGACAGCGACACTCGTTATAACCCGAGCTTC
CAGGGTCAAGTTACCATTAGCGCGGATAAAAGCATTAGCACCGCATATCTGCAGTGGTCTAGCCT
GAAAGCGAGCGACACCGCCGTGTATTACTGTGCCCGTGTTGATGATTATTATTACCGTGGTTACT
ACATGGACATCTGGGGTCAGGGCACCCTGGTCACTGTCTCGAGT

>3A2 VL (SEQ ID NO. 61)

CAGTCTGTGCTGACTCAGCCTCCGAGCGTTAGCGCAGCACCGGGTCAGAAAGTGACCATTAGTT
GTAGCGGTAGCAGCAGCAACATCGGCAACTACTACGTCTCTTGGTATCAGCAGCTGCCTGGCAC
CGCACCGAAACTGCTGATTTATCGTAACTCTAACCGCCCATCTGGTGTGCCGGATCGTTTTAGCG
GTAGTAAAAGCGGCACCAGCGCAAGCCTGGCAATTAGCGGTCTGCAGAGCGAAGATGAAGCAG
ATTATTACTGTGCGGCTTGGGACGATTCTCTTTCTGGTTGGGTTTTTGGTGGTGGGACCAAGCTG
ACCGTCCTA

>20F6 VL (same for 49G5, 49A6, 55G9 and 55A3) (SEQ ID NO. 62)

CAGTCTGTGCTGACTCAGCCTCCGAGCGTTAGCGCAGCACCGGGTCAGAAAGTGACCATTAGTT
GTAGCGGTAGCAGCAGCAACATCGGCTCTAACTACGTCTCTTGGTATCAGCAGCTGCCTGGCAC
CGCACCGAAACTGCTGATTTATAGTAACTCTAACCGCCCATCTGGTGTGCCGGATCGTTTTAGCG
GTAGTAAAAGCGGCACCAGCGCAAGCCTGGCAATTAGCGGTCTGCAGAGCGAAGATGAAGCAG

ATTATTACTGTGCGGCTTGGGACGATTCTCTTTCTGGTTGGGTTTTTGGTGGTGGGACCAAGCTG
ACCGTCCTA

>53D11 (same for 77F3 and 126A8B) (SEQ ID NO. 63)

CAGTCTGTGCTGACTCAGCCTCCGAGCGTTAGCGCAGCACCGGGTCAGAAAGTGACCATTAGTT
GTAGCGGTAGCAGCAGCAACATCGGCTCTAACTACGTCTCTTGGTATCAGCAGCTGCCTGGCAC
CGCACCGAAACTGCTGATTTATAGTAACTCTAACCGCCCATCTGGTGTGCCGGATCGTTTTAGCG
GTAGTAAAAGCGGCACCAGCGCAAGCCTGGCAATTAGCGGTCTGCAGAGCGAAGATGAAGCAG
ATTATTACTGTGCGGCTTGGGATAATTCTGTTGCGGGTTGGGTTTTTGGTGGTGGGACCAAGCT
GACCGTCCTA

>129D5B VL (SEQ ID NO. 64)

CAGCCTGTGCTGACTCAGCCTCCGAGCGTTAGCGCAGCACCGGGTCAGAAAGTGACCATTAGTT
GCAGCGGTAGCAGCAGCAACATCGGCTCTAACTACGTCTCTTGGTATCAGCAGCTGCCTGGCAC
CGCACCGAAACTGCTGATTTATAGTAACTCTAACCGCCCATCTGGTGTGCCGGATCGTTTTAGCG
GTAGTAAAAGCGGCACCAGCGCAAGCCTGGCAATTAGCGGTCTGCAGAGCGAAGATGAAGCAG
ATTATTACTGTGCGGCTTGGGATAATTCTGTTGCAGGTTGGGTTTTTGGTGGTGGGACCAAGCTG
ACCGTCCTA

>129D5BTY VL (SEQ ID NO. 199)

CAGCCTGTGCTGACTCAGCCTCCGAGCGTTAGCGCAGCACCGGGTCAGAAAGTGACCATTAGTT
GCAGCGGTAGCAGCAGCAACATCGGCTCTAACTACGTCTCTTGGTATCAGCAGCTGCCTGGCAC
CGCACCGAAACTGCTGATTTATAGTAACTACAACCGCCCATCTGGTGTGCCGGATCGTTTTAGCG
GTAGTAAAAGCGGCACCAGCGCAAGCCTGGCAATTAGCGGTCTGCAGAGCGAAGATGAAGCAG
ATTATTACTGTGCGGCTTGGGATAATACGGTTGCAGGTTGGGTTTTTGGTGGTGGGACCAAGCT
GACCGTCCTA

>139B2 VL (SEQ ID NO. 65)

CAGTCTGTGCTGACTCAGCCTCCGAGCGTTAGCGCAGCACCGGGTCAGAAAGTGACCATTAGTT
GTAGCGGTAGCAGCAGCAACATCGGCTCTAACTACGTCTCTTGGTATCAGCAGCTGCCTGGCAC
CGCACCGAAACTGCTGATTTATAGTAACTCTAACCGCCCATCTGGTGTGCCGGATCGTTTTAGCG
GTAGTAAAAGCGGCACCAGCGCAAGCCTGGCAATTAGCGGTCTGCAGAGCGAAGATGAAGCAG
ATTATTACTGTGCGGCTTGGGATAATTCTGTTGCGGGTTGGGTTTTTGGTGGTGGGACCCAGCT
GACCGTCCTA

>139D2 VL (same for 139D7) (SEQ ID NO. 66)

CAGTCTGTGCTGACTCAGCCTCCGAGCGTTAGCGCAGCACCGGGTCAGAAAGTGACCATTAGTT
GTAGCGGTAGCAGCAGCAACATCGGCTCTAACTACGTCTCTTGGTATCAGCAGCTGCCTGGCAC
CGCACCGAAACTGCTGATTTATAGTAACTCTAACCGCCCATCTGGTGTGCCGGATCGTTTTAGCG

GTAGTAAAAGCGGCACCAGCGCAAGCCTGGCAATTAGCGGTCTGCAGAGCGAAGATGAAGCAG
ATTATTACTGTGCGGCTTGGGATAATTCTGTTGCGGGTTGGGTTTTTGGTGGTGGGACCCGGCT
GACCGTCCTA

>26B5 VL (SEQ ID NO. 67)

CAGTCTGTGCTGACTCAGCCTCCGAGCGTTAGCGCAGCACCGGGTCAGAAAGTGACCATTAGTT
GTAGCGGTAGCAGCAGCAACATCGGCTCTTACGTTGTCTACTGGTATCAGCAGCTGCCTGGCAC
CGCACCGAAACTGCTGATTTATGACAACACTAACCGCCCATCTGGTGTGCCGGATCGTTTTAGCG
GTAGTAAAAGCGGCACCAGCGCAAGCCTGGCAATTAGCGGTCTGCAGAGCGAAGATGAAGCAG
ATTATTACTGTGCGACTTGGGACGATTCTCTTAACGGTCCGGTTTTTGGTGGTGGGACCAAGCTG
ACCGTCCTA

>83B11D VL (same for 94C2, 94C3, 94E6, 112F2 and 112G4) (SEQ ID NO. 68)

CAGTCTGTGCTGACTCAGCCTCCGAGCGTTAGCGCAGCACCGGGTCAGAAAGTGACCATTAGTT
GTAGCGGTAGCAGCAGCAACATCGGCTCTTACGTTGTCTACTGGTATCAGCAGCTGCCTGGCAC
CGCACCGAAACTGCTGATTTATGACAACAACCAGCGCCCATCTGGTGTGCCGGATCGTTTTAGC
GGTAGTAAAAGCGGCACCAGCGCAAGCCTGGCAATTAGCGGTCTGCAGAGCGAAGATGAAGCA
GATTATTACTGTGCGTCTTGGGACGATTCTCTTAACGGTCCGGTTTTTGGTGGTGGGACCAAGCT
GACCGTCCTA

>115D1D VL (same for 116A5 and 121H3B) (SEQ ID NO. 69)

CAGTCTGTGCTGACTCAGCCTCCGAGCGTTAGCGCAGCACCGGGTCAGAAAGTGACCATTAGTT
GTAGCGGTAGCAGCAGCAACATCGGCCCTTACGTTGTCTACTGGTATCAGCAGCTGCCTGGCAC
CGCACCGAAACTGCTGATTTATGACAACAACCAGCGCCCATCTGGCGTGCCGGATCGTTTTAGC
GGTAGTAAAAGCGGCACCAGCGCAAGCCTGGCAATTAGCGGTCTGCAGAGCGAAGATGAAGCA
GATTATTACTGTGCGACTTGGGACGATTCTCTTAACGGTCCGGTTTTTGGTGGTGGGACCAAGCT
GACCGTCCTA

>131D5S VL (SEQ ID NO. 70)

CAGTCTGTGCTGACGCAGCCTCCGAGCGTTAGCGCAGCACCGGGTCAGAAAGTGACCATTAGTT
GTAGCGGTAGCAGCAGCAACATCGGCCCTTACGTTGTCTACTGGTATCAGCAGCTGCCTGGCAG
CGCACCGAAACTGCTGATTTATGACAACAACCAGCGCCCAACTGGCGTGCCGGATCGTTTTAGC
GGTAGTAAAAGCGGCACCAGCGCAAGCCTGGCAATTAGCGGTCTGCAGAGCGAAGATGAAGCA
GATTATTACTGTGCGACTTGGGACGATTCACTTAACGGTCCGGTTTTTGGTGGTGGGACCAAGCT
GACCGTCCTA

>49A6 VH (SEQ ID NO. 154)

GAGGTTCAGCTGGTTCAGAGCGGTGCCGAAGTTAAAAAACCGGGTGAAAGCCTGAAAATTTCAT
GTAAAGGTAGCGGCTATTCTTTCACTACTTATTGGATCGGTTGGGTGCGCCAGATGCCTGGTAAA

GGTCTGGAATGGATGGGCATCATCAACCCCGCTGACAGCAACACTCGTTATAACCCGAGCTTCC
AGGGTCAAGTTACCATTAGCGCGGATAAAAGCATTAGCACCGCAtATCTGCAGTGGTCTAGCCTG
AAAGCGAGCGACACCGCCGTGTATTACTGTGCCCGTCATGGTGGTCGTGGTCGTCTTGCTTATT
GGGGTCAGGGCACCCTGGTCACCGTCTCGAGT

>55G9 VH (SEQ ID NO. 155)

GAGGTTCAGCTGGTTCAGAGCGGTGCCGAAGTTAAAAAACCGGGTGAAAGCCTGAAAATTTCAT
GTAAAGGTAGCGGCTATTCTTTCACTACTTATTGGATCGGTTGGGTGCGCCAGATGCCTGGTAAA
GGTCTGGAATGGATGGGCATCATCAACCCCGCTGACAGCAACACTCGTTATAACCCGAGCTTCC
AGGGTCAAGTTACCATTAGCGCGGATAAAAGCATTAGCACCGCATATCTGCAGTGGTCTAGCCT
GAAAGCGAGCGACACCGCCGTGTATTACTGTGCCCGTCATGGTGGTCGTGGGAGGCTTGAGCG
TTGGGGTCAGGGCACCCTGGTCACCGTCTCGAGT

>55A3 VH (SEQ ID NO. 156)

GAGGTTCAGCTGGTTCAGAGCGGTGCCGAAGTTAAAAAACCGGGTGAAAGCCTGAAAATTTCAT
GTAAAGGTAGCGGCTATTCTTTCACTACTTATTGGATCGGTTGGGTGCGCCAGATGCCTGGTAAA
GGTCTGGAATGGATGGGCATCATCAACCCCGCTGACAGCAACACTCGTTATAACCCGAGCTTCC
AGGGTCAAGTTACCATTAGCGCGGATAAAAGCATTAGCACCGCATATCTGCAGTGGTCTAGCCT
GAAAGCGAGCGACACCGCCGTGTATTACTGTGCCCGTCATGGTGGTCGTGGTCGTCTGCCTTAT
TGGGGTCAGGGCACCCTGGTCACCGTCTCGAGT

>74C3 VH (SEQ ID NO. 157)

GAGGTTCAGCTGGTTCAGAGCGGTGCCGAAGTTAAGAAACCGGGTGAAAGCCTGAAAATTTCAT
GTAAAGGTAGCGGCTATTCTTTCACTACTTATTGGATCGGTTGGATGCGCCAGATGCCTGGTAAA
GGTCTGGAATGGATGGGCATCATCAACCCCGCTGACAGCAACACTCGTTATAACCCGAGCTTCC
AGGGTCAAGTTACCATTAGCGCGGATAAAAGCATTAGCACCGCATATCTGCAGTGGTCTAGCCT
GAAAGCGAGCGACACCGCCGTGTATTACTGTGCCCGTCATGGTGGTCGTGGTCGTCTGGACGTT
TGGGGTCAGGGCACCCTGGTCACCGTCTCGAGT

>64B2 VH (SEQ ID NO. 158)

GAGGTTCAGCTGGTTCAGAGCGGTGCCGAAGTTAAAAAACCGGGTGAAAGCCTGAAAATTTCAT
GCGAAGGTAGCGGCTATTCTTTCACTACTTATTGGATCGGTTGGGTGCGCCAGATGCCTGGTAA
AGGTCTGGAATGGATGGGCATCATCAACCCCGCTGACAGCAACACTCGTTATAACCCGAGCTTC
CAGGGTCAAGTTACCATTAGCGCGGATAAAAGCATTAGCACCGCATATCTGCAGTGGTCTAGCCT
GAAAGCGAGCGACACCGCCGTGTATTACTGTGCCCGTCATGGTGGTCGTGGTCGTCTGGACGTT
TGGGGTCAGGGCACCCTGGTCACCGTCTCGAGT

>71D4 VH (SEQ ID NO. 159)

GAGGTTCAGCTGGTTCAGAGCGGTGCCGAAGTTAAAAAACCGGGTGAAAGCCTGAAAATTTCAT
GTAAAGGTAGCGGCTATTCTTTCACTACTTATTGGGTCGGTTGGGTGCGCCAGATGCCTGGTAAA
GGTCTGGAATGGATGGGCATCATCAACCCCGCTGACAGCAACACTCGTTATAACCCGAGCTTCC
AGGGTCAAGTTACCATTAGCGCGGATAAGAGCATTAGCACCGCATATCTGCAGTGGTCTAGCCT
GAAAGCGAGCGACACCGCCGTGTATTACTGTGCCCGTCATGGTGGTCGTGGTCGTCTGGACGTT
TGGGGTCAGGGCACCCTGGTCACCGTCTCGAGT

>126A8B VH (SEQ ID NO. 160)

GAGGTTCAGCTGGTTCAGAGCGGTGCCGAAGTTAAAAAACCGGGTGAAAGCCTGAAAATTTCAT
GTAAAGGTAGCGGCTATTCTTTCACTACTTATTGGATCGGTTGGGTGCGCCAGATGCCTGGTAAA
GGTCTGGAATGGATGGGCATCATCAACCCCGCTGACAGCAACACTCGTTATAGCCCGAGCTTCC
AGGGTCAAGTTACCATTAGCGCGGATAAAAGCATTAGCACCGCATATCTGCAGTGGTCTAGCCT
GAAAGCGAGCGACACCGCCGTGTATTACTGTGCCCGTCATAGCGGTCGTGGGCGTTTGTGGCC
GTGGGGTCAGGGCACCCTGGTCACCGTCTCGAGT

>94C3 VH (same for 116A5) (SEQ ID NO. 161)

GAGGTTCAGCTGGTTCAGAGCGGTGCCGAAGTTAAAAAACCGGGTGAAAGCCTGAAAATTTCAT
GTAAAGGTAGCGGCTATACTTTCGATACTTATTGGATCGGTTGGGTGCGCCAGATGCCTGGTAA
AGGTCTGGAATGGATGGGCATCATCAACCCCGGTGACAGCGACACTCGTTATAACCCGAGCTTC
CAGGGTCAAGTTACCATTAGCGCGGATAAAAGCATTAGCACCGCATATCTGCAGTGGTCCAGCC
TGAAAGCGAGCGACACCGCCGTGTATTACTGTGCCCGTACGGATGATTATTATTACCGTGGTTAC
TACATGGACATCTGGGGTCAGGGCACCCTGGTCACCGTCTCGAGT

>94E6 VH (SEQ ID NO. 162)

GAGGTTCAGCTGGTTCAGAGCGGTGCCGAAGTTAAAAAACCGGGTGAAAGCCTGAAAATTTCAT
GTAAAGGTAGCGGCTATACTTTCGATACTTATTGGATCGGTTGGGTGCGCCAGATGCCTGGTAA
AGGTCTGGAATGGATGGGCATCATCAACCCCGGTGACAGCGACACTCGTTATAACCCGAGCTTC
CAGGGTCAAGTTACCATTAGCGCGGATAAAAGCATTAGCACCGCATATCTGCAGTGGTCTAGCCT
GAAAGCGAGCGACACCGCCGTGTATTACTGTGCCCGTACGAATGATGAGTATTACCGTGGTTAC
TACATGGACATCTGGGGTCAGGGCACCCTGGTCACCGTCTCGAGT

>112F2 VH (same for 113A3) (SEQ ID NO. 163)

GAGGTTCAGCTGGTTCAGAGCGGTGCCGAAGTTAAAAAACCGGGTGAAAGCCTGAAAATTTCAT
GTAAAGGTAGCGGCTATACTTTCGATACTTATGGGATCGGTTGGGTGCGCCAGATGCCTGGTAA
AGGTCTGGAATGGATGGGCATCATCAACCCCGGTGACAGCGACACTCGTTATAACCCGAGCTTC
CAGGGTCAAGTTACCATTAGCGCGGATAAAAGCATTAGCACCGCATATCTGCAGTGGTCTAGCCT
GAAAGCGAGCGACACCGCCGTGTATTACTGTGCCCGTGTTGATGATTTTTATTACCGTGGTTACT
ACATGGACATCTGGGGTCAGGGCACCCTGGTCACCGTCTCGAGT

>112G4 VH (same for 113G8) (SEQ ID NO. 164)

GAGGTTCAGCTGGTTCAGAGCGGTGCCGAAGTTAAAAAACCGGGTGAAAGCCTGAAAATTTCAT
GTAAAGGTAGCGGCTATACTTTCGATACTTATGGGATCGGTTGGGTGCGCCAGATGCCTGGTAA
AGGTCTGGAATGGATGGGCACCATCGACCCCGGTGACAGCGACACTCGTTATAACCCGAGCTTC
CAGGGTCAAGTTACCATTAGCGCGGATAAAAGCATTAGCACCGCATATCTGCAGTGGTCTAGCCT
GAAAGCGAGCGACACCGCCGTGTATTACTGTGCCCGTACGGATGATTATTATTACCGTGGTTACT
ACATGGACATCTGGGGTCAGGGCACCCTGGTCACCGTCTCGAGT

>115C7 VH (SEQ ID NO. 165)

GAGGTTCAGCTGGTTCAGAGCGGTGCCGAAGTTAAAAAACCGGGTGAAAGCCTGAAAATTTCAT
GTAAAGGTAGCGGCTATACTTTCGATACTTATcAGATCGGTTGGGTGCGCCAGATGCCTGGTAAA
GGTCTGGAATGGATGGGCATCATCAACCCCGGTGACAGCGACACTCGCTATAACCCGAGCTTCC
AGGGTCAAGTTACCATTAGCGCGGATAAAAGCATTAGCACCGCATATCTGCAGTGGTCTAGCCT
GAAAGCGAGCGACACCGCCGTGTATTACTGTGCCCGTGTTGATGATTTTTATTACCGTGGTTACT
ACATGGACATCTGGGGTCAGGGCACCCTGGTCACCGTCTCGAGT

>121H3B VH (SEQ ID NO. 166)

GAGGTTCAGCTTGTTCAGAGCGGTGCCGAAGTTAAAAAACCGGGTGAAAGCCTGAAAATTTCAT
GTAAAGGTAGCGGCTATACTTTCGATACTTATTGGATCGGTTGGGTGCGCCAGATGCCTGGTAA
AGGTCTGGAATGGATGGGCATCATCAACCCCGGTGACAGCGACGCTCGTTATAACCCGAGCTTC
CAGGGTCAAGTTACCATTAGCGCGGATAAAAGCATTAGCACCGCATATCTGCAGTGGTCCAGCC
TGAAAGCGAGCGACACCGCCGTGTATTACTGTGCCCGTGCGGATGATTATTATTACCGTGGTTAC
TACATGGACATCTGGGGTCAGGGCACCCTGGTCACCGTCTCGAGT

>59D5 VL (SEQ ID NO. 167)

CAGTCTGTGCTGACTCAGCCTCCGAGCGTTAGCGCAGCACCGGGTCAGAAAGTGACCATTAGTT
GTAGCGGTAGCAGCAGCAACATCGGCTCTAACTACGTCTCTTGGTATCAGCAGCTGCCTGGCAC
CGCACCGAAACTGCTGATTTATAGTAACTCTAACCGCCCATCTGGTGTGCCGGATCGTTTTAGCG
GTAGTAAAAGCGGCACCAGCGCAAGCCTGGCAATTAGCGGTCTGCAGAGCGAAGATGAAGCAG
ATTATTACTGTGCGGCTTGGGATAATCCTAGTGGGGGTTGGGTTTTTGGTGGTGGGACCAAGCT
GACCGTCCTA

>54E11 VL (SEQ ID NO. 168)

CAGTCTGTGCTGACTCAGCCTCCGAGCGTTAGCGCAGCACCGGGTCAGAAAGTGACCATTAGTT
GTAGCGGTAGCAGCAGCAACATCGGCTCTAACTACGTCTCTTGGTATCAGCAGCTGCCTGGCAC
CGCACCGAAACTGCTGATTTATAGTAACTCTAACCGCCCATCTGGTGTGCCGGATCGTTTTAGCG
GTAGTAAAAGCGGCACCAGCGCAAGCCTGGCAATTAGCGGTCTGCAGAGCGAAGATGAAGCAG

ATTATTACTGTGCGGCTTGGGATCAGATTTCTGGGGGTTGGGTTTTTGGTGGTGGGACCAAGCT
GACCGTCCTA

>59D4 VL (SEQ ID NO. 169)

CAGTCTGTGCTGACTCAGCCTCCGAGCGTTAGCGCAGCACCGGGTCAGAAAGTGACCATTAGTT
GTAGCGGTAGCAGCAGCAACATCGGCTCTAACTACGTCTCTTGGTATCAGCAGCTGCCTGGCAC
CGCACCGAAACTGCTGATTTATAGTAACTCTAACCGCCCATCTGGTGTGCCGGATCGTTTTAGCG
GTAGTAAAAGCGGCACCAGCGCAAGCCTGGCAATTAGCGGTCTGCAGAGCGAAGATGAAGCAG
ATTATTACTGTGCGGCTTGGGATCAGGAGTTTGGGGGTTGGGTTTTTGGTGGTGGGACCAAGCT
GACCGTCCTA

>59A10 VL (SEQ ID NO. 170)

CAGTCTGTGCTGACTCAGCCTCCGAGCGTTAGCGCAGCACCGGGTCAGAAAGTGACCATTAGTT
GTAGCGGTAGCAGCAGCAACATCGGCTCTAACTACGTCTCTTGGTATCAGCAGCTGCCTGGCAC
CGCACCGAAACTGCTGATTTATAGTAACTCTAACCGCCCATCTGGTGTGCCGGATCGTTTTAGCG
GTAGTAAAAGCGGCACCAGCGCAAGCCTGGCAATTAGCGGTCTGCAGAGCGAAGATGAAGCAG
ATTATTACTGTGCGGCTTGGGATCAGGGTTATAATGGTTGGGTTTTTGGTGGTGGGACCAAGCT
GACCGTCCTA

>65C2 VL (SEQ ID NO. 171)

CAGTCTGTGCTGACTCAGCCTCCGAGCGTTAGCGCAGCACCGGGTCAGAAAGTGACCATTAGTT
GTAGCGGTAGCAGCAGCAACATCGGCTCTAACTACGTCTCTTGGTATCAGCAGCTGCCTGGCAC
CGCACCGAAACTGCTGATTTATAGTAACTCTAACCGCCCATCTGGTGTGCCGGATCGTTTTAGCG
GTAGTAAAAGCGGCACCAGCGCAAGCCTGGCAATTAGCGGTCTGCAGAGCGAAGATGAAGCAG
ATTATTACTGTGCGGCTTGGGATCAGAGTACTGATGGTTGGGTTTTTGGTGGTGGGACCAAGCT
GACCGTCCTA

>53G1 VL (SEQ ID NO. 172)

CAGTCTGTGCTGACTCAGCCTCCGAGCGTTAGCGCAGCACCGGGTCAGAAAGTGACCATTAGTT
GTAGCGGTAGCAGCAGCAACATCGGCTCTAACTACGTCTCTTGGTATCAGCAGCTGCCTGGCAC
CGCACCGAAACTGCTGATTTATAGTAACTCTAACCGCCCATCTGGTGTGCCGGATCGTTTTAGCG
GTAGTAAAAGCGGCACCAGCGCAAGCCTGGCAATTAGCGGTCTGCAGAGCGAAGATGAAGCAG
ATTATTACTGTGCGGCTTGGAGTAATTATGCTGCTGGTTGGGTTTTTGGTGGTGGGACCAAGCTG
ACCGTCCTA

>65A3 VL (SEQ ID NO. 173)

CAGTCTGTGCTGACTCAGCCTCCGAGCGTTAGCGCAGCACCGGGTCAGAAAGTGACCATTAGTT
GTAGCGGTAGCAGCAGCAACATCGGCTCTAACTACGTCTCTTGGTATCAGCAGCTGCCTGGCAC
CGCACCGAAACTGCTGATTTATAGTAACTCTAACCGCCCATCTGGTGTGCCGGATCGTTTTAGCG

GTAGTAAAAGCGGCACCAGCGCAAGCCTGGCAATTAGCGGTCTGCAGAGCGAAGATGAAGCAG
ATTATTACTGTGCGGCTTGGGAGAATTATGCTGCTGGTTGGGTTTTTGGTGGTGGGACCAAGCT
GACCGTCCTA

>65G6 VL (SEQ ID NO. 174)

CAGTCTGTGCTGACTCAGCCTCCGAGCGTTAGCGCAGCACCGGGTCAGAAAGTGACCATTAGTT
GTAGCGGTAGCAGCAGCAACATCGGCTCTAACTACGTCTCTTGGTATCAGCAGCTGCCTGGCAC
CGCACCGAAACTGCTGATTTATAGTAACTCTAACCGCCCATCTGGTGTGCCGGATCGTTTTAGCG
GTAGTAAAAGCGGCACCAGCGCAAGCCTGGCAATTAGCGGTCTGCAGAGCGAAGATGAAGCAG
ATTATTACTGTGCGGCTTGGGAGAATTGGGAGGCGGGTTGGGTTTTTGGTGGTGGGACCAAGCT
GACCGTCCTA

>53G9 VL (SEQ ID NO. 175)

CAGTCTGTGCTGACTCAGCCTCCGAGCGTTAGCGCAGCACCGGGTCAGAAAGTGACCATTAGTT
GTAGCGGTAGCAGCAGCAACATCGGCTCTAACTACGTCTCTTGGTATCAGCAGCTGCCTGGCAC
CGCACCGAAACTGCTGATTTATAGTAACTCTAACCGCCCATCTGGTGTGCCGGATCGTTTTAGCG
GTAGTAAAAGCGGCACCAGCGCAAGCCTGGCAATTAGCGGTCTGCAGAGCGAAGATGAAGCAG
ATTATTACTGTGCGGCTTGGGATTTGACGGAGGCTGGTTGGGTTTTTGGTGGTGGGACCAAGCT
GACCGTCCTA

>58H11 VL (SEQ ID NO. 176)

CAGTCTGTGCTGACTCAGCCTCCGAGCGTTAGCGCAGCACCGGGTCAGAAAGTGACCATTAGTT
GTAGCGGTAGCAGCAGCAACATCGGCTCTAACTACGTCTCTTGGTATCAGCAGCTGCCTGGCAC
CGCACCGAAACTGCTGATTTATAGTAACTCTAACCGCCCATCTGGTGTGCCGGATCGTTTTAGCG
GTAGTAAAAGCGGCACCAGCGCAAGCCTGGCAATTAGCGGTCTGCAGAGCGAAGATGAAGCAG
ATTATTACTGTGCGGCTTGGGACACGGATCAGGCGGGGTGGGTTTTTGGTGGTGGGACCAAGCT
GACCGTCCTA

>59E5 VL (SEQ ID NO. 177)

CAGTCTGTGCTGACTCAGCCTCCGAGCGTTAGCGCAGCACCGGGTCAGAAAGTGACCATTAGTT
GTAGCGGTAGCAGCAGCAACATCGGCTCTAACTACGTCTCTTGGTATCAGCAGCTGCCTGGCAC
CGCACCGAAACTGCTGATTTATAGTAACTCTAACCGCCCATCTGGTGTGCCGGATCGTTTTAGCG
GTAGTAAAAGCGGCACCAGCGCAAGCCTGGCAATTAGCGGTCTGCAGAGCGAAGATGAAGCAG
ATTATTACTGTGCGGCTTGGGATTCTGAGGAGGCGGGTTGGGTTTTTGGTGGTGGGACCAAGCT
GACCGTCCTA

>59H2 VL (SEQ ID NO. 178)

CAGTCTGTGCTGACTCAGCCTCCGAGCGTTAGCGCAGCACCGGGTCAGAAAGTGACCATTAGTT
GTAGCGGTAGCAGCAGCAACATCGGCTCTAACTACGTCTCTTGGTATCAGCAGCTGCCTGGCAC

CGCACCGAAACTGCTGATTTATAGTAACTCTAACCGCCCATCTGGTGTGCCGGATCGTTTTAGCG
GTAGTAAAAGCGGCACCAGCGCAAGCCTGGCAATTAGCGGTCTGCAGAGCGAAGATGAAGCAG
ATTATTACTGTGCGGCTTGGGATTCTTCGTATGGTGGTTGGGTTTTTGGTGGTGGGACCAAGCTG
ACCGTCCTA

>59A6 VL (SEQ ID NO. 179)

CAGTCTGTGCTGACTCAGCCTCCGAGCGTTAGCGCAGCACCGGGTCAGAAAGTGACCATTAGTT
GTAGCGGTAGCAGCAGCAACATCGGCTCTAACTACGTCTCTTGGTATCAGCAGCTGCCTGGCAC
CGCACCGAAACTGCTGATTTATAGTAACTCTAACCGCCCATCTGGTGTGCCGGATCGTTTTAGCG
GTAGTAAAAGCGGCACCAGCGCAAGCCTGGCAATTAGCGGTCTGCAGAGCGAAGATGAAGCAG
ATTATTACTGTGCGGCTTGGGATTCGGCTAATGCGGGTTGGGTTTTTGGTGGTGGGACCAAGCT
GACCGTCCTA

>59A2 VL (SEQ ID NO. 180)

CAGTCTGTGCTGACTCAGCCTCCGAGCGTTAGCGCGGCACCGGGCCAGAAAGTGACCATTAGTT
GTAGCGGTAGCAGCAGCAACATCGGCTCTAACTACGTCTCTTGGTATCAGCAGCTGCCTGGCAC
CGCACCGAAACTGCTGATTTATAGTAACTCTAACCGCCCATCTGGTGTGCCGGATCGTTTTAGCG
GTAGTAAAAGCGGCACCAGCGCAAGCCTGGCAATTAGCGGTCTGCAGAGCGAAGATGAAGCAG
ATTATTACTGTGCGGCTTGGGATAGTAGTGCTGCTGGTTGGGTTTTTGGTGGTGGGACCAAGCT
GACCGTCCTA

>59D10 VL (SEQ ID NO. 181)

CAGTCTGTGCTGACTCAGCCTCCGAGCGTTAGCGCAGCACCGGGTCAGAAAGTGACCATTAGTT
GTAGCGGTAGCAGCAGCAACATCGGCTCTAACTACGTCTCTTGGTATCAGCAGCTGCCTGGCAC
CGCACCGAAACTGCTGATTTATAGTAACTCTAACCGCCCATCTGGTGTGCCGGATCGTTTTAGCG
GTAGTAAAAGCGGCACCAGCGCAAGCCTGGCAATTAGCGGTCTGCAGAGCGAAGATGAAGCAG
ATTATTACTGTGCGGCTTGGGATGGTAATGATGATGGTTGGGTTTTTGGTGGTGGGACCAAGCT
GACCGTCCTA

>58A9 VL (SEQ ID NO. 182)

CAGTCTGTGCTGACTCAGCCTCCGAGCGTTAGCGCAGCACCGGGTCAGAAAGTGACCATTAGTT
GTAGCGGTAGCAGCAGCAACATCGGCTCTAACTACGTCTCTTGGTATCAGCAGCTGCCTGGCAC
CGCACCGAAACTGCTGATTTATAGTAACTCTAACCGCCCATCTGGTGTGCCGGATCGTTTTAGCG
GTAGTAAAAGCGGCACCAGCGCAAGCCTGGCAATTAGCGGTCTGCAGAGCGAAGATGAAGCAG
ATTATTACTGTGCGGCTTGGGACAATCATCAGGCTAGTTGGGTTTTTGGTGGTGGGACCAAGCT
GACCGTCCTA

>74C3 VL (SEQ ID NO. 183)

CAGTCTGTGCTGACTCAGCCTCCGAGCGTTAGCGCAGCACCGGGTCAGAAAGTGACCATTAGTT
GTAGCGGTAGCAGCAGCAACATCGGCTCTAACTACGTCTCTTGGTATCAGCAGCTGCCTGGCAC
CGCACCGAAGCTGCTGATTTATAGTAACTCTAACCGCCCATCTGGTGTGCCGGATCGTTTTAGCG
GTAGTAAAAGCGGCACCAGCGCAAGCCTGGCAATTAGCGGTCTGCAGAGCGAAGATGAAGCAG
ATTATTACTGTGCGGCTTGGGATAATCCTGAGGCGGGTTGGGTTTTTGGTGGTGGGACCAAGCT
GACCGTCCTA

>59H6 VL (SEQ ID NO. 184)

CAGTCTGTGCTGACTCAGCCTCCGAGCGTTAGCGCAGCACCGGGTCAGAAAGTGACCATTAGTT
GTAGCGGTAGCAGCAGCAACATCGGCTCTAACTACGTCTCTTGGTATCAGCAGCTGCCTGGCAC
CGCACCGAAACTGCTGATTTATAGTAACTCTAACCGCCCATCTGGTGTGCCGGATCGTTTTAGCG
GTAGTAAAAGCGGCACCAGCGCAAGCCTGGCAATTAGCGGTCTGCAGAGCGAAGATGAAGCAG
ATTATTACTGTGCGGCTTGGGATCAGGATTGGTCGGGTTGGGTTTTTGGTGGTGGGACCAAGCT
GACCGTCCTA

>64B2 VL (SEQ ID NO. 185)

CAGTCTGTGCTGACTCAGCCTCCGAGCGTTAGCGCAGCACCGGGTCAGAAAGTGACCATTAGTT
GTAGCGGTAGCAGCAGCAACATCGGCTCTAACTACGTCTCTTGGTATCAGCAGCTGCCTGGCAC
CGCACCGAAACTGCTGATTTATAGTAACTCTAACCGCCCATCTGGTGTGCCGGATCGTTTTAGCG
GTAGTAAAAGCGGCACCAGCGCAAGCCTGGCAATTAGCGGTCTGCAGAGCGAAGATGAAGCAG
ATTATTACTGTGCGGCTTGGGACCAGCAGTTTGCTGGTTGGGTTTTTGGTGGTGGGACCAAGCT
GACCGTCCTA

>52G1 VL (SEQ ID NO. 186)

CAGTCTGTGCTGACTCAGCCTCCGAGCGTTAGCGCAGCACCGGGTCAGAAAGTGACCATTAGTT
GTAGCGGTAGCAGCAGCAACATCGGCTCTAACTACGTCTCTTGGTATCAGCAGCTGCCTGGCAC
CGCACCGAAACTGCTGATTTATAGTAACTCTAACCGCCCATCTGGTGTGCCGGATCGTTTTAGCG
GTAGTAAAAGCGGCACCAGCGCAAGCCTGGCAATTAGCGGTCTGCAGAGCGAAGATGAAGCAG
ATTATTACTGTGCGGCTTGGGACTCGATTGCTCATAATTGGGTTTTTGGTGGTGGGACCAAGCTG
ACCGTCCTA

>58A2 VL (SEQ ID NO. 187)

CAGTCTGTGCTGACTCAGCCTCCGAGCGTTAGCGCAGCACCGGGTCAGAAAGTGACCATTAGTT
GTAGCGGTAGCAGCAGCAACATCGGCTCTAACTACGTCTCTTGGTATCAGCAGCTGCCTGGCAC
CGCACCGAAACTGCTGATTTATAGTAACTCTAACCGCCCATCTGGTGTGCCGGATCGTTTTAGCG
GTAGTAAAAGCGGCACCAGCGCAAGCCTGGCAATTAGCGGTCTGCAGAGCGAAGATGAAGCAG
ATTATTACTGTGCGGCTTGGGACTCTAATCCTTCGCATTGGGTTTTTGGTGGTGGGACCAAGCTG
ACCGTCCTA

>52D5 VL (SEQ ID NO. 188)

CAGTCTGTGCTGACTCAGCCTCCGAGCGTTAGCGCAGCACCGGGTCAGAAAGTGACCATTAGTT
GTAGCGGTAGCAGCAGCAACATCGGCTCTAACTACGTCTCTTGGTATCAGCAGCTGCCTGGCAC
CGCACCGAAACTGCTGATTTATAGTAACTCTAACCGCCCATCTGGTGTGCCGGATCGTTTTAGCG
GTAGTAAAAGCGGCACCAGCGCAAGCCTGGCAATTAGCGGTCTGCAGAGCGAAGATGAAGCAG
ATTATTACTGTGCGGCTTGGGACATTGCTAGTGCGAATTGGGTTTTTGGTGGTGGGACCAAGCT
GACCGTCCTA

>71D4 VL (SEQ ID NO. 189)

CAGTCTGTGCTGACTCAGCCTCCGAGCGTTAGCGCAGCACCGGGTCAGAAAGTGACCATTAGTT
GTAGCGGTAGCAGCAGCAACATCGGCTCTAACTACGTCTCTTGGTATCAGCAGCTGCCTGGCAC
CGCACCGAAACTGCTGATTTATAGTAACTCTAACCGCCCATCTGGTGTGCCGGATCGTTTTAGCG
GTAGTAAAAGCGGCACCAGCGCAAGCCTGGCAATTAGCGGTCTGCAGAGCGAAGATGAAGCAG
ATTATTACTGTGCGGCTTGGGATCAGATTTCGGCGGGTTGGGTTTTTGGTGGTGGGACCAAGCT
GACCGTCCTA

>75G7 VL (SEQ ID NO. 190)

CAGTCTGTGCTGACTCAGCCTCCGAGCGTTAGCGCAGCACCGGGTCAGAAAGTGACCATTAGTT
GTAGCGGTAGCAGCAGCAACATCGGCTCTAACTACGTCTCTTGGTATCAGCAGCTGCCTGGCAC
CGCACCGAAACTGCTGATTTATAGTAACTCTAACCGCCCATCTGGTGTGCCGGATCGTTTTAGCG
GTAGTAAAAGCGGCACCAGCGCAAGCCTGGCAATTAGCGGTCTGCAGAGCGAAGATGAAGCAG
ATTATTACTGTGCGGCTTGGGATAATCATTATGCGGGTTGGGTTTTTGGTGGTGGGACCAAGCTG
ACCGTCCTA

>71C2 VL (SEQ ID NO. 191)

CAGTCTGTGCTGACTCAGCCTCCGAGCGTTAGCGCAGCACCGGGTCAGAAAGTGACCATTAGTT
GTAGCGGTAGCAGCAGCAACATCGGCTCTAACTACGTCTCTTGGTATCAGCAGCTGCCTGGCAC
CGCACCGAAACTGCTGATTTATAGTAACTCTAACCGCCCATCTGGTGTGCCGGATCGTTTTAGCG
GTAGTAAAAGCGGCACCAGCGCAAGCCTGGCAATTAGCGGTCTGCAGAGCGAAGATGAAGCAG
ATTATTACTGTGCGGCTTGGGATAATACTAGTGCTGGTTGGGTTTTTGGTGGTGGGACCAAGCTG
ACCGTCCTA

>71F11 VL (SEQ ID NO. 192)

CAGTCTGTGCTGACTCAGCCTCCGAGCGTTAGCGCAGCACCGGGTCAGAAAGTGACCATTAGTT
GTAGCGGTAGCAGCAGCAACATCGGCTCTAACTACGTCTCTTGGTATCAGCAGCTGCCTGGCAC
CGCACCGAAACTGCTGATTTATAGTAACTCTAACCGCCCATCTGGTGTGCCGGATCGTTTTAGCG
GTAGTAAAAGCGGCACCAGCGCAAGCCTGGCAATTAGCGGTCTGCAGAGCGAAGATGAAGCAG

ATTATTACTGTGCGGCTTGGGATAATTCTCTTGCGGGTTGGGTTTTTGGTGGTGGGACCAAGCTG
ACCGTCCTA

>113A3 VL (SEQ ID NO. 193)

CAGTCTGTGCTGACTCAGCCTCCGAGCGTTAGCGCAGCACCGGGTCAGAAAGTGACCATTAGTT
GTAGCGGTAGCAGCAGCAACATCGGCTCTTACGTTGTCTACTGGTATCAGCAGCTGCCTGGCAC
CGCACCGAAACTGCTGATTTATGACAACAACCAGCGCCCATCTGGTGTGCCGGATCGTTTTAGC
GGTAGTAAAAGCGGCACCAGCGCAAGCCTGGCAATTAGCGGTCTGCAGAGCGAAGATGAAGCA
GATTATTACTGTGCGTCTTGGGACGATGTTGATTCTGCTCCGGTTTTTGGTGGTGGGACCAAGCT
GACCGTCCTA

>113G8 VL (SEQ ID NO. 194)

CAGTCTGTGCTGACGCAGCCTCCGAGCGTTAGCGCAGCACCGGGTCAGAAAGTGACCATTAGTT
GTAGCGGTAGCAGCAGCAACATCGGCTCTTACGTTGTCTACTGGTATCAGCAGCTGCCTGGCAC
CGCACCGAAACTGCTGATTTATGACAACAACCAGCGCCCATCTGGTGTGCCGGATCGTTTTAGC
GGTAGTAAAAGCGGCACCAGCGCAAGCCTGGCAATTAGCGGTCTGCAGAGCGAAGATGAAGCA
GATTATTACTGTGCGTCTTGGGACGATCCTAATAATGCGCCGGTTTTTGGTGGTGGGACCAAGCT
GACCGTCCTA

>115C7 VL (SEQ ID NO. 195)

CAGTCTGTGCTGACGCAGCCTCCGAGCGTTAGCGCAGCACCGGGTCAGAAAGTGACCATTAGTT
GTAGCGGTAGCAGCAGCAACATCGGCTCTTACGTTGTCTACTGGTATCAGCAGCTGCCTGGCAC
CGCACCGAAACTGCTGATTTATGACAACAACCAGCGCCCATCTGGTGTGCCGGATCGTTTTAGC
GGTAGTAAAAGCGGCACCAGCGCAAGCCTGGCAATTAGCGGTCTGCAGAGCGAAGATGAAGCA
GATTATTACTGTGCGACTTGGGACGATCCTAGTCAGCAGCCTGTTTTTGGTGGTGGGAcCAAGCT
GACCGTCCTA

CLAIMS

1. An antibody or antigen-binding fragment thereof that specifically binds to the MET receptor (cMET), wherein: (i) the antibody or antigen-binding fragment thereof comprises a heavy chain variable region (VH) comprising the Complementarity Determining Regions (CDRs) CDR-H1, CDR-H2, and CDR-H3 of SEQ ID NO. 1, or a variant thereof having at least 90% sequence identity to SEQ ID NO. 1, and comprises a light chain variable region (VL) comprising the CDRs CDR-L1, CDR-L2, and CDR-L3 of SEQ ID NO. 196 or SEQ ID NO. 2, or a variant thereof having at least 90% sequence identity with SEQ ID NO. 196 or SEQ ID NO. 2; or (ii) the antibody or antigen-binding fragment thereof comprises a heavy chain variable region (VH) comprising the Complementarity Determining Regions (CDRs) CDR-H1, CDR-H2, and CDR-H3 of SEQ ID NO. 21, or a variant thereof having at least 90% sequence identity to SEQ ID NO. 21, and comprises a light chain variable region (VL) comprising the CDRs CDR-L1, CDR-L2, and CDR-L3 of SEQ ID NO. 22, or a variant thereof having at least 90% sequence identity with SEQ ID NO. 22.

2. The antibody or antigen-binding fragment of claim 1, wherein the antibody or antigen-binding fragment is an antigen-binding fragment.

3. The antibody or antigen-binding fragment of claim 1, wherein the VH comprises the CDRs of SEQ ID NO. 1 and the VL comprises the CDRs of SEQ ID NOs. 196 or 2.

4. The antibody or antigen-binding fragment of any of the preceding claims, wherein the VH comprises the following CDRs:

a) CDR-H1: **[SEQ ID NO. 23]** or an amino acid sequence having at least 80% identity therewith, for example at least 85%, 90%, 91%, 92%, 93%, 94%, 95%, 96%, 97%, 98%, or 99% identity, preferably with at least 80% identity; and/or
b) CDR-H2: **[SEQ ID NO. 28]** or an amino acid sequence having at least 80% identity therewith, for example at least 85%, 90%, 91%, 92%, 93%, 94%, 95%, 96%, 97%, 98%, or 99% identity, preferably with 88% identity; and/or
c) CDR-H3: **[SEQ ID NO. 32]** or an amino acid sequence having at least 73% identity therewith, for example at least 85%, 90%, 91%, 92%, 93%, 94%, 95%, 96%, 97%, 98%, or 99% identity, preferably with at least 67% identity.

5. The antibody or antigen-binding fragment of any of the preceding claims, wherein the VH comprises the CDRs of SEQ ID NOs 23, 28, and 32.

6. The antibody or antigen-binding fragment of any of the preceding claims comprising a VH having the amino acid sequence of SEQ ID NO. 1, or a variant having at least 80% sequence identity therewith, for example at least 85%, 90%, 91%, 92%, 93%, 94%, 95%, 96%, 97%, 98%, or 99% identity, preferably having around 93% identity.

7. The antibody or antigen-binding fragment of any of the preceding claims, wherein the VL comprises the following CDRs:

a) CDR-L1: **[SEQ ID NO. 37]** or an amino acid sequence having at least 80% identity therewith, for example at least 85%, 90%, 91%, 92%, 93%, 94%, 95%, 96%, 97%, 98%, or 99% identity, preferably having 85% identity; and/or
b) CDR-L2: **[SEQ ID NOs. 197 or 41]** or an amino acid sequence having at least 80% identity therewith, for example at least 85%, 90%, 91%, 92%, 93%, 94%, 95%, 96%, 97%, 98%, or 99% identity, preferably having at least 71% identity; and/or
c) CDR-L3: **[SEQ ID NOs. 198 or 46]** or an amino acid sequence having at least 55% identity therewith, for example at least 60%, 65%, 70%, 75%, 80%, 85%, 90%, 91%, 92%, 93%, 94%, 95%, 96%, 97%, 98%, or 99% identity, preferably having at least 55% identity.

8. The antibody or antigen-binding fragment of any of the preceding claims, wherein the VL comprises the CDRs of SEQ ID NOs 37, 197 or 41, and 198 or 46, preferably wherein the VL comprises the CDRs of SEQ ID NOs 37, 197, and 198 or SEQ ID NOs. 37, 41, and 46.

9. The antibody or antigen-binding fragment of any of the preceding claims comprising a VL having the amino acid sequence of SEQ ID NOs. 196 or 2, or a variant having at least 80% sequence identity therewith, for example at least 85%, 90%, 91%, 92%, 93%, 94%, 95%, 96%, 97%, 98%, or 99% identity, preferably having around 91% identity.

10. The antibody or antigen-binding fragment of any of the preceding claims comprising the following CDRs:

a) CDR-H1: **[SEQ ID NO. 23]** or an amino acid sequence having at least 80% identity therewith, for example at least 85%, 90%, 91%, 92%, 93%, 94%, 95%, 96%, 97%, 98%, or 99% identity, preferably with at least 80% identity; and/or

b) CDR-H2: **[SEQ ID NO. 28]** or an amino acid sequence having at least 80% identity therewith, for example at least 85%, 90%, 91%, 92%, 93%, 94%, 95%, 96%, 97%, 98%, or 99% identity, preferably with 88% identity; and/or
c) CDR-H3: **[SEQ ID NO. 32]** or an amino acid sequence having at least 73% identity therewith, for example at least 85%, 90%, 91%, 92%, 93%, 94%, 95%, 96%, 97%, 98%, or 99% identity, preferably with at least 67% identity; and/or
d) CDR-L1: **[SEQ ID NO. 37]** or an amino acid sequence having at least 80% identity therewith, for example at least 85%, 90%, 91%, 92%, 93%, 94%, 95%, 96%, 97%, 98%, or 99% identity, preferably having 85% identity; and/or
e) CDR-L2: **[SEQ ID NO. 197 or 41]** or an amino acid sequence having at least 80% identity therewith, for example at least 85%, 90%, 95%, or 99% identity, preferably having at least 71% identity; and/or
f) CDR-L3: **[SEQ ID NO. 198 or 46]** or an amino acid sequence having at least 55% identity therewith, for example at least 60%, 65%, 70%, 75%, 80%, 85%, 90%, 91%, 92%, 93%, 94%, 95%, 96%, 97%, 98%, or 99% identity, preferably having at least 55% identity.

11. The antibody or antigen-binding fragment of claim 1, wherein the VH comprises the CDRs of SEQ ID NO. 21 and the VL comprises the CDRs of SEQ ID NO. 22.

12. The antibody or antigen-binding fragment of any of the preceding claims, wherein the VH comprises the following CDRs:

a) CDR-H1: **[SEQ ID NO. 27]** or an amino acid sequence having at least 60% identity therewith, for example at least 60%, 65%, 70%, 75%, 80%, 85%, 90%, 91%, 92%, 93%, 94%, 95%, 96%, 97%, 98%, or 99% identity, preferably with at least 60% identity; and/or
b) CDR-H2: **[SEQ ID NO. 29]** or an amino acid sequence having at least 80% identity therewith, for example at least 85%, 90%, 91%, 92%, 93%, 94%, 95%, 96%, 97%, 98%, or 99% identity, preferably with at least 82% identity; and/or
c) CDR-H3: **[SEQ ID NO. 35]** or an amino acid sequence having at least 60% identity therewith, for example at least 65%, 70%, 75%, 80%, 85%, 90%, 91%, 92%, 93%, 94%, 95%, 96%, 97%, 98%, or 99% identity, preferably with at least 69% identity.

13. The antibody or antigen-binding fragment of any of the preceding claims, wherein the VH comprises the CDRs of SEQ ID NOs 27, 29, and 35.

14. The antibody or antigen-binding fragment of any of the preceding claims comprising a VH having the amino acid sequence of SEQ ID NO. 21, or a variant having at least 80% sequence identity therewith, for example at least 85%, 90%, 91%, 92%, 93%, 94%, 95%, 96%, 97%, 98%, or 99% identity, preferably having around 91% identity.

15. The antibody or antigen-binding fragment of any of the preceding claims, wherein the VL comprises the following CDRs:

a) CDR-L1: **[SEQ ID NO. 39]** or an amino acid sequence having at least 80% identity therewith, for example at least 85%, 90%, 91%, 92%, 93%, 94%, 95%, 96%, 97%, 98%, or 99% identity, preferably having at least 92% identity; and/or
b) CDR-L2: **[SEQ ID NO. 44]** or an amino acid sequence having at least 55% identity therewith, for example at least 60%, 65%, 70%, 75%, 80%, 85%, 90%, 91%, 92%, 93%, 94%, 95%, 96%, 97%, 98%, or 99% identity, preferably having at least 57% identity; and/or
c) CDR-L3: **[SEQ ID NO. 47]** or an amino acid sequence having at least 55% identity therewith, for example at least 60%, 65%, 70%, 75%, 80%, 85%, 90%, 91%, 92%, 93%, 94%, 95%, 96%, 97%, 98%, or 99% identity, preferably having at least 55% identity.

16. The antibody or antigen-binding fragment of any of the preceding claims, wherein the VL comprises the CDRs of SEQ ID NOs 39, 44, and 47.

17. The antibody or antigen-binding fragment of any of the preceding claims comprising a VL having the amino acid sequence of SEQ ID NO. 22, or a variant having at least 80% sequence identity therewith, for example at least 85%, 90%, 91%, 92%, 93%, 94%, 95%, 96%, 97%, 98%, or 99% identity, preferably having around 91% identity.

18. The antibody or antigen-binding fragment of any of the preceding claims comprising the following CDRs:

a) CDR-H1: **[SEQ ID NO. 27]** or an amino acid sequence having at least 60% identity therewith, for example at least 60%, 65%, 70%, 75%, 80%, 85%, 90%, 91%, 92%, 93%, 94%, 95%, 96%, 97%, 98%, or 99% identity, preferably with at least 60% identity; and/or
b) CDR-H2: **[SEQ ID NO. 29]** or an amino acid sequence having at least 80% identity therewith, for example at least 85%, 90%, 91%, 92%, 93%, 94%, 95%, 96%, 97%, 98%, or 99% identity, preferably with at least 82% identity; and/or

c) CDR-H3: **[SEQ ID NO. 35]** or an amino acid sequence having at least 60% identity therewith, for example at least 65%, 70%, 75%, 80%, 85%, 90%, 91%, 92%, 93%, 94%, 95%, 96%, 97%, 98%, or 99% identity, preferably with at least 69% identity; and/or

d) CDR-L1: **[SEQ ID NO. 39]** or an amino acid sequence having at least 80% identity therewith, for example at least 85%, 90%, 91%, 92%, 93%, 94%, 95%, 96%, 97%, 98%, or 99% identity, preferably having at least 92% identity; and/or

e) CDR-L2: **[SEQ ID NO. 44]** or an amino acid sequence having at least 55% identity therewith, for example at least 60%, 65%, 70%, 75%, 80%, 85%, 90%, 91%, 92%, 93%, 94%, 95%, 96%, 97%, 98%, or 99% identity, preferably having at least 57% identity; and/or

f) CDR-L3: **[SEQ ID NO. 47]** or an amino acid sequence having at least 55% identity therewith, for example at least 60%, 65%, 70%, 75%, 80%, 85%, 90%, 91%, 92%, 93%, 94%, 95%, 96%, 97%, 98%, or 99% identity, preferably having at least 55% identity.

19. The antibody or antigen-binding fragment thereof according to claim 1 comprising any one of the following combinations of CDRs:

(i) SEQ ID NOs. 23, 28, 32, 37, 197, and 198 (clone 129D5BTY);
(ii) SEQ ID NOs. 23, 28, 32, 37, 41, and 46 (clone 129D5B);
(iii) SEQ ID NOs. 23, 115, 30, 36, 40, and 45 (clone 3A2);
(iv) SEQ ID NOs. 23, 115, 30, 37, 41, and 45 (clone 20F6);
(v) SEQ ID NOs. 23, 115, 31, 37, 41, and 45 (clone 49G5);
(vi) SEQ ID NOs. 23, 115, 30, 37, 41, and 46 (clone 53D11);
(vii) SEQ ID NOs. 23, 115, 31, 37, 41, and 46 (clone 77F3);
(viii) SEQ ID NOs. 23, 29, 33, 38, 42, and 47 (clone 26B5);
(ix) SEQ ID NOs. 23, 29, 33, 38, 43, and 48 (clone 83B11D);
(x) SEQ ID NOs. 23, 29, 34, 38, 43, and 48 (clone 94C2);
(xi) SEQ ID NOs. 23, 29, 35, 39, 43, and 47 (clone 115D1D); and
(xii) SEQ ID NOs. 27, 29, 35, 39, 44, and 47 (clone 131D5s).

20. The antibody or antigen-binding fragment thereof according to any of the preceding claims wherein the antigen-binding fragment is selected from: scFv, Fv, Fab, F(ab)2, Fab-SH, dsFv, sdAb, di-scFvs bi-scFv, Fcabs, diabodies, scFv-Fc/minibody, triabody, tetrabody, tandAb, half antibody (Unibody) and domain antibodies.

21. The antibody or antigen-binding fragment thereof according to any of the preceding claims wherein the antigen-binding fragment binds cMET with an affinity KD of less than 1nM.

22. The antibody or antigen-binding fragment thereof according to any of the preceding claims further comprising a payload, optionally wherein the payload is a toxin, further optionally wherein the payload is coupled to the antibody or antigen-binding fragment thereof via a linker.

23. The antibody or antigen-binding fragment thereof of claim 22, wherein the payload is coupled to the antibody or antigen-binding fragment thereof with a coupling ratio (payload:antibody or antigen-binding fragment) of at least 2:1, at least 3:1, at least 4:1, at least 5:1, at least 6:1, at least 7:1, at least 8:1, at least 9:1, or at least 10:1.

24. The antibody or antigen-binding fragment thereof of claim 23, wherein the payload is coupled to the antibody or antigen-binding fragment thereof with a coupling ratio (payload:antibody or antigen-binding fragment) of at least 6:1.

25. The antibody or antigen-binding fragment thereof of claims 22-24, wherein the payload is directly conjugated to the antibody or antigen-binding fragment thereof at an amino acid, optionally wherein the direct coupling is via a lysine or cysteine residue on the surface of the antibody or antigen-binding fragment thereof, preferably wherein the coupling is via a lysine residue.

26. The antibody or antigen-binding fragment thereof of claims 22-24, wherein the payload is indirectly conjugated to the antibody or antigen-binding fragment thereof at an amino acid, optionally wherein the indirect coupling is via a thiol or maleimide.

27. The antibody or antigen-binding fragment thereof of claims 22-26, wherein the payload is a microtubule inhibitor (MTI), a DNA-damaging agent, a topoisomerase inhibitor, a steroid, a tyrosine kinase inhibitor, an immuno-modulatory drug.

28. The antibody or antigen-binding fragment thereof of claim 27, wherein the MTI is an auristatin or a derivative thereof.

29. The antibody or antigen-binding fragment thereof of claims 27-28, wherein the DNA-damaging agent is a nicking agent, an alkylator, or an intercalating agent.

30. The antibody or antigen-binding fragment thereof of claims 27-29, wherein the topoisomerase inhibitor is a camptothecin or a derivative thereof, optionally wherein the topoisomerase inhibitor is exatecan.

31. The antibody or antigen-binding fragment thereof of claims 27-30, wherein the steroid is dexamethasone.

32. The antibody or antigen-binding fragment thereof of claims 27-31, wherein the tyrosine kinase inhibitor is nintedanib.

33. The antibody or antigen-binding fragment thereof of claims 27-32, wherein the immuno-modulatory drug is a Toll-Like Receptor 7/8 agonist drug.

34. The antibody or antigen-binding fragment thereof of claims 22-28, wherein the antigen-binding fragment is a single chain Fv (scFv) and the payload is MMAE, and wherein the payload is coupled to the scFv with a coupling ratio (payload:scFv) of 6:1.

35. The antibody or antigen-binding fragment thereof of claims 22-28, wherein the antigen-binding fragment is a single chain Fv (scFv) and the payload is a mono-methyl auristatin E (MMAE) comprising a glucuronide and branched PEG linker, wherein the MMAE is conjugated onto surface lysine residues of the scFv.

36. The antibody or antigen-binding fragment thereof of claims 22-35 wherein the FDC binds cMET with an affinity KD of less than 10nM.

37. A pharmaceutical composition comprising the antibody or antigen-binding fragment of any of Claims 1-36 and a pharmaceutically-acceptable carrier, excipient or diluent.

38. An antibody or antigen-binding fragment or pharmaceutical composition as defined in any of Claims 1 to 37 for use in medicine.

39. An antibody or antigen-binding fragment or pharmaceutical composition as defined in any of Claims 1 to 37 for use in the diagnosis, treatment and/or prevention of a disease wherein the disease is selected from cancer, benign tumours, infectious diseases including bacterial, viral, fungal, trypanosome, nematode and prion infections, cardiovascular disease, autoimmune disease.

40. An antibody or antigen-binding fragment or pharmaceutical composition as defined in any of Claims 1 to 37 for use in the manufacture of a medicament for the treatment and/or prevention of a disease selected from cancer, benign tumours, infectious diseases

including bacterial, viral, fungal, trypanosome, nematode and prion infections, cardiovascular disease, and autoimmune disease.

41. The antibody or antigen-binding fragment for use according to any of Claims 38 to 40 wherein the disease is cancer of the colon, lung, breast, head/neck, prostate, skin, stomach/gastrointestinal, oesophageal, bladder, glioma, renal, ovarian, thyroid and bone and

42. A process of making a compound as defined in any of Claims 1 to 36 comprising the steps of:

(i) providing a small molecule payload;
(ii) providing the antibody or antigen-binding fragment as defined in any of Claims 1 to 21;
(iii) conjugating the payload and the antibody or antigen binding fragment thereof.

43. The process according to Claim 42 further comprising the step of:

(iv) combining the compound with a pharmaceutically-acceptable carrier to form a pharmaceutical composition.